



CIMSS Cooperative Agreement Report
1 January 2007-31 December 2007



University of Wisconsin-Madison

**Cooperative Institute for
Meteorological Satellite Studies (CIMSS)**

Cooperative Agreement Annual Report

**for the period
1 January 2007 to 31 December 2007
Cooperative Agreement Number: NA06NES4400002**

**Submitted to:
National Oceanic and Atmospheric Administration
(NOAA)**



Cooperative Agreement Annual Report
1 January 2007 to 31 December 2007

Steve Ackerman
Director, CIMSS

Tom Achteor
Executive Director, Editor

CIMSS Contributing Authors:

Tom Achteor
Steve Ackerman
Scott Bachmeier
Bryan Baum
Chris Bedka
Ralf Bennartz
Fred Best
Eva Borbas
Li Bi
Corey Calvert
Amato Evan
Wayne Feltz
Rich Frey
Ray Garcia
Iliana Genkova
Jordan Gerth
Tom Greenwald
Liam Gumley
Mat Gunshor
Pat Heck
Allen Huang
Bormin Huang
Jim Jung
Jim Kossin
Dan LaPorte
Jun Li
Jinlong Li
Yinghui Liu
Scott Lindstrom
W. Paul Menzel
Chris Moeller
James P. Nelson III
Tim Olander
Jason Otkin

Ralph Petersen
Youri Plokhenko
Elaine Prins
Hank Revercomb
Tom Rink
Chris Rozoff
Dave Santek
Todd Schaack
Chris Schmidt
Tony Schreiner
Matthew Sitkowski
Maciej Smuga-Otto
William Straka III
Dave Tobin
Paul van Delst
Chris Velden
Dee Wade
Andi Walther
Xuanji Wang
Steve Wanzong
Tony Wimmers
Tom Zapotocny

NOAA Collaborators

Jeff Key
Bob Aune
Andy Heidinger
Mike Pavolonis
Brad Pierce
Tim Schmit
Gary S. Wade
Jaime Daniels
Don Hillger

The work conducted as part of the CIMSS Cooperative Agreement for 1 January 2007 to 31 December 2007 is detailed in this report. In the Table of Contents and in the report, the primary author, either the UW-Madison PI or PM, or the NOAA collaborator working on the particular effort is indicated for each section. While primary authors are noted, the research discussed in this report has been a result of numerous collaborations with other CIMSS and NOAA colleagues.



CIMSS Cooperative Agreement Annual Report 1 January 2007 to 31 December 2007

Table of Contents

1. GIMPAP (GOES Improved Measurements and Product Assurance Program)	6
1.1. GOES single field-of-view sounding retrieval science – Jun Li	6
1.2. Global Observing System Studies: Intercalibration – Mat Gunshor	10
1.3. GOES / POES Intercalibration - Mat Gunshor	12
1.4. GOES Winds – Chris Velden	14
1.5.1. GOES Tropical Cyclone Applications - Chris Velden	16
1.5.2. Analysis and Application of GOES IR Imagery Toward Improving Hurricane Intensity Change Prediction – Jim Kossin and Christopher Rozoff.....	17
1.6. Biomass Burning – Chris Schmidt and Elaine Prins	22
1.7. GOES Imager SATellite Convection AnalySis and Tracking (SATCAST) System Product Evaluation by NOAA/NESDIS Operations – Wayne Feltz and Kris Bedka	26
1.8. GOES GEOCAT and Cloud Products – Corey Calvert, Andrew Heidinger and Michael Pavlonis	29
2. CIMSS Support for Polar and Geostationary Satellite Science Topics (P&G_PSDI)	30
2.1. Product Quality Assurance and Science (PQAS) Support for Operational GOES Imager and Sounder Products – James P. Nelson III, Chris Velden, Anthony Schreiner, Gary Wade, Tim Schmit and Jaime Daniels.....	30
2.2. GOES Surface and Insolation Project Processing (GSIP) – William Straka III and Andy Heidinger	33
2.3. GOES Sounder and Imager Spectral Response Function & Transmittance Files – Mat Gunshor and Tim Schmit.....	34
2.4. GOES-N (13) Routine Checkout and Data Archive –Tony Schreiner, Chris Velden, Scott Bachmeier, Tim Schmit and Don Hillger	35
2.5. GOES Wildfire Fire Automated Biomass Burning Algorithm – Chris Schmidt and Elaine Prins	37
2.6. Derived Products from GOES-10 Sounder – Tony Schreiner, James P. Nelson III, Tim Schmit, and Gary Wade	39
2.7. Implementation of the CIMSS Advanced Dvorak Technique into NESDIS Operations – Tim Olander and Chris Velden	41
2.8. Polar Winds (MODIS) - Dave Santek, Jeff Key and Chris Velden	42
3. Ground Systems Research	43
3.1. Global Fire Detection - Elaine Prins, Chris Schmidt	43
3.2. A Dedicated Processing System for Infusion of Satellite Products in AWIPS – Scott Bachmeier, Gary Wade and Jordan Gerth	46
4. GOES R Risk Reduction	51
4.1. Algorithm Development – Allen Huang and Chris Velden, Team Leaders	51
4.1.1. GOES-R Risk Reduction Sounding Algorithm Development – Jun Li and Allen Huang	51
4.1.2. GOES-R Risk Reduction Activities and Achievements: Winds – Chris Velden, Steve Wanzong and Iliana Genkova	56
4.1.3. GOES-R Risk Reduction Ozone Algorithm Development – Jun Li, Jinlong Li and Chris Schmidt	59



4.1.4. Radiative Transfer Modeling – Steve Ackerman and Tom Greenwald.....	61
4.1.5. Land Surface Properties – Bob Knuteson	63
4.1.6. Biomass Burning – Chris Schmidt and Elaine Prins.....	69
4.1.7. SATCAST/Convective Initiation – Wayne Feltz and Kristopher Bedka	71
4.1.8.1 Tropical Cyclones Research – Chris Velden.....	75
4.1.8.2 Constructing an Objective Tool for Identifying Hurricane Secondary Eyewall Formation – James Kossin and Matthew Sitkowski	78
4.1.9. Visualization (HYDRA Integration) – Tom Rink and Tom Achtor.....	85
4.2. Cal/Val Efforts in support of GOES – Dave Tobin	88
4.3. Nowcasting Activities – Ralph Petersen, Robert Aune	89
4.4. Data Assimilation/Simulations – Jason Otkin and Allen Huang	94
4.5. Ground Systems Processing – Maciej Smuga-Otto and Robert Knuteson.....	97
5. GOES R Algorithm Working Group	99
5.1. GOES-R Proxy Data Sets - Allen Huang and Tom Greenwald	99
5.2. GOES-R Analysis Facility Instrument for Impacts on Requirements (GRAFIIR) – Allen Huang.....	105
5.3. Development of the Multilayer Cloudy Radiative Transfer Model for GOES-R Advanced Baseline Imager (ABI) - Bormin Huang	108
5.4. Algorithm Integration Team (AIT) Technical Support – Ray Garcia and Maciej Smuga- Otto.....	111
5.5. Total Ozone from ABI – Chris Schmidt, Jun Li	112
5.6. GOES-R Cloud Properties –Corey Calvert, Andrew Heidinger, Michael Pavolonis, Andi Walther and Pat Heck.....	113
5.7. Static Libraries for Retrieval of Cloud Optical and Microphysical Properties - Bryan Baum	116
5.8. GEOCAT Enhancements and Documentation – Graeme Martin and Michael Pavolonis	116
5.9. ABI Fire Detection and Characterization Algorithm Development and Evaluation– Chris Schmidt and Elaine Prins	118
5.10. GOES-R Legacy Profile Algorithm Evaluation and Selection - Jun Li and Tim Schmit	122
5.11. Sounding Product Evaluation and Validation – Dave Tobin and Tom Achtor	125
5.12. GOES-R AWG Winds – Chris Velden, Steve Wanzong and Iliana Genkova	125
5.13. GPSDI Hurricane Intensity from ABI – Chris Velden and Tim Olander	129
5.14. Aviation – Wayne Feltz	131
5.14.1. Volcanic Ash and SO ₂ – Wayne Feltz and Michael Pavolonis	131
5.14.2. Fog/Low Cloud – Wayne Feltz and Michael Pavolonis	133
5.14.3. Turbulence – Wayne Feltz and Tony Wimmers	134
5.15 Estimation of Sea and Lake Ice Characteristics with GOES-R ABI - Xuanji Wang, Yinghui Liu and Jeff Key.....	135
6. GOES-R (and beyond) instrument and requirement studies – Jun Li and Tim Schmit	137
7. A CIMSS Research Study of the Next Generation Geostationary Operational Environmental Satellite (GOES) Data Compression - Bormin Huang	145
8. Joint Center for Satellite Data Assimilation (JCSDA)	147
8.1. The Development of IASI radiance and AIRS cloudy radiance assimilation techniques within the NCEP’s Global Forecast System – James Jung, Tom Zapotocny and Todd Schaack.....	147
8.2. Enhanced Cloud Height Assignment using CALIPSO – Steve Ackerman.....	152



8.3. Assimilating and Determining the Forecast Impact of Sea Surface Winds Measured by WindSat/Coriolis in the NCEP GDAS/GFS – Li Bi, James Jung and Steve Ackerman	153
8.4. Observation error characterization for radiance assimilation of clouds and precipitation – Ralf Bennartz, Tom Greenwald and Andrew Heidinger	159
9. Continued Development of the Community Radiative Transfer Model (CRTM) – Paul van Delst	160
10. NCEP International Modeling Support - Ralph Petersen	160
11. Support for the WVSS-II Field Program – Ralph Petersen and Wayne Feltz	161
12. VISIT Activities – Steve Ackerman, Scott Bachmeier and Scott Lindstrom	172
13. SHyMet Activities – Steve Ackerman and Scott Bachmeier	175
14. Polar Winds from Satellite Imagers and Sounders – Chris Velden, Jeff Key and Dave Santek	175
15. Monitoring Global Variability with PATMOS-x – Amato Evan and Andrew Heidinger	177
16. Developing Training Materials for McIDAS-X Users and Programmers – Dee Wade	179
17. NPOESS Studies	179
17.1. Generating and Validating Snow and Ice Products in Polar Regions – William Straka III and Jeff Key	179
17.2. Cloud Studies for NPOESS – Richard Frey, Andrew Heidinger and Michael Pavolonis	181
17.3. VIIRS Radiance Calibration / Validation, VIIRS / CrIS Cloud Property Investigations, and CrIS / ATMS / GPS Soundings – Paul Menzel, Eva Borbas, Yuri Plokhenko, Chris Moeller and Dan LaPorte	183
17.4. Cal/Val Verification and Validation Activities – Hank Revercomb and Fred Best	187
17.5. The International Polar Orbiting Processing Package for Direct Broadcast Users - Allen Huang and Liam Gumley	197



1. GIMPAP (GOES Improved Measurements and Product Assurance Program)

1.1. GOES single field-of-view sounding retrieval science – Jun Li

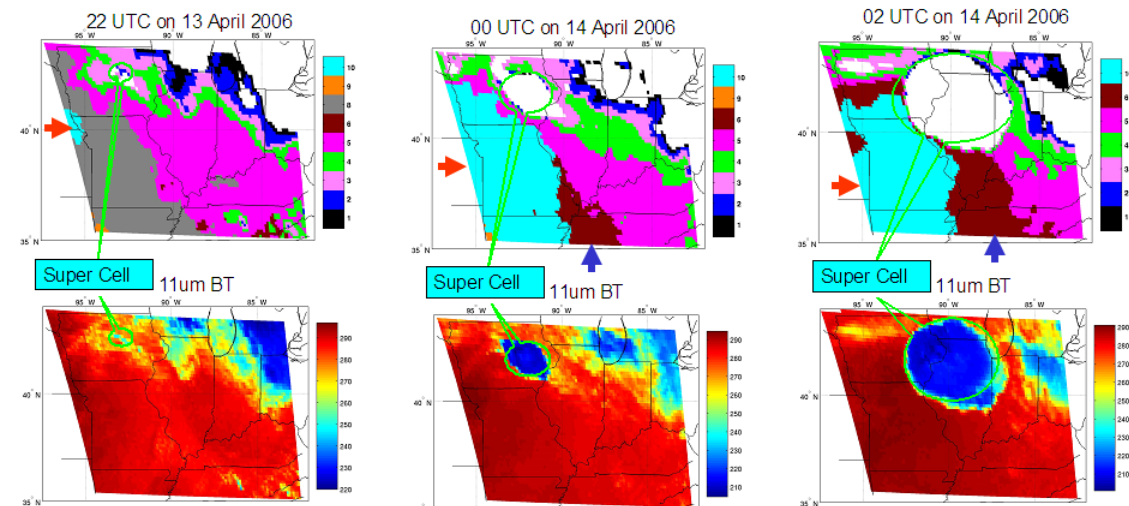
Proposed Work

In 2007, we proposed to:

1. Investigate the use of spectral, temporal information, spatial information and noise filtering in single FOV sounding and ozone retrieval;
2. Study the synergy with GPS and other low orbiter observations;
3. Use clear channels for cloudy sounding;
4. Enhance international collaboration for geostationary sounding studies.

Summary of 2007 Accomplishments and Findings

Clustering technique for GOES Sounder radiances



April 13 – 14, 2006 hail storm in Madison area, WI

New way of using GOES Sounder data to help severe weather forecast. Sounder multi-spectral brightness temperatures are classified into cloudy sky (see white area) and different clear air masses (see different colors). From 22 UTC (13 April) to 00 UTC (14 April), the clear sky air mass 10 moves fast towards east, and the super cell is also developing (see the 11 μm brightness temperature images). From 00 UTC to 02 UTC, air mass 6 moves fast toward north and the super cell is further developed to Madison area. The clear sky air mass movement pre and during the convection is very useful for the storm forecast. For example, using the Lifted Index (LI) to help the forecast and now cast. (Zhenglong Li, W. Paul Menzel and Jun Li)

Figure 1.1.1: Clear air mass classes from clustering (upper panels) and 11 μm brightness temperature images at 22 UTC on 13 April, 00 UTC and 02 UTC on 14 April 2006.

According to GIMPAP Technical Advisory Committee (TAC) guidance, we implemented the clustering technique to GOES Sounder radiance measurements. Results show that this technique is very useful for convective storm nowcasting using the GOES Sounder data. The hailstorm of 13 – 14 April 2006 caused damage to many houses in and around Madison, Wisconsin. The storm produced large hailstones. The



GOES Sounder 11- μ m image at 22 UTC on 13 April showed that a super cell was likely to develop. The multispectral band classification (Li et al. 2003, JAM) showed that there are four typical classes (4, 5, 6, 10) of clear air mass surrounding the super cell (see Figure 1.1.1). Two hours later (00 UTC on 14 April), the class 10 (which was a dry air mass according to the relative humidity retrieval) moved east while a class 6 (which is a wet air mass) moved north. The clear sky atmosphere was very unstable from 22 UTC to 00 UTC as the super cell started to develop. From 00 UTC on 13 April to 02 UTC on 14 April, the air mass continued to move (classes 6 and 10), and the super cell developed quickly and became a convective system. The soundings observed by the GOES Sounder before and during the convective storm are very useful for short-range storm forecasts.

Time continuity and noise filtering in GOES SFOV sounding retrieval

We continued to study time continuity (TC). We have tested a few approaches using previous time step information (e.g., retrieval or forecast information from previous time step) in the current time step sounding retrieval. The time continuity does show slight improvement over the use of a single time step for soundings. However, after analysis, we think that using time continuity might not provide a significant advantage over the single time step method with current GOES Sounder data for soundings. Possible reasons are: (1) the temporal resolution of GOES Sounder is not high enough to show advantage in TC for soundings; (2) GOES Sounder retrieval algorithm uses a forecast as first guess and the forecast already contains TC information through dynamic process; and (3) collocation between two time steps for SFOV will create additional error. However, time continuity should work well for surface emissivity and skin temperature retrieval. For example, by the assumption that emissivity is temporally invariable while surface skin temperature is temporally variable, radiance observations from more than two time steps can be used. We will investigate the TC approach for surface property retrieval. For example, time continuity is expected to show a positive impact on ABI (Advanced Baseline Imager) retrieval due to its very high temporal resolution (better than 15 minutes).

CIMSS GIMPAP sounding group helped GOES-13 Sounder technical report, we find that GOES-13 Sounder has striping noise for some spectral bands due to the calibration, and the striping noise can be removed by a noise filtering technique.

Successful integration of GOES improved sounding algorithm and software into the CIMSS merged retrieval system

The GOES improved sounding algorithm and software has been successfully implemented into the CIMSS merged real time retrieval system. The derived total precipitable water (TPW) images show that the improved DPI has less noise than the legacy one. We are running the legacy and improved retrieval systems simultaneously to quantitatively evaluate the results against radiosonde observations (RAOBs). The new algorithm and software can be transferred to the operational implementation through PSDI program.

GOES-12 Sounder improved single field-of-view (SFOV) soundings show very important nowcasting information for a tornado that occurred in Texas on 24 April 2007, killing 10 people and injuring more than 120 persons. Unfortunately, the short range forecast did not reflect this needed information. A severe convection developed ahead of a frontal boundary that was moving southward across the Rio Grande Valley region late in the day on 24 April 2007. This storm produced large hail (up to **2.75 inches** in diameter), strong winds (up to **76 mph**), and an EF-3 tornado. We used hourly GOES-12 Sounder data to retrieve the soundings and lifted index (LI) product. The retrieved LI from the improved method is better than the legacy product and much better than the actual forecast. Figure 1.1.2 shows the forecast LI (upper left) and the GOES-12 Sounder LI retrievals (upper right) at 22 UTC on 24 April 2007. The NOAA-16 AVHRR image is also shown (lower panel). The storm is rapidly developing at 22 UTC. The LI index at 20 and 21 UTC from forecast does not reflect any atmospheric instability in that region, while



new retrievals before and during the storm development show important atmospheric instability information. Although the legacy LI also provided instability information for this case, it is not as good as new retrievals. An article summarizing the GOES sounding improvement and applications will be published in *Geophysical Research Letters* (Li et al. 2008).

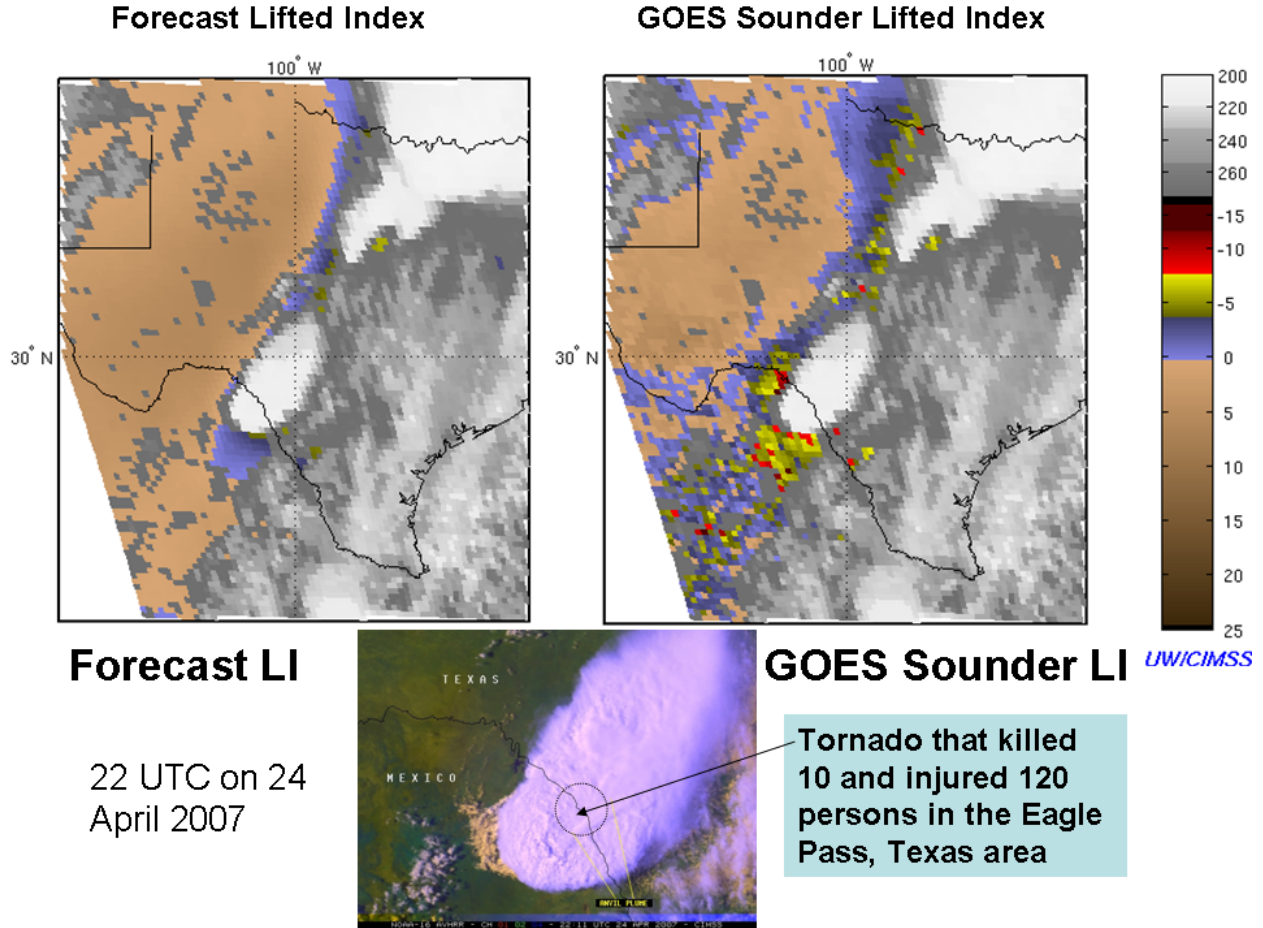


Figure 1.1.2: The forecast LI (upper left) and the GOES-12 Sounder LI retrievals (upper right) at 22 UTC on 24 April 2007.

GOES single field-of-view cloudy sounding research started

Forecasts in cloudy regions usually are worse than those in clear regions. Moisture soundings in cloudy skies are very important to the forecast model. The goal is to derive soundings from GOES Sounder radiances contaminated with thin or low clouds. One-layer cloudy radiative transfer model accounting for atmospheric molecule absorption, cloud absorption and scattering, is used in the cloudy sounding retrieval. The cloudy training data set over Continental United States (CONUS) is developed, the data set contains temperature profile, moisture profile, surface skin temperature, surface infrared emissivities at GOES Sounder spectral bands, cloud-top pressure, cloud optical depth, and cloud particle size in radius. The cloudy training data set is used to generate cloudy regression coefficients for ice cloudy and water cloudy situations. Initial results show that the cloudy LI in thin or low cloudy situations expands the unstable region that links to the supercell development.



International collaboration on geostationary sounding study

As part of the capacity building effort of the Global Earth Observation System of Systems (GEOSS)-America, CIMSS delivered processing software to generate temperature and moisture profiles from GOES-10 Sounder data to Rodrigo Souza of Instituto de Pesquisas Espaciais (INPE, Brazil). The new algorithms and software provided to South American GOES-10 user community are developed under GIMPAP support. Luiz Augusto Toledo Machado, Chief of Satellite and System Division at INPE, has reported their GOES-10 sounding test results at the GOES-10 workshop held on 26 June 2007 in San Jose, Costa Rica.

Invited by Dr. Marcelino Manso, Manager of EUMETSAT NoWCasting Satellite Application Facility (NWCSAF) at Instituto Nacional de Meteorología (INM) in Madrid, Spain, Jun Li visited NWCSAF 19 – 30 November 2007. Li collaborated with INM scientists on implementing the legacy profile algorithm for SEVIRI (Spinning Enhanced Visible and InfraRed Imager) operational nowcasting products at NWCSAF, and on the use of SEVIRI for algorithm development and improvement. He also attended the “Workshop on Physical Retrieval of Clear Air Parameters” held 28-29 November and gave a talk entitled “Development of physical retrieval algorithm for clear sky legacy profiles from SEVIRI and ABI infrared radiances.” About 30 researchers and scientists attended the workshop. Jun Li’s travel was supported by EUMETSAT.

Publications, Presentations and Conference Reports

Jin, Xin, J. Li, C.C. Schmidt, T.J. Schmit and J. Li, 2007. Retrieval of Total Column Ozone from Imagers Onboard Geostationary Satellites, *IEEE Transactions on Geosciences and Remote Sensing* (in press).

Li, Jinlong, J. Li, C.C. Schmidt, J.P. Nelson III, and T.J. Schmit, 2007. High Temporal Resolution GOES Sounder Single Field of View Ozone Improvements, *Geophysical Research Letters*, 34, L01804, doi:10.1029/2006GL028172.

Li, Jun, T.J. Schmit, J. Daniels, J. Li, Z. Li, W.P. Menzel, and J.J. Gurka, 2007. GOES infrared sounders - the current applications and future needs, *Proceedings of 32nd International Symposium on Remote Sensing of Environment*, June 25 - 29, 2007, San José, Costa Rica.

Li, Jun, 2007. Single Field-of-View Soundings from Geostationary Infrared Sounder Radiances, presentation at the EUMETSAT/AMS joint satellite conference, 24 - 28 September 2007, Amsterdam, The Netherlands.

Li, Jun. et al. 2007. GOES Sounding Product Improvement and Applications to Storm Cases, supplementary PPT for GIMAP TAC.

Li, Zhenglong, W.P. Menzel, T. J. Schmit, J.P. Nelson, J. Daniels and S.A. Ackerman, 2008. GOES sounding improvement and applications to severe storm nowcasting, *Geophysical Research Letters* (in press).

Schmit, Timothy J., 2007. The GOES-10 Sounder, presentation at the GOES-10 Workshop, 26 June 2007, San José, Costa Rica.



1.2. Global Observing System Studies: Intercalibration – Mat Gunshor

Proposed Work

CIMSS continued to investigate how to address, or compensate for, the effect of spectral gaps in AIRS coverage on intercalibration results. CIMSS continued to investigate the radiometric characteristics of old instruments, both domestic and international, and new instruments as data become available. New IASI and Meteosat-9 were expected to come online in 2007. CIMSS also planned to continue to collaborate with scientists from NOAA and other institutions to assess the radiometric accuracy of satellite instruments. In the past, this work has included investigating such topics as the effects of changes to the Modern Sensor Processing System (MSPS) software, the effects of direct solar radiation on GOES-13 imagery during eclipse, and diagnosing the calibration (gain) mode of the sounder. CIMSS plans to continue to address these types of issues as they arise.

Summary of Accomplishments and Findings

Scientists from CIMSS attended the 1st meeting of the Global Space-Based Inter-Calibration System (GSICS) Research Working Group (GRWG-I) on 22-23 January 2007 in the NOAA Science Center in Camp Springs, Maryland. CIMSS attendees presented summaries of intercalibration work done over the past decade. The research covered a wide-range of satellite-to-satellite intercalibration, aircraft-based validation, and ground-based validation of satellite instrument calibration. We made recommendations to the international GSICS council on how to proceed with coordinated efforts to intercalibrate the world's geostationary imagers using polar-orbiting high spectral resolution instruments such as the Atmospheric InfraRed Sounder (AIRS) onboard Aqua (United States) and eventually the Infrared Atmospheric Sounding Interferometer (IASI) onboard MetOp-A (Europe).

Based on a relatively small sample size from 23 September to 10 October of 2006, preliminary results showed that METEOSAT-9 compared well to AIRS and to METEOSAT-8 (vicariously through AIRS). With our counterparts in EUMETSAT, we electronically presented these results to the GSICS committee in March 2007—before the switchover in operations to METEOSAT-9 on 11 April 2007.

During the GOES-13 post-launch test analysis, comparisons with AIRS data and HIRS data on NOAA-15 and NOAA-16 show that there appears to be a cold bias on the order of -2 K in band 6 (13.3 micrometer) of the GOES-13 Imager. This may be mitigated using a bias correction. Preliminary work shows that shifting the Spectral Response Function (SRF) -4.7 inverse centimeters reduces the apparent bias (compared to AIRS) from -2.4 to 0 K. A memo was written on this subject and circulated among interested parties in March 2007. In subsequent communications with NOAA and ITT, including a teleconference, it became apparent that the proposed method of correcting this problem has merit and it is possible that the official GOES-13 Imager SRF for that band will be changed before GOES-13 becomes operational.

We continued to research improvements to methods of filling AIRS spectral gaps. This research was presented as a poster and paper at the SPIE conference: Atmospheric and Environmental Remote Sensing Data Processing and Utilization III: Readiness for GEOSS (27-28 August, 2007). The paper was titled “Intercalibrating geostationary imagers via polar orbiting high spectral resolution data” and included results from GOES-12 and Meteosat-8 compared to AIRS over 2006. This research was also presented at the 15th American Meteorological Society (AMS) Satellite Meteorology & Oceanography Conference in Amsterdam, the Netherlands 24-28 September 2007. This paper included an error-analysis method to estimate the amount of error introduced by the adopted method of gap-filling. We compensate for AIRS spectral gaps by filling them with generic information from the US Standard Atmosphere, adjusted to mimic the AIRS data. Part of the paper focuses on this method and testing it against a series of known atmospheres (calculated spectra from radiosonde data using a line-by-line radiative transfer model) that



were made to look like AIRS. The results showed that the method worked very well for most spectral bands and reasonably well in tropical atmospheres for the other bands. Work continued in this area to expand the results to other geostationary imagers and to expand the SPIE conference paper for submission to a peer-reviewed publication.

Work has begun to use IASI data for comparisons to the world's geostationary imagers. There is a separate effort at CIMSS to provide IASI data to a number of scientists and that work will most likely be leveraged in the next year. While that is developing, there is a more rudimentary method of obtaining data. So far, several dozen cases have been collected of IASI matched with GOES-12, GOES-11, GOES-10, METEOSAT-9, MTSAT, and FY-2C (at the GEO sub-points). There are also efforts underway to develop the software tools needed to process IASI/GEO comparisons. The collection of data will continue, as the infrastructure for beginning more frequent IASI/GEO comparisons is built, and analysis will begin in the next fiscal year.

Publications and Conference Reports

Gunshor, Mathew M., T.J. Schmit, W.P. Menzel and D. Tobin. Intercalibrating geostationary imagers via polar orbiting high spectral resolution data. Atmospheric and Environmental Remote Sensing Data Processing and Utilization III: Readiness for GEOSS, San Diego, CA, 27-28, 30 August 2007. *Proc. SPIE Int. Soc. Opt. Eng.* 6684, 66841H (2007).

Schmit, Timothy J. and M. Gunshor. Intercalibrating the world's geostationary imagers via polar orbiting high spectral resolution data. Joint 2007 EUMETSAT Meteorological Satellite Conference and the 15th Satellite Meteorology and Oceanography Conference of the American Meteorological Society, Amsterdam, the Netherlands, 24-28 September 2007.

Table 1.2.1: Comparison of GOES-13 Imager to Atmospheric InfraRed Sounder (AIRS). The sample size is 19.

Imager Band	Bias (K)	Standard Deviation of Differences (K)
2 (3.9 μm)	0.2	0.6
3 (6.5 μm)	-0.4	0.3
4 (10.7 μm)	-0.1	0.4
6 (13.3 μm)	-2.4	0.6

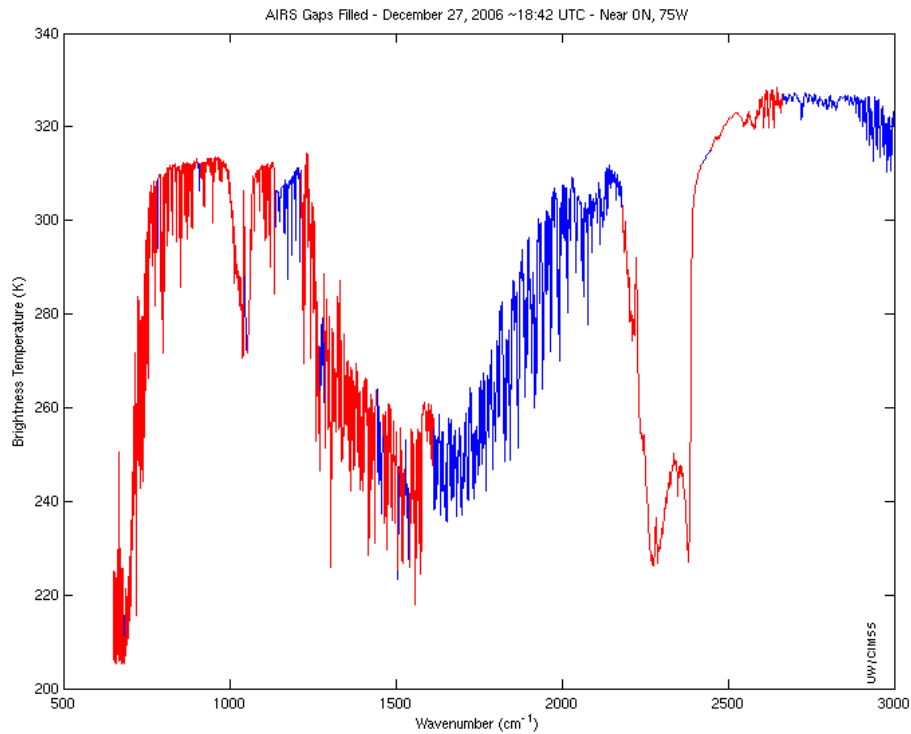


Figure 1.2.1: Example of an AIRS spectrum (red) with spectral gaps being filled in blue by an adjusted US Standard Atmosphere spectrum.

1.3. GOES / POES Intercalibration - Mat Gunshor

Proposed Work

In 2007, our primary focus was to continue routine intercalibration using NOAA-15 and -16 AVHRR, and HIRS compared to GOES-11, -12, Meteosat-5, -7 and -8. This effort requires regular maintenance and periodic archiving. CIMSS continued to write, update, and maintain a large volume of software directly related to this project. Results are posted to a web page for the user community. When the SSEC Data Center began receiving GOES-10 data, routine intercalibration processing of GOES-10 data began for its new location over South America.

Summary of Accomplishments and Findings

This year, we made a concerted effort to give regular oversight to the automated features of this process. The data collection and processing results were monitored as were the output generated for the internet.

GOES-10 returned to operational status near the end of 2006 (21 December) for service over South America at 60 West. Automated intercalibration with NOAA-15 and NOAA-16 AVHRR and HIRS soon followed with results being posted to the CIMSS intercalibration web page.

We also had to address the several changes in the international line-up of geostationary imagers. METEOSAT-7 replaced METEOSAT-5 over the Indian Ocean at 65 degrees east longitude. METEOSAT-5 was moved to the archive section of the web page.



In addition, we have switched to MTSAT HRIT data from MTSAT HiRID data formats because NESDIS dropped the HiRID format and switched to HRIT. This change required upgrading the portion of the intercalibration software that runs in McIDAS. McIDAS is used to collect data for intercalibration and older versions of the McIDAS servers that cannot properly handle this newer data format for MTSAT. We used to use version 2005a of McIDAS, but have switched to the 2007 version of McIDAS.

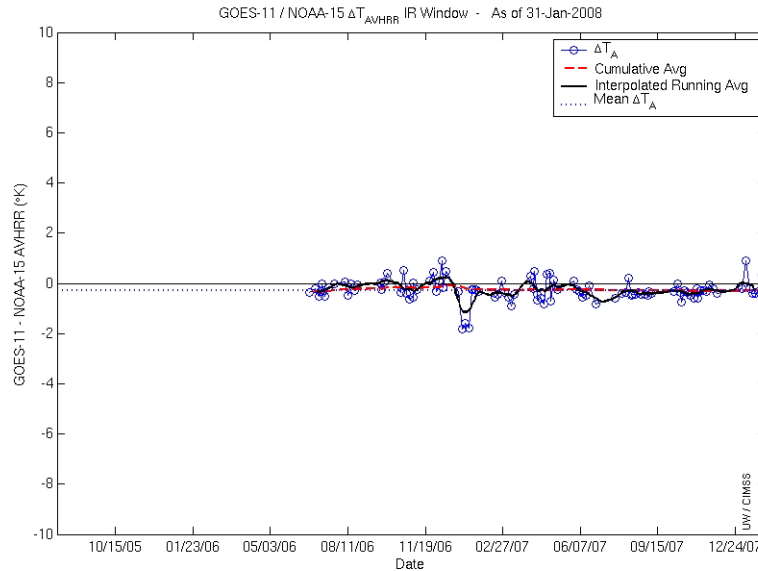


Figure 1.3.1: Time series of GOES-11-NOAA-15 AVHRR intercalibration cases from mid-June 2006 through the present. Similar plots for GOES-9, -10, -11, and -12 compared to NOAA-15 and NOAA-16 HIRS and AVHRR are updated daily on the CIMSS intercalibration web site: <http://cimss.ssec.wisc.edu/goes/intercal>



Intercalibration at CIMSS

Intercalibration of Geostationary and Polar Orbiting Instruments

- Home
- Overview
- Results**
- Examples
- Publications
- Links

Results

Current Summary

NOAA-15 Infrared Window Channel
August 22, 2005 to January 31, 2008

Delta (geo-leo)		GOES-11 IRW	GOES-12 IRW	GOES-10 IRW	MET-8 IRW	MET-7 IRW
Number of Comparisons	ΔT_{HIRS}	103	209	237	132	156
	ΔT_{AVHRR}	103	209	237	132	156
Mean	ΔT_{HIRS}	0.8	0.49	0.89	0.44	-1.83
	ΔT_{AVHRR}	-0.28	1.16	0.17	0.4	-2.08
Standard Deviation	ΔT_{HIRS}	2.43	1.66	1.78	1.02	1.18
	ΔT_{AVHRR}	0.42	2.52	0.58	0.35	0.81

Figure 1.3.2: Snapshot of results posted to intercalibration Web page on 31 January 2008. Results here show the mean and standard deviation of all cases processed to date.

1.4. GOES Winds – Chris Velden

Proposed Work

CIMSS continued to develop new diagnostic fields derived from GOES data and analyses for applications to Tropical Cyclones (TCs).

Summary of Accomplishments and Findings

1. The CIMSS winds-tracking software continues to be modified to allow for easy adaptation to new instruments. Satellite-specific parts of the software were identified and isolated, minimizing the effort required for adding new satellites and sensors. In this reporting period, a specific example is the adaptation of the code to process data from the successfully launched GOES-13 satellite. The algorithm linkages that were needed to ingest and process the GOES-13 data were tested in the science checkout period, and have been successfully integrated.



2. We are investigating the idea that the vectors best represent a mean *layer* of motion rather than a single level. To test this hypothesis, GOES-12 Operational winds (IR and WV) are compared to collocated rawinsonde data at both individual levels and layers of varying thickness. RMS differences are calculated for groups of vectors binned by assigned pressure. In general, upper-level winds agree best with a mean layer motion of ~ 100 hPa in thickness. Mid- and lower-level winds correspond best to a broader layer ~ 150 hPa thick. The representativeness of mid-level WV winds can be a very broad layer. Assigning the vector heights to a tropospheric *layer* can increase GOES wind-rawinsonde agreement by ~ 1 - 2 m/s. Our findings suggest that the vector representativeness error can be reduced by attributing the vectors to a tropospheric layer rather than a discrete single tropospheric level.
3. CIMSS is supporting elements of a tropical cyclone (TC) predictability study in conjunction with scientists at the Naval Research Lab. Special GOES-12 rapid-scan wind data sets were processed during major hurricane events in the 2005 and 2006 Atlantic hurricane seasons. Produced at hourly intervals using 5-min rapid scans, these data sets are being tested for forecast impact in global models using variational assimilation methods. It is anticipated that the GOES winds will cover important areas of the model initial analyses identified by targeting techniques as potential high impact regions. These concepts are being tested.
4. The data assimilation community continues to struggle with effective integration of satellite-derived winds into current variational analysis schemes. As a result, observing system experiments show the winds offer only a modest positive impact on NWP forecasts. One of the strong messages from recent International Winds Workshops is that the data assimilation community could use more information on vector characterization and quality. During this reporting period we have continued to test and modify a new regression-based quality indicator referred to as the "Expected Error" (EE). This index is designed to attach to every vector record and indicate the confidence in the form of an expected vector RMSE. Our analyses suggest the EE is a better indicator of quality than the existing operational Quality Indicator (QI). We are in the process of examining this new EE for data assimilation screening properties and eventually for observation weighting in NWP applications.

Publications

Velden, C., and K. Bedka, 2007: Identifying the Uncertainty in Determining Satellite-Derived Atmospheric Motion Vector Height Assignments. Submitted to *JAMC*.

Berger, H. and C. Velden: The impact of GOES rapid-scan Atmospheric Motion Vectors (AMVs) on global numerical weather prediction model forecasts. Joint 2007 EUMETSAT Meteorological Satellite Conference and Satellite Meteorology and Oceanography Conference, 15th, of the American Meteorological Society, Amsterdam, the Netherlands, 24-28 September 2007.

Berger, H., C. Velden, S. Wanzong and J. Daniels: Evaluation of a new quality indicator to estimate satellite-derived Atmospheric Motion Vector observation error. Joint 2007 EUMETSAT Meteorological Satellite Conference and Satellite Meteorology and Oceanography Conference, 15th, of the American Meteorological Society, Amsterdam, the Netherlands, 24-28 September 2007.



1.5.1. GOES Tropical Cyclone Applications - Chris Velden

Proposed Work

CIMSS continues to develop new diagnostic fields derived from GOES data and analyses for applications to Tropical Cyclones (TCs).

Summary of Accomplishments and Findings

1. The CIMSS Tropical Cyclones group continues to develop diagnostic fields derived from GOES winds analyses for applications to TCs. These products include analyses of vertical wind shear, vorticity, upper-level divergence, vertical wind shear tendency, steering currents, and surface adjusted cloud-drift winds. All of these products are featured on the CIMSS Tropical Cyclones web site (<http://cimss.ssec.wisc.edu/tropic2/>), which has become an extremely popular site for both the general public and forecasters during TC events. We continue to upgrade these products and develop new ones often based on community/user feedback. Also, GOES data sets and products are continuously requested by and provided to the user community for scientific research on TCs.
2. Previous reports have included information on research on identifying the Saharan Air Layer (SAL) using GOES and other satellite data, and the dust's influence on TC intensity. The research has resulted in the submission of a paper to *GRL*.
3. We continue to upgrade the Advanced Dvorak Technique (ADT) algorithm, which is now used by several of NOAA's tropical cyclone analysis centers. The algorithm upgrades have focused on the following primary areas: 1) examination and mitigation of logic/rules as applied in situations of rapid intensity changes, and 2) statistical evaluation of the performance in specific TC cases to better understand the behavior and areas of weakness. Several new schemes were tested and implemented into the experimental ADT code.
3. The CIMSS TC group continues to explore an integrated approach to satellite-based TC intensity estimation through a weighted consensus of ADT, and AMSU methods derived at CIMSS and at CIRA. First we identified the strengths and weaknesses of each individual method, which we then used to assign weights for a consensus algorithm. The consensus algorithm is designed to better estimate TC intensity. This new approach was tested in near real time during the 2007 hurricane season. A statistical analysis is underway. For more information, see: <http://cimss.ssec.wisc.edu/tropic2/real-time/satcon/>

Publications and Conference reports

Herndon, D., and C. Velden, 2007: CIMSS Satellite Consensus (SATCON) Tropical Cyclone Intensity Algorithm. 61st Interdepartmental Hurricane Conference, New Orleans, LA.

Herndon, D., and C. Velden, 2007: CIMSS TC Satellite Consensus (SATCON). 2007 Tropical Cyclone Conference, Pearl Harbor, HI.

Olander, T.L., and C.S. Velden, 2007: The Advanced Dvorak Technique: Continued Development of and Objective Scheme to Estimate Tropical Cyclone Intensity Using Geostationary Infrared Satellite Imagery, *Wea. Forecasting*, 22, 287-298.

Olander, T.L. and C.S. Velden, 2007: The UW-CIMSS Advanced Dvorak Technique (ADT): An IR-Based Method to estimate Hurricane Intensity. The Joint 2007 EUMETSAT Meteorological Satellite



Conference and the 15th American Meteorological Society (AMS) Satellite Meteorology & Oceanography Conference, September 24-28.

Olander, T. L. and C.S. Velden, 2007: The Advanced Dvorak Technique (ADT). Tropical Cyclone Coordinators Conference, Pearl Harbor, HI, 5-9 February.

Evan, A.T., R. Bennartz, V. Bennington, H. Corrada-Bravo, A.K. Heidinger, N. M. Mahowald, C.S. Velden, G. Myhre and J.P. Kossin, 2007: Ocean temperature forcing by aerosols across the Atlantic tropical cyclone development region. *Geochem. Geophys. Geosyst.*, (accepted in January 2008 pending minor revision).

Evan, A.T., et al., 2007: Satellite-Observed West African Dust Outbreaks and the Relationship with North Atlantic Hurricane Activity, 15th AMS Conference on Satellite Meteorology, Amsterdam, Netherlands.
Evan, A. T., et al., 2007: Quantifying the impact of dust on tropical Atlantic Ocean temperatures, Joint AGU Meeting, Acapulco, Mexico.

Evan, A. T., et al., 2007: Saharan dust forcing of North Atlantic sea surface temperature. European Geosciences Union 2007 Annual Meeting, Vienna, Austria.

Evan, A.T., and C.S. Velden. 2007: Dust in the 2006 hurricane season. 61st Interdepartmental Hurricane Conference, New Orleans, Louisiana.

1.5.2. Analysis and Application of GOES IR Imagery Toward Improving Hurricane Intensity Change Prediction – Jim Kossin and Christopher Rozoff

Proposed Work

The goal of this research is to extract more information from GOES IR imagery that is related to changes in hurricane intensity, and apply this information to increasing intensity forecast skill through modification of the SHIPS model. Previous work has demonstrated that information gleaned from GOES IR imagery about the state of the hurricane inner-core can also be related to intensity change. This was shown by the addition of GOES IR-based predictors to the existing environment-based predictor suite of SHIPS, which increased skill. Another goal is to explore and ultimately construct a new algorithm for predicting rapid intensification.

Summary of Accomplishments and Results

A part of our research included updating, repairing, and extending the GOES infrared database, which now spans the period 1978 to 2006. Each GOES image was recalibrated and re-navigated to a hurricane-centric coordinate system. We then reprocessed the data and constructed and executed algorithms to extract the required GOES-based SHIPS predictors, significantly extending the GOES data for inclusion in the SHIPS model. We are presently testing the effects that these new data have on SHIPS performance.

We also performed a short side-project for the SHIPS model development. The goal of this short side-project was to determine whether the skill of the SHIPS model might be increased by removing dependencies among the predictors. The SHIPS model is a linear model based on multivariate regression. It is well known that the skill of such models, when measured through *independent* testing, can be degraded by the inclusion of new predictors that are correlated with the existing predictors. A method for removing predictor correlation from multivariate regression models was introduced to the meteorology community by Lorenz in 1956. The procedure requires performing principal component analysis on the



predictor suite, which rotates the predictors into new predictors that are orthogonal to each other (i.e., they are completely independent of one another). These new predictors are ordered in terms of the amount of explained variance of the original predictor suite. The idea is that most of the model's independent skill will come from the leading predictors (which explain most of the variance of the actual predictors), while the trailing predictors contain mostly noise that is uncorrelated with the model predictand. Since the SHIPS model utilizes a large number of predictors, we felt that there was a reasonable chance that we could increase skill through this method. As it turns out, this is not the case.

Our procedure is outlined here:

1. We ingested the SHIPS Atlantic developmental data set (spans 1982–2006).
2. Then we formed predictor suite. We chose the $t = 24$ h forecast interval as the predictand for this experiment. In this case, we had 226 potential predictors and 4613 fixes.
3. We performed a forward stepping procedure to reduce the predictor suite dimensionality. Here we used the MATLAB utility “stepwise.” Doing so reduced the number of predictors to 43. The evolution of dependent RMS error during the forward stepping procedure is shown in Figure 1.5.1.1. For the final step (43 predictors), the dependent RMS error within the full ($n = 4613$) sample was **11.72 kt**.
4. Independent testing was then performed with a “leave one out” procedure in which we removed each of the 25 years, trained the model on the remaining years, and tested on the year that was removed. The errors for each year were accumulated for all years. The resulting independent RMS error was **11.99 kt**.
5. From the above, it became clear that there was little room for improvement. RMS error can never be reduced below the dependent RMS error of 11.72 kt, and the 43-predictor model already has an independent RMS error of 11.99 kt.
6. Despite there being little room for improvement, at this stage of the project it was simple enough to perform the principal component analysis on the 43 predictors, and repeat the independent test with the rotated predictors. The evolution of independent RMS error with the incremental additions of the new predictors is shown in Figure 1.5.2.1b. The point of diminishing returns occurs at around the 11th predictor, similarly to the forward stepping procedure shown in Figure 1.5.2.1. This evidence suggests that the forward stepping already does a good enough job of eliminating predictors that correlate too strongly with other predictors relative to the desired correlation with the predictand.

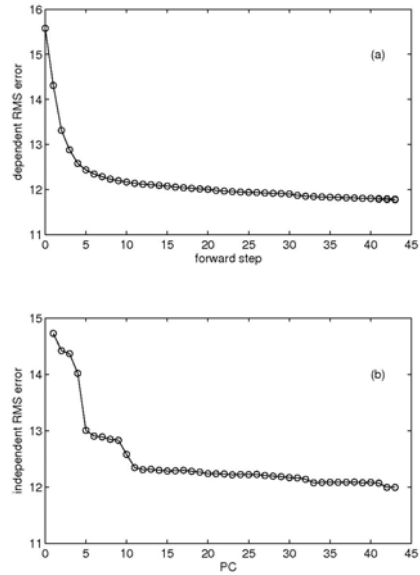


Figure 1.5.2.1: (a) Evolution of dependent RMS error during forward stepping procedure. (b) Evolution of independent RMS error as the new rotated predictors are added. The rotated predictors are the principal components of the original predictor suite. They are ordered in terms of variance explained of the original predictors.

In addition to the brief side-project described above, we have also started our work toward constructing a new rapid intensification index for Atlantic and Eastern Pacific hurricanes. Here we used the National Hurricane Center and Statistical Hurricane Intensity Prediction Scheme (SHIPS) databases and probabilistic tools to study the large-scale properties of rapidly intensifying Atlantic basin tropical cyclones. As a first step, we re-examined the results of Kaplan and DeMaria (2003) (hereafter KD) constructing composite differences between tropical cyclones that rapidly intensified and those that did not. As in KD, we defined rapid intensification (RI) as the 95th percentile of over-water 24-h intensity changes over the entire dataset, which is about 30 kt over a 24-h period in both KD and the current results (see Fig. 2). The dataset of KD covered all tropical cyclones that developed from 1989 to 2000, whereas our results extend the dataset through the end of the 2006 hurricane season. Overall, our results are largely confirmatory of their earlier results and provide greater statistical confidence in KD's key indicators of Atlantic tropical cyclone rapid intensification.

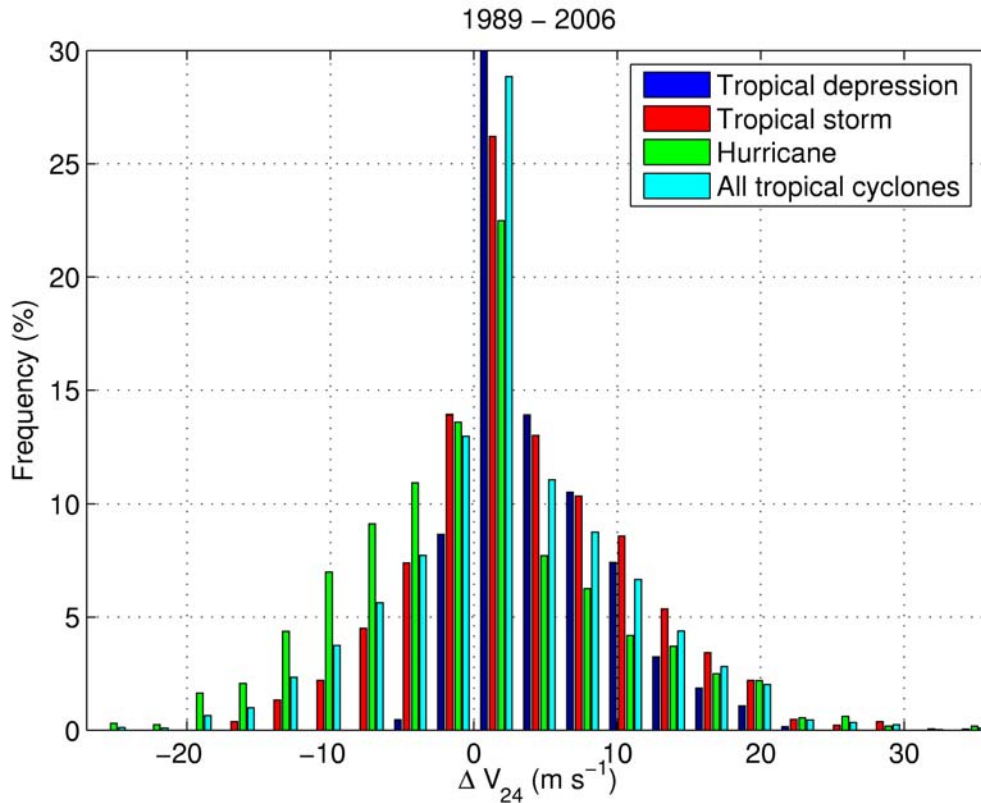


Figure 1.5.2.2: The frequency distribution of 24-hour intensity change stratified by tropical cyclone intensity at all data over sea.

Table 1.5.2.1 shows the mean differences in essential variables between storms that underwent rapid intensification (RI) and those that did not (non-RI). The variables VMX, LAT, LON, DVMX, and USTM, which are obtained from the HURDAT database, are the maximum surface wind speed, the latitude and longitude of the storm center, the intensity change over the previous 12 hours, and the zonal component of storm motion, respectively. The remaining variables obtained from the SHIPS archive are the Reynolds sea surface temperature (SST), potential intensity (POT), the vertical wind shear obtained from subtracting the 850- and 200-hPa wind vectors averaged over $r = 200 - 800$ km. (SHR), the 200-hPa zonal wind (U200), 850 – 700-hPa average relative humidity averaged from $r = 200 - 800$ km (RHLO), the area average ($r = 0 - 1000$ km) 850-hPa vorticity averaged over $r = 200 - 800$ km (Z850), the steering layer averaged over $r = 200 - 800$ km (SLYR), and the relative eddy momentum flux convergence (REFC) evaluated from

$$\text{REFC} = -r^{-2} \frac{\partial}{\partial r} \left(r^2 \overline{U'_L V'_L} \right)$$

where U and V are the storm relative 200-hPa radial and tangential winds, the overbar represents an azimuthal average, and the primes are the perturbations from the mean.

Table 1.5.2.1: The mean magnitudes of the initial ($t = 0$ h) climatological and synoptic variables of the RI and non-RI samples from 1989 to 2006. Differences (RI – non-RI) are also shown. A single, double, or triple asterisk is placed beside the differences if the difference is statistically significant (using a two-sided t test) at the 95 %, 99 %, or 99.9 % level, respectively.

Variable	Units	RI Mean	Non-RI Mean	Difference
----------	-------	---------	-------------	------------



VMX	m s^{-1}	30.56	30.54	0.02
LAT	$^{\circ}\text{N}$	19.48	24.09	-4.61***
LON	$^{\circ}\text{W}$	62.21	57.81	4.41***
DVMX	m s^{-1}	4.81	1.18	3.63***
USTM	m s^{-1}	-3.50	-1.71	-1.79***
SST	$^{\circ}\text{C}$	28.54	27.50	1.05***
POT	m s^{-1}	61.45	51.27	10.19***
SHR	m s^{-1}	5.23	8.59	-3.37***
U200	m s^{-1}	-0.77	3.76	-4.53***
RHLO	%	70.55	66.25	4.31***
Z850	10^{-7} s^{-1}	36.44	23.24	13.20***
REFC	$\text{m s}^{-1} \text{ day}^{-1}$	0.97	2.39	-1.42**
SLYR	hPa	582.46	622.71	-40.26***

Our results contain 234 tropical cyclones, which is 71 more tropical cyclones than in the original KD data set yielding 252 and 3910 RI and non-RI samples compared to KDs 159 and 2462 RI and non-RI samples. As a result, our composites contain greater statistical significance than the original KD data set, though the updated results are consistent with KDs composites. Climatologically, Atlantic tropical cyclone RI is favored further south and west as well as for storms that have more of a westward track motion. Also, storms that were intensifying more rapidly over the previous 12 hours are more likely to experience rapid intensification over the next 24 hours. From a thermodynamic standpoint, enhanced SSTs, potential intensity, and low-level relative humidity are more favorable for RI. Enhanced shear, westerly upper level flow, eddy momentum flux convergence and a lower altitude of storm steering are less favorable for RI. Finally, KDs results suggested that periods of RI were preceded by greater low-level vorticity (i.e., Z850), but their results were not statistically significant at the 95 % level whereas our larger data set provides greater confidence in this result with statistical significance at the 99.9 % level. Because the mean maximum surface winds of RI and non-RI samples are essentially the same, we conclude that enhanced area-averaged low-level vorticity seems to be an important requirement for rapid intensification.

Another benefit of our larger data set is the greater confidence in stratifying our results in terms of tropical depressions ($\text{VMX} < 18 \text{ m s}^{-1}$), tropical storms ($18 \text{ m s}^{-1} \leq \text{VMX} < 33 \text{ m s}^{-1}$) and hurricanes ($\text{VMX} \geq 33 \text{ m s}^{-1}$). While RI for all tropical cyclones favor lower REFC and contain no significant differences in 200-hPa temperatures, RI in tropical depressions is slightly more favored in the situation of enhanced REFC and lower 200-hPa temperatures. This trend indicates that upper level disturbances may be important in the rapid intensification in the weaker tropical cyclones. This is not the case for tropical storms and hurricanes. Finally, although there is no difference in VMX between RI and non-RI storms for all tropical cyclones, RI cases occurring in hurricanes occur for initially lower wind speeds than non-RI cases. Part of the explanation for this is that RI systems are further from their potential intensities. This tendency is borne out in the frequency distribution of 24-h intensity change, as depicted in Figure 1.5.2.2. Tropical depressions and tropical storms are more likely to intensify and hurricanes contain a higher probability of weakening due to the thermodynamic upper bound of tropical cyclones.

Our preliminary results toward a new algorithm for predicting rapid intensification are shown in Figure 1.5.2.3. We will continue developing this algorithm and will perform error and skill analyses. One exciting prospect of applying our Bayes classification algorithm to the rapid intensification problem is that our algorithm allows more than two classes (binary classification). Thus we can predict probabilities for different intensification thresholds, removing some of the subjective constraints from the problem. We are looking more deeply into this concept now.

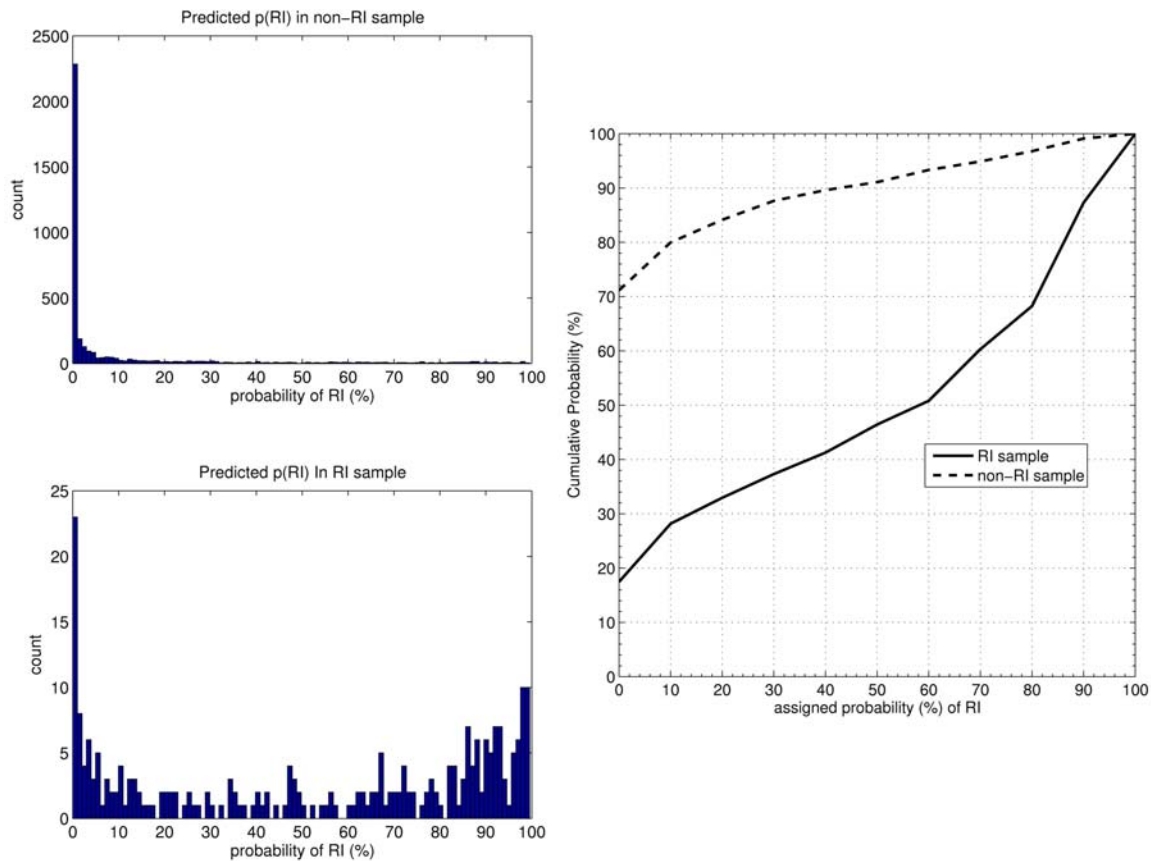


Figure 1.5.2.3: Preliminary results using Bayes classification on a small number of features.

1.6. Biomass Burning – Chris Schmidt and Elaine Prins

Proposed Work

The CIMSS fire team proposed four major tasks for 2007. CIMSS proposed to continue the GOES WF_ABBA trend analysis throughout the western hemisphere to assess changes in biomass burning and collaborate with the user community in environmental applications of the WF_ABBA data base. These collaborations include ongoing activities with the atmospheric modeling community to assimilate geostationary WF_ABBA fire products into aerosol/trace gas transport models. In collaboration with Dr. R. Rabin (NOAA/NSSL) and Dr. P. Bothwell (NOAA/NWS, Storm Prediction Center), a new effort focuses on applications of Rapid Scan GOES fire products for early detection of wildfires and agricultural burning and diurnal monitoring of fire variability. Finally, CIMSS proposed to continue to work with GTOS GOFD/GOLD, CGMS, and GEOSS to foster the development and implementation of a global geostationary fire-monitoring network with international involvement.

Summary of Accomplishments and Findings

Over the past year the CIMSS biomass burning team continued to provide the WF_ABBA database (2000 – present) to the user community via an ftp site at CIMSS and an online database (<http://www.nrlmry.navy.mil/flambe/index.html>). As part of a cost-sharing effort with funds provided by NASA LBA ECO Phase III, CIMSS delivered the GOES WF_ABBA (version 6.0) fire product for the years 2000-2005 to the LBA-DIS. The data set includes information on satellite coverage for each time period that was processed with the WF_ABBA to account for variable satellite schedules affecting



coverage over South America during the peak of the fire season that coincides with the hurricane season in North America.

Interannual trend analyses of fire activity in the western hemisphere were expanded to include 2007. Figure 1.6.1 provides a summary of GOES WF_ABBA fire detection from 2000 through 2007 by latitude. The figure does not include fire activity in the Western Hemisphere from 4-12 December 2007 because GOES-12 was unavailable during this time. This time period typically accounts for only 1% of the annual burning for the Western Hemisphere and the lack of this data should not significantly affect the annual results for 2007. There was an overall increase of 50% in fire activity in the Western Hemisphere during 2007. In North America, the WF_ABBA recorded a 12 % increase in fire activity associated with burning in California, Florida, Utah, Montana, Florida, Georgia, and across Canada. In South America, the increase was the largest observed over the past eight years with nearly a 64% increase over 2006 and a 45% increase over the annual average for the previous seven years. The 2006 fire season showed a substantial reduction in fire activity that had been attributed to a tri-national policy put into effect to reduce catastrophic burning associated with drought conditions. As prices for soy and cattle surged in 2007, deforestation and soybean production and associated burning also soared in states along the southern and eastern perimeters of the Amazon (Mato Grosso, Para, Tocantins, Amazonas) (<http://news.mongabay.com/2007/1021-amazon.html>).

In collaboration with Dr. R. Rabin (NOAA/NSSL) and Dr. P. Bothwell (NOAA/NWS, Storm Prediction Center) CIMSS evaluated three case studies of time series of rapid scan observations of wildfire activity and ancillary information (local meteorological conditions and fire observations if available). These case studies included the Westside Fire in southern California in December 2006, the East Amarillo Complex Fire in March 2006, and the Hayman and Rodeo Chediski Fires in June 2002. The focus of this investigation was to determine the utility of providing time series of value-added information to fire weather forecasters for specific wildfires. This additional information might include a combination of time series of rapid scan observed and background brightness temperatures in the 3.9- and 10.7-micrometer bands, satellite derived products, fire radiative power, and meteorological information. Figure 1.6.2 shows plots of time series of GOES-12 rapid scan observed and background 3.9- and 10.7-micrometer brightness temperatures (K) as well as derived power (kW per unit area) and ASOS winds observations (Borger, TX) for the East Amarillo Complex fire in March 2006. For the East Amarillo case study, preliminary analyses seem to indicate that observations of fire radiative power (FRP) in conjunction with other meteorological information may be useful to evaluate fire intensity and diurnal variability, although the results are not definitive. Based on this preliminary analysis more case studies are being identified to further explore this application.

The CIMSS biomass burning team continues to collaborate with the international aerosol/emissions modeling and data assimilation communities. CIMSS provided guidance for a multi-agency funded effort to assess the impact of utilizing satellite derived fire products for construction of the National Emissions Inventory (NEI). Soja, et al, has submitted for publication a manuscript titled "Assessing satellite-based fire data for use in the National Emissions Inventory." During the past year most of our interactions with the model data assimilation community have been with NRL-Monterey and FNMOC regarding the assimilation of GOES and MODIS fire products in the NRL Aerosol Analysis and Prediction System (NAAPS). In 2007, the NAAPS model went operational in FNMOC. We also continued our collaborations with the air quality transport modeling team at INPE/CPTEC in Brazil. Collaborators at INPE/CPTEC published a manuscript in *Atmospheric Chemistry and Physics* titled "Including the sub-grid scale plume rise of vegetation fires in low resolution atmospheric transport models." CIMSS researchers served as co-authors on this manuscript.



On 12-14 December, CIMSS scientists attended a Fire Locating and Monitoring of Burning Emissions (FLAMBE) workshop at NRL in Monterey, CA to discuss progress and future plans in support of the FLAMBE program funded by multiple agencies (NASA, NOAA, DOD) to assimilate real-time fire products in operational Navy aerosol transport models. Specific topics included: assimilation of global geostationary fire products beginning in 2008, assessment and characterization of fire radiative power (FRP), MODIS and GOES fire product validation studies, plans to account for cloud obscured fire activity, a second generation FLAMBE source function, and assimilation of fire data in COAMPS-OS.

CIMSS continues to work with the GTOS GOFC/GOLD Fire Implementation Team as the lead on global geostationary fire monitoring network activities. An executive summary of the [2nd GOFC/GOLD Workshop on Geostationary Fire Monitoring and Applications](#) held at EUMETSAT in Darmstadt, Germany (4-6 December 2006) was completed and is available online at <http://gofc-fire.umd.edu/implementation/Events/meetings/past.asp>. A list of presentations can also be found at this web site. This activity also fits within the framework of GEOSS and falls under the GEO Tasks DI-06-13 and DI-06-09. A paper titled “Global Observation of Forest and Land Cover Dynamics (GOFC-GOLD): monitoring and early warning systems for wildland fire disaster reduction” was accepted for publication in the Group on Earth Observations (GEO) Summit Publication, *The Full Picture*. The article discusses global near-real time wildland fire monitoring from both polar and geostationary systems and the development of a global early warning system for wildland fire. Co-authors include representatives from Natural Resources Canada, the University of Maryland, CIMSS, and the Global Fire Monitoring Center.

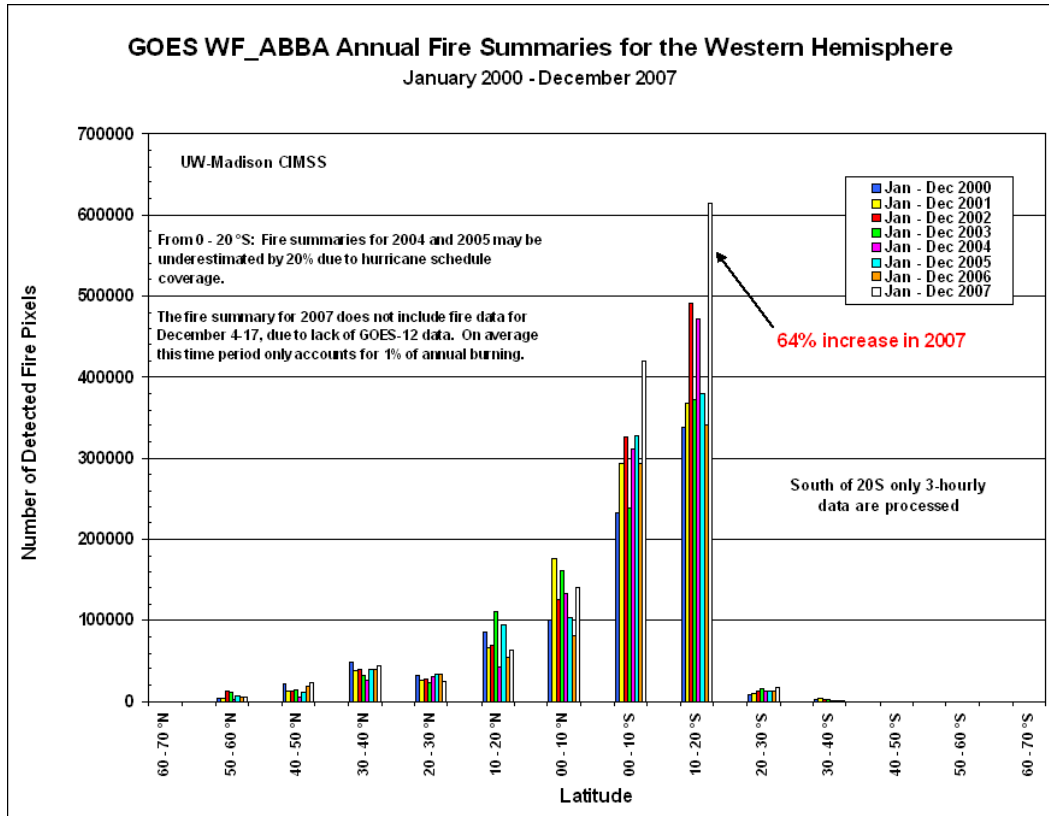
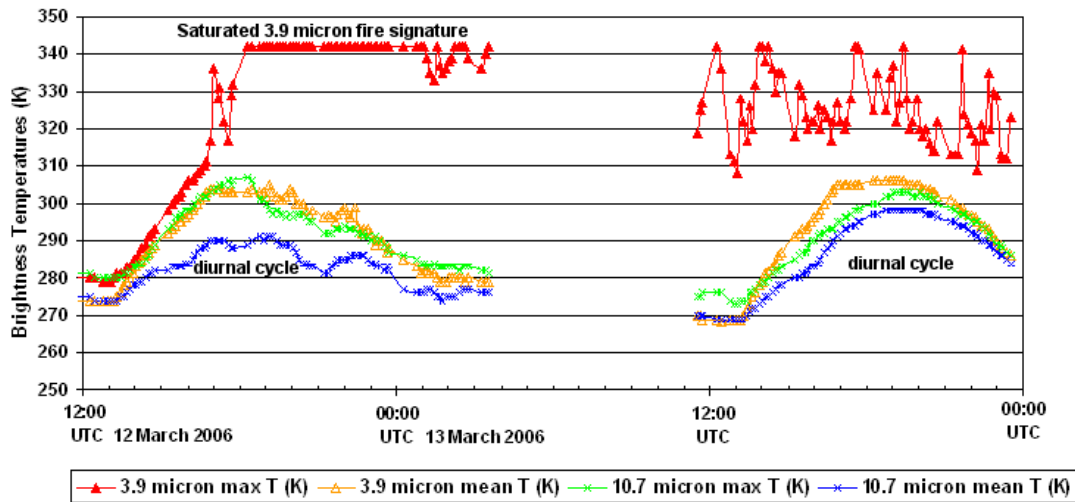


Figure 1.6.1: A summary of GOES WF_ABBA fire detection from 2000 through 2007 by latitude.



GOES-12 Rapid Scan 3.9 and 10.7 micron Observations East Amarillo Complex Fire 12-13 March 2006



GOES-12 Rapid Scan Derived Power and Borger, TX ASOS East Amarillo Complex Fire 12-13 March 2006

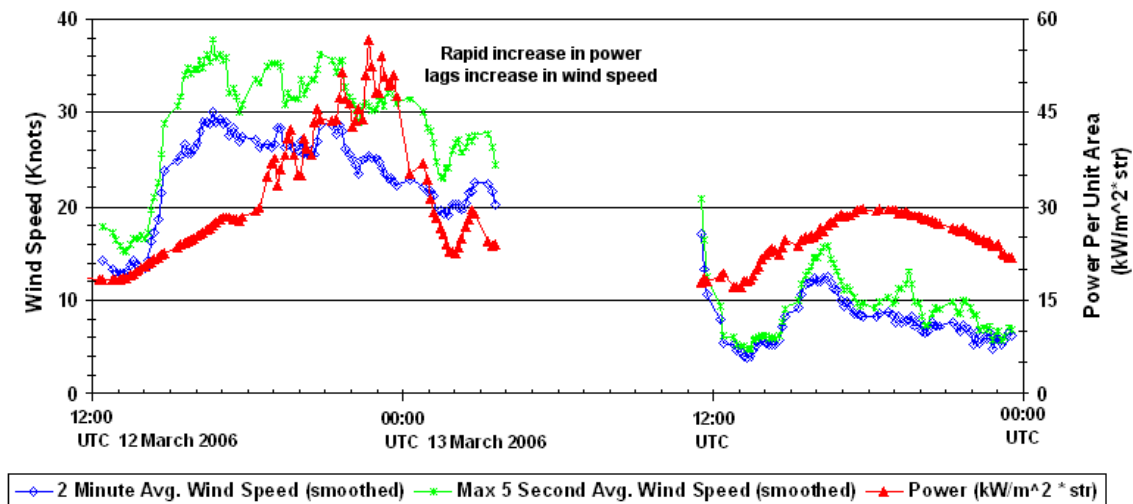


Figure 1.6.2: Time series of GOES-12 rapid scan observed and background 3.9- and 10.7-micrometer brightness temperatures (K) as well as derived power (kW per unit area) and ASOS winds observations (Borger, TX) for the East Amarillo Complex fire in March 2006.

Publications and Conference Reports

De Groot, W., T. Lynham, M. Brady, I. Csiszar, D. Davies, C. Justice, E. Prins, and J. Goldammer, 2007: Global Observation of Forest and Land Cover Dynamics (GOF-C-GOLD): monitoring and early warning systems for wildland fire disaster reduction. Group on Earth Observations (GEO) Summit Publication: *The Full Picture*.

Prins, E. M., Y. Govaerts, I. Csiszar, 2007: GOF-C/GOLD Fire Monitoring and Mapping Implementation Team 2nd Workshop on Geostationary Fire Monitoring and Applications – Executive Summary, EUMETSAT, Darmstadt, Germany, 4 – 6 December 2006.



Freitas, S.R., K. M. Longo, R. Chatfield, D. Latham, M.A.F. Silva Dias, M. O. Andreae, E. Prins, J. C. Santos, R. Gielow, and J. A. Carvalho Jr., 2007: Including the sub-grid scale plume rise of vegetation fires in low resolution atmospheric transport models, *Atmospheric Chemistry and Physics*, 7, 3385-3398.

1.7. GOES Imager SATellite Convection AnalySis and Tracking (SATCAST) System Product Evaluation by NOAA/NESDIS Operations – Wayne Feltz and Kris Bedka

Proposed work

CIMSS, in collaboration with the University of Alabama in Huntsville, currently produces a set of GOES-12 Imager satellite-derived products for diagnosing and nowcasting thunderstorm development, evolution, and motion. These products have been under development for four years under the NASA-supported Advanced Satellite Aviation-weather Products initiative for use in aviation safety applications (Mecikalski et al., 2006). CIMSS is currently providing these products to several groups, including the NOAA/NESDIS Satellite Application Branch (SAB) precipitation desk, in near real-time. The goal of this collaboration is to improve on existing SAB satellite-derived guidance and precipitation forecasts. CIMSS convective weather products can identify rapidly developing convective storms, which should be monitored for heavy rainfall and flash flooding potential. SAB precipitation estimates are provided directly to National Weather Service Forecast Offices and Regional Forecast Centers and contribute to forecasts disseminated to the general public. The proposal tasks for this work included: collaborating with NOAA/SAB analysts in optimal display, interpretation, and use of CIMSS satellite-derived convection diagnostic and nowcasting products; optimizing the algorithm to operate on larger real-time domains; visiting local NWS offices to acquire user feedback and product improvement information; making the products accessible through AWIPS; and coordinating our research with NSSL and CIRA.

Summary of accomplishments and findings

1. SAB evaluated the CI algorithm in spring and summer of 2007. We have been working with Jay Hanna at NOAA/SAB. They have been producing SATCast products in a test mode and were able to reallocate the domain location and view results using McIDAS. Wayne Feltz and Kristopher Bedka visited NOAA NESDIS SAB branch on 29-30 August 2007 to discuss optimal display, NWS end-user feedback, data interpretation, and plans for FY2008. Convective initiation algorithm testing is ongoing. A new box-average cooling rate field is now being provided to NOAA SAB for user evaluation.
2. A training PowerPoint has been constructed and provided to interested users, including the NOAA NESDIS SAB team.
3. The software now operates on larger real-time domains. The CI domain is operating in two modes. First over Storm Prediction Center (SPC) convective risk domains and second over the upper Midwest in support of local forecast offices. SATCast is now operating over AWIPS Upper Midwest “States” domain. Cooling rate and convective initiation results are being evaluated locally at CIMSS prior to distribution to local NWS office. A new cooling rate technique using radiance box averaging has been developed to improve product temporal latency and reduce false alarm rate.
4. Local NWS offices were visited to acquire user feedback and improve upon products where necessary. The SATCast mesoscale winds and convective initiation work was presented to forecasters at the Sullivan (Milwaukee), La Crosse and Green Bay NWS offices. They have expressed strong interest in receiving mesoscale wind fields via AWIPS. Distribution of Mesoscale winds commenced in May 2007 via AWIPS to Milwaukee and La Crosse NWS offices and feedback survey has been constructed. An example of the display can be seen in Figure 1.7.1. Jordan Gerth has developed a mesoscale winds web site: <http://cimss.ssec.wisc.edu/~jordang/awips-goes/meso/>. Kristopher Bedka and Jordan Gerth



attended the NWS Great Lakes Operational Meteorologist Workshop 5-7 September 2007 to present the GOES satellite-derived mesoscale winds and convective initiation. A cloud top cooling rate and convective initiation product is also now available via AWIPS is currently undergoing local evaluation of product display and quality. An example of this product can be seen in Figure 1.7.2.

5. We have coordinated our research with scientists at NSSL and CIRA on CIMSS aviation activities.

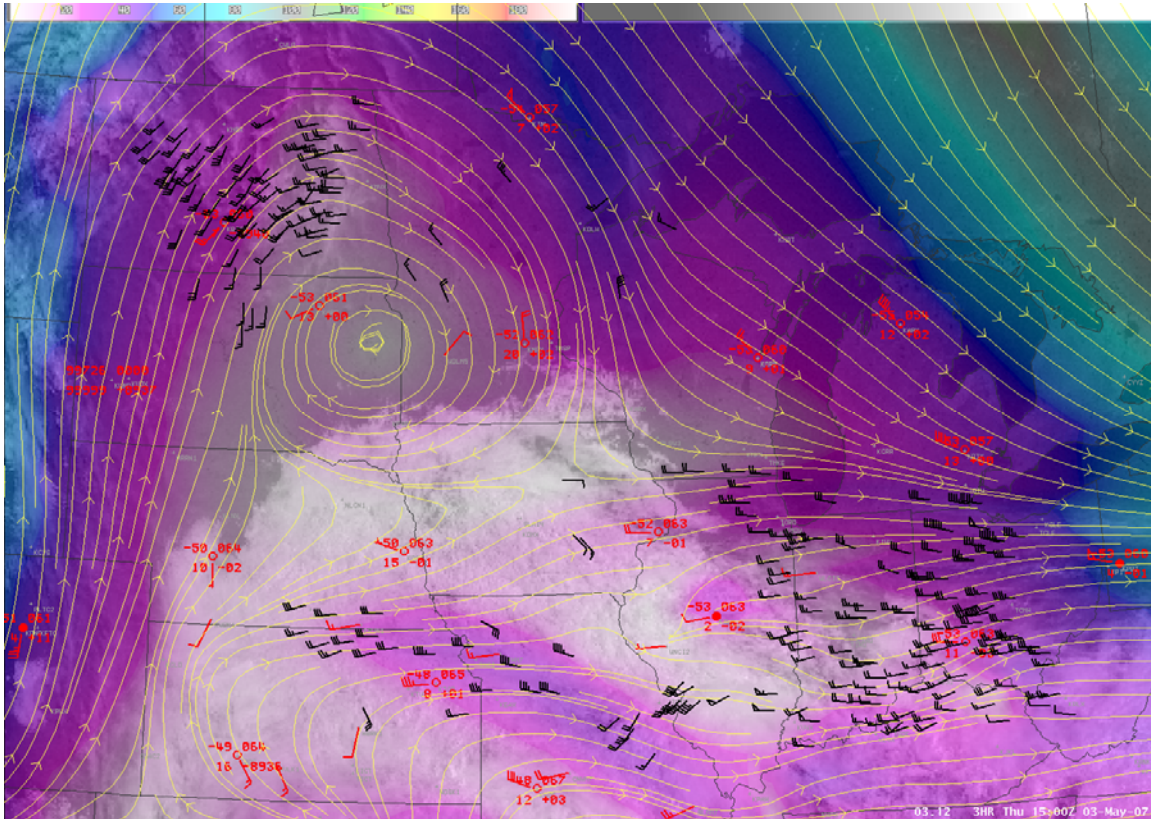


Figure 1.7.1: GOES-12 upper-tropospheric mesoscale winds (black) plotted on top of NAM model wind streamlines (yellow lines), NAM model wind speed (color shaded), and time/height matched WSR-88D and Wind Profiler wind barbs (red) within the AWIPS software. Plots such as these allow us to evaluate the quality of these mesoscale winds in a framework to which NWS forecasters can relate.

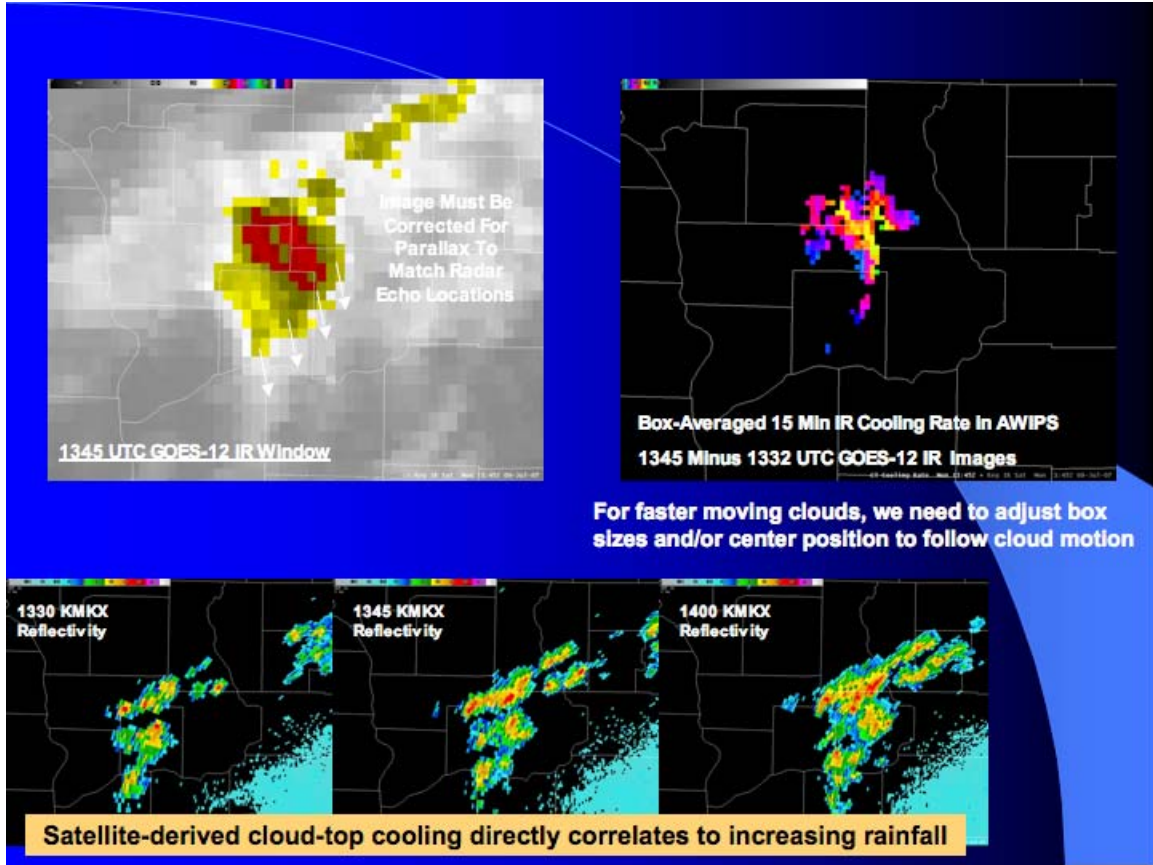


Figure 1.7.2: The box average cooling rate product is been sent to AWIPS station for near real-time monitoring. Parallax will be addressed in FY2008 for the product to be useful for local forecast offices. Notice the box averaged CTC product (upper right) matches the shape of precipitation structure within the radar imagery but is shifted NW by 15-20 km (due to parallax).

Publications and Conference Reports

Bedka, K., W. F. Feltz, J. Gerth, 2007: UW-CIMSS Satellite-derived Convective Storm Nowcasting and Aviation products, 16th Great Lakes Operational Meteorology Workshop, 5-7 September 2007, Milwaukee, Wisconsin.

Bedka, K. M., C. Velden, W. Feltz, R. Petersen, 2007: Statistical comparisons between satellite-derived mesoscale atmospheric motion vectors, rawinsondes, and NOAA wind profiler observations, The Joint 2007 EUMETSAT Meteorological Satellite Conference and the 15th AMS Satellite Meteorology and Oceanography Conference. 24-28 September 2007. Amsterdam, Netherlands.

Bedka, K. M. and C. Velden, 2007: Improved representation of satellite atmospheric motion vectors by attributing assigned heights to tropospheric layers. The Joint 2007 EUMETSAT Meteorological Satellite Conference and the 15th AMS Satellite Meteorology and Oceanography Conference. 24-28 September. Amsterdam, Netherlands.



1.8. GOES GEOCAT and Cloud Products – Corey Calvert, Andrew Heidinger and Michael Pavolonis

Work proposed

With the advent of the GOES-R Algorithm Working Groups, NOAA has begun to develop consensus prototype algorithms for GOES-R. Particularly, the cloud application team has developed a prototype system for testing cloud algorithms applied to geostationary imager data (GEOCAT). GEOCAT can process geostationary imager data from GOES, MSG/SEVIRI and MTSAT. Beyond the cloud height and effective cloud amount product from the GOES-12 imagers and the cloud mask from Clear-sky Brightness Temperature (CSBT), NOAA makes no other operational cloud products from the GOES imager. Most of the proposed GOES-R cloud products can in fact be produced from the current GOES imagers albeit with reduced accuracy. We propose to implement GEOCAT applied to the GOES imager data in real time at CIMSS and to make cloud products available to all interested users for evaluation and comment.

Summary of Accomplishments

The main activity over the past year involved the implementation of the version 1 GOES-R AWG Cloud Application Team (CAT) cloud algorithms into GEOCAT and into the real-time stream of data provided by SSEC. GEOCAT proved to be a reliable system after running for several months without crashing or causing any major issues. In addition to implementing the direct, GOES-R AWG CAT algorithms, significant time was spent modifying them to operate on the GOES I-M and GOES-NOP imager data. While the modifications were significant, the physical approaches in the real-time algorithms are consistent with those developed for the ABI. The current GOES-R ABI cloud products being generated in near real-time from the GOES-11 data are listed below.

- Cloud Mask
- Cloud Type
- Cloud Phase
- Cloud Height
- Cloud Temperature
- Cloud Pressure
- Cloud Liquid Water Path
- Cloud Ice Water Path
- Cloud Visible Optical depth
- Cloud Particle Size
- Cloud 11 micrometer Emissivity

The only GOES-R AWG Cloud application algorithm not included in the real-time GOES processing is the Nighttime Optical Properties Algorithm from NASA LaRC. It will be included once we secure permission from the author of the algorithm (Patrick Minnis). It takes approximately 5 minutes to run the algorithms listed above on a full disk of GOES-11 data. An example output of the cloud phase algorithm run on GOES-11 is shown below. A web site is currently under construction that will display all the cloud products as they become available. New hardware has been ordered that will allow the number of platforms run in real time to be increased. Once setup is complete real-time cloud products will be produced and displayed for GOES-11, GOES-12, and SEVIRI (dependant on data lag).

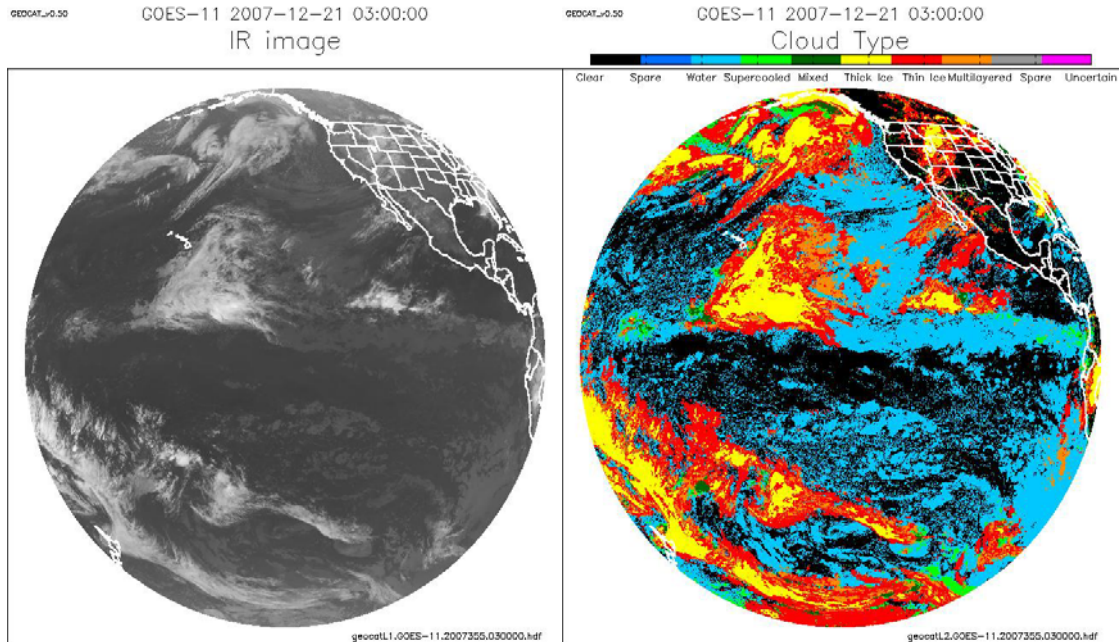


Figure 1.8.1: Example cloud phase product (right) produced by GEOCAT for GOES-11. The corresponding IR image is also shown on the left. The image time is 12/21/2007, 03:00 UTC.

2. CIMSS Support for Polar and Geostationary Satellite Science Topics (P&G_PSDI)

2.1. Product Quality Assurance and Science (PQAS) Support for Operational GOES Imager and Sounder Products – James P. Nelson III, Chris Velden, Anthony Schreiner, Gary Wade, Tim Schmit and Jaime Daniels

Proposed Work

This project supports GOES Imager and Sounder data quality assurance and science algorithm maintenance. It is broad in scope, involving aspects of both computer software and hardware. One example of work conducted for this project is the modification of software to handle special atmospheric or computing environment conditions. Work supported through this project is vital to maintaining and improving the integrity of all the GOES Imager and Sounder research products that CIMSS makes available to the meteorological community via the following websites:

<http://cimss.ssec.wisc.edu/goes/rt/>

<http://cimss.ssec.wisc.edu/tropic/real-time/atlantic/winds/winds.html>

In this project, CIMSS strives to search for generic, robust solutions to problems. When a problem arises, we often improve the software in some way while correcting the problem. Even cosmetic improvements can be useful when it makes the software easier to interpret for the next generation of scientists who will need to interface with the code. Software improvement is a process, and the accumulation of incremental improvements over time results in better Imager and Sounder software to support NESDIS operations.

From the most recent CIMSS Product Systems Development and Implementation (PSDI) proposal, covering the period 01 May 2007 through 31 December 2007, the following items were targeted for work during the latter half of 2007:



- 1) Provide software to display statistics on the web showing temperature and moisture retrieval quality compared to nearby radiosondes.
- 2) Migrate GOES Sounder Single Field-of-View (SFOV) total ozone retrieval capabilities to STAR/OPDB, and eventually into NOAA/NESDIS within OSDPD/SSD.
- 3) Improve GOES Sounder SFOV cloud retrievals and the GOES Imager cloud product.
- 4) Update the GOES Imager Clear Sky Brightness Temperature (CSBT) product.
- 5) Develop improvements to the automated satellite winds processing code.
- 6) Provide software upgrades incorporating new satellites to NOAA/NESDIS/STAR and AFWA.
- 7) Activate new retrieval/RAOB collocation files as new temperature/moisture retrieval algorithms come online.
- 8) Continue software development to allow retrieval quality evaluation against high-resolution numerical model data (both point and gradient comparisons).
- 9) Continue monitoring GOES Imager and Sounder product systems hardware, interfacing with technical computing personnel within SSEC as needed.
- 10) Make CIMSS software more robust in terms of multi-platform use, enhanced code documentation and appearance, etc.
- 11) Even though our computing environment at CIMSS was scheduled to become entirely Linux-based, software development will continue with a goal of portability to other platforms.
- 12) Add more software and ancillary data files to the CVS repository.
- 13) Write a variety of new utility software.
- 14) Continue to add UNIX make and tar utilities into the development environment of all CIMSS GOES Sounder and Imager research product software.
- 15) Install McIDAS software updates as needed to upgrade the CIMSS GOES research product computing environment.

Summary of Accomplishments and Findings

Software upgrades to windco (the GOES CIMSS/NESDIS winds retrieval software package) added the capability to process GOES-13 and GOES-R ABI, including satellite calibration. Additionally, windco Atmospheric Motion Vector (AMV) cloud height software was repaired, and the capability to bias-adjust the GOES CO2 channels was added. CIMSS provided Air Force Weather Agency with new windco distributions that incorporate all of the above changes.

Updated cloud-detection software (Schreiner et al. 2007) was incorporated into the GOES Sounder retrieval software. A prototype true Single Field-of-View (SFOV) cloud product utilizing a spatial cloud mask (as opposed to a spectral cloud mask) was developed during 2007, and is now being run in parallel at CIMSS.

Some progress was also made early in the year on software to objectively compare retrieval parameters with corresponding gridded model data. Using McIDAS, we worked to increase the number of image levels/colors used when generating retrieval Derived Product Imagery (DPI). Also, Bill Bellon made significant progress revamping the GOES Real time web page (<http://cimss.ssec.wisc.edu/goes/rt/>). UNIX/McIDAS-X assistance was provided to various personnel throughout the year, and the current version of McIDAS-X was installed on multiple CIMSS workstations. Numerous updates were made to the software that generates GOES retrievals of temperature and moisture. Late in the year, work was done to investigate use of the Linux GPROF utility to allow users to derive detailed system usage statistics for a given program.

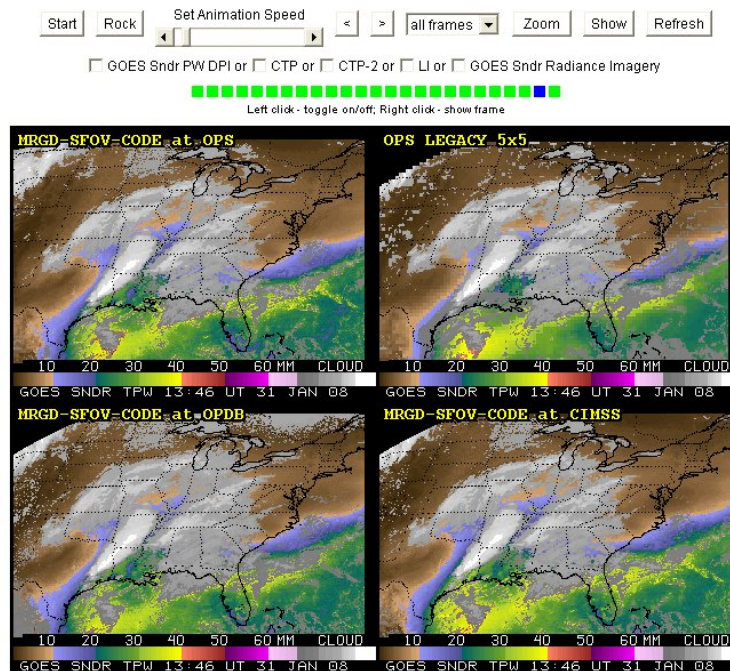


Initial work was performed to implement by means of a single “include” file a consistent methodology for gross error quality control of data used during product generation that can be used in all relevant software. Routine but important system maintenance was performed at various times throughout 2007, such as alerting various CIMSS personnel when a certain disk drive became too full.

A new and exciting phase of the CIMSS GOES Sounder and Imager archive began to ramp up in the latter part of 2007. Plans are moving forward to transfer all archived data since late 2002 from tape to a new RAID disk system, allowing continual online access. This will be a dramatic improvement, since users will then be able to retrieve data of interest without having to request a data restoration by SSEC Datacenter staff. It is anticipated that the new online archive might also be very useful to users outside of CIMSS; e.g., NOAA/NESDIS/STAR.

Some time was spent late in 2007 working on McIDAS-X needs that should be included in the next generation of McIDAS. McIDAS-V will be a very good visualization tool, and this should in turn lead to enhanced GOES product quality assurance and science support capabilities and opportunities. Software was also written to allow easy access to output file information for specified jobs, while other software updates provide more complete email error messages to users upon job failure.

Lastly, data restoration requests were fulfilled during the year for scientists in Washington, D.C., the National Center for Atmospheric Research (NCAR), the European Center for Medium Range Weather Forecasts (ECMWF), and the University of Alabama-Huntsville, and GOES-12 Sounder DPI imagery was supplied to a graduate student at Plymouth St. University.



Back to [CIMSS Realtime GOES Page](#) or [archive of comparisons of versions of GOES Sounder DPI](#). [More details.](#)

Figure 2.1.1: A sample display showing a 4-panel comparison of TPW from the GOES Sounder from 14 UTC on 31 Jan 2008. The display shows a synoptic pattern with moist return flow from the Gulf of Mexico spreading into the lower Mississippi Valley, with a strong inverted surface trough near the Texas-Louisiana border. Although this type of display is not new to 2007, such easy comparison of the different versions of the GOES Sounder retrieval algorithm speaks concretely of the ongoing monitoring of the GOES Sounder DPI at CIMSS. Plans call for displays such as this to be incorporated into <http://cimss.ssec.wisc.edu/goes/rt/> during 2008.



Publications and Conference Reports

Schreiner, A, J., S.A. Ackerman, and B.A. Baum, 2007: A multispectral technique for detecting low-level cloudiness near sunrise. *J. Atmos. Oceanic Technol.*, 24, 1800-1810.

2.2. GOES Surface and Insolation Project Processing (GSIP) – William Straka III and Andy Heidinger

Proposed Work

GOES Surface and Insolation Project Processing (GSIP) is a flexible fortran-90 GOES imager processing system. The work proposed is to continue developing, modifying and adapting algorithms to include into the processing system. The primary work done this year was focused on developing a new version of GSIP, `gsip_v2`, which will replace the current operational version of GSIP at NOAA/NESDIS. Operationally, GSIP provides estimations of solar insolation and surface temperature to NCEP for the land data assimilation system (LDAS). GSIP is a high spatial resolution solar radiation product to be used in models for predicting coral bleaching and the hydrological cycle. GSIP currently has operational community including coral reef managers, users of NOAA/HotSpot product suite; NCEP and the hydrology community. Testing has been done at both NESDIS and CIMSS comparing the output of GSIP to data from SURFRAD, ARM and the Tropical Atmosphere Ocean/Triangle Trans-Ocean Buoy Network (TAO/TRITON) array of buoys. This comparison is being performed on a daily basis at NOAA/NESDIS operationally and at CIMSS for case study analysis. This system will continue until such time that the new geostationary testbed (GEOCAT) becomes operational.

Summary of Accomplishments and Findings

The second version of GSIP, `gsip_v2`, was developed for NOAA/NESDIS to replace the current operational version. Development of this version was a continuation of work begun last year, including improvements to the data processing memory efficiency. Data processing in `gsip_v2` is accomplished in small segments, rather than by reading in the entire AREA file and processing it two scan lines at a time. Another major improvement is that `gsip_v2` is a single executable for any NOAA geostationary satellite. The satellite information is determined by data inside of the band separated AREA files. This feature means that GSIP processing can be adjusted without disruption even when a GOES satellite is replaced due to maintenance issues. NOAA/NESDIS had such an interruption when GOES-10 temporarily replaced GOES-12 as the operational GOES-EAST satellite in December 2007. A processing problem occurred because it was using two separate executables, each hard wired for a specific satellite. In `gsip_v2`, science and other operations are done outside the main program, and `gsip_v2` can take program inputs via the command line. These features make the code more user friendly and make it easier for users to write operational scripts. Several algorithms have been updated, including some from the Cloud AWG group that are currently being used in the GOES-R testbed. Also, higher resolution ancillary data sets were used in `gsip_v2`, and it has the ability to use the new 0.5 degree GFS model data.

There are three types of outputs of `gsip_v2`. Level 1 consists of all of the calculated angles, reflectances and brightness temperatures at pixel level. Level 2 consists of the pixel-level products, such as the cloud mask, land surface temperature and others. The Level 3 output is the grid level output, which is the most important for NOAA/NESDIS. All of the data that was agreed on by NOAA/NESDIS and NCDC in their "SPSRB Data Submission Agreement." In this agreement, they stipulate that output should be at 1/8-degree resolution, a significant improvement over the 1/2-degree data that was previously being archived at NCDC. All of the data types are output in a common HDF4 format. In addition, to satisfy requirements by NCDC, the Level 3 data is output in binary format that is then converted into a netCDF format file



using a separate program. Currently gsip_v2 is being tested in a pseudo-operational environment and will eventually be transitioned into operations.

As a data check, CIMSS compared the Level 3 data to similar dates/times as a previous version of gsip. We accomplished this check by looking at data over specific sites in the GOES-EAST and GOES-WEST domain. It was found that the data between the old version and new versions of the GSIP code were consistent.

In addition to upgrading the current code, GSIP solar insolation estimates were compared to shortwave downwelling radiation observed by various SURFRAD sites and the TAO/TRITON set of buoys in the Pacific. Although TAO/TRITON data availability was extremely sporadic, it was found that there was an overall slight underestimation of the downward surface shortwave radiation. However, there was a moderate spread in the data, particularly during the hours around local sunrise and sunset. Other buoy data sets (PIRATA in the Atlantic, for example) have been found to have similar issues with sporadic data availability, and this issue has been encountered previously by NESDIS personnel conducting similar near-real time validations of downwelling surface radiation and Photosynthetically Active Radiation (PAR).

2.3. GOES Sounder and Imager Spectral Response Function & Transmittance Files – Mat Gunshor and Tim Schmit

Proposed Work

The research goal is to maintain a high level of accuracy in the calculations and products obtained from the GOES series of Sounders and Imagers. Specifically, this project addresses future needs with GOES-O as well as arising needs with the current operational GOES (-10, -11, and -12) instruments. We planned to calculate the Planck Function Coefficients needed to convert radiances into temperature for the GOES Imager and Sounder. GOES Sounding retrievals use Pressure Layered Optical Depth (PLOD), also called Pressure layer Fast Algorithm for Atmospheric Transmittances (PFAAST), as the fast forward model; PLOD transmittance files will be generated and tested for GOES Imager and Sounder. We planned to maintain and possibly update the CIMSS GOES real-time weighting function web page to meet user requests.

Summary of Accomplishments/Findings

The GOES weighting functions web page received several updates. The first was a reworking of the code that provides a more user-friendly and interactive interface. Along with this update the US Standard Atmosphere was added. Additional educational features have also been added. To assist with CIMSS and NOAA ASPB personnel with a training workshop on GOES-10 in Brazil, a training module page was added. This new page has GOES-10 weighting functions calculated for various combinations of band, atmosphere, zenith angle, column moisture, and skin temperature. A user can see the effect of varying the zenith angle between 0 and 70 degrees, removing as much as 90% of the column moisture, or adjusting the skin temperature between -10 and +10 K on the weighting functions of any GOES-10 Imager or Sounder band for four calculated atmospheres including the standard tropical and the US Standard Atmosphere. A similar page was created for the Advanced Baseline Imager (ABI) on GOES-R, as well as for GOES-13, which has a slightly different channel lineup on the Imager than GOES-10. In reviews of the training in Brazil, several participants specifically named the GOES-10 weighting function lab as a favorite session.

GOES-O spectral response functions (SRFs) were acquired, detectors were averaged for each band, and Planck Function coefficients (PFCs) were calculated. PFCs were made available to the general



community by implementing them in a 2007 version of McIDAS, and were given to the wildfire detection team at CIMSS. Total transmittances for ABI were also provided to the wildfire detection team for use in their algorithm development work for GOES-R. Forward model transmittance coefficient files have not yet been calculated for GOES-O or -P, pending completion of the update to the line-by-line radiative transfer model (LBLRTM). Calculation of coefficient file updates for GOES imagers and sounders will occur in 2008.

MTSAT-2 SRFs were also acquired this year and PFCs were calculated and made available through McIDAS. Transmittance coefficient files were also calculated and made available for MTSAT-2.

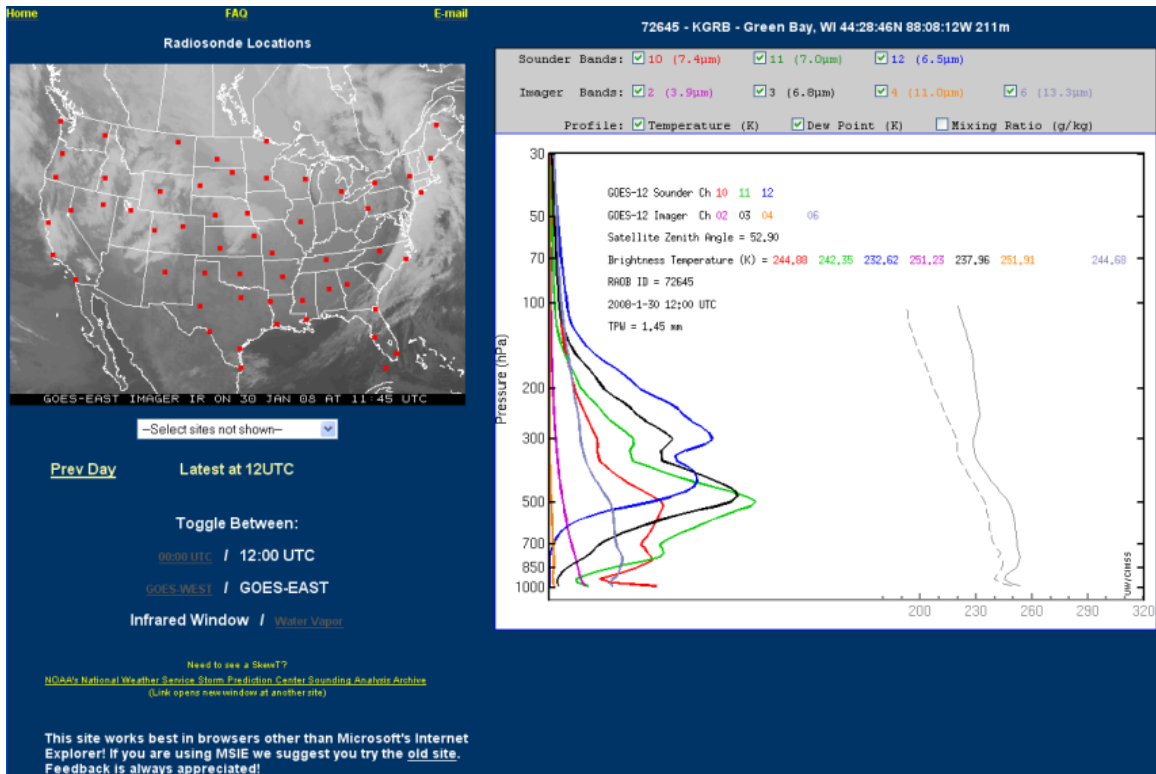


Figure 2.3.1: Snapshot of the CIMSS Real-time GOES Weighting Function web page. Users can choose which bands to view, as well as plot profile temperature, dew point, and/or mixing ratio. The most recent five days are kept online and users can also choose between GOES-East and GOES-West, 00 and 12 UTC raobs, and from a wide range of U.S. stations from CONUS, Hawaii, Alaska, and now the U.S. Standard Atmosphere.

2.4. GOES-N (13) Routine Checkout and Data Archive –Tony Schreiner, Chris Velden, Scott Bachmeier, Tim Schmit and Don Hillger

Proposed Work

CIMSS proposed to conduct research with GOES-13 as part of the NOAA science checkout. This includes additional analysis of the radiance data and product generation and validations. This checkout of GOES-13 is a critical step toward operational use of the data.

GOES-13 was launched on 24 May 2006. A post launch engineering (July – December 2006) and science (December 2006 – January 2007) checkout was conducted. In addition, GOES-13 operated for approximately one month during the summer of 2007. The GVAR (GOES Variable) data were acquired



and saved by the SSEC Data Center. While GOES-13 will not likely be operational in the near future, it is currently the back-up satellite.

Summary of Accomplishments and Findings

At CIMSS, considerable research and additional work in the checkout for GOES-13 has been completed. Nine CIMSS scientists contributed to the GOES-13 NOAA Technical Report. This report included the results of the science tests and comparisons. Calibration work was completed, including Imager and Sounder noise estimates. Products were generated and validated as well, including Total Precipitable Water (TPW), lifted index (LI), cloud parameters, atmospheric motion vectors, clear sky brightness temperature, and fire detection. The improved image registration was noted in two case studies, one of wildfires in the upper peninsula of Michigan and the other on ice floes in Hudson Bay. The GOES-13 Science Test Report was produced in cooperation with colleagues from NOAA NESDIS STAR, CIRA, CICS, Perot Systems, and others. The report has been posted online:

http://rammb.cira.colostate.edu/projects/goes_n/

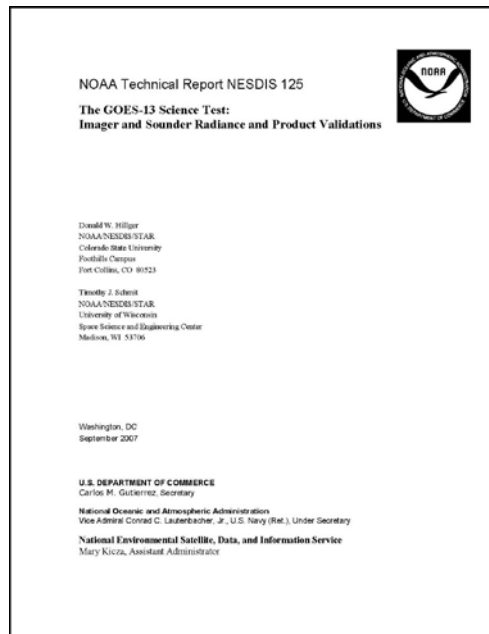


Figure 2.4.1: Cover of the GOES-13 NOAA Science Test Technical Report #125.

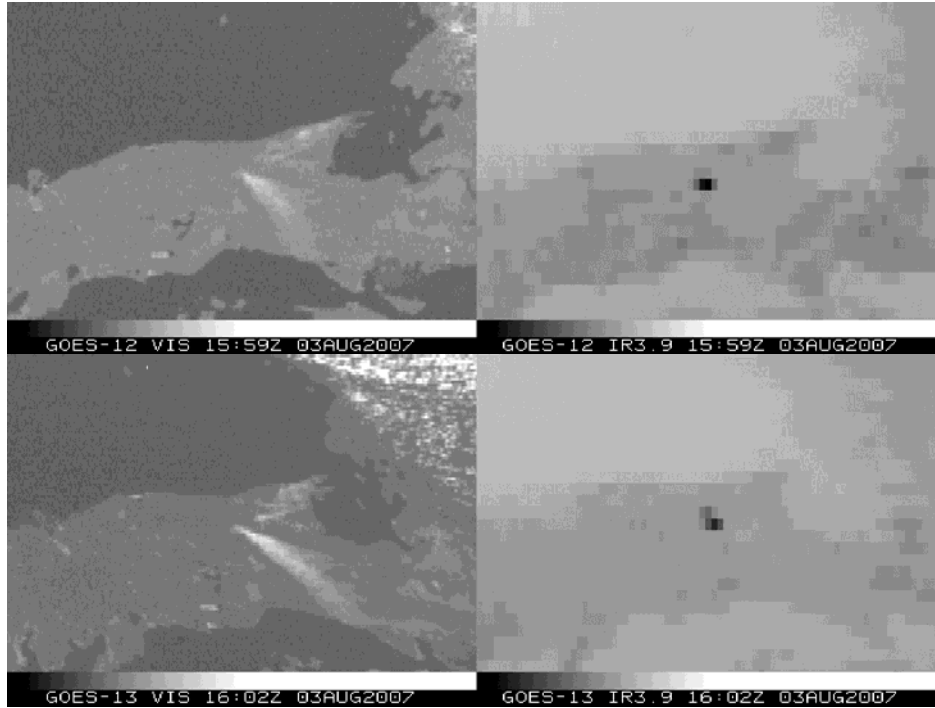


Figure 2.4.2: Above is still-shot of an animation of GOES-12 (upper 2 panels) and GOES-13 (lower 2 panels) visible channel and 3.9 micrometer IR images showing a smoke plume (drifting southeastward) and “hot spots” (black IR pixels) associated with a large wildfire burning in the eastern Upper Peninsula of Michigan on 03 August 2007. Improved image navigation and registration (INR) is evident with the GOES-13 satellite: the coastline features and the fire hot spots remain fairly steady from image to image, while the GOES-12 images exhibit a good deal of "wobble" in the animation (not shown).

Publications and Conference Reports

Hillger, D. W., and T. J. Schmit, 2007. The GOES-13 Science Test: Imager and Sounder Radiance and Product Validations. *NOAA/NESDIS Technical Report 125*. U.S. Department of Commerce, Washington, DC.

2.5. GOES Wildfire Fire Automated Biomass Burning Algorithm – Chris Schmidt and Elaine Prins

Proposed Work

The GOES Wildfire Automated Biomass Burning Algorithm (WF_ABBA) was developed at CIMSS to monitor diurnal fire activity throughout the Western Hemisphere. Over the past six years, funding from a variety of sources has been used to develop and implement version 6.0 of the GOES-8/-10/-12 Wildfire ABBA (WF_ABBA) for applications throughout the Western Hemisphere with real-time products made available via the CIMSS Biomass Burning web site (<http://cimss.ssec.wisc.edu/goes/burn/wfabba.html>) and anonymous FTP. Currently GIMPAP funding of biomass burning efforts at CIMSS focuses primarily on research applications of the GOES WF_ABBA fire data including trend analyses, collaborations with the user community on environmental applications and model data assimilation, fire weather, and participation in international fire working groups. Ground Systems funding supports research needed to adapt the GOES WF_ABBA fire algorithm to current and future global geostationary satellites (e.g. Met-8/-9, MTSAT-1R, INSAT-3D, and GOMS Electro N2). GOES-R funding also enhances product development for the current GOES WF_ABBA by supporting research on aspects of the algorithm that



are not otherwise addressed, and some of the benefits of that work are applicable to the current GOES Imagers.

In 2007 CIMSS proposed to continue real-time processing of GOES data with the WF_ABBA and to provide support for the WF_ABBA code running at NESDIS Operations. CIMSS proposed to continue testing and implementing the WF_ABBA processing system for new geostationary satellites for use by users of fire data such as the fire warning community. It also proposed effort toward achieving decreased latency, and proposed adjustments to the WF_ABBA system to enable processing of all data from a given platform. This included transitioning support for Met-8/-9 and MTSAT-1R to OSDPD (WF_ABBA with global and RSO support); implementing the improvements to the WF_ABBA that include metadata on opaque cloud coverage, block-out zones, etc.; working with ORA to investigate utilizing Moon for visible calibration (relevant to WF_ABBA cloud masking); implementing support for GOES-13; continuing development of innovative ways to look at GOES/MODIS comparisons for future satellite fire data fusion applications and cal/val; and continuing collaborations with Wilfrid Schroeder of University of Maryland (UMd) on comparing WF_ABBA fires to high resolution sources such as ASTER and Landsat ETM+.

Summary of Accomplishments and Findings

Support for the operational WF_ABBA has continued and issues have been addressed as they arose. Among those issues was the unexpected replacement of GOES-12 with GOES-10 when GOES-12 suffered anomalies following an orbital maneuver in December. While the WF_ABBA system had historically supported GOES-10 it was not anticipated that GOES-10 would serve as the Eastern satellite and thus modifications were necessary in order to provide support for real-time operations. GOES-12 returned to service after a couple of weeks and the transition back was seamless for the WF_ABBA.

GOES-13 support was also implemented in 2007 and the WF_ABBA is ready should GOES-13 be pressed into service.

CIMSS continued working with Wilfrid Schroeder of UMD on intercomparing the WF_ABBA with high-resolution data such as that from ASTER and Landsat ETM+. It was found that the WF_ABBA and MODIS have comparable commission errors (on the order of 2-3%) and that the WF_ABBA has an omission error rate only twice that of MODIS despite having a 4 km versus a 1 km footprint. It was also found that the WF_ABBA was showing a consistent, sub-pixel bias in position, which is still under investigation. The biggest challenge for this type of analysis was confirmed to be the registration of GOES pixels in general, which varies on the order of 1 to 2 pixels typically during the course of a day. While the sub-pixel position bias can be fixed, it is unclear if the random variation in navigation accuracy can be addressed. The navigation issues are of particular concern to the analysts who prepare the data for the Hazard Mapping System though they are of general interest to all users of fire data.

Version 6.5 of the WF_ABBA has been undergoing continued development in response to the GOES-R Algorithm Working Group (AWG) and Risk Reduction work, and as a result has not been transitioned to Operations at this time. In 2008, we expect to move Version 6.5 (with support for Rapid Scan Operations and for the global geostationary satellite constellation) into testing on the new IBM AIX machines at NESDIS Operations.

During the course of 2007, the Navy confirmed that they would not request WF_ABBA support of FY-2C. This source of support has been removed from the roadmap for the future. It was also determined that INSAT-3D and GOMS Electro N2 would be removed from the 2007 and 2008 work plans and rather be considered as a new start once the availability of those satellites was confirmed. It was also confirmed that MTSAT-1R data would be limited to 4 km High Resolution Information Transmission (HRIT) data and that 2 km data would not be available. Given the low saturation of MTSAT-1R this development



severely limits the fire detection and characterization abilities for this satellite, but support for it is still planned.

Publications and Conference Reports

Schroeder, W., M. Ruminski, I. Csiszar, L. Giglio, E. Prins, C. Schmidt and J. Morisette: Validation Analyses of an Operational Fire Monitoring Product: The Hazard Mapping System, *International Journal of Remote Sensing*, submitted.

Schroeder, W, E. Prins, L. Giglio, I. Csiszar, C. Schmidt, J. Morisette, D. Morton, 2007: Validation of GOES and MODIS Active Fire Detection Products Using ASTER and ETM+ Data, accepted for publication in *Remote Sensing of the Environment*.

2.6. Derived Products from GOES-10 Sounder – Tony Schreiner, James P. Nelson III, Tim Schmit, and Gary Wade

Proposed Work

The transfer of GOES-10 to routinely scan the Southern Hemisphere is a part of the Global Earth Observation System of Systems (GEOSS) project, which is a collaborative effort between NOAA and partners in the Americas and the Caribbean. GOES-10 is the first geostationary Sounder to routinely gather data over South America in more than 20 years. With appropriate data sharing, GOES-10 data are available for other uses. These include temperature and moisture profiles, cloud product information, and the monitoring of ash and SO₂ by the Washington DC Volcanic Ash Advisory Center (VAAC) as well as improvement of the Antarctica satellite composites used to monitor weather-related aviation hazards.

Many countries receiving geostationary Sounder data for the first time in 20 years were not ready to produce meteorological products from the GOES-10 Sounder. These countries can access (via the web) the derived products from GOES-10 made at CIMSS. Countries that are prepared to locally generate such products can use those produced at CIMSS for validation purposes.

Two main tasks were proposed for 2007:

1. Acquire and save the GOES-10 GVAR signal.
2. Derive and post GOES-10 Sounder products.

Summary of Accomplishments and Findings

The SSEC Data Center completed the first task, while CIMSS science staff and NOAA collaborators are conducting the second. The tracking antenna and ancillary mounting, power, and connection equipment were purchased and installed in June of 2007.

As part of the second phase of this project:

1. GOES-10 Sounder data ingested into McIDAS (Man computer Interactive Data Access System) are being used to process retrieval profiles and other products over South America.
2. Derived products from GOES-10 were incorporated into the recently redesigned CIMSS GOES Real time Derived Products web page (<http://cimss.ssec.wisc.edu/goes/rt/>). Products include derived product images (DPI) of cloud-top pressure as well as Total Precipitable Water (TPW) and Lifted Index (stability) from the Sounder temperature and moisture profiles.
3. A data archive was created for GOES-10 Sounder data and derived products, and continues to grow.
4. Routine monitoring of the GOES-10 data products continues.



In addition, significant work was performed to make available a new research version of the CIMSS Sounder Single Field of View (SFOV) retrieval algorithm to Brazilian scientists during 2007, so that they could perform GOES-10 retrieval production on-site.

This project does not cover training. In November 2007, the GEOSS (Global Earth Observation System of Systems) - Americas/Caribbean Remote Sensing Workshop was held in Brazil with instruction provided by a team of CIMSS and NOAA/NESDIS scientists. Although the workshop was not directly supported (financially) by this PSDI task, the efforts of this PSDI work were fundamental to the workshop goal of providing understanding and experience of the GOES sounding process to the attendees, who came from all corners of South and Central America.



Figure 2.6.1: The GOES-10 tracking antenna (center foreground) which sits on top of the SSEC building, amidst the other (fixed) GOES antennas and the MODIS (MODerate Resolution Imaging Spectroradiometer) Direct Broadcast antenna (right).

The screenshot shows the 'CIMSS GOES Realtime Derived Products' web page. The main heading is 'GOES-10 @ 60W (S. America)'. Below this, there is a navigation menu on the left with categories like 'GOES Home', 'Sounder DPI', 'Imager DPI', 'GOES-10 @ 60W', and 'Other Products'. The main content area is divided into several sections:

- Radiances**: Contains two sub-sections: 'GOES-10 Sounder - single sector' and 'GOES-10 Imager'. Each has a 'Compare' button and a list of bands with checkboxes. The sounder section lists bands 5, 8, 11, and 19. The imager section lists bands 1 through 5.
- GOES-10 Sounder - all bands**: A section with a 'Compare' button and a list of sectors (14N, DTS, 15S, 33S).
- GOES-10 Sounder - combined sectors**: A section with a 'Compare' button and a list of sectors (Band 8).
- Derived Product Imagery**: Contains two sub-sections: 'GOES-10 Cloud Products' and 'GOES-10 Retrieval Products'. Each has a 'Compare' button and a list of products with checkboxes. The cloud products section lists 'Cloud Top Pressure' and 'Cloud Top Pressure - combined sectors'. The retrieval products section lists 'Total Precipitable Water', 'Total Precipitable Water - Combined Sectors', 'Lifted Index', and 'Lifted Index - Combined Sectors'.
- Related Links**: A list of links including 'GOES-10 imager and sounder schedules from NOAA/NESDIS/OSO', 'Earth Observation Partnership of the Americas (EOPA) project', 'CIMSS GOES Blog - GOES-10', and 'ASCII Data Files' with sub-links for various retrieval products and documentation.

Figure 2.6.2: The main selection page for near realtime GOES-10 Sounder and Imager data—a portion of the CIMSS GOES Real time Derived Products web page (<http://cimss.ssec.wisc.edu/goes/rt/goes10.php>).

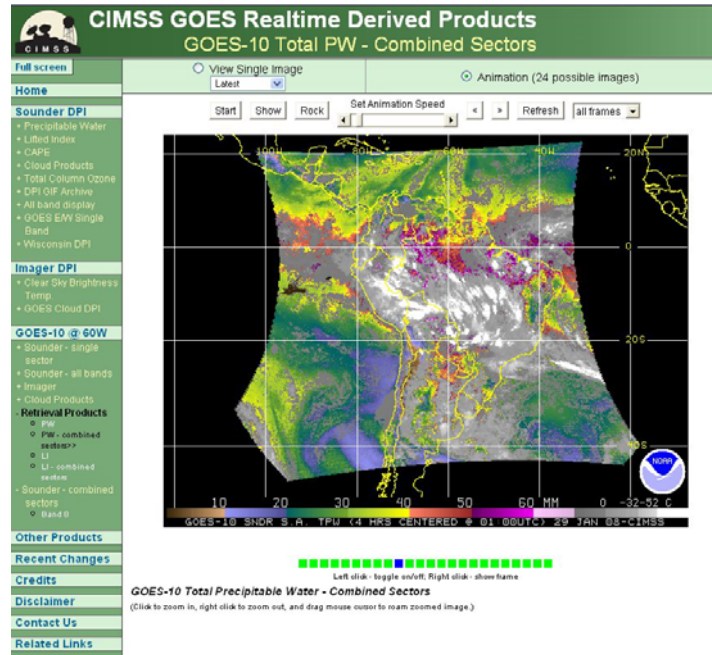


Figure 2.6.3: A screen capture from the CIMSS GOES Real time web page showing a GOES-10 Sounder Derived Product Image (DPI) of total precipitable water (TPW), from 29 January 2008. This DPI image consists of four individual GOES-10 Sounder swaths, progressing from north to south (at start times of 23:30, 00:30, 01:30 and 02:30 UTC), which are remapped and merged together into one composite image.

2.7. Implementation of the CIMSS Advanced Dvorak Technique into NESDIS Operations – Tim Olander and Chris Velden

Proposed Work

The latest McIDAS-based version of the Advanced Dvorak Technique (ADT) (Version 7.2.1) was released to NOAA/NESDIS Satellite Analysis Branch (SAB) forecasters for evaluation before the 2007 Atlantic and West Pacific tropical cyclone (TC) season. The ADT provides intensity estimates for all global TCs using multi-platform geostationary, infrared satellite imagery. The objective ADT algorithm complements the use of the more subjective and time-consuming Dvorak Technique (DT), which has been in use operationally since the 1970s and is the method on which the ADT is based. SAB forecasters have provided an evaluation of the ADT performance and recommended areas of concern to be investigated by CIMSS prior to the 2008 TC season. The evaluation will also serve to guide the official PSDI recommendation by SAB to implement the ADT operationally during the 2008 TC season.

Summary of Accomplishments and Findings

SAB forecasters provided a thorough feedback regarding the performance of the ADT during the 2007 TC season. In general, SAB forecasters are happy with the performance and will recommend full implementation to operational tool status to the SPSRB in February 2008. One primary and two secondary areas of concern were highlighted during evaluation discussions and will be addressed further prior to the 2008 TC season. The primary area of concern involves estimation of TC intensity during the weaker hurricane/typhoon intensity stages prior to eye formation, which has been a historically difficult intensity range to accurately analyze using infrared satellite imagery alone. Several possible avenues will be investigated to alleviate this performance shortfall, including the use of ancillary satellite information.



Publications and Conference Reports

Olander, T.L. and C.S. Velden, 2007: The Advanced Dvorak Technique: Continued Development of and Objective Scheme to Estimate Tropical Cyclone Intensity Using Geostationary Infrared Satellite Imagery, *Wea. Forecasting*, 22, 287-298.

Olander, T.L. and C.S. Velden, The UW-CIMSS Advanced Dvorak Technique (ADT): An IR-Based Method to estimate Hurricane Intensity, The Joint 2007 EUMETSAT Meteorological Satellite Conference and the 15th American Meteorological Society (AMS) Satellite Meteorology & Oceanography Conference, 24-28 September.

Olander, T.L. and C.S. Velden, The Advanced Dvorak Technique (ADT), 2007 Tropical Cyclone Coordinators Conference, Pearl Harbor, HI, 5-9 February.

2.8. Polar Winds (MODIS) - Dave Santek, Jeff Key and Chris Velden

Proposed Work

Geostationary satellite radiance measurements have been used to generate cloud-drift winds in the low- and mid-latitudes of the western hemisphere for more than two decades. Fully automated cloud-drift wind production from GOES became operational in 1996, and wind vectors are routinely used in operational numerical models of the National Centers for Environmental Prediction (NCEP). Unfortunately, GOES is of little use at high latitudes due to the poor viewing geometry.

The objective of this project is to generate wind vectors over the polar regions from polar-orbiting satellites. Of primary interest is the MODIS instrument on NASA's Terra and Aqua satellites. We have developed an experimental wind product that can be used in numerical weather prediction systems, and have helped transition the product to NESDIS operations. Under this PSDI funding, we continue to evaluate, improve, and extend the product suite.

The project Principal Investigator at CIMSS is Christopher Velden. David Santek performs the analyses, and oversees the implementation and modification of McIDAS and heritage wind generation software for use with MODIS. Steve Wanzong also assists in code modification and testing. Jeff Key, NOAA/NESDIS, works on the project in collaboration with CIMSS scientists, and is the NESDIS point of contact for the project.

Summary of Accomplishments and Findings

Over the past year we have continued the real-time generation of the MODIS polar winds product from both Terra and Aqua. The data are made available to users via anonymous FTP. MODIS data are acquired from the NOAA Real-Time System, which is a NOAA computer at NASA Goddard Space Flight Center. The experimental MODIS wind product is routinely generated by CIMSS for scientific research. The product transitioned to NESDIS operations in November 2005. We continue to work with our STAR and OSDPD colleagues on code differences and any discrepancies that arise between the CIMSS and OSDPD winds.

At CIMSS we are generating a mixed satellite product. Previously, MODIS winds were only generated from the Terra and Aqua satellites separately. The mixed satellite system uses data from both by tracking features in swaths from alternating satellites. This technique improves the timeliness and the equatorward extent of the product, though coverage is reduced in the poleward regions and changes in viewing geometry between passes result in fewer wind vectors. Therefore, this product is complementary and is not a replacement for the individual satellite product. We are assisting OSDPD with transitioning the code and processing scripts from CIMSS to their environment.



We have extended the polar wind generation algorithm for use with the Advanced Very High Resolution Radiometer (AVHRR) on the NOAA polar-orbiting satellites. The winds are derived only in the 11-micrometer infrared channel from the NOAA-15, -16, -17, and -18 satellites. The Global Area Coverage (GAC) data from these satellites are used in order to maximize the product coverage in the polar regions. However, there are fewer AVHRR winds generated compared to MODIS due to the lower spatial resolution GAC and the lack of a water vapor channel. By using the four NOAA satellites, the areal coverage at a specific time is potentially more complete than the winds derived only from MODIS. These AVHRR winds are generated routinely at CIMSS and evaluations are beginning at some NWP centers. Preliminary feedback is encouraging.

Ten numerical weather prediction centers worldwide continue use the MODIS winds in their operational systems: the Joint Center for Satellite Data Assimilation (JCSDA), the European Centre for Medium-Range Weather Forecasts (ECMWF), the NASA Global Modeling and Assimilation Office (GMAO), the U.K. Met Office, the Canadian Meteorological Centre (CMC), the Japan Meteorological Agency (JMA), the U.S. Navy's, Fleet Numerical Meteorology and Oceanography Center (FNMOC), Deutscher Wetterdienst (DWD; Germany), MeteoFrance, and the National Center for Atmospheric Research (NCAR).

Velden, Key and Santek attended and presented at the joint 2007 EUMETSAT Meteorological Satellite Conference and the 15th American Meteorological Society Satellite Meteorology and Oceanography Conference held in Amsterdam in September 2007.

Publications and Conference Reports

Santek, D., J. Key, C.S. Velden, 2007: Feature-tracked winds from polar satellites: Status and outlook, Proceedings of the 15th Conf. on Satellite Meteorology and Oceanography, American Meteorological Society, Amsterdam, Netherlands, 23-28 September 2007.

Santek, D.A., 2007: The global impact of satellite-derived polar winds on model forecasts. PhD dissertation. University of Wisconsin-Madison, 141 pp.

3. Ground Systems Research

3.1. Global Fire Detection - Elaine Prins, Chris Schmidt

Proposed Work

As part of a two-year effort CIMSS proposed to participate in cost-sharing activities with NASA and other NOAA programs to adapt the GOES WF_ABBA to Met-8/-9, FY-2C, MTSAT-1R, INSAT-3D and the GOMS Electro-L MSU-GS. The goal is to create a global consistent fire product utilizing the capabilities of each of these unique systems and a common fire detection algorithm, the GOES Wildfire Automated Biomass Burning Algorithm (WF_ABBA). During the first year, development focused on adapting the WF_ABBA to Met-8, MTSAT-1R, and preliminary studies for adaptation to FY-2C. During the second year, CIMSS proposed to adapt the WF_ABBA to INSAT-3D and GOMS Elektro-L MSU-GS and characterize the differences between the fire monitoring capabilities of each of the instruments. In response to requests from the international GOFD/GOLD Fire user community, CIMSS also proposed to adapt the WF_ABBA for each platform to include a fire mask and meta data regarding processing regions, block-out zones (associated with biome types, regions of saturation, etc.), and the presence of opaque clouds.



Summary of Accomplishments and Findings

CIMSS began to develop and implement a global geostationary fire-monitoring network in June 2006. Initial efforts focused on adapting the GOES WF_ABBA to Met-8 SEVIRI and MTSAT-1R HRID data. During 2007, CIMSS developed version 6.5 of the WF_ABBA and adapted it for application with Met-8/-9 SEVIRI and MTSAT-1R HRID and HRIT data. CIMSS has decided not to pursue the adaptation of the WF_ABBA to FY-2C due to the reduced capability of locating and monitoring fires with FY-2C. Initially CIMSS felt that there might be an issue with calibration of the 3.9-micrometer band on FY-2C that could be addressed, but Dr. Lui Cheng of the National Satellite Meteorological Center of the China Meteorological Administration has investigated this and there does not appear to be any issues with the 3.9-micrometer calibration. There may be a possibility that FY-2D will be more conducive to fire monitoring and this will be investigated in the coming year. Due to the delayed launch of INSAT-3D (September 2008) and GOMS Elektro-L MSU-GS (end of 2008), much of year 2 funding has been reserved for this activity in the final quarter of 2008.

Version 6.5 of the WF_ABBA was developed and implemented to provide additional parameters and metadata as requested by the international user community and in accordance with GOCF-GOLD – Fire recommendations (<http://gofc-fire.umd.edu/products/pdfs/Events/2nd GOCF Geo Workshop Report%20final.pdf>).

Improvements in version 6.5 include the following:

- 1) An opaque cloud product to indicate regions where fire detection is not possible;
- 2) A Fire Radiative Power (FRP) product in addition to Dozier output of instantaneous estimates of fire size and temperature;
- 3) Metadata on processing region, opaque cloud coverage, block-out zones due to solar reflectance, clouds, extreme view angles, saturation, biome type, etc;
- 4) Fire/meta data mask imagery;
- 5) Revised ASCII fire product output including: latitude, longitude, satellite view angle, pixel size, observed 4 and 11 micrometer brightness temperatures, instantaneous estimates of fire size and temperature, fire radiative power, biome type, fire confidence flag.

Version 6.5 of the WF_ABBA also provides for a consistent global geostationary fire product that enables characterization of the similarities and differences between each instrument and their fire monitoring capabilities. This addition is essential for global geostationary fire product model data assimilation and trend analyses.

Over the past year, the Met-8/-9 WF_ABBA (version 6.5) has been applied in case study mode to monitor fires in Europe, Africa, and eastern Brazil. The code has been modified to address issues associated with SEVIRI re-sampling/re-gridding for fire detection, but the re-gridding protocol continues to impact the accuracy of sub-pixel characterization. This issue will persist until users are provided pre-gridded SEVIRI data. CIMSS has also observed that large, hot saturated fire pixels can produce a “stuck bit” effect on subsequent pixels along a scan line resulting in a false elongation of the fire signal. This has been observed by others as well and was reported to EUMETSAT.

In the summer of 2007, Greece experienced the worst fire season in nearly 50 years resulting in the loss of 84 lives, a burned area in excess of 650,000 acres and an estimated cost of approximately \$3 billion. The most devastating conflagrations began on 23 August and extended into September resulting in the loss of 70 lives. The Met-9 WF_ABBA was able to monitor the outbreak and chart the diurnal variability in fire activity with 15-minute updates on the fire progression. Figure 3.1.1 shows an example of the WF_ABBA fire mask for 25 August 2007 at 11:45 UTC (1:45 pm local time). Fires are evident in numerous locations throughout Greece and surrounding countries. Qualitative comparison with the



MODIS fire products for this fire event showed good agreement, although the Met-9 WF_ABBA fire product provided additional information on the diurnal variability.

The MTSAT-1R WF_ABBA (version 6.5) has been tested on several case studies in 2007. Figure 3.1.2 shows an example of the MTSAT-1R WF_ABBA fire product for 26 September 2007 at 02:33 UTC. This example shows that the MTSAT-1R WF_ABBA is able to document fire activity throughout SE Asia, but the low saturation in the 3.7-micrometer band results in large areas of saturation over continental regions within several hours of local noon. The saturation block-out region is in addition to the solar and reflectance angle block-out region assigned by the WF_ABBA code. Saturation continues to be a major limiting factor in MTSAT-1R fire monitoring capabilities, requiring conservative thresholds to eliminate false alarms associated with non-fire pixel saturation during peak solar heating. It is encouraging to note that even with these limitations, daily composites of WF_ABBA fire products provide additional information on short-lived agricultural and deforestation fires throughout the region that are not detected by MODIS. The MTSAT-1R WF_ABBA was applied to two weeks of data in August 2007 in support of the 7 SEAS Virtual Biomass Burning Experiment (VBBE) in Southeast Asia and will be made available in the first quarter of 2008 online at <http://www.nrlmry.navy.mil/flambe/7seas/7seas.html>.

Met-9 SEVIRI WF_ABBA Observations of Wildfires in Greece
Date: 25-Aug-2007 Time: 11:45 UTC (1:45 pm local time)

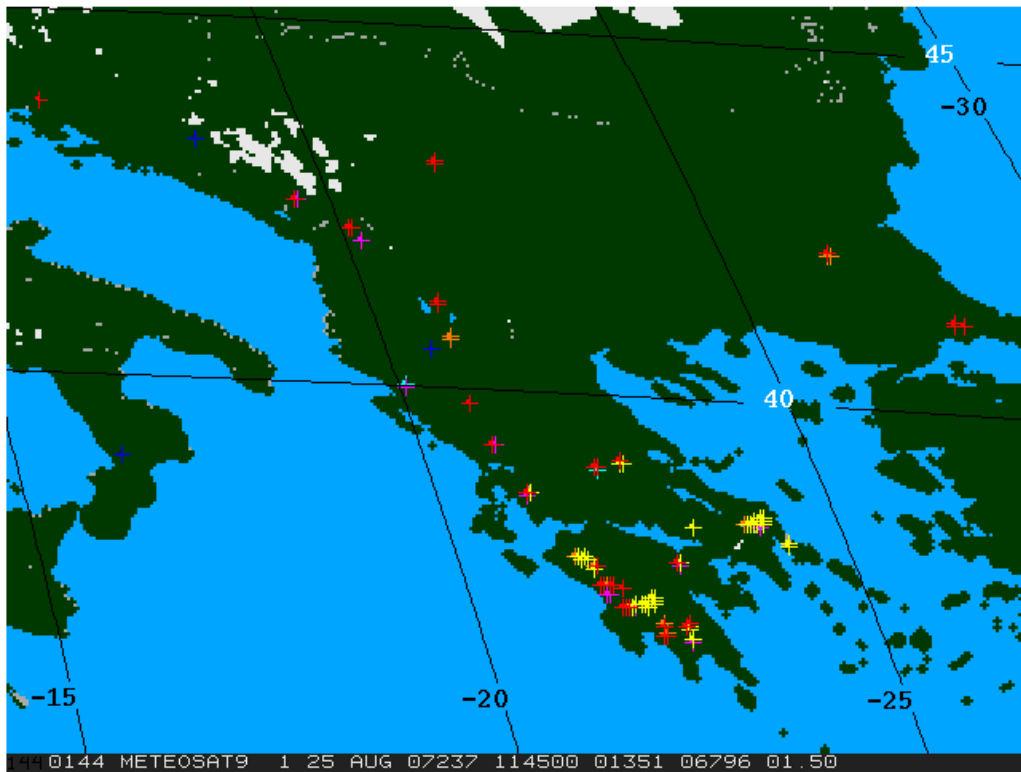


Figure 3.1.1: Met-9 SEVIRI WF_ABBA (version 6.5) observations of wildfires in Greece on 25 August 2007.



Fire Monitoring with MTSAT-1R JAMI WF_ABBA

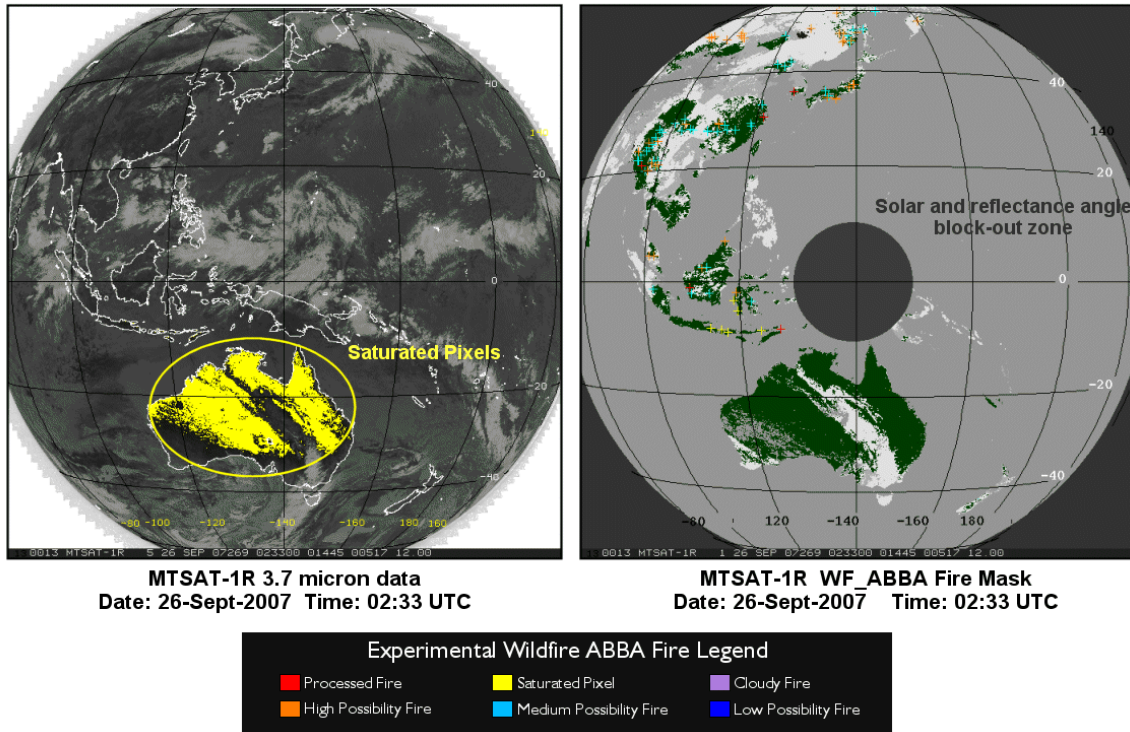


Figure 3.1.2: Fire monitoring with the MTSAT-1R JAMI WF_ABBA in Southeast Asia on 26 September 2007. Large regions of Australia are saturated due to the low saturation in the 3.7-micrometer band.

Publications and Conference reports

Prins, E., 2007: Status and Plans for Global Geostationary Fire Monitoring, Joint 2007 EUMETSAT Meteorological Satellite and 15th AMS Satellite Meteorology and Oceanography Conference, Amsterdam, Netherlands, 24-28 September 2007.

Prins, E., C. Schmidt, J. Hoffman, J. Brunner, S. Lindstrom, 2007: Status and Plans for Global Geostationary Fire Monitoring with the WF_ABBA (version 6.5), FLAMBE Workshop, NRL-Monterey, Monterey, CA, 17-19 December 2007.

3.2. A Dedicated Processing System for Infusion of Satellite Products in AWIPS – Scott Bachmeier, Gary Wade and Jordan Gerth

Proposed Work

CIMSS planned to continue to expand its recent successful integration capability to insert some of its new satellite derived products into the NWS Advanced Weather Information Processing System (AWIPS) data stream. CIMSS proposed to follow up on that capability and work with select offices to realize their enhanced potential to use new experimental satellite products in their duties. Application focused on use of data from the polar-orbiting MODIS and the geostationary GOES Sounder. This development effort, with accompanying education and support, brought together university and NESDIS researchers with operational NWS forecasters to foster practical use of satellite resources.



Summary of Accomplishments and Results

1. Jordan Gerth has provided numerous NWS Forecast Offices with coordination, details and packaged sets of scripts for the continuation and enhancement of access to experimental CIMSS satellite products via the NWS AWIPS. Interest is high for assorted products, ranging from high resolution MODIS sea surface temperature data to CIMSS Regional Assimilation System (CRAS) forecast cloud and water vapor images as well as dynamic nearcasts of instability (the latter both utilizing data from the GOES Sounder).

Many Forecast Offices are participating including:

Aberdeen, SD	LaCrosse, WI
Billings, MT	Nashville, TN
Davenport, IA (Quad Cities)	Riverton, WY
Des Moines, IA	Springfield, MO
Green Bay, WI	Wichita, KS
Indianapolis, IN	
Milwaukee/Sullivan, WI	

One way to track the actual use of any of these new satellite products in the Forecast Offices has been by noting any Area Forecast Discussions (AFD) issued where these products are mentioned. Nearly 100 hits were recorded in 2007.

2. Daylong visits were made (or were planned within this reporting period) to Milwaukee/Sullivan, WI (09 Jan 2007), LaCrosse, WI (06 Mar 2007), and Green Bay, WI (10 Jan 2008). A team of CIMSS scientists presented numerous applications of satellite data, specifically emphasizing MODIS and GOES (especially the Sounder). These interactions have continued to promote and realize good collaborations and dialogue between the researcher/provider side and the forecaster/user side. The following talks, which were given during our visit to Green Bay, are available online at <http://cimss.ssec.wisc.edu/~garyw/nws-visits/grb-2008/>.

MODIS applications Kathy Strabala and Scott Bachmeier
Current GOES Sounder applications Gary Wade
Satellite applications for aviation needs Wayne Feltz
Synthetic forecast imagery from the CRAS Robert Aune
Dynamic “nearcasting” of GOES Sounder data Ralph Petersen

3. The CIMSS team made a significant contribution to the NWS Great Lakes Operational Meteorology (GLOM) Workshop, which was held in Milwaukee, WI from 05-07 Sep 2007. CIMSS researchers presented four talks in the session on satellite applications, all emphasizing the new products being provided in AWIPS.
4. A script was made by Jordan Gerth to show “true color” imagery products from MODIS in the AWIPS environment. The display, involving red, green, and blue spectral bands from MODIS, is not part of the AWIPS core, but runs in AWIPS. This MODIS true color imagery viewer has been provided to many NWS offices.
5. New additions to the suite of high horizontal resolution MODIS products being provided by CIMSS to participating NWS FOs include the Normalized Difference Vegetation Index and LST Land Surface Temperature data.



6. Examples of these successful transitions, taking satellite products generated at CIMSS and displaying them in NWS FOs in their own AWIPS environments, can be found at: <http://cimss.ssec.wisc.edu/goes/blog/cimss-satellite-proving-ground>.

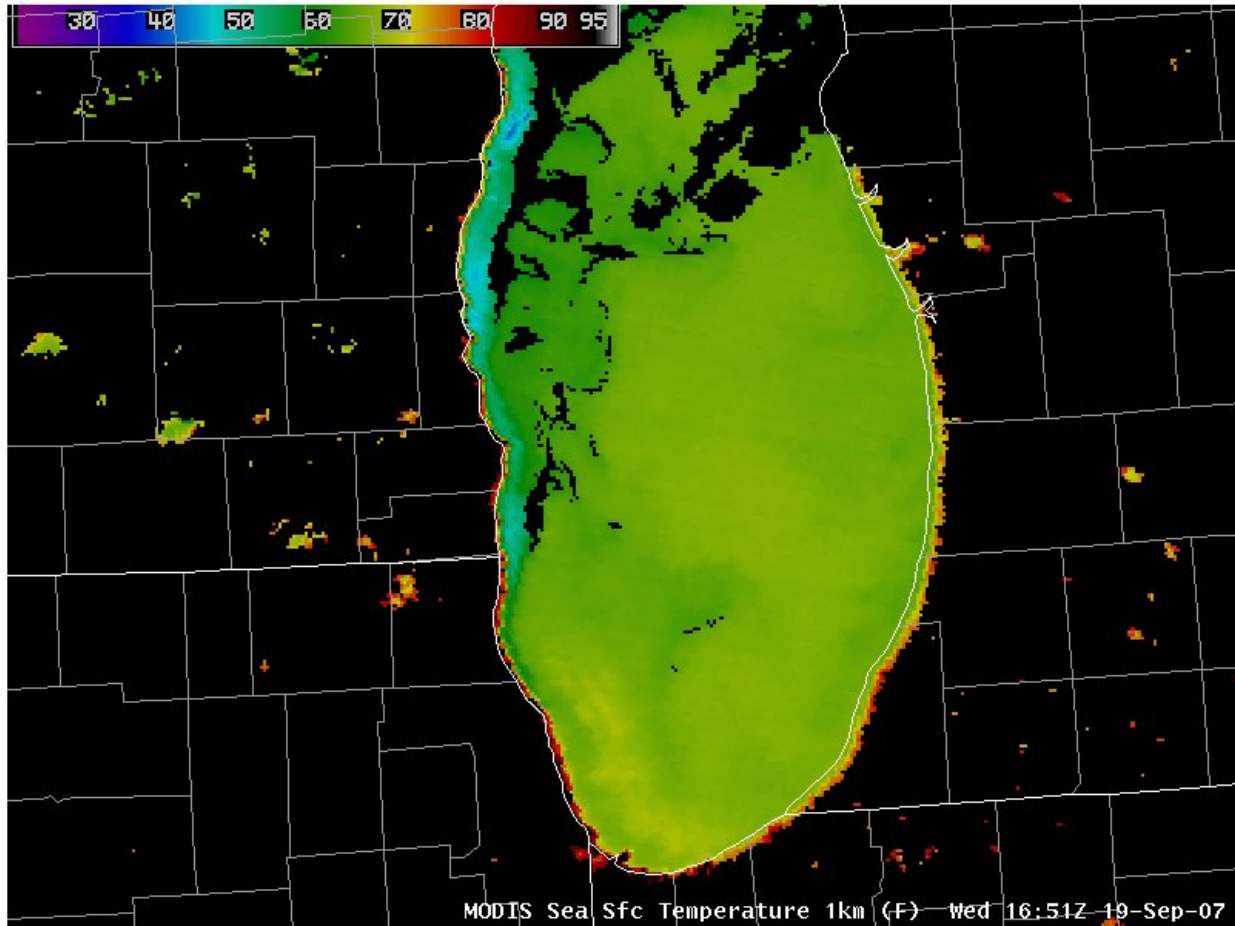


Figure 3.2.1: An SST image derived from MODIS over Lake Michigan at 16:51 UTC on 19 Sep 2007, displayed in AWIPS. Cold upwelling noted along the west shore of the lake is of interest to forecasters, due to effects on nearby land temperatures as well cloud formation.

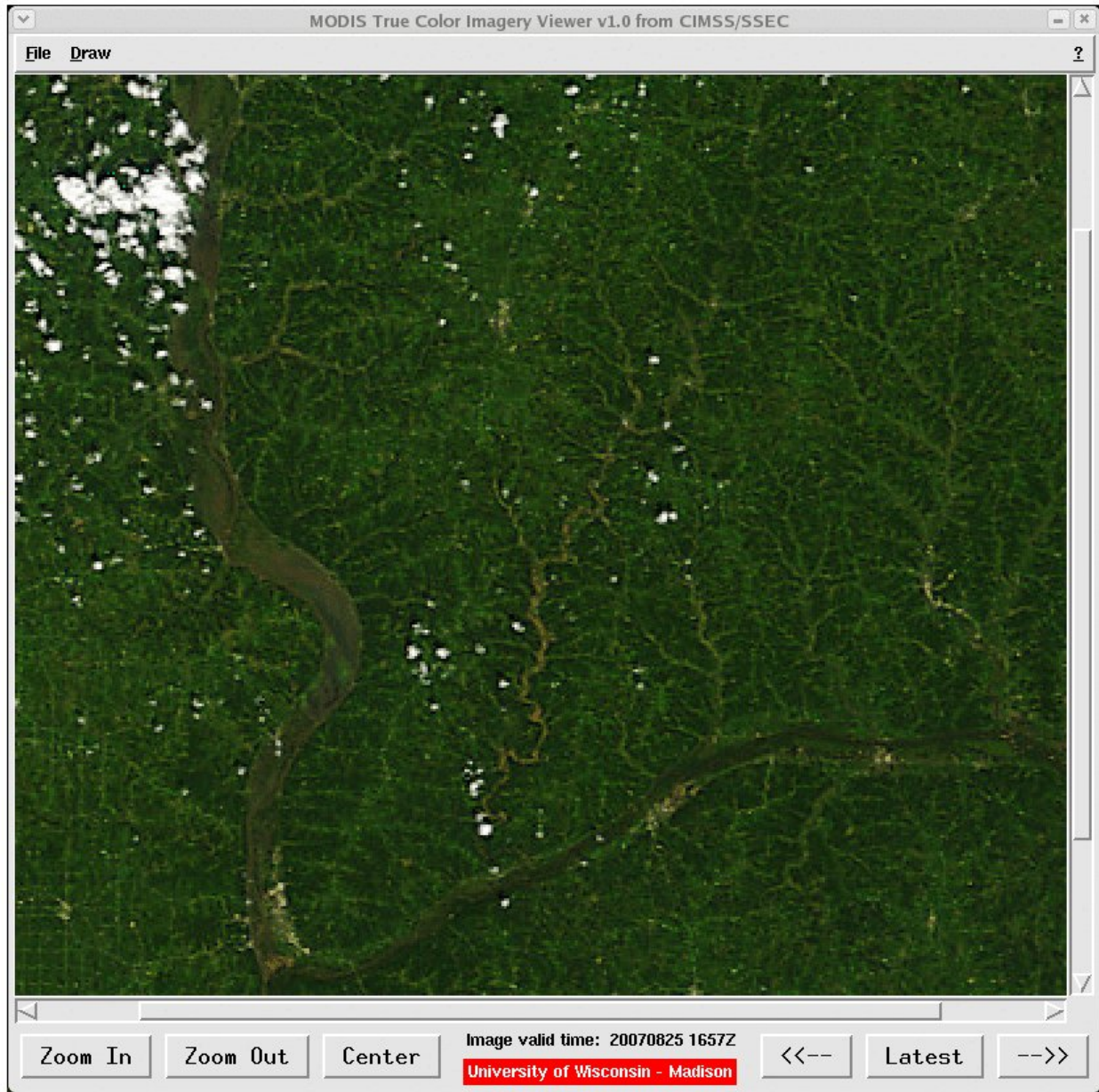


Figure 3.2.2: A sample screen capture of the MODIS True Color Imagery Viewer script, which runs in the AWIPS environment, showing southwestern Wisconsin at 1657 UTC on 25 Aug 2007. When compared with earlier imagery, river flooding is evident, especially along the Mississippi River (interior left side of image). The Wisconsin River is seen coming in from the east (across the lower third of the image).

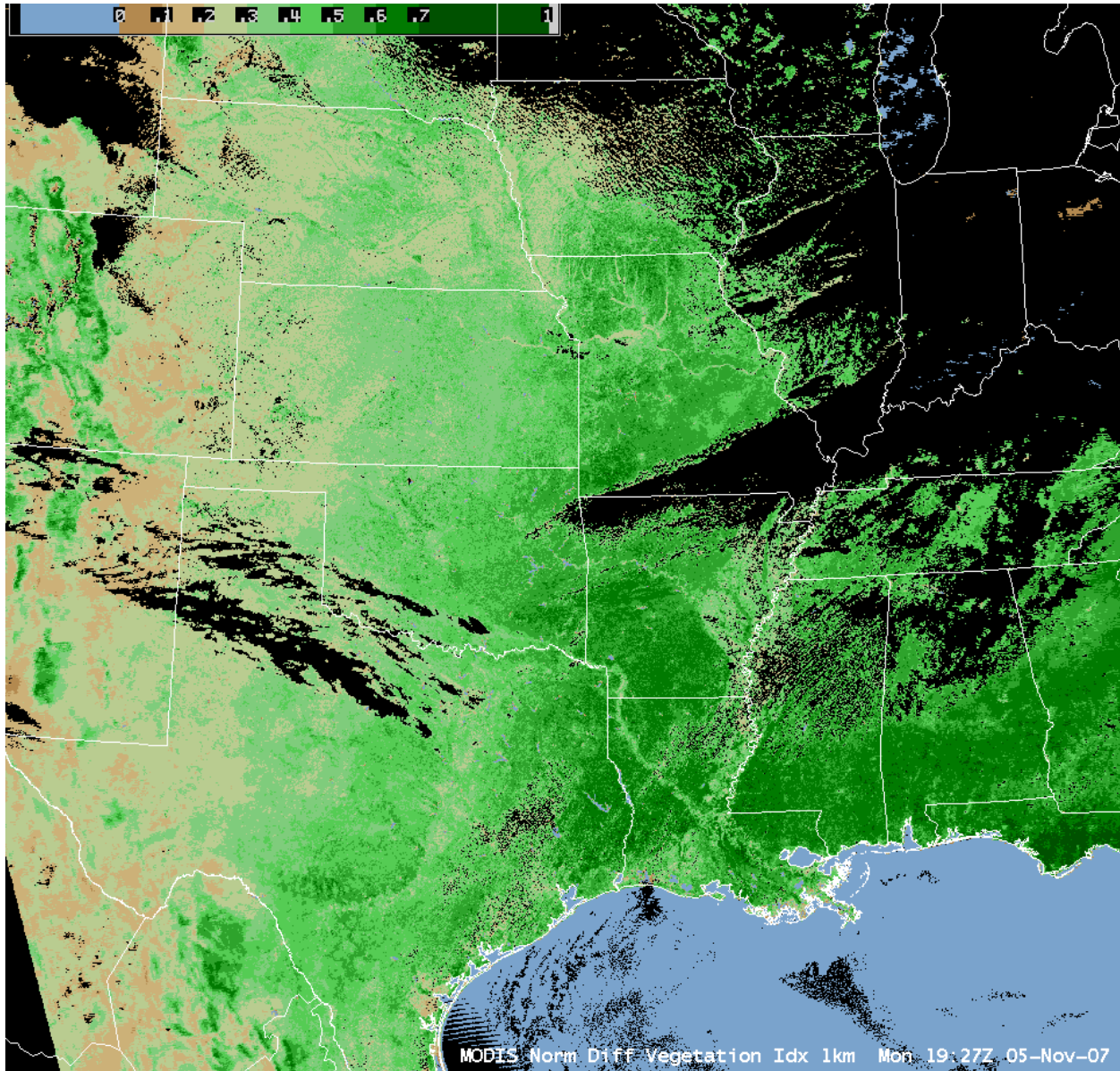


Figure 3.2.3: An NDVI image from MODIS at 19:27 UTC on 05 Nov 2007 over the central US, displayed in AWIPS. Less vegetated areas (beige and very light green) are seen throughout the High Plains of the central US, while lower through mid Mississippi Valley as well as southeast US areas (darker green) show more vegetative response.



4. GOES R Risk Reduction

4.1. Algorithm Development – Allen Huang and Chris Velden, Team Leaders

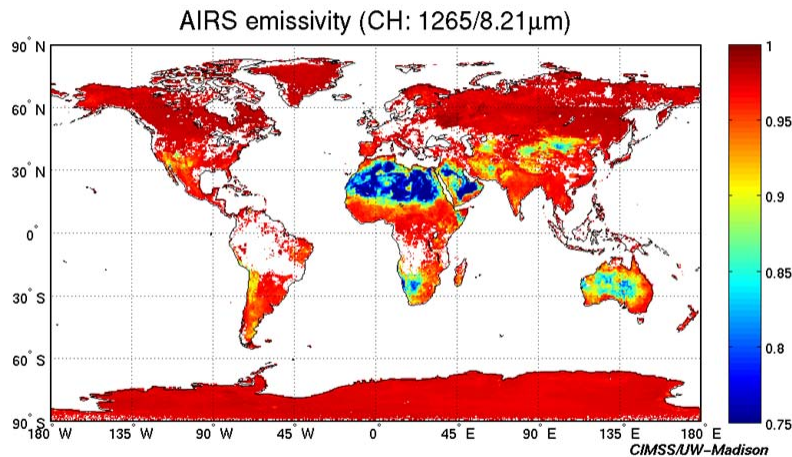
4.1.1. GOES-R Risk Reduction Sounding Algorithm Development – Jun Li and Allen Huang

Proposed Work

1. Take advantage of time continuity and high spatial resolution in retrieval.
2. Better handling cloud in retrieval.
3. Better handling surface emissivity in retrieval.
4. Synergy of LEO hyperspectral IR sounder and ABI for legacy profile evolution.

Summary of Accomplishments and Findings

Global AIRS emissivity map – CIMSS research product



Algorithm can also be applied to IASI for global emissivity product

Figure 4.1.1.1: Global 8-day (01 – 08 January 2004) composite of AIRS single field-of-view (SFOV) retrievals at 8.21 μm (single channel).

Global map of hyperspectral IR emissivity spectra developed

The GOES-R3 Technical Advisory Committee (TAC) advised using surface emissivity from LEO hyperspectral InfraRed (IR) radiances for Advanced Baseline Imager (ABI) products. Following on that advice, we generated a global map of Atmospheric InfraRed Sounder (AIRS) emissivity spectra for demonstration. The hyperspectral IR emissivity physical retrieval algorithm (Li et al. 2007–*GRL*) was used to generate the emissivity production. Collocated output from the operational MODIS 1 km cloud mask product was used for AIRS sub-pixel cloud detection (Li et al. 2004–*JAM*), only radiances from clear sky AIRS fields-of-view (FOVs) are used for surface emissivity retrieval. Figure 4.1.1.1 shows global 8-day (01 – 08 January 2004) composite of AIRS single field-of-view (SFOV) retrievals at 8.21 μm (single channel). Figure 4.1.1.2 shows the emissivity spectra over Arizona and Utah (right panel) area which contains diversified surface types, and the emissivity spectra show large spatial and spectral variations. The emissivity varies from 0.80 to 1.00 depends on the surface type and IR spectral region. This is a unique global hyperspectral IR emissivity product that has not seen before. Studies also show that AIRS emissivity map at MODIS band center wavelength agrees with the operational MODIS



broadband emissivity product. Figure 4.1.1.3 shows the global emissivity map from AIRS at 4.3 μm (single channel, upper panel) along with the operational MODIS broadband emissivity product (lower panel). The two emissivity maps agree well. MODIS provides global emissivity product at 6 spectral IR bands. In order to better compare AIRS emissivity product (CIMSS) with operational MODIS product, the MODIS spectral response functions (SRFs) will be used to generate “Pseudo MODIS emissivity” from AIRS.

The same algorithm will be applied to process IASI (Infrared Atmospheric Sounding Interferometer), unlike AIRS, IASI can provide emissivity spectrum without spectral gap, which is ideal for GEO product processing.

Emissivity spectra over Arizona and Utah

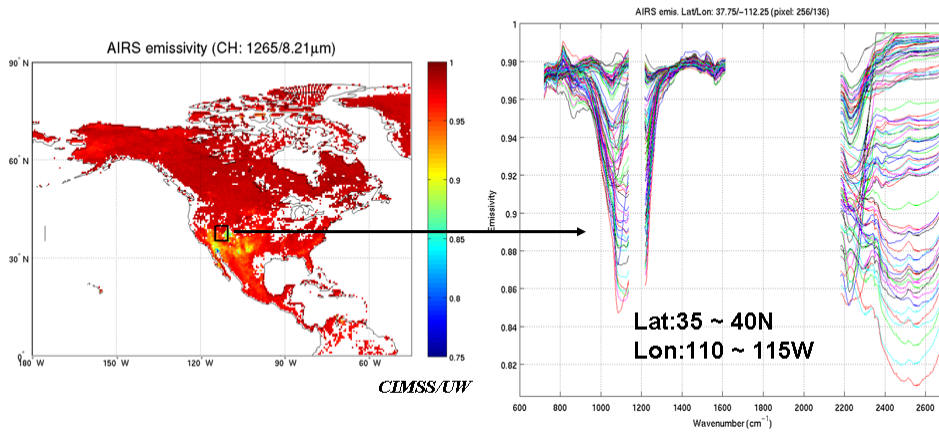


Figure 4.1.1.2: The emissivity spectra over Arizona and Utah (right panel) area which contains diversified surface types.

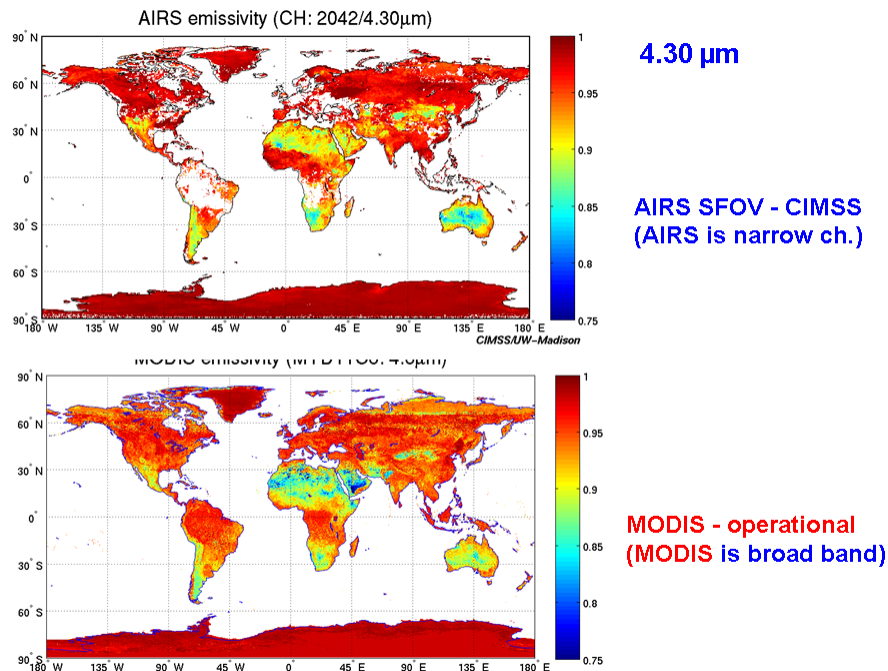


Figure 4.1.1.3: The global emissivity map from AIRS at 4.3 μm (single channel, upper panel) along with the operational MODIS broadband emissivity product (lower panel).

Improved cloud handling in soundings

In order to study synergy of LEO hyperspectral infrared (IR) and GEO imager for sounding evolution, the LEO hyperspectral IR alone single field-of-view (FOV) approach is studied as a first step. Single FOV cloudy sounding approach using hyperspectral IR radiances is successfully tested with AIRS radiance measurements from EOS Aqua. Two articles on cloudy sounding retrieval were published in 2007 (Weisz et al. 2007a, 2007b). Since the cloud properties (cloud-top pressure, optical thickness, particle radius) are simultaneously retrieved with sounding, we found that the AIRS retrieved SFOV CTP (cloud-top pressure) and the operational MODIS (Moderate Resolution Imaging Spectroradiometer) CTP product are close each other, both agree with CloudSat and CALIPSO measurements (Weisz et al. 2007b), MODIS and AIRS have similar CTP retrievals for most cloudy cases except for very low cloud cases. We also compared the cloudy sounding with radiosonde observations. Figure 4.1.1.4 shows the AIRS BT image at a window channel (upper left), the AIRS BT spectrum at Atmospheric Radiation Measurement (ARM) CART Site (lower left), AIRS SFOV cloudy temperature and dew point sounding retrievals (red line), two RAOBs at ARM CART Sites with different times of AIRS overpass. The AIRS BT image shows cirrus clouds over Southern Great Plains, the slope in the longwave IR window spectral region (low left) shows the cirrus cloud signature, on the other hand, the clouds are not thick so the AIRS sees the low level temperature (the water vapor absorption lines are up in the longwave IR window region). Therefore, both cirrus cloud signature and low-level temperature inversion are reflected in AIRS BT spectrum. The AIRS SFOV cloudy sounding approach does retrieve the inversion structure. The RAOBs also reveal the low-level temperature inversion. The cloud properties from AIRS are also reasonable, for example, the CTP is 308 hPa for this cirrus case. Note that this AIRS footprint at ARM CART Site is overcast according to MODIS cloud mask, but since it is not optically thick clouds, the AIRS sees sounding down to the surface. The temperature sounding differences between AIRS and RAOBs might be due to the 3-hour time difference.

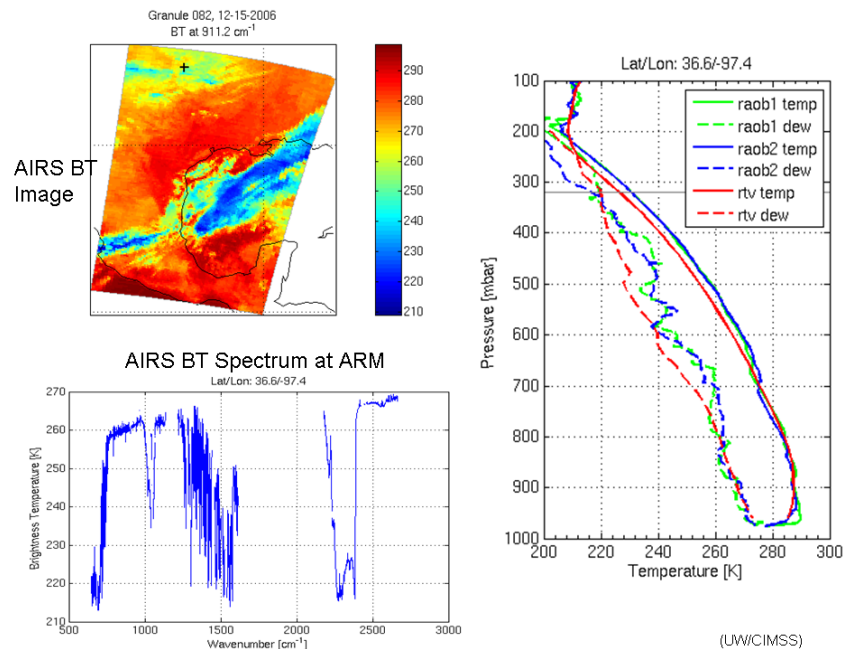


Figure 4.1.1.4: The AIRS BT image at a window channel (upper left), the AIRS BT spectrum at ARM CART Site (lower left), AIRS SFOV cloudy temperature and dew point sounding retrievals (red line), two RAOBs at ARM CART Sites with different times of AIRS overpass



LEO/GEO combination of profile evolution is under investigation

After establishing a reliable sound approach using only hyperspectral IR data, the next step is to combine LEO hyperspectral IR sounder (e.g., IASI, CrIS) and GEO imager (e.g., SEVIRI, ABI) for profile evolution. We are also developing the algorithm for legacy profile retrieval using combined ABI and forecast. Spinning Enhanced Visible and Infra-Red Imager (SEVIRI) data has been used for testing the algorithm. Some results were presented at Hyperspectral Imaging and Sounding of the Environment (HISE) topical meeting held in Santa Fe, New Mexico from 11-15 February 2007, and at the SPIE annual meeting held from 25-30 August 2007 in San Diego, CA. We have started on the simulation for CrIS/ABI combination, using observations from SEVIRI and IASI as proxy data. Some results are expected in early 2008.

Time continuity and high spatial resolution in retrievals

The advantage of time continuity of SEVIRI/ABI can be uniquely taken into account in emissivity retrievals. For example, ABI radiances from many time steps can be used to retrieve temporally invariable emissivity and variable surface skin temperatures. The algorithm has been developed and is being tested with SEVIRI data. In addition, we found that hyperspectral IR alone single FOV cloudy soundings have the capability on depicting hurricane eye warm core. Study on hurricane Isabel (13 September 2003) with AIRS onboard EOS Aqua platform shows that the temperature difference between hurricane eye and its environment can be as large as 20 K. The AIRS alone soundings are verified with dropsonde data in this case. See Figure 4.1.1.5 for details. Combination of ABI and hyperspectral IR data from polar orbits will provide better picture of hurricane.

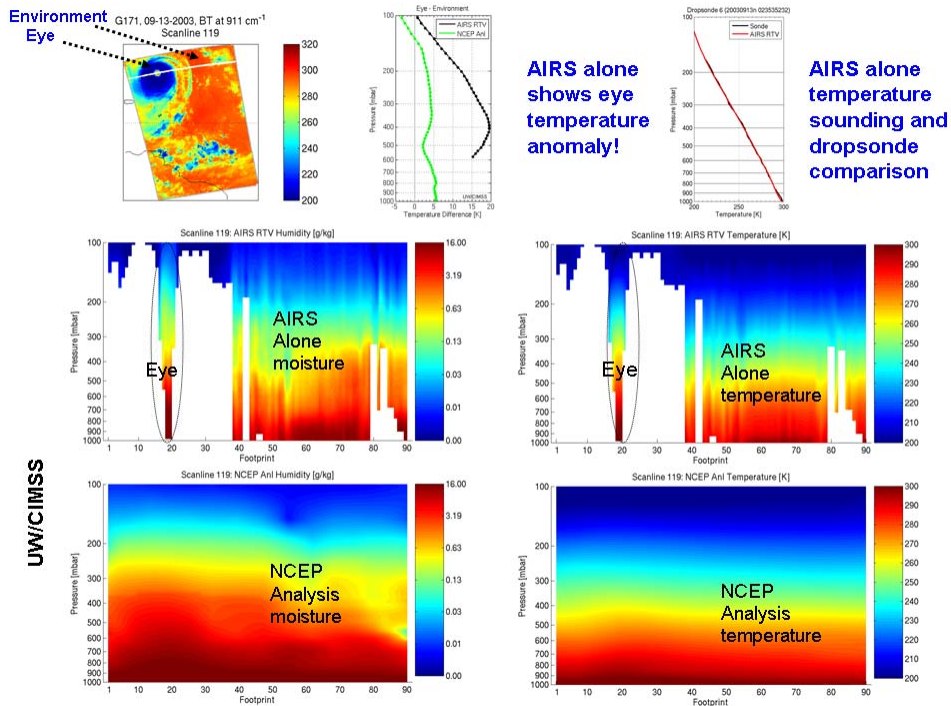


Figure 4.1.1.5. The AIRS brightness temperature image at 11 μm channel (top left), hurricane eye temperature anomaly from AIRS alone single footprint soundings and NCEP analysis (top middle), AIRS validation with dropsonde (top right), AIRS moisture (lower left) and temperature (lower right) single footprint (~13.5 km) sounding cross-section along the scan line across the eye, along with the NCEP analysis (bottom panels).



Publications and Conference Reports

Peer-Reviewed Publications

Li, Jun, J. Li, E. Weisz, and D.K. Zhou, 2007: Physical retrieval of emissivity spectrum from hyperspectral IR radiances. *Geophysical Research Letters*. 34, L16812, doi:10.1029/2007GL030543.

Schmit, T.J., J. Li, J.J. Gurka, M.D. Goldberg, K. Schrab, Jinlong Li, and W. Feltz, 2007: The GOES-R ABI (Advanced Baseline Imager) and the continuation of GOES-N class sounder products, *J. of Appl. Meteorol. Cli.* (conditionally accepted)

Weisz, E., J. Li, J. Li, D.K. Zhou, H.-L.Huang, M. Goldberg, and P. Yang, 2007: Cloudy sounding and cloud-top height retrieval from AIRS alone single field-of-view radiance measurements. *Geophysical Research Letters*, 34, L12802, doi:10.1029/2007GL030219.

Weisz, E., J. Li, W.P. Menzel, A. Heidinger and B. Kahn, 2007: Comparison of AIRS, MODIS, CloudSat and CALIPSO cloud top height retrievals, *Geophysical Research Letters*, 34, L17811, doi:10.1029/2007GL030676, 2007.

Conference Papers/Posters

Jin, Xin, J. Li, J.P. Nelson III, C.C. Schmidt, Z. Li, T.J. Schmit, and M. D. Goldberg, 2007: An improved atmospheric profile retrieval system for GOES Sounder and SEVIRI data, *Proceedings of SPIE 6684*.

Li, Jinlong, J. Li, E. Weisz, T. J. Schmit, M.D. Goldberg, and D.K. Zhou, 2007: Simultaneous retrieval of hyperspectral IR emissivity spectrum along with temperature and moisture profiles from AIRS, *Proceedings of SPIE 6684*.

Li, Jinlong, et al. 2007: Hyperspectral IR emissivity retrieval, poster presentation at *EUMETSAT/AMS satellite conference*, 24 – 28 September 2007, Amsterdam, the Netherlands. (Presented by Jun Li)

Li, Jun et al., 2007: Development and demonstration of hyperspectral infrared only sounding retrieval, *Hyperspectral Imaging and Sounding of the Environment (HISE) topical meeting*, 11 – 15 February 2007, Santa Fe, New Mexico, Optical Society of America.

Li, Jun, 2007: Single field-of-view cloudy sounding retrieval from IR hyperspectral radiances, invited talk at *AIRS science team meeting*, 27 - 30 March 2007, Pasadena, California.

Li, Jun, 2007: Research on All Sky Single field-of-view Infrared Only Sounding, *the GOES-R Algorithm Working Group (AWG) meeting*, 15 - 18 May 2007, the National Conference Center, VA.

Li, Jun, E. Weisz, J. Li, X. Jin, C. Liu, T.J. Schmit, A. Huang, and M.D. Goldberg, 2007: All sky sounding retrievals from hyperspectral infrared radiances alone, *Proceedings of SPIE 6684*.

Li, Jun, et al. 2007: Single Field-of-View Soundings from Geostationary Infrared Sounder Radiances, *EUMETSAT/AMS satellite conference*, 24 – 28 September 2007, Amsterdam, the Netherlands.

Li, Jun, 2007: Single footprint sounding, surface emissivity and cloud property retrievals from hyperspectral infrared radiances under all sky conditions, *the first IASI conference*, Anglet, France, 13 - 16 November 2007.



Weisz, Elisabeth, et al. 2007: Hyperspectral IR SFOV cloudy sounding retrieval, poster presentation at *EUMETSAT/AMS satellite conference*, 24 – 28 September 2007, Amsterdam, the Netherlands. (Presented by Jun Li)

4.1.2. GOES-R Risk Reduction Activities and Achievements: Winds – Chris Velden, Steve Wanzong and Iliana Genkova

Proposed Work

Previous GOES-R Risk Reduction work on Atmospheric Motion Vectors (AMVs) concentrated on demonstrating the ability of the AMV algorithm to target and track features found in WRF modeled moisture fields and simulated moisture retrievals. In 2007, the ATReC and Ocean Winds data sets were used to successfully demonstrate the feasibility of the concept of altitude-resolved vectors from the derived retrieval constant-pressure moisture analyses.

Summary of Accomplishments and Findings

During 2007, another WRF data set was thoroughly investigated. The so called FULL DISK case features 6km spatial and 40 min temporal resolution imagery produced from WRF model output over the projected full disk coverage of GOES-R. The output had to be converted from Unidata’s Common Data Form (NetCDF) individual ‘cube’ (a ‘cube’ refers to a smaller domain) files to HES-like sounding retrieval blocks. Each cube contains temperature and moisture field information, but also U and V wind field data needed for AMV validation and quality assessment. ‘Stitching’ and ‘data conversion’ tools were developed and implemented for AMV tracking purposes.

The processing of the FULL DISK case yielded height-resolved wind fields from 34 constant pressure levels (from 300hPa down to 986hPa). Figure 4.1.2.1 illustrates a) the spatial coverage of the targets from a single moisture field (729hPa), and b) example of moisture-tracked wind vectors over a selected segment of the FULLDISK.

Evaluation of the AMV quality was achieved through inter-comparisons with the WRF model U/V fields. Table 4.1.2.1 illustrates the statistics derived from comparing the OCEAN WINDS case AMVs to WRF U and V fields. The AMV RMSE statistics are comparable to those for real time GOES AMVs.

Table 4.1.2.1: Statistics derived from comparing the OCEAN WINDS case AMVs to WRF U and V fields.

100km Vector Match Distance	Winds with QI > 50
Simulated Retrieval Wind Count	1555
WRF Wind Count	983040
Match Count	1555
Speed Bias (m/s)	-3.3
Vector RMS (m/s)	5.7

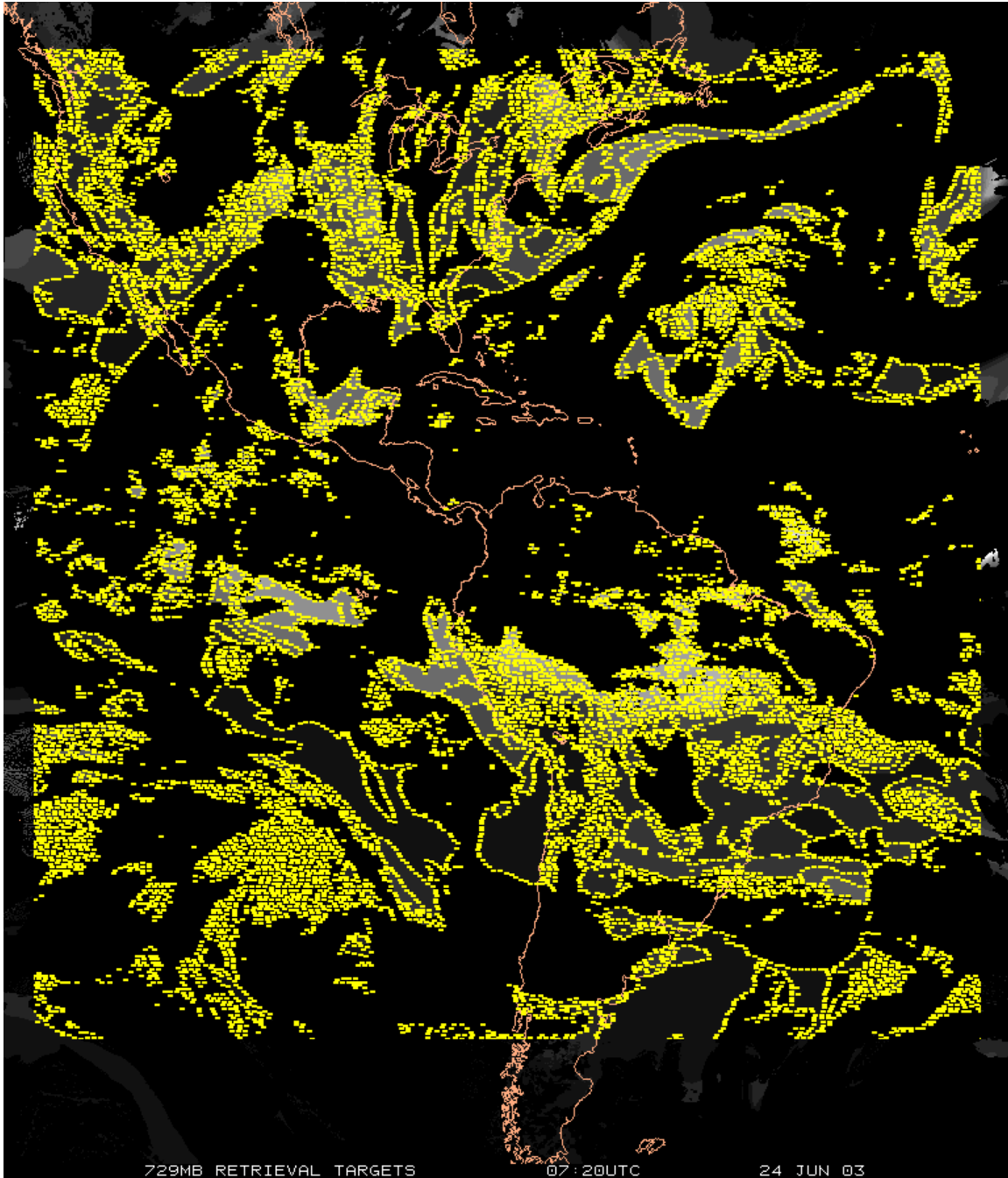


Figure 4.1.2.1: (a) Initial moisture gradient “targets” for a selected constant pressure level analysis (729 hPa) based on simulated HES moisture retrievals. (b) An example of moisture-tracked wind vectors derived from constant pressure level simulated HES retrieved fields for a selected sector of the FULLDISK case, off of the eastern Atlantic seaboard. The plot emphasizes the marine levels, and shows the vertical resolution achievable. To complement the research described above, we have also applied the same physical temperature and relative humidity retrieval algorithm to real GOES sounder radiances to derive moisture analysis fields, and then applied the winds extracting scheme to the constant pressure dew point images. The benefit of applying this approach to cloud free regions is shown in Figure 4.1.2.2, where the sounder moisture winds are plotted along with the real time cloud tracked winds vectors to illustrate the better AMV vertical coverage that is attained.

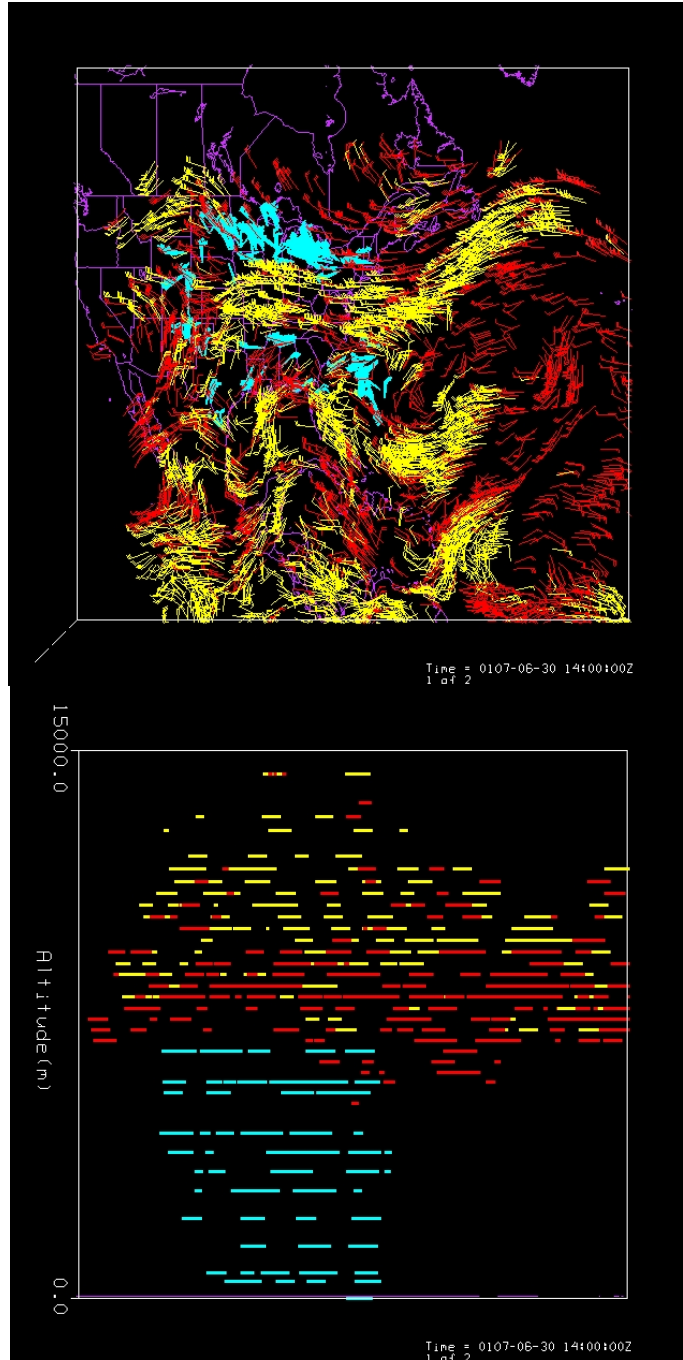


Figure 4.1.2.2: GOES sounder moisture analysis winds (cyan) are plotted along with the real time GOES cloud tracked (yellow) and water vapor (red) vectors. Top: plan view. Bottom: vertical view.

Publications and Conference Reports

Velden, Christopher S., S. Wanzong, I. Genkova, D.A. Santek, J. Li, E.R. Olson, and J.A. Otkin. Clear sky atmospheric motion vectors derived from the GOES Sounder and simulated GOES-R hyperspectral moisture retrievals. Symposium on Future National Operational Environmental Satellites, 3rd, San Antonio, TX, 14-18 January 2007 (preprints). American Meteorological Society, Boston, MA, 2007, Manuscript not available for publication.



Wanzong, Steve, C.S. Velden, I. Genkova, D.A. Santek, N. Bormann, J. Thepaut, D. Salmond, M. Hortal, J. Li, E.R. Olson and J.A. Otkin. The use of simulated data sets in atmospheric motion vector research. Joint 2007 EUMETSAT Meteorological Satellite Conference and the 15th Satellite Meteorology and Oceanography Conference of the American Meteorological Society, Amsterdam, The Netherlands, 24-28 September 2007.

Genkova, Iliana, C.S. Velden, S. Wanzong, and W.P. Menzel. Height-resolved wind vectors from GOES sounder moisture analyses. Joint 2007 EUMETSAT Meteorological Satellite Conference and the 15th Satellite Meteorology and Oceanography Conference of the American Meteorological Society, Amsterdam, The Netherlands, 24-28 September 2007.

4.1.3. GOES-R Risk Reduction Ozone Algorithm Development – Jun Li, Jinlong Li and Chris Schmidt

Proposed Work

In 2007, we proposed to:

1. Improve ABI TCO retrieval accuracy and coverage;
2. Study the ABI TCO retrieval under low cloud conditions.

Summary of Accomplishments and Findings

ABI total column ozone algorithm developed and tested with SEVIRI

An algorithm has been developed for total column ozone (TCO) retrieval from Advanced Baseline Imager (ABI) infrared (IR) radiances. We found that we can generate total column ozone retrievals using ABI and SEVIRI with accuracy similar to current GOES Sounder (4 ~ 5 %) if forecast temperature information is used in combination with IR spectral bands. The temperature information is not required in the current GOES Sounder SFOV TCO retrieval because the CO₂ spectral bands provide the temperature information already. A manuscript titled “Retrieval of Total Column Ozone from Imagers Onboard Geostationary Satellites” by Xin Jin, Jun Li, Christopher C. Schmidt, Timothy J. Schmit, and Jinlong Li was published in *IEEE Transactions on Geoscience and Remote Sensing*.

ABI total column ozone spatial resolution studied

To increase the ABI TCO retrieval coverage, clear radiances within 5 by 5 field of views (FOVs), the area can be averaged for TCO retrieval. After averaging the area, the spatial resolution of the TCO product will be 10 km, which is the same as that of the current GOES Sounder research TCO product (Li et al. 2001—*JTECH*; Li et al. 2007—*GRL*). We then wanted to determine if the 10 km ABI TCO preserved the spatial gradient of TCO when compared with the ABI single FOV TCO product with 2 km spatial resolution. To answer this question, the Spinning Enhanced Visible and InfraRed Imager (SEVIRI) 3 km radiances are used for this study. SEVIRI TCO with approximate 10 km spatial resolution from radiances averaged within 3 by 3 FOV area is compared with single FOV TCO product. Results show that the derived TCO images with 10 km and 3 km resolutions are similar. Figure 4.1.3.1 shows the 10 km and 3 km TCO products derived from SEVIRI radiances at 1200 UTC on 14 February 2006. The 10 km TCO has more retrieval coverage and better accuracy than the 3 km TCO. Note that TCO results from SEVIRI averaging might not fully reflect ABI data because ABI has much better spatial resolution (2 km) than SEVIRI’s 3 km (which is actually the re-sampling resolution). The spatial gradient versus noise reduction for ABI TCO product needs to be further studied. Since the ozone observation derived once everyday from Ozone Monitoring Instrument (OMI) onboard the NASA’s Earth Observing System (EOS) Aura platform has much larger spatial resolution (13 km by 25 km), the TCO product provided by ABI with



both good spatial and temporal information is very important for environmental forecasting and nowcasting.

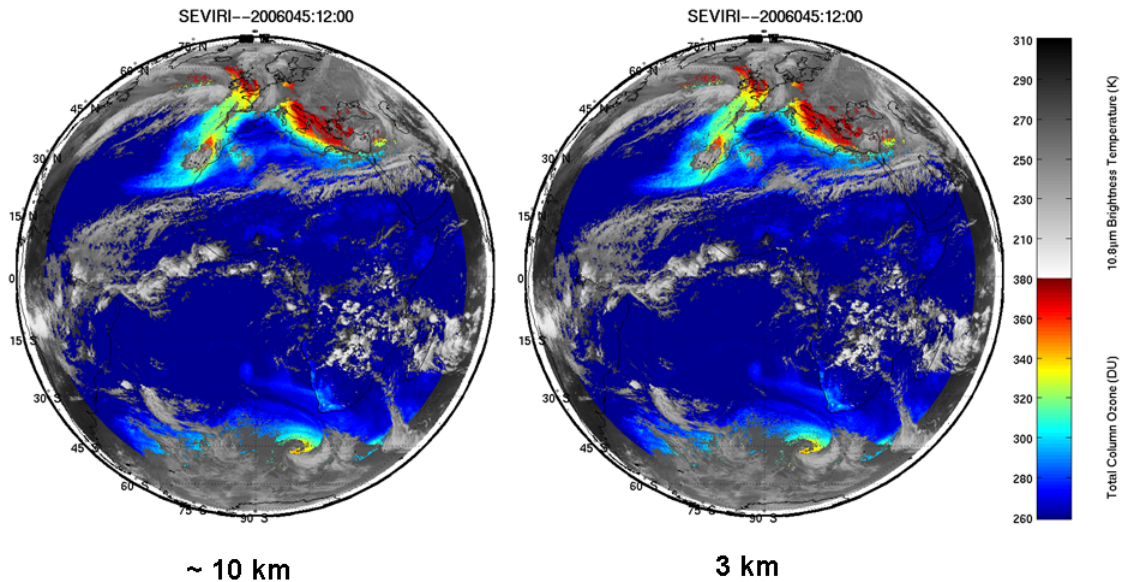


Figure 4.1.3.1: The 10 km and 3 km TCO products derived from SEVIRI radiances at 1200 UTC on 14 February 2006.

Total column ozone bias studied

We have applied ABI TCO algorithm to process SEVIRI. We found that SEVIRI underestimates TCO over the ocean. We believe that some of the bias may be due to the low cloud contamination over ocean, which leads to apparently colder skin temperatures and effectively lowers the TCO value. Given the same atmosphere and same observed brightness temperatures, a cooler skin temperature will appear to have less ozone above it than a warmer skin temperature. This trend results in an underestimate of the ozone column because the 9.6 μm band is an absorption band, and the radiance difference between it and other window channels is the largest single source of ozone information in the algorithm. Decreasing that difference decreases the apparent TCO. Another possible reason is that the training database contains fewer samples over ocean, and the regression is likely biased toward cooler skin temperatures for given surface air temperatures. To reduce the bias over ocean, it is important to improve how the algorithm handles low clouds and expand the training database to include more samples over ocean.

SEVIRI TCO compared with AIRS ozone product

We compared the collocated TCO products between SEVIRI, AIRS and OMI using the data between 14 and 15 February 2006. To minimize the errors caused by the different spatial resolutions, we only compared the pixels within 5 km. Using OMI as standard, comparisons show that SEVIRI and AIRS have similar TCO accuracy over land while AIRS has larger root mean square difference (RMSD) over ocean. The larger RMSD over ocean might be due to the cloud contamination in AIRS field of regard (FOR, 45 km). Table 4.1.3.1 shows the SEVIRI and AIRS TCO RMSD over land and ocean, respectively.

In addition, using AIRS SFOV cloudy sounding approach developed at CIMSS, the ozone profile above the cloudy can be reliably achieved with hyperspectral IR radiances. The cloudy approach will be tested with SEVIRI and the impact of partial cloudiness on TCO retrieval will be investigated.



Table 4.1.3.1: RMSD between OMI and SEVIRI/AIRS TCO.

Instruments	SEVIRI	AIRS
Over Land	12.6	13.1
Over Ocean	13.3	22.5

Publications and Conference Reports

Li, Jinlong, J. Li, C. Schmidt, J. Nelson III, and T. Schmit, 2007: High Temporal Resolution GOES Sounder Single Field of View Ozone Improvements, *Geophysical Research Letters*, 34, L01804, doi:10.1029/2006GL028172.

Jin, Xin, J. Li, C.C. Schmidt, T.J. Schmit, and J. Li, 2008: Retrieval of Total Column Ozone from Imagers Onboard Geostationary Satellites, *IEEE Transactions on Geosciences and Remote Sensing*, 46, 479 – 488.

Xin Jin, Jun Li, et al. 2007: Study of high temporal ozone product from imagers onboard geostationary satellites, *Proceeding of Hyperspectral Imaging and Sounding of the Environment (HISE) topical meeting*. 11–15 February 2007, Santa Fe, New Mexico, Optical Society of American.

4.1.4. Radiative Transfer Modeling – Steve Ackerman and Tom Greenwald

Proposed Work

This project extends our previous radiative transfer model (RTM) work by significantly modifying the Successive Order of Interaction (SOI) RTM to make it run in the solar spectrum. The SOI RTM is attractive because it can provide rapid calculation of top-of-atmosphere reflectances needed for the practical generation of proxy data sets for the ABI solar bands (1-7). In addition, an RTM that is applicable through the microwave, infrared and solar spectrums can provide a more unified framework from which to compute radiances for supporting not only ABI proxy data development but also other multi-spectral applications. To test the performance of the SOI RTM in the thermal infrared, comparisons are also made against the FIRTM-AD, a fast model for hyperspectral applications developed at Texas A&M University.

Summary of Accomplishments and Findings

The main accomplishments in RTM development were the construction of a new solar version of the SOI RTM and the generation of lookup tables for scattering/absorption properties (including phase functions) of water drops and ice particles for each of the ABI solar bands. The SOI RTM is very flexible and has a number of different options including running as a traditional doubling/adding model and supporting both specular and Lambertian surfaces. As an example of the capability of the new model and lookup tables, Figure 4.1.4.1 shows a simulated full-disk image of ABI band 2 based on over eight million WRF model grid points. The performance of the SOI RTM was very impressive. In 8-stream mode these calculations took only a few hours of wall clock time to complete on Zara, our 80-core Opteron cluster.

The comparison of the SOI RTM (at 32 streams) and the FIRTM-AD was somewhat limited but showed relatively good agreement. The differences in the window region were typically under 0.2-0.3 K (see Figure 4.1.4.2). The difficulty in this comparison was how to match the vertical location of the clouds in the two models since each model treats cloud vertical placement in a different way. Although the SOI RTM was found to be roughly three to four times slower than the FIRTM-AD, this is expected since the SOI RTM computes cloud reflection and transmission properties explicitly whereas the FIRTM-AD retrieves these properties from a large, multi-dimensional lookup table.



ABI band 2 (0.64 μm) reflectance 2005-06-04

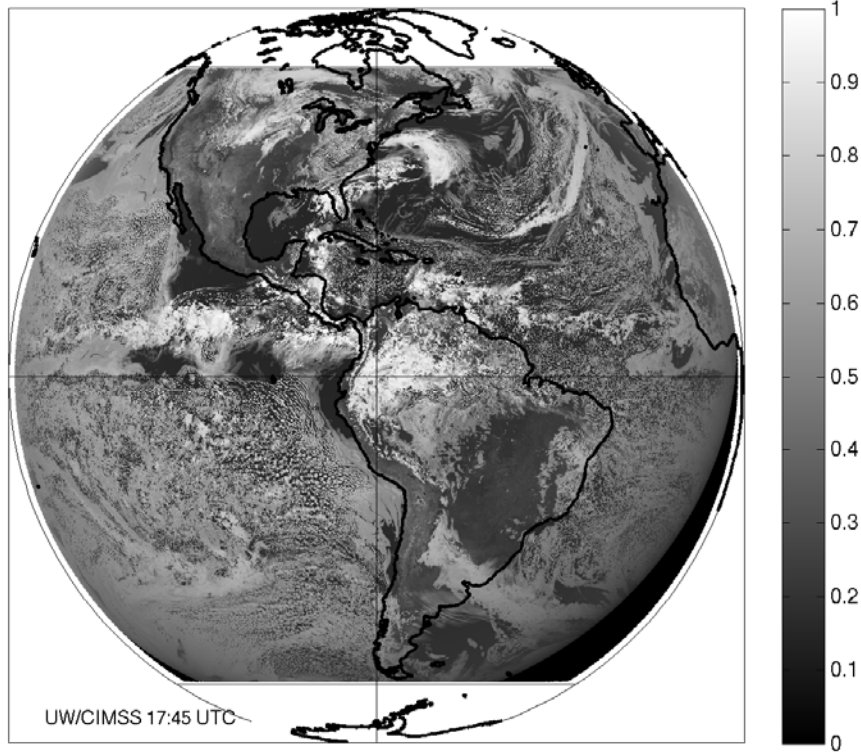


Figure 4.1.4.1: Simulation of ABI band 2 reflectance based on the SOI RTM and a WRF model 6-km resolution simulation.

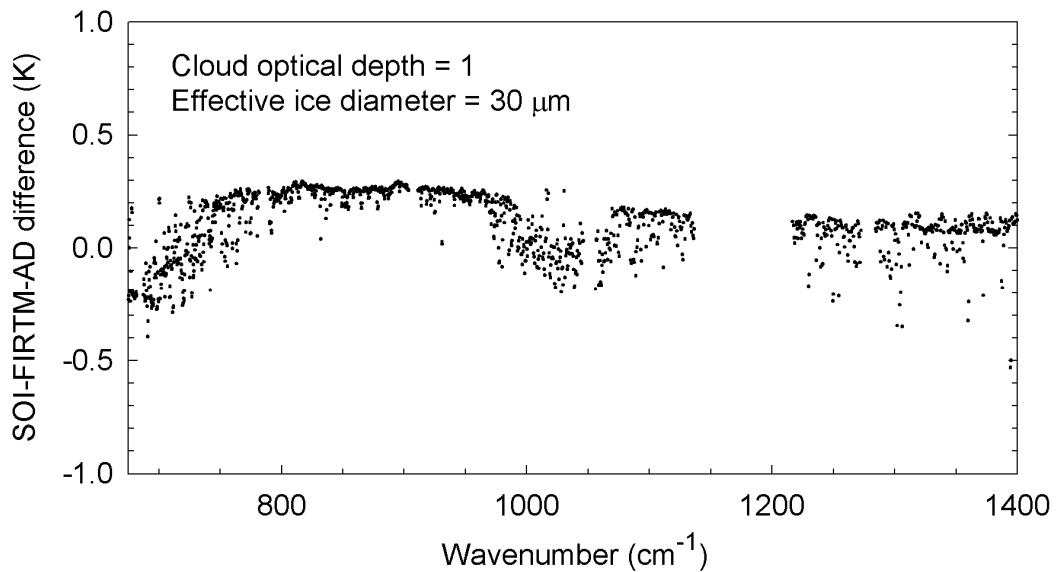


Figure 4.1.4.2: Comparison of top-of-atmosphere brightness temperature differences between the SOI RTM and the FIRTM-AD for a single-layer ice cloud. The cloud layer in the SOI RTM existed between 162.23 and 175.23 hPa, while the cloud layer in the FIRTM-AD was set at 168 hPa.



Publications and Conference Reports

Greenwald, T. J., J. Sieglaff, Y.-K. Lee, H.-L. Huang, J. Otkin, E. Olson, M. Gunshor, 2007: Verifying large-scale, high-resolution simulations of clouds for GOES-R activities, Submitted to 5th GOES Users' Conference, American Meteorological Society Meeting, New Orleans, Louisiana.

Zhang, Z., P. Yang, G. Kattawar, H.-L. Huang, T. Greenwald, J. Li, B. A. Baum, D.K. Zhou, and Y. Hu, 2007: A fast infrared radiative transfer model based on the adding-doubling method for hyperspectral remote sensing applications. *Journal of Quantitative Spectroscopy and Radiative Transfer*, 105, 243-263.

4.1.5. Land Surface Properties – Bob Knuteson

Proposed Work

In 2006, the CIMSS GOES-R Risk Reduction team studying land surface properties focused on the development of a global gridded high spatial resolution multi-year infrared emissivity database for use by: 1) the AWG proxy data team for simulation of realistic Earth emitted radiation, 2) the sounder team for temperature and water vapor retrieval algorithm development, and 3) for data assimilation in Numerical Weather Prediction models. A paper was submitted in late 2006 to the *Journal of Applied Meteorology and Climate* by lead author Suzanne Wetzel-Seemann that describes the methodology used to create this database from a combination of MODIS observations and laboratory measurements. This development was conducted in collaboration with the MODIS land products team and has been used for the comparison of against AIRS products produced by NOAA STAR.

We proposed to continue this work in 2007 with an emphasis on deriving land surface temperature and surface emissivity for the ABI sensor. We planned to collaborate with the EUMETSAT Land Satellite Applications Facility (LAND SAF) in Portugal, particularly Dr. Isabel Trigo, to develop an algorithm that uses the temporal change of the SEVIRI instrument measurements to determine infrared emissivity for the SEVIRI infrared channels. We proposed to create a prototype algorithm for ABI that takes advantage of the time change of surface temperature to separate surface temperature and surface emissivity. We also planned to apply this algorithm to the SEVIRI observations over Africa and Europe for a case study. The independent emissivity product created from the SEVIRI infrared channels was used to validate the UW emissivity database. EUMETSAT Climate SAF is using the UW database over land to generate temperature and water vapor profiles. We will collaborate with Ralf Bennartz (UW-AOS) on the impact of improvements in the land surface emissivity on profile retrievals SEVIRI as a proxy for ABI.

Summary of Accomplishments and Findings

Two accomplishments can be reported under this GOES-R risk reduction task in 2007: 1) an assessment of land surface emissivity from SEVIRI observations, and 2) an extension of the MODIS-based UW BF database to high spectral resolution. Both results have been presented at conferences (see reference list). Unfortunately the planned development of a land surface temperature and emissivity separation algorithm was not possible due to what appears to be significant calibration errors in the SEVIRI observations. These errors are apparent in the comparison of derived emissivities from SEVIRI when compared to results derived from MODIS and AIRS observations. This result is unexpected and requires further investigation. An update to the SEVIRI calibration is expected in 2008 from EUMETSAT. This work shows the importance of the sensor radiometric calibration requirement for the ABI in the GOES-R program in that it suggests that the full information content of the observations will not be exploited unless the relative and absolute calibration of each of the infrared channels is fully characterized.



Assessment of Land Surface Emissivity from SEVIRI

Diurnal signatures of land surface emission were investigated using SEVIRI data from August 2006. The diurnal change of observed brightness temperature is shown for seven sites near the Eastern Mediterranean in Figure 4.1.5.1. These geostationary observations can be used to develop an inversion method for obtaining land surface emissivity from the SEVIRI data that takes advantage of the time variation of the measurements. The data were obtained from Michael Pavalonis using GEOCAT. The observed top of atmosphere radiation is the sum of atmospheric, surface, and reflected contributions. Using an RTM to make calculations for each term in the RTM, we can easily evaluate the TOA radiation assuming any given surface emissivity. We compare these calculated radiances to observed SEVIRI radiances to evaluate of the different emissivity products.

The atmospheric state was determined from ECMWF model runs for 18 August 2006 at 00UTC. The radiative transfer model (LBLRTM by AER, Inc.) was used to calculate the TOA radiation given by the atmosphere, the surface, and reflected terms in a 1 by 1 degree grid over North Africa. The calculations were then interpolated onto the finer SEVIRI grid, and convolved to the SEVIRI spectral resolution (see Figure 4.1.5.2). We assumed the surface temperatures used by LSA SAF, and the surface emissivities given by: LSA SAF, UW MODIS BF, and NASA L2 AIRS. The LSA SAF emissivities are daily averages for 18 August 2006, the UW MODIS BF emissivities are monthly averages, and the AIRS Level 2 emissivities are for 16 August 00UTC values (18 August was not available). Results are presented in Figures 4.1.5.3 and 4.1.5.4.

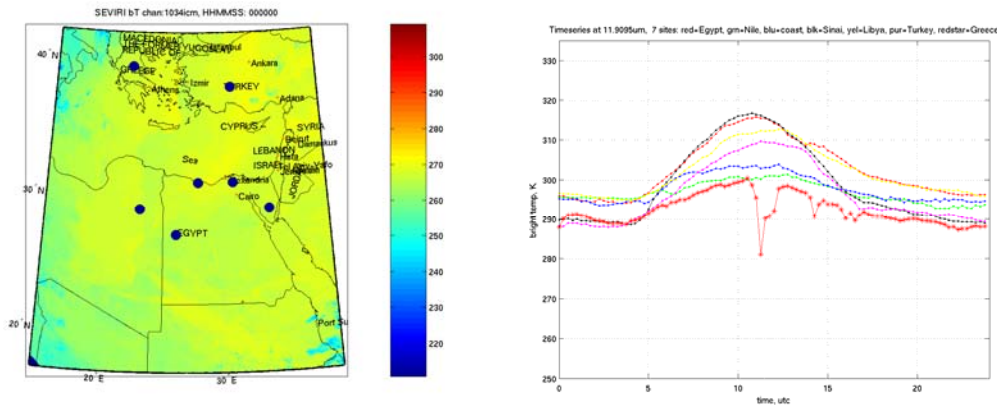


Figure 4.1.5.1: Diurnal change in the observed SEVIRI brightness temperature (right) at the seven sites shown as dots on the map (left) representing a range of land cover types.

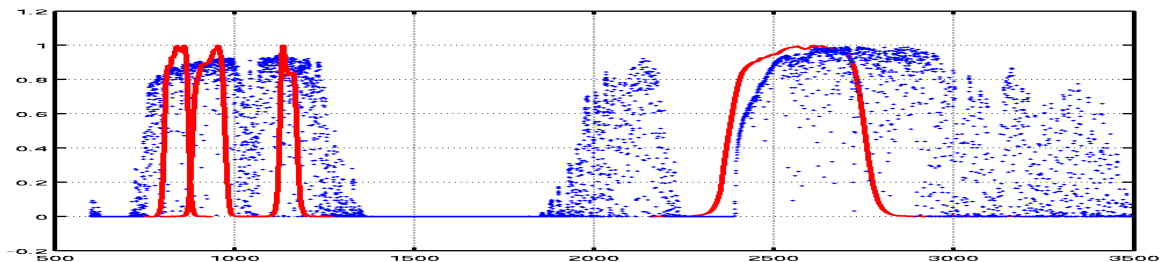
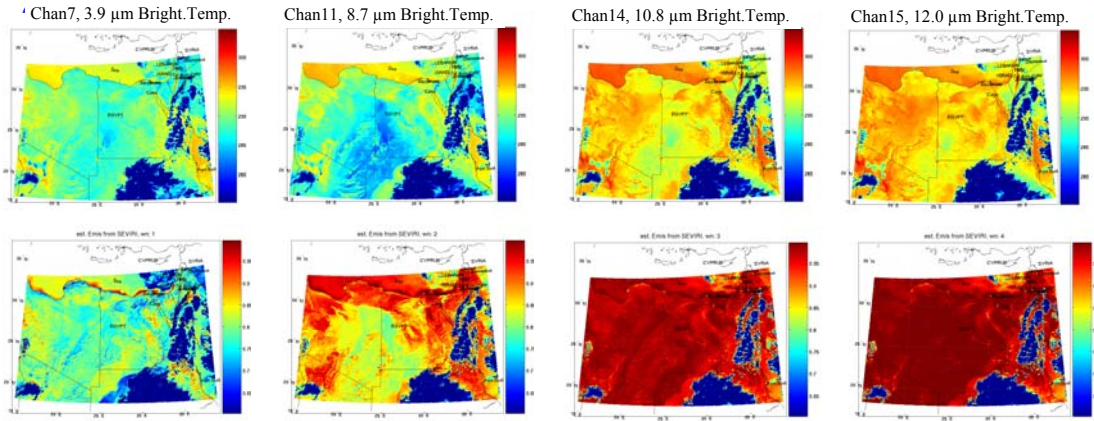


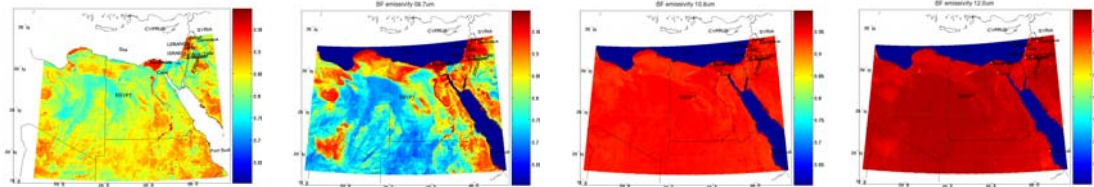
Figure 4.1.5.2: The four IR SEVIRI filter functions overlaid on a transmission calculation.



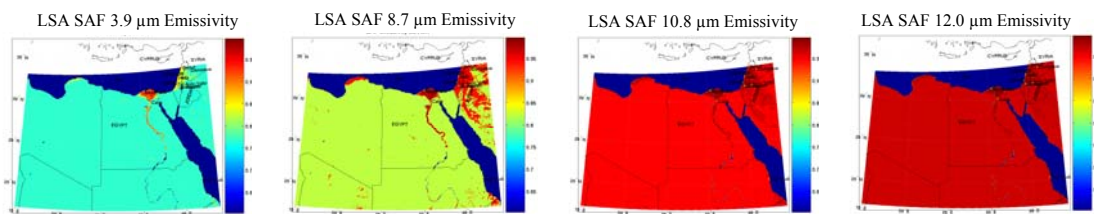
SEVIRI observed Brightness Temperature and Emissivity, 18 August 2006



Emissivity from UW MODIS BF, monthly average August 2006



Emissivity from LSA SAF, 18 August 2006 00UTC



Emissivity from AIRS L2, 16 August 2006 00UTC

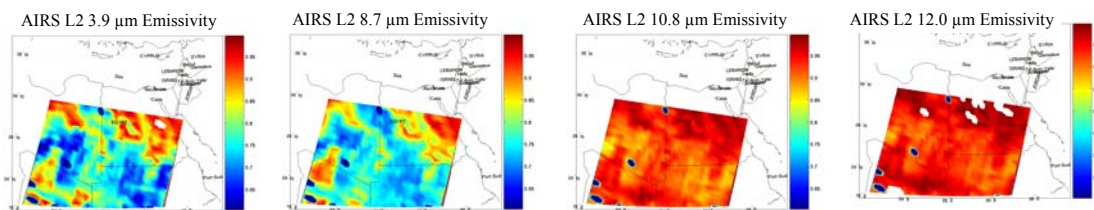


Figure 4.1.5.3: The top two rows of panels are the observed SEVIRI brightness temperature and the emissivity derived from the same observations using a surface temperature obtained from the EUMETSAT Land SAF (courtesy of Trigo). Comparisons to MODIS emissivities for the same time (third row of panels) show large discrepancies at 8.5 micrometers, and smaller discrepancies at 3.9 and 10.8 micrometers. The actual spatial variation is much more realistic than that used by the Land SAF (fourth row). The bottom row shows results from the AIRS L2 product for reference.



Emissivity by Channel

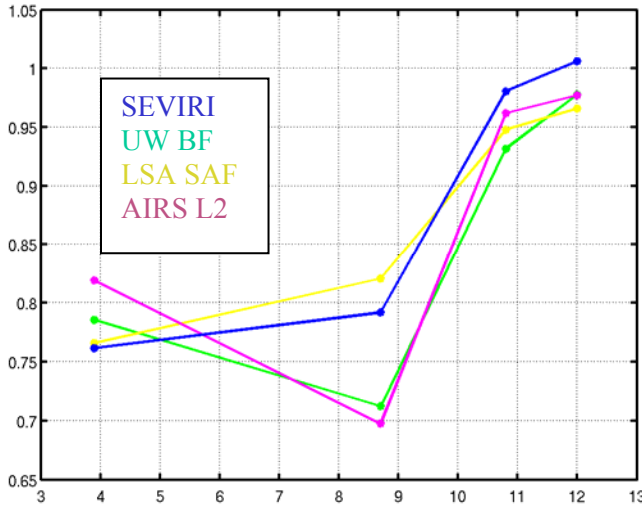


Figure 4.1.5.4: A single pixel at the Egypt One validation site illustrates the spectral discrepancies among the SEVIRI, MODIS (UW BF), Land SAF, and AIRS L2 products.

The calculated brightness temperature using the three different emissivity products agrees well with SEVIRI observations at 12.0 μm ; about +0.1 K, +0.1 K and -0.4 K respectively for UW MODIS BF, LSA SAF, and AIRS Level 2. Agreement at 10.8 μm is also good; approximately +0.4, +0.6, and -0.02 K respectively. However all the emissivity models lead to a disagreement with SEVIRI observations of about +3 K at 8.7 μm , and between +2.3 to +2.9 K at 3.9 μm . The use of 12.0 and 10.8 μm for the determination of land surface temperature appears to be valid however. UW MODIS BF and AIRS L2 emissivities are in generally good agreement with each other while the LSA SAF emissivity is limited by its lack of spatial detail.

Extension of the UW MODIS BF database to High Spectral Resolution (HSR)

In 2007, an algorithm was developed to derive a high spectral resolution (HSR) IR land surface emissivity from 3.6 to 14.3 μm for a given month, for every latitude/longitude point globally at 0.05-degree spatial resolution. The HSR emissivity is derived from a combination of high spectral resolution laboratory measurements of selected materials, and the UW/CIMSS Baseline Fit (BF) global infrared land surface emissivity database (Seemann et al., 2007) by using a principal component analysis (PCA) regression. The beta version of the algorithm to extract the high spectral resolution emissivity database from the UW/CIMSS BF emissivity data set is available for testing.

The HSR emissivity is derived from a statistical regression. The first Principal Components (PCs, eigenvectors) of 123 selected laboratory spectra (in this study the spectral resolution between 2-4 cm^{-1} , at 416 wavenumbers) were regressed against the 10 hinge points (3.6, 4.3, 5.0, 5.8, 7.6, 8.3, 9.3, 10.8, 12.1, and 14.3 μm) of the monthly UW/CIMSS BF emissivity (available at <http://cimss.ssec.wisc.edu/iremis/>). After calculating the PCA coefficients, the high spectral resolution emissivity values are determined at the same MYD11 latitude and longitude point given in the BF data. The accuracy of the new HSR emissivity data depends on the input BF emissivity data and the MODIS monthly MYD11 measurements.

In the PCA technique, the first PCs with highest eigenvalues represent real variations in the data while the last, least significant PCs most often represent random white noise. The number of PCs allowed is ten due to the number of spectral points of the input BF emissivities. However, using the maximum number



or close to the maximum number of PCs makes the solution unstable. Some tests (see Borbas et al., 2007) indicate that the optimal number of PCs is six. The number of PCs is an input to the algorithm. An example creating high spectral resolution emissivity spectra using the land profiles of the SeeBor training database over two IGBP types is shown on Figure 4.1.5.1.

Comparison of the UW/CIMSS BF and UW/CIMSS HSR emissivities at ten different locations of the Earth can be seen on Figure 4.1.5.5. The comparisons indicated that the largest differences occur around at 13, 10.2-9.7, 8.5, 7.8 and 4 μm for arid and semi arid regions and the HSR emissivity data can capture the quartz-reststrahlen band with the peak around 8.5 μm .

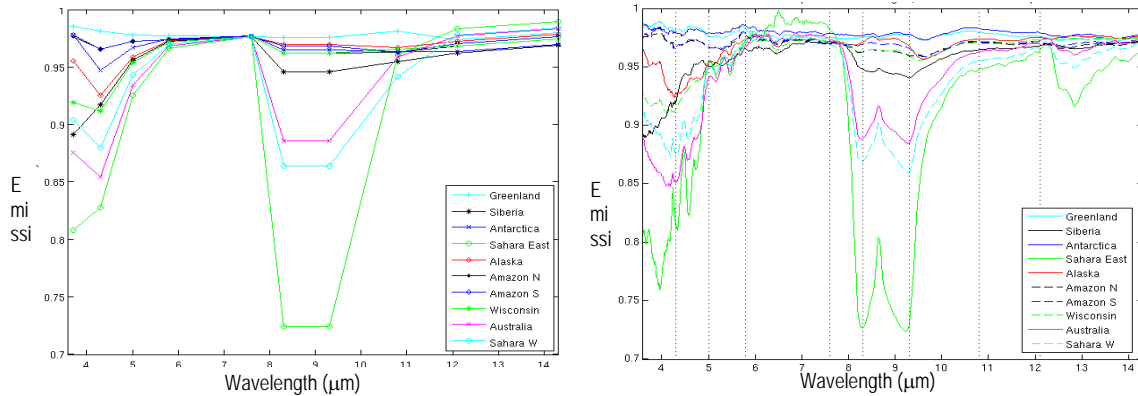


Figure 4.1.5.5: Emissivity spectra for August 2003 at ten different locations created by the BF (*right*) and PCA regression method (*left*).

We wanted to assess the importance of emissivity on retrieved atmospheric temperature, moisture, ozone profiles and land surface products as well as on use in data assimilation. To make this assessment, we performed sensitivity analysis of forward model calculated IR brightness temperatures (BT) is performed for the high spectral resolution AIRS spectral channels. The impacts of varying the emissivity on the calculated top-of-atmosphere BT across the infrared spectral regions are examined, then an analysis of the effects of a change in emissivity on retrieved temperature and moisture profiles is presented.

The pCRTM transmittance model was used to calculate BT for 8583 clear sky land profiles from the SeeBor training data set. Average differences of calculated BT using BF emissivity and HSR emissivity are plotted for some selected IGBP ecosystem types on Figure 4.1.5.6. The largest differences between BT calculated with these two emissivities occur around at 13, 10.2-9.7, 8.5, 7.8 and 4 μm for the IGBP barren/desert land classification.

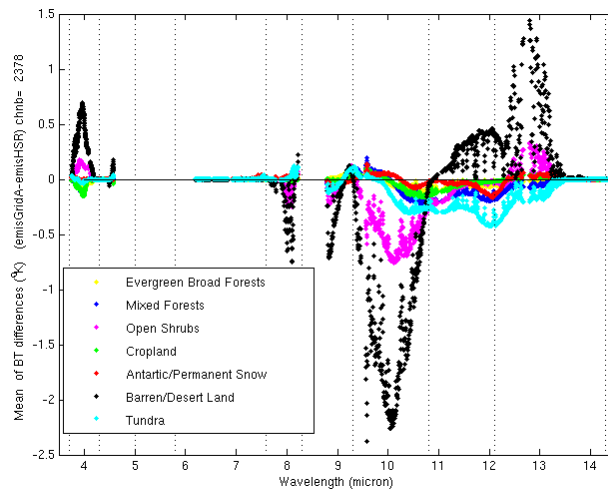


Figure 4.1.5.6: Averaged differences of BT calculated with BF emissivity minus those calculated with HSR emissivity. Each point represents a forward model calculation for one profile, and the colors indicate the land cover classification of the profile location, as defined by the IGBP categories.

Clear sky AIRS retrievals were compared to the ECMWF analyses from 2 September 2003 to assess the effects of a change in emissivity on retrieved temperature and moisture profiles. The UW-Madison IMAPP single FOV AIRS algorithm was used to generate temperature, moisture and ozone retrievals. A constant emissivity of 1.0, the UW/CIMSS BF emissivity and the UW/CIMSS HSR emissivity were each assigned to the SeaBor training data set and subsequently used to derive the synthetic regression coefficients for the AIRS retrievals. The MODIS MYD35 cloud mask products were used to find the clear sky scenes. Bias and RMS differences between the differently derived AIRS retrievals and ECMWF analyses at low latitudes (between $\pm 30^\circ$) are shown on Figure 4.1.5.7.

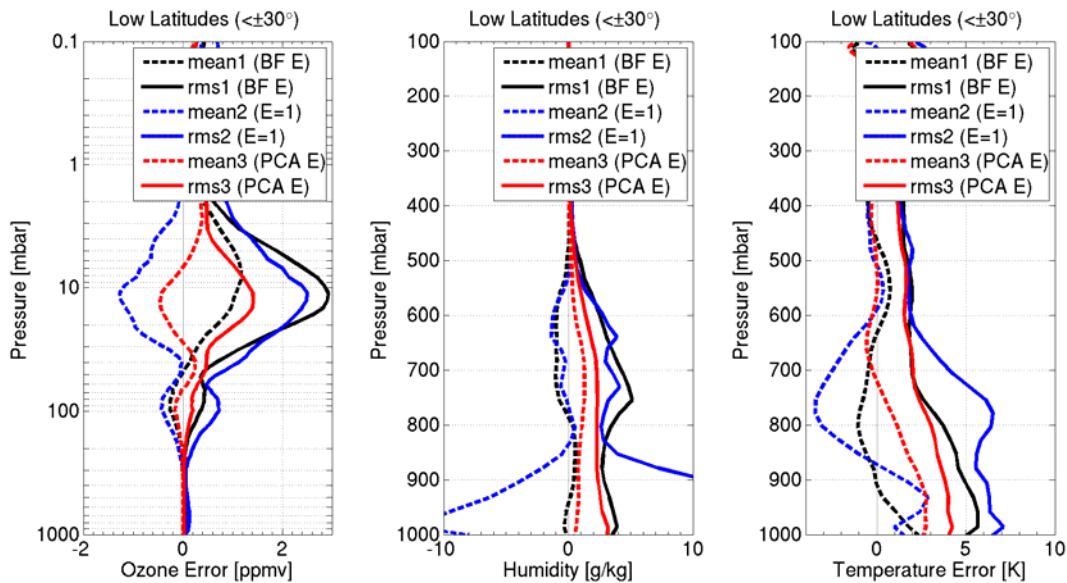


Figure 4.1.5.7: Profiles of mean and RMS differences between ECMWF analyses and AIRS ozone (*left*), moisture (*middle*) and temperature (*right*) retrievals for low latitudes (between 30° S and 30° N) calculated using emissivity=1 (blue), the UW/CIMSS BF emissivity (black) and UW/CIMSS HSR (PCA) emissivity (red) assigned to the training profiles for clear sky scenes on 02 September 2003.



Using the HSR emissivity data in the IMAPP AIRS algorithm showed a positive effect on temperature, moisture and ozone retrievals when compared with using a constant emissivity or the BF emissivity data. This case study also indicated that the HSR emissivity data could better capture the emissivity spectra in the ozone absorption band.

Publications and Conference Reports

Borbos, Eva, L. Moy, S. Seemann, R. Knuteson, I. Trigo, P. Antonelli, J. Li and H.L. Huang. A global infrared land surface emissivity database and its validation. 11th Symposium on Integrated Observing and Assimilation Systems for Atmosphere, Oceans, and Land Surface, San Antonio, TX, 14-18 January 2007 (preprints). American Meteorological Society, Boston, MA, 2007, Paper P2.7. Call Number: Reprint # 5285.

Borbos, Eva, R.O. Knuteson, S.W. Seemann, E. Weisz, L. Moy, Leslie and H.L. Huang. A high spectral resolution global land surface infrared emissivity database. 15th Joint 2007 EUMETSAT Meteorological Satellite Conference and Satellite Meteorology and Oceanography Conference of the American Meteorological Society, Amsterdam, the Netherlands, 24-28 September 2007. Proceedings. European Organization for the Exploitation of Meteorological Satellites (EUMETSAT), Darmstadt, Germany, 2007, Unpagged. Call Number: Reprint # 5563.

Moy, Leslie; et al., Comparison of Land Surface Emissivity from MODIS, AIRS, and SEVIRI, 15th Joint 2007 EUMETSAT Meteorological Satellite Conference and Satellite Meteorology and Oceanography Conference of the American Meteorological Society, Amsterdam, the Netherlands, 24-28 September 2007. Proceedings. European Organization for the Exploitation of Meteorological Satellites (EUMETSAT), Darmstadt, Germany, 2007.

Seemann, S.W., E.E. Borbas, R.O. Knuteson, G. R. Stephenson, H.- L. Huang. A global infrared surface emissivity database for clear sky atmospheric sounding retrievals from satellite-based radiance measurements. *Journal of Applied Meteorology and Climatology*, accepted April 2007, DOI:10.1175/2007JAM1590.1, Volume 47.

4.1.6. Biomass Burning – Chris Schmidt and Elaine Prins

Proposed work

GOES-R ABI biomass burning research and development activities for 2007 focused on active fire detection and sub-pixel characterization utilizing simulated and current global geostationary multi-spectral data. CIMSS investigated application of the dynamic Baseline Emissivity data set, which contains monthly estimates of spectral band emissivities derived from MODIS data, to improve sub-pixel fire characterization. CIMSS utilized 15-minute MSG SEVIRI data and the MSG WF_ABBA product over Africa to investigate how to exploit high temporal data to identify and monitor small fast burning agricultural and grass fires. CIMSS continued to investigate fire characterization using both Dozier estimates of instantaneous sub-pixel fire size, and temperature and fire radiative power (FRP) as derived from both MODIS simulated ABI data and other sensors as appropriate. Collaborations continued with NRL-Monterey and NESDIS on emission studies and data assimilation into the NAAPS model. These risk reduction activities ensure enhanced future fire detection, monitoring and characterization.

Summary of Accomplishments and Findings

Continued from 2006, we worked to create simulated ABI data from MODIS data. In 2007, simulated ABI data has been created from MODIS data. When generating the simulated imagery, the CIMSS technique accounts for the viewing geometries of the two satellites and the spatial response function of



the ABI. This remapped data is being used as proxy data for the GOES-R ABI WF_ABBA development effort. MODIS has two 3.9 μm channels, bands 21 and 22. Band 21 has higher radiometric noise than 22 but also saturates pixels at a higher temperature. The modified technique now utilizes band 22 unless it has saturated, in which case band 21 is substituted. This technique provides a more accurate simulation of the ABI dynamic range. We then applied this technique to the Southern California fires of 2007 (23, 24, and 26 October). CIMSS now has eight such MODIS to ABI case studies representing fires in North, Central, and South America. In the process of refining this remapping technique, a more direct comparison was made between remapped data with the Point-Spread Function (PSF) applied and that without, and it was confirmed that simple remapping produces virtually useless data. It should be noted that the PSF used dated from several years ago before the current design of ABI was conceived. Efforts to acquire the current PSF for ABI are underway.

Figure 4.1.6.1 compares the output from the new CIMSS remapping technique and the standard nearest-neighbor technique. Noise and moiré patterns are clearly visible in the nearest-neighbor image, while the CIMSS technique produces a much more realistic-looking image.

CIMSS continued to work with the proxy data team at CIRA to develop model-derived ABI proxy data for use with the WF_ABBA. CIRA delivered three cases: fires of constant size and temperature over the course of several hours with no clouds, fires of constant size and varying temperature over the course of several hours with no clouds, and fires of constant size and temperature with a field of convectively induced clouds. CIMSS has applied the WF_ABBA to the three cases and the WF_ABBA has performed well, with the most difficulty being introduced by the clouds in the third test data set, as expected. In the clear sky cases WF_ABBA derived fire size are within 50% of “truth”, which is within specification. Fire Radiated Power (FRP) was also calculated, and FRP values derived from radiances agreed with FRP values derived from instantaneous fire size and temperature as calculated by the WF_ABBA for reasonably large fires with temperatures between 650 K and 1200 K. Outside of that range of size and temperatures derived the two FRPs were poorly correlated. The same result was obtained when 2004-2006 GOES data was analyzed. Calculating FRP “truth” in the case of the model-based proxy data is a difficult task given the large number of saturated pixels present in the model-derived case. The two groups jointly worked out the correct way to simulate the FRP that ABI should be able to detect given simulated viewing conditions using a simplified Gaussian bivariate PSF. CIMSS also provided CIRA with current GOES WFABBA fire location and characterization data to use as inputs to the second model-generated case, which simulated fires over Central America.

Work has continued to increase use of the Baseline Emissivity data set (formerly referred to as the SeeBor), and collaborations strengthened with NRL-Monterey and NESDIS on emission studies and data assimilation into the NAAPS model. Application of the Baseline Emissivity data set resulted in detection of more fires with the WFABBA, though the fire characterization estimates were lower.

The WFABBA uses total precipitable water (TPW) from Numerical Weather Prediction (NWP) models to estimate the attenuation of the 3.9 μm signal. New look-up tables were generated for the ABI WFABBA as part of the algorithm development.

The WFABBA relies on a screen to identify clouds that are opaque in the 3.9 μm band, effectively requiring an “attenuation mask.” In an effort to upgrade the cloud screen for ABI, the simple thresholding scheme used by the WFABBA was compared to the GOES Surface and Insolation Program (GSIP) cloud method. It was determined that the WFABBA’s simple thresholds were a better fit for the algorithm. This “attenuation mask” is different from a cloud detection algorithm and something such as the ABI cloud detection algorithm cannot be used as a substitute.

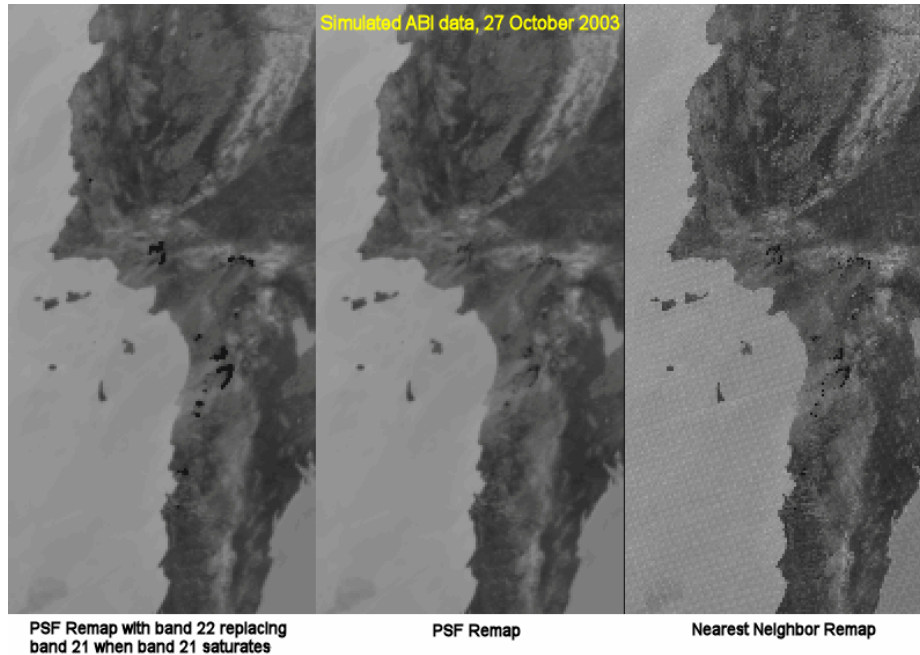


Figure 4.1.6.1: Three-way comparison between MODIS data remapped using the PSF and replacing band 21 data with band 22 when band 21 saturates, PSF remap on band 21 only, and a nearest neighbor remap. The PSF remaps are superior to the nearest neighbor remap, and fidelity of the fire detection is maintained when band 22 is used in conjunction with band 21.

Publications and Conference Reports

Schmidt, Christopher C., E.M. Prins, J.P. Hoffman, J.C. Brunner, S. Lindstrom, M. Gunshor, D. Santek, and G. Martin, 2007: GOES-R Fire Detection and Characterization, Algorithm Working Group Annual Meeting, National Conference Center, Landsowne, VA, 14-18 May 2007.

Schmidt, Christopher C., E.M. Prins, J.P. Hoffman, S. Lindstrom, J.C. Brunner, and J. Feltz, 2007: GOES-R ABI fire detection and monitoring with the WildFire ABBA, The joint 2007 EUMETSAT Meteorological Satellite Conference and the 15th America Meteorological Society (AMS) Satellite Meteorology & Oceanography Conference, RAI Center, Amsterdam, Netherlands, 24-28 September 2007.

4.1.7. SATCAST/Convective Initiation – Wayne Feltz and Kristopher Bedka

Purposed Work

This research task planned to adapt a GOES imager infrared cooling rate and convective initiation algorithm for use with MSG SEVIRI imager radiance data in anticipation of application on the GOES-R ABI imager. The CIMSS Satellite Nowcasting and Aviation APplications (SNAAP) team has conducted this research.

We proposed to take advantage of the current Convective and Orographically-induced Precipitation Study (COPS) being conducted in Southern Germany and Eastern France in the summer of 2007. CIMSS collaborated with Dr. Volker Gaertner (EUMETSAT), Dr. Marianne Koenig (EUMETSAT), and Dr. Volker Wulfmeyer (University of Stuttgart) to transition the SNAAP/ASAP convection initiation and mesoscale atmospheric motion vector applications into using SEVIRI radiances. This experiment ended,



but it provided an opportunity to use a current imager containing more ABI channels than currently possessed by GOES imager. New radiance channels can be used to optimize the convective initiation algorithm.

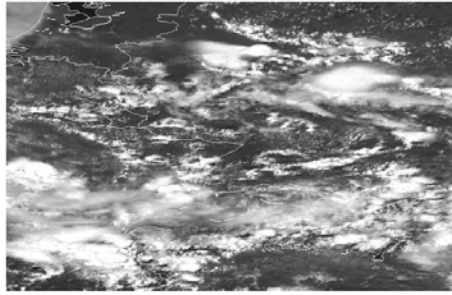
Summary of Accomplishments and Findings

GOES imager SATCAST algorithm (in collaboration with Prof. John Mecikalski of the University of Alabama – Huntsville) has been successfully adapted to use SEVIRI radiances as input data stream. Additional channels including 8.5 and 12.0 μm have been used to optimize algorithm performance. This additional radiance information has reduced the False Alarm Rate (FAR) when compared to GOES imager version of SATCAST algorithm. SATCAST has been implemented at EUMETSAT in collaboration with Marianne Koenig and Volker Gaertner, and was used for operational support during the COPS experiment that ended on 31 August 2007. The convective initiation data sets have been archived for further study and Marianne Koenig has requested that members of our SNAAP team return to Darmstadt after COPS has ended to review possible cases of interest for study. Figure 4.1.7.1 shows an example of nowcasting products shown on the COPS SATCAST product archive. The archive is located at this address: <http://cimss.ssec.wisc.edu/snaap/cops/quicklooks.php>

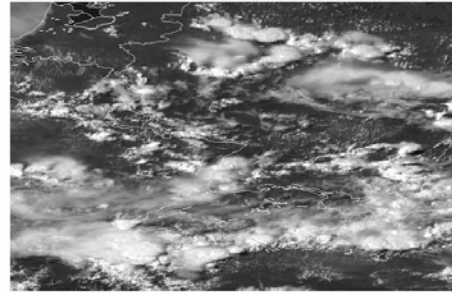
The SATCAST algorithm is currently using 15-minute resolution SEVIRI data. A special 5-minute temporal resolution mode has been invoked over the COPS domain during intensive operational periods. This 5-minute SEVIRI data has been archived at EUMETSAT and is accessible for case study use. Currently, we are investigating a new methodology for calculating cooling rate by taking advantage of higher temporal resolution SEVIRI and GOES imager data. The current SATCAST algorithm requires calculation of mesoscale winds, which will most likely not be needed for 30-sec or 5-minute resolution ABI modes of operation. Removing the requirement to calculate mesoscale wind reduces computational expense and improves temporal latency of satellite derived convective fields. Preliminary validation of the SATCAST SEVIRI CI products is being conducted in collaboration with EUMETSAT. New box-average CI cooling rate will be investigated, taking advantage of higher temporal resolution expected from ABI. A case study was also produced for a convective case occurring over South Africa in support of Marianne Koenig (EUMETSAT) and Estelle de Coning (South African Weather Service) to demonstrate cooling rate/CI algorithm flexibility over various geographical domains. Figure 4.1.7.2 show results from applying the cooling rate/convective initiation methodology over a storm in South Africa.



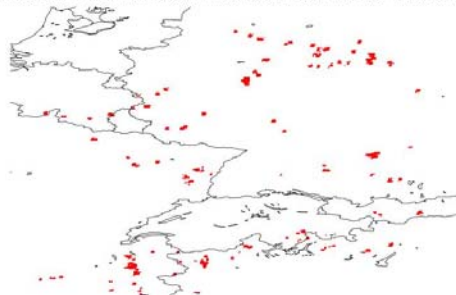
MSG High Resolution Visible Reflectance: 2007162 at 1230 UTC



MSG High Resolution Visible Reflectance: 2007162 at 1400 UTC



MSG Convective Initiation Nowcast: 2007162 at 1230 UTC



CI Nowcast Locations in Red

1 km MSG Convective Cloud Classification: 2007162 at 1400 UTC

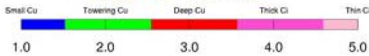
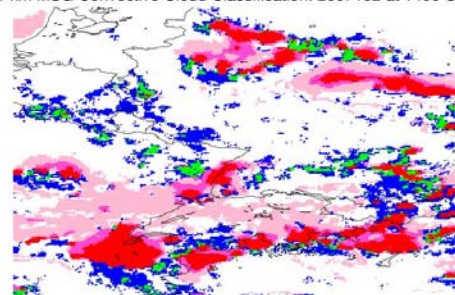


Figure 4.1.7.1: Convective initiation nowcast (bottom-left) compared to MSG 1 km visible channel imagery at the time of the nowcast (upper-left) and imagery 1.5 hours later, illustrating that many of the cumulus identified by the nowcast later developed into deep convection (bottom-right).

Marianne Koenig visited SSEC/CIMSS and focused on validating the convective initiation product. Kris Bedka will continue to work with her to optimize the algorithm using 5-minute SEVIRI data. The CTCR and CI algorithm will be executed over South Africa during the convective season from November 2007 – January 2008. The results constitute another rich validation data set to help transition algorithm to ABI. An abstract titled “Improving Nowcasting of convective storm development using MSG SEVIRI, MODIS, and GOES-12 imagery as risk reduction for GOES-R ABI” was presented at the 2008 AMS GOES User’s Conference that describes this GOES-R risk reduction effort.

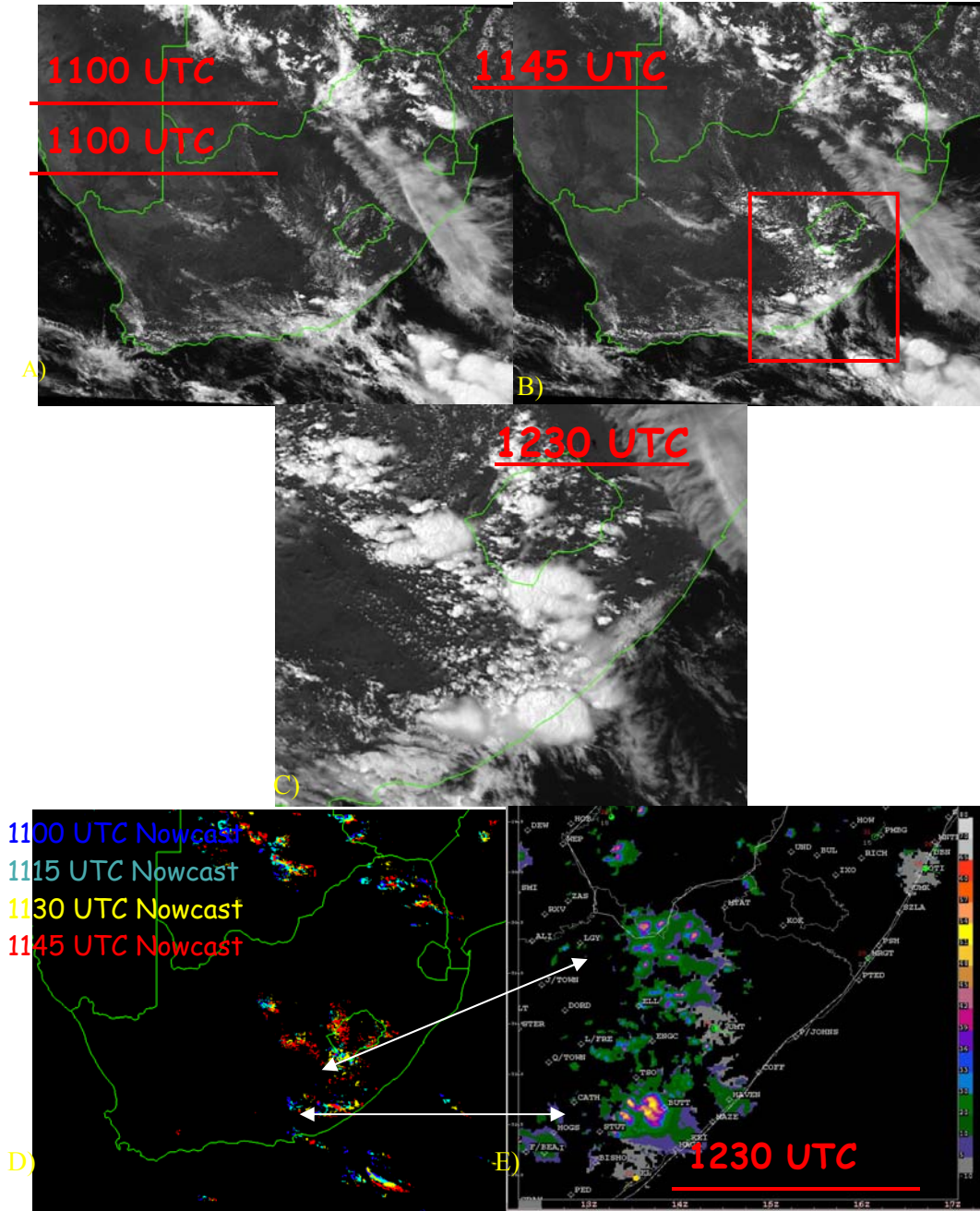


Figure 4.1.7.2: SEVIRI visible images in panels A-C indicate rapid development of convection over the S. Africa region between 1100 and 1230 UTC. Panel D shows the SEVIRI imager based box-average convective initiation nowcast for consecutive 15-minute data. Panel E indicated radar echo intensification in very near proximity of nowcast convective development.

To summarize, GOES imager convective diagnostic products were produced for the summer 2007 COPS experiment. Results from this activity were presented at the EUMETSAT/AMS Satellite conference in Amsterdam in September 2007. This activity has inspired a new collaboration with the South African Weather Service, which has a fairly dense radar network. SEVIRI convective diagnostic products are being produced and provided in a near real-time manner for weather decision support for South Africa. The additional SEVIRI radiance channels (as compared to the GOES imager) allow spectral and temporal



optimization of the algorithm for future GOES-R ABI use. New FY2008 GOES-R RISK REDUCTION convective cooling rate, convective initiation, and mesoscale wind research have been outlined and accepted for continued progress.

Publications and Conference Reports

Bedka, K. M., et al., 2007: Geostationary convective storm diagnostic and nowcasting products: Applications with GOES-12 and MSG. Seminar given at EUMETSAT, 26 February 2007.

Bedka, K.M., W. Feltz, J. Mecikalski, R. Rabin, J. Sieglaff, J. Brunner, P. Antonelli, and C. Velden, 2007: An end-to-end convection diagnostic and nowcasting approach for MSG SEVIRI and GOES-R Risk Reduction. The EUMETSAT-IMWM Convective Workshop. 15-17 November 2007. Krakow, Poland.

Feltz, W. F., et al., 2007: Satellite-based Nowcasting and Aviation Weather Applications for Convection, Turbulence, and Volcanic Ash. Seminar given at EUMETSAT, 26 March 2007.

Koenig, M. and K. M. Bedka, 2007: Meteosat Second Generation: Convective storm nowcasting tools. The Joint 2007 EUMETSAT Meteorological Satellite Conference and the 15th AMS Satellite Meteorology and Oceanography Conference. 24-28 September. Amsterdam, Netherlands.

4.1.8.1 Tropical Cyclones Research – Chris Velden

Proposed Work

One of the objectives of our GOES-R risk reduction work was to demonstrate what would be possible with ABI. Some existing GOES observing strategies mimic what will be possible with ABI and can provide a good idea of what we will be able to do with ABI data. For example, the upper-level outflow is thought to be an important contributor to intensity changes in tropical storms. Using Atmospheric Motion Vectors (AMVs) derived from special GOES 5-minute rapid-scan (r/s) imaging operations, we can create an effective simulation of what will be available on a routine basis once GOES-R is launched.

To demonstrate this capability, GOES-11 AMVs were derived from 5-minute r/s imagery during as NASA's Tropical Cloud Systems and Processes (TCSP) experiment in July 2005. Hurricane Emily traversed the sampling domain and provided a good case study because the storm's intensity fluctuated during the period of observation. GOES-11 r/s AMVs and selected kinematic analyses for a time period during Emily were analyzed. This caliber of high-resolution data will be routinely possible from the GOES-R ABI. In 2007, we planned to see what we could observe and learn from current GOES special observing modes in advance of this deployment.

Summary of Accomplishments and Findings

Time series of upper-level quantities derived from the GOES r/s AMVs over Emily and other TCs were derived. From these data sets, we identified trends and potential associations with a hurricane's structure and intensity fluctuations. To investigate kinematic quantities such as vorticity and divergence, the AMVs had to be analyzed on a uniform grid. This analysis was done using an iterative Barnes scheme. The Barnes scheme allows an analysis to fit the observations coarsely where observations are sparse and a tightly where the observations are dense.

For example, we analyzed AMVs during Hurricane Emily (11–21 July 2005) on a 0.2-degree grid. Included in the analyses were AMVs assigned a height between 150 hPa and 200 hPa and located approximately 700 kilometers from the NHC best-track storm center. In regions without AMVs, a 1-



degree numerical weather prediction background was used. Figure 4.1.8.1.1 shows an example of a storm-centered vorticity field calculated from the analysis of Emily valid 18z on 18 July 2005. The observation wind barbs (ms^{-1}) that made up the analysis are also plotted on top of the vorticity field. Although Emily was a weak category-one hurricane at this time, she intensified 10 kts during the following six hours. The analysis captures the cyclonic circulation over the storm's center, and the asymmetric, anti-cyclonic outflow region to the north and northeast of the storm.

To examine the trends in vorticity over the lifecycle of the storm, average vorticity values were calculated and compared with Emily's intensity. For each analysis, we averaged a circular region in the inner 200 kilometers and the outer 200 kilometers. This process allowed us to examine the inner cyclonic flow in the storm's eye-wall and its anti-cyclonic outflow. A time series of the average values of these two quantities was compared to the Emily's maximum wind-speed (shown in Figure 4.1.8.1.2). The comparison shows how the two vorticity averages changed as Emily's intensity changed. In general, as Emily intensified, its inner vorticity increased. The one period where this relationship was not as strong was during Emily's peak intensity. This observation may be related to the difficulty generating AMVs over a TC's center when the storm is very intense due to uniformity (or an absence of clouds) in the eye-region. The vorticity-intensity relationship is much clearer during the final intensification period around 20 July (day 201). The inner-vorticity increased significantly while the outer-region became more negative, corresponding to increased anticyclonic outflow. The inner-vorticity average correlates to Emily's intensity at around 60%.

The geographic constraints of our AMV data sets prevented us from capturing the very early stages of Emily. However, it is clear that the two-vorticity quantities do not differ appreciably prior to intensification or after it dissipates. It is possible that these quantities can be used to investigate genesis, and will be examined more thoroughly for additional storms. Although this analysis only represents one case study, it shows the potential of analyzing the upper-level flow and relating it to TC intensity and intensity change. Further investigation into these and other parameters should lead to a better understanding as to how the upper-levels impact and are modified by TC intensity change.

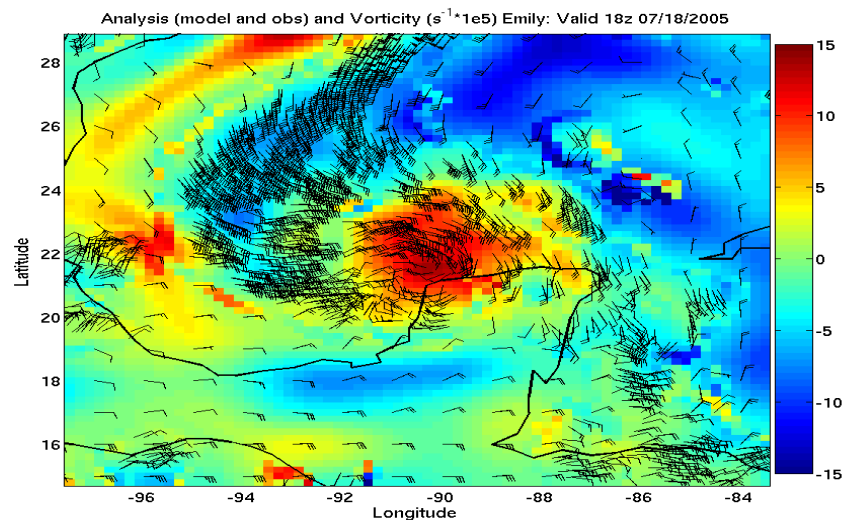


Figure 4.1.8.1.1: Storm-Centered vorticity analysis and observed AMVs at 18Z on 18 July 2005 for Hurricane Emily. The color-contours show vorticity (10^5s^{-1}) and the wind barbs show the observations in ms^{-1} . The analysis captures the cyclonic structure in the storm's center and the anti-cyclonic outflow to Emily's north. These asymmetric outflow channels are often associated with storm strengthening. Emily is a weak hurricane at this time, but subsequently intensifies 10-kts in 6 hours, and 55-kts in 30-hours.

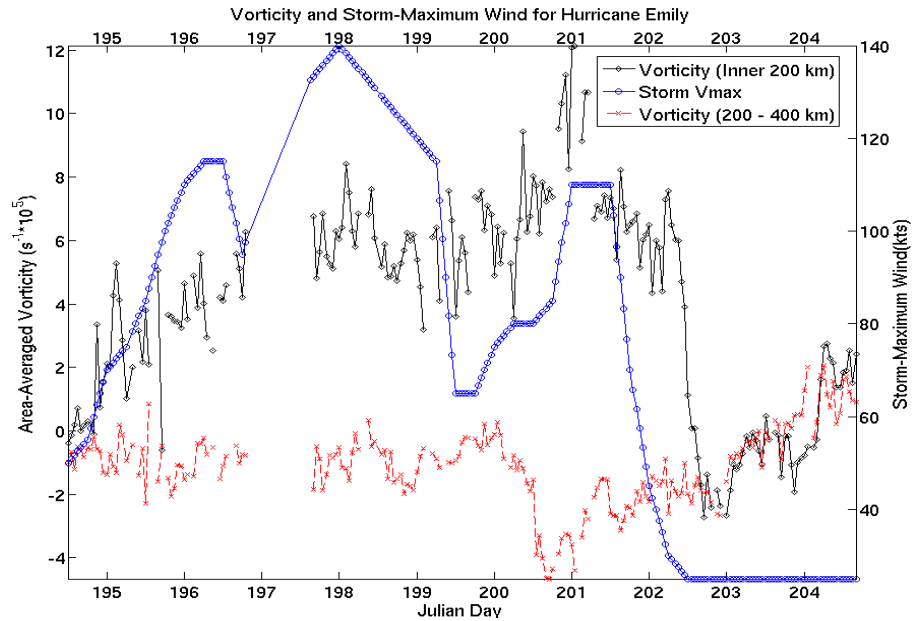


Figure 4.1.8.1.2: Hurricane Emily (2005) time series of inner 200km averaged vorticity (black-diamond curve, left-axis), outer 200-400 km averaged vorticity (red-x curve, left axis) and best-track storm maximum wind-speed (blue-circles, right axis). As Emily intensifies, the inner vorticity increases. During the re-intensification around day 201 (July 20th), the inner-region increases even more and the outer vorticity average becomes more negative. The inner-vorticity and storm maximum wind speed are correlated at about 60%. The missing points in the time series are due to times of missing or poor quality data.

We next expanded our data set to include analyses from other 2005 storms, namely Katrina, Rita, Wilma, and Ophelia and Eugene. These analyses have been sorted by storm maximum wind and azimuthally averaged. Figure 4.1.8.1.3 shows the azimuthal averages for storm-relative tangential wind, relative vorticity, storm-relative radial wind, and divergence. These profiles show the stronger cyclonic rotation (seen in the vorticity and tangential wind plots) in the more intense systems, even at upper-levels. One can also see the heightened divergence for lower-strength storms (Category 1 to Category 3), probably due to increased convective vigor in strengthening storms. By the time the storms are at Category 4 or Category 5 strength, the upper-level divergence over the core region is actually shown to be weaker. For further analysis, it may be worth normalizing many of these quantities by some size parameter to take into account the differing spatial structures of each storm.

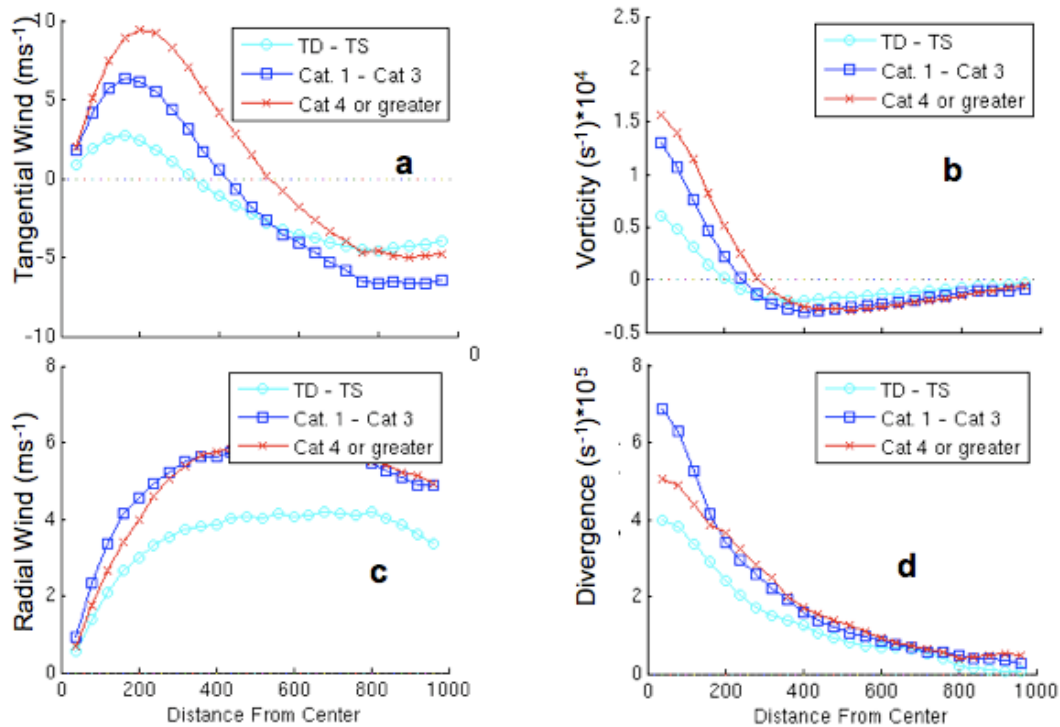


Figure 4.1.8.1.3: Azimuthally averaged profiles of upper-level: a) SR Tangential Wind b) Relative Vorticity c) SR-Radial Wind d) Divergence binned by intensity. These profiles suggest that the upper level kinematics are sensitive/related to storm intensity.

Publications

Berger, H., and C. Velden, 2007: Diagnosing Upper-level Mass Flux Characteristics during TC Formation and Intensification using GOES Rapid-Scan Winds. TCSP/NAMMA Workshop 15-17 May.

Berger, H., and C. Velden, 2007: Tropical cyclone outflow diagnostics as observed in GOES Rapid-Scan Atmospheric Motion Vector analyses. Joint 2007 EUMETSAT/AMS Conference, Amsterdam, 24-28 September.

4.1.8.2 Constructing an Objective Tool for Identifying Hurricane Secondary Eyewall Formation – James Kossin and Matthew Sitkowski

Proposed Work

Hurricanes, and particularly major hurricanes, will often organize a secondary eyewall at some distance around the primary eyewall. These events are generally associated with marked changes in the intensity and structure of the inner core, such as large and rapid deviations of the maximum wind and significant broadening of the surface wind field. The latter has particularly dangerous consequences in terms of sea state, storm surge and wind damage extent during landfall events. Despite the importance of secondary eyewall formation in hurricane forecasting, there is presently no objective guidance to diagnose or forecast these events. Forecasters need to rely on aircraft reconnaissance data, coastal radar imagery, or satellite microwave imagery to make a subjective determination of whether SEF is occurring or not. These data are not always available in a timely manner. In this project our goal is to construct a new index, based on readily available data, which will provide forecasters with a probability of imminent secondary eyewall formation (SEF). The algorithm is based on environmental and GOES infrared



satellite features from the SHIPS-model developmental data set applied to a Bayesian classification scheme.

Summary of Accomplishments and Findings

Our first milestone was the completion of an exhaustive and unprecedented database of global SEF occurrence. More than 4,500 SSMI, SSMIS, TRMM, and AQUA microwave images were downloaded from the Naval Research Laboratory web site. In combination with aircraft, radar, and additional satellite data, these images were used to examine nearly 175 tropical cyclones to determine the approximate time of SEF. *Note that, while microwave imagery was applied to identify SEF, our algorithm will not rely on microwave data. The microwave data was used only to create the database on which to train the GOES-based algorithm.*

A catalogue of major tropical cyclones and the number of these that experience SEF are shown in the top two rows of Table 4.1.8.2.1. Some storms experience more than one occurrence of SEF in their lifetime, which is reflected in the bottom row of the table.

Table 4.1.8.2.1: Inventory of major tropical cyclones (TC), and climatology of SEF occurrence.

	1997	1998	1999	2000	2001	2002	2003	2004	2005	2006	Sum
Major TCs	21	14	14	12	18	19	14	23	19	19	173
SEF TCs	11	5	6	7	9	13	10	14	10	13	98
SEF Cases	15	5	7	7	10	16	16	28	20	21	145

The inventory shown in Table 4.1.8.2.1 is global. For this project we are interested in the future application of GOES-R imagery in the North Atlantic and Eastern North Pacific, where about 35% of SEF occurrence takes place (Figure 4.1.8.2.1).

For each fix where a storm had maximum winds greater than 100 kt, our new database allows us to determine if the storm formed a secondary eyewall in the following 12 hours. The climatology of SEF counts from our new inventory tells us that there is a 26% probability of SEF *on average*. Our second milestone for this quarter is the addition of skill to this climatological probability based on environmental conditions.

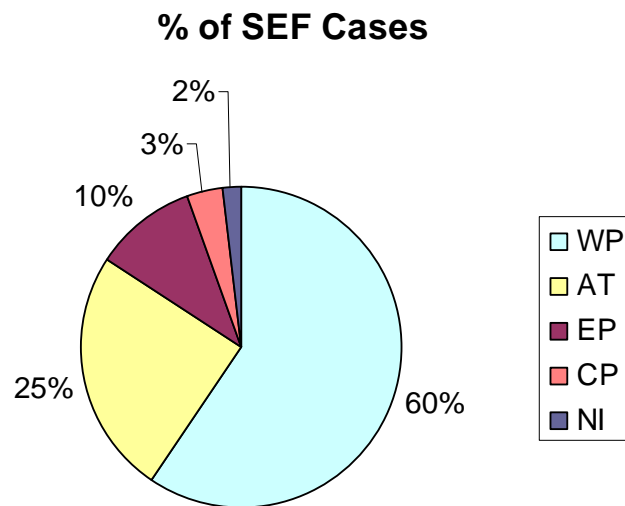


Figure 4.1.8.2.1: Distribution of SEF occurrence by ocean basin.



We have identified a number of environmental features that relate significantly to SEF. These include: the amplitude and meridional structure of the ambient SST anomalies, low-level and mid-level moisture, vertical wind shear, and lapse rates. To identify these environmental features, we first centered the environmental reanalysis fields about the storm center at every 6-hourly storm position fix, and then we performed composite analyses, which were subsequently subjected to statistical significance tests. Additionally, Principal Component Analysis (PCA) was applied to the storm-centric environmental fields and the expansion coefficients of the leading modes of environmental variability were stratified by cases of SEF and tested for statistical significance. For example, the composite analysis for sea surface temperature (SST) is shown in Figure 4.1.8.2.2. We find that SEF is associated with warmer SST in general, and the differences are particularly pronounced to the north of the storm center. This association indicates a reduction of meridional SST gradient associated with SEF, which is physically reconcilable with the hypothesis that SEF is more likely in an environment that is more symmetric around the storm.

We then applied the features identified in the composite analyses and PCA in a Bayesian classification framework that combines climatological probabilities of SEF with “class conditioned” probability density functions for the environmental features. Here, we have two classes (binary classification). Class 1 comprises tropical cyclone fixes with intensities greater than 100 kt but no SEF occurrence in the following 12 hours. Class 2 comprises the sample of cases where SEF did occur within 12 hours. The Bayesian classifier provides probabilities that a particular group of features belongs to a particular class. Figure 4.1.8.2.3 shows how much additional information beyond climatology is gained with the inclusion of the feature matrix. The climatological probability of 26% is what we would always predict if we had no other information. With the inclusion of the feature matrix, we correctly predict, on average, significantly higher probabilities in class 2 and lower probabilities in class 1, as desired.

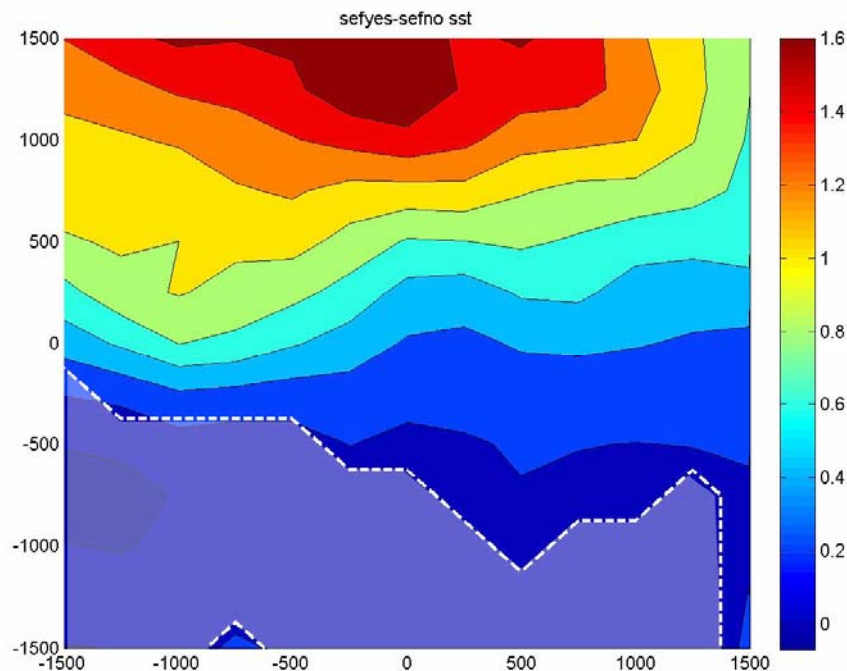


Figure 4.1.8.2.2: Composite differences in storm-centered sea surface temperature between cases where SEF occurred at some time in the following 12 hours versus cases where no SEF occurred. All differences outside the shaded region are significant at 95% in a two-sided t-test.

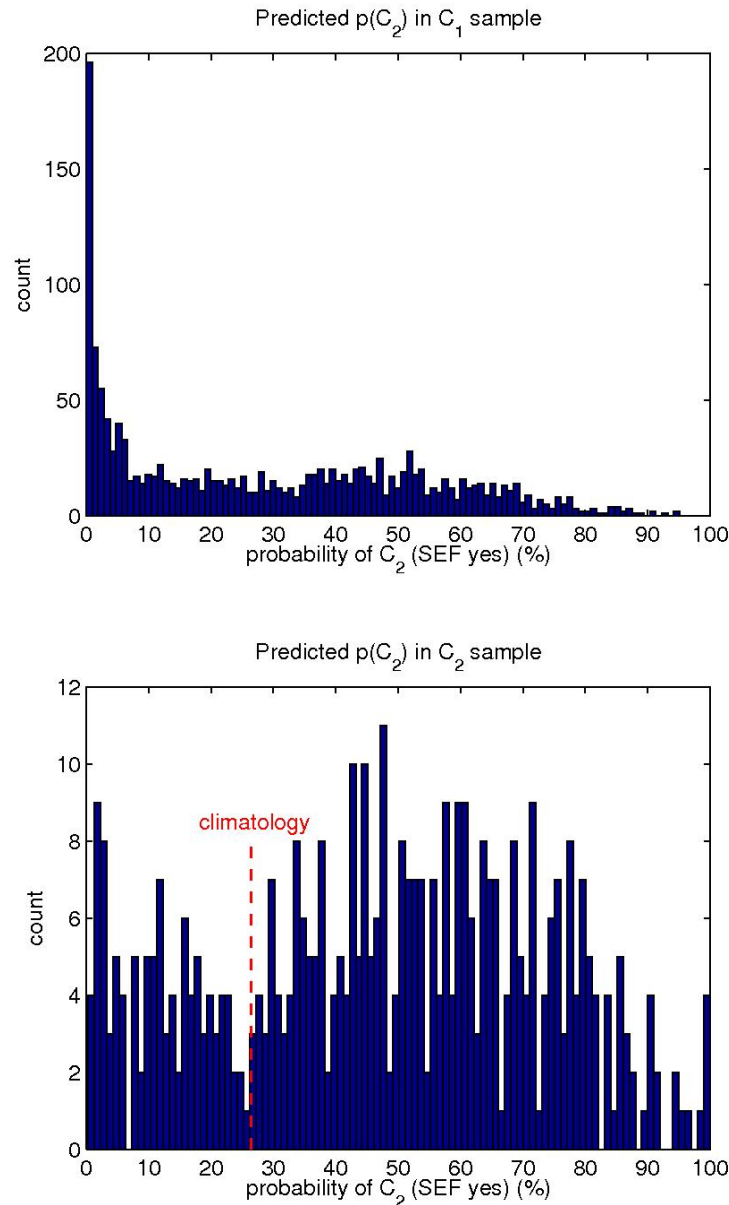


Figure 4.1.8.2.3: Distribution of predicted probabilities that SEF will occur within the next 12 hours. Top panel: cases when SEF did not occur. Bottom panel: cases when SEF did occur. All points to the right of climatology in the bottom panel represent cases where the feature matrix provided useful information.

Our next milestone was the adaptation of our algorithm to operate in the SHIPS-model framework, which will facilitate the potential transition to operations and the eventual merger of our index with the “Annular Hurricane Index” being developed by our NOAA/NESDIS collaborators at CIRA/CSU. The next, and perhaps most important, milestone was the inclusion of satellite information from GOES.

We constructed a new SEF index based on environmental features from the SHIPS-model developmental data set applied to a Bayesian classification scheme. Utilizing the SHIPS data set allows for a very simple merging of our index with the annular hurricane index being developed by our CIRA/NESDIS collaborators, which also uses the SHIPS developmental data set. Some of our results are shown in



Figure 4.1.8.2.4. The Bayes classifier considers climatological probability of SEF in concert with probabilities based on the storm environment. For example, if we had no environmental information at all, we would simply assign a probability of SEF based on previously documented frequencies of occurrence. For storms of intensity greater than 100 kt that did not just complete an eyewall replacement cycle, the North Atlantic climatological probability of SEF in the following 12 hour is around 30% on average.

The improvement of the algorithm when the GOES data is included is shown and described in Figure 4.1.8.2.5. Compared to Figure 4.1.8.2.4, Figure 4.1.8.2.5 reflects improvements made through our continuing analysis of the SHIPS environmental features and modifications to our SEF climatology based on the inclusion of new data. Table 4.1.8.2.2 shows the “confusion matrix” for the present forms of the algorithm applied to the North Atlantic. To create this, we reduced our continuous probability estimates to a simple binary classifier by using 50% as a threshold between predicting SEF and non-SEF. The effects that the environmental features and the GOES satellite-derived features have on the accuracy of the predictions can be seen by the changes in the elements of the matrix, and are further quantified in Table 4.1.8.2.3. Table 4.1.8.2.3 shows the Brier Skill Score, Success Rate (correct predictions), False Positive Rate (false alarms), and False Negative Rate (misses) for climatology, and the algorithm with and without the inclusion of the satellite information. The algorithm performs skillfully and the satellite information measurably increases the skill. When the satellite information is included, the skill level is 31% above climatology. Cross-validation of the algorithm is in progress and we can expect some reduction of this skill in an operational setting. These preliminary results are very encouraging, and we’re presently looking more deeply into how to optimize the GOES-based improvements to our model.

We have also made progress toward a more flexible climatology to apply to the Bayes classifier. For example, we have enough cases now to stratify the classes (SEF and non-SEF) by current intensity, which has a significant effect on the climatological probability of SEF. In the future we hope to conduct a more thorough cross-validation of our algorithm so that we can get a better idea of what to expect in an operational setting. We are also looking at ways to objectively measure skill beyond the application of confusion matrices, which is a method for quantifying the skill of classifiers but does not utilize the additional information of probabilities that our algorithm provides (beyond, for example, a linear discriminant method). We would like to extend this to measure the skill of our assigned probabilities. We are also looking at ways to reduce the effect that the storms themselves have on the SHIPS environmental features. The storms tend to contaminate a large surrounding region, making it difficult to measure the true storm environment. Using reanalysis fields, we are looking at variance maps to determine whether measuring the environment at a location some time before the storm arrives is a reasonable proxy for the environment at the time of the storm’s arrival at that location.

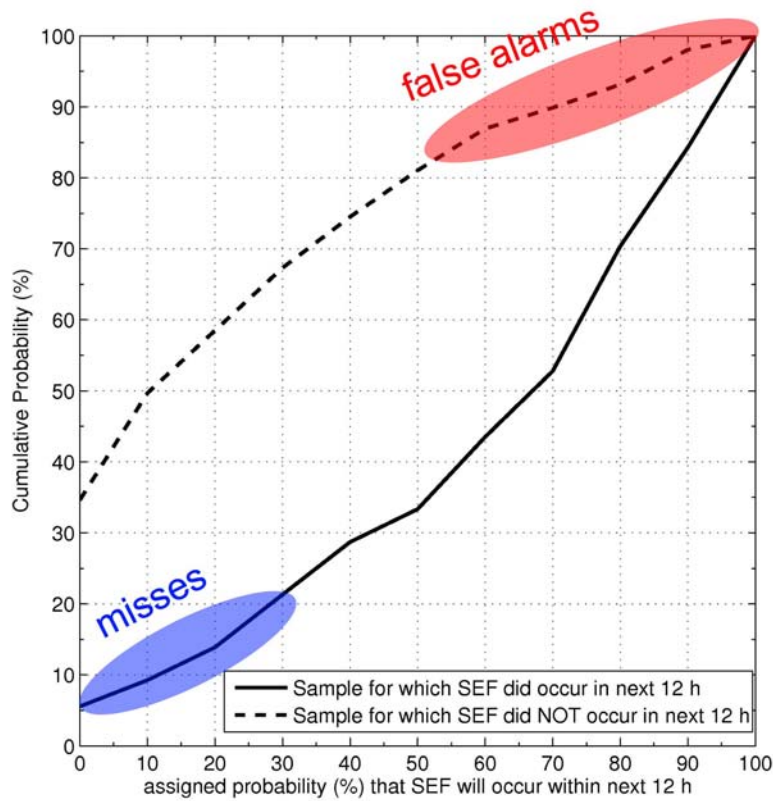


Figure 4.1.8.2.4: Cumulative probability of the probability that secondary eyewall formation (SEF) will occur within the next 12 hour, as assigned by our new SHIPS developmental data set-based algorithm. Solid line: probability of SEF assigned to storms that did undergo SEF. Dashed line: probability of SEF assigned to storms that did not undergo SEF. The algorithm is skillful, assigning higher probability than the climatological probability (of around 30%) in 80% of SEF cases. This is analogous to a success rate of 80%. The algorithm also assigns a probability of SEF that is greater than 50% in about 20% of non-SEF cases. This is a subjective measure of our false-alarm rate.

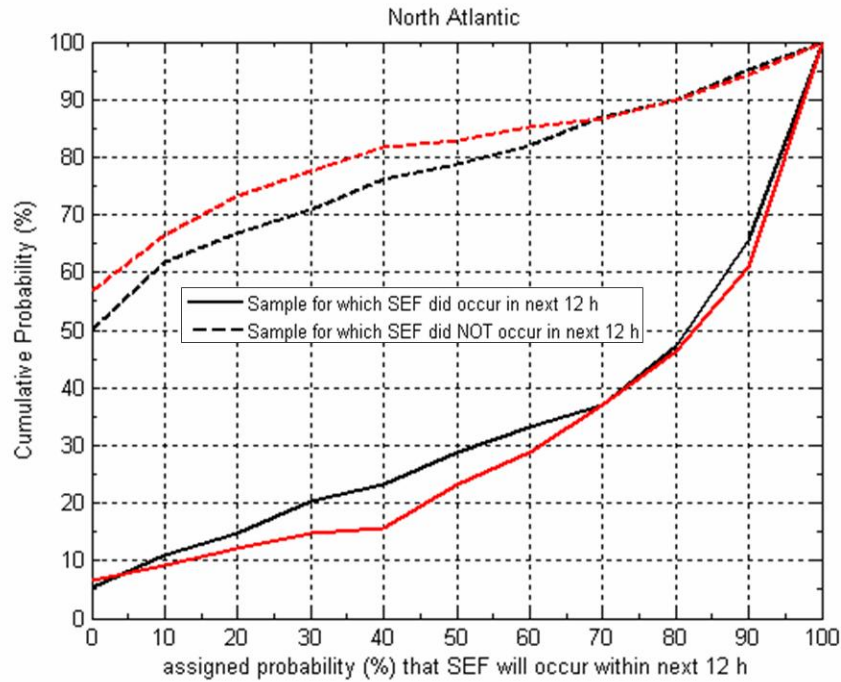


Figure 4.1.8.2.5: Similar to Figure 4.1.8.2.4, but with modifications to the algorithm, and with the inclusion of the SHIPS GOES-based features. The black lines show the algorithm performance in the North Atlantic without the GOES-based features, and the red lines show the improvement with the GOES-based features. Our assigned probabilities for both the SEF and non-SEF cases improve measurably and there is consistent improvement (no degradation of skill). For example, the probability of assigning a low probability of SEF ($P < 30\%$) to non-SEF cases increases from 70% to roughly 80%. The probability of assigning a high probability of SEF ($P > 30\%$) to SEF cases increases from 80% to 85%.

Table 4.1.8.2.2: Confusion matrix resulting from North Atlantic climatology (top rows), and for the algorithm without the GOES features (middle rows) and with the GOES features (bottom rows). The two columns represent instances of the *predicted* class and the rows represent instances of the *observed* class. For the case of climatology, we would simply always predict no SEF (we would be correct about 70% of the time and would miss all actual SEF). The improvements can be seen with the inclusion of the environmental features, and again with the further inclusion of the GOES information.

		SEF-YES (predicted)	SEF-NO (predicted)
Climatology	SEF-YES (observed)	0 (success)	108 (miss)
	SEF-NO (observed)	0 (false alarm)	251 (success)
Environmental	SEF-YES (observed)	81 (success)	27 (miss)
	SEF-NO (observed)	51 (false alarm)	200 (success)
Env. plus GOES	SEF-YES (observed)	85 (success)	23 (miss)
	SEF-NO (observed)	42 (false alarm)	209 (success)

Table 4.1.8.2.3: Performance metrics of the algorithm.

	Brier Skill Score	Success Rate	False Alarm Rate	Miss Rate
Climatology	0%	70%	0%	100%
Environmental	23%	78%	20%	25%
Env. plus GOES	31%	82%	17%	21%



4.1.9. Visualization (HYDRA Integration) – Tom Rink and Tom Achtor

Proposed Work

The primary goal of the Visualization project is the integration of HYDRA into the GOES-R visualization and data analysis environment. The first phase of this work is to explore and make an assessment of the process required to integrate the strengths of HYDRA into the Unidata Integrated Data View (IDV), and subsequently into McIDAS-V. The focus of this development will enhance the analysis of high spectral, spatial and temporal resolution remote sensing data produced by the next generation GOES suite of instruments. It was deemed important to create some demonstrations of how this can be accomplished, and some examples of what the initial system might look like. Figure 4.1.9.1 shows MODIS Aerosol Optical Thickness, and MODIS Cloud Optical Properties combined with the CALIPSO Lidar in a 3D display.

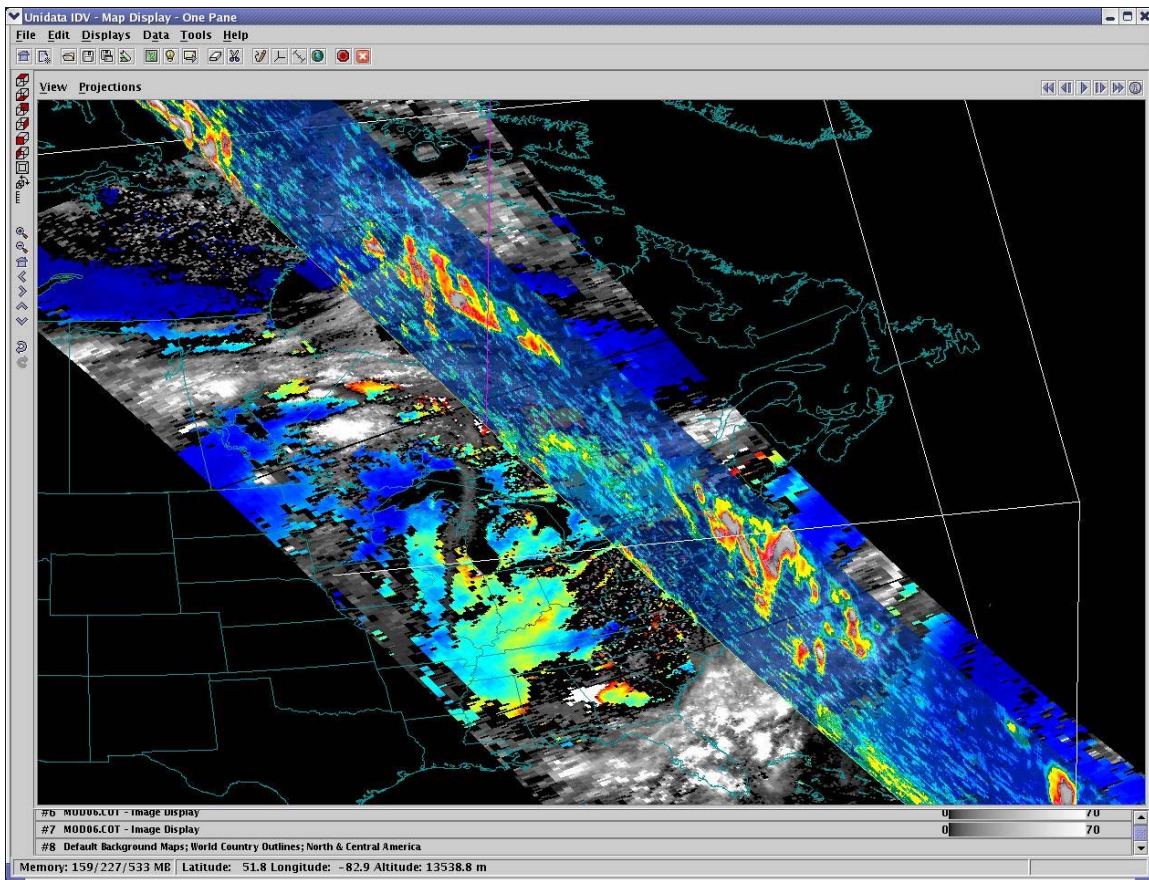


Figure 4.1.9.1: 3D display of MODIS Aerosol Optical Thickness, and MODIS Cloud Optical Properties combined with the CALIPSO Lidar

Summary of Accomplishments and Findings

A key implementation goal is to generalize HYDRA's abstract data access layer for multi- and hyper-spectral Level 1B and Level 2 data sets. Work is in progress to open up HYDRA's local read access to HDF4 via Java, and to create adapters to HYDRA's data access classes that can be used within McIDAS-V. There are two concurrent development paths here: the first involves the Level 2 products, e.g. MODIS and AIRS, and the second involves primarily the Level 1B hyper-spectral data products. The former is a more natural fit to the IDV/McIDAS-V because of the analogous relationship to the display and internal



data representation of meteorology grids. The later is more involved, and will likely take the most effort of the two because of the specialized strategies employed in HYDRA to visualize, analyze and interrogate multi and hyper-spectral Level1B data. Good progress has been made on adapting HYDRA data to the IDV/McIDAS-V display environment, and this process was expedited by the fact that both HYDRA and the IDV/McIDAS-V have their own adapters to the VisAD data model. The goal of the current work is to more cleanly integrate the functionality of both applications.

New development also includes class extensions for data sources and controls specific to hyper-spectral radiances (Level 1B, Level 1C), which have been mostly completed and tested on AIRS and IASI data. Excellent cooperation with Unidata on the data storage format issues will enable Java access to HDF5 and HDF4 file formats. Testing is underway now using the HDF5 format IASI Level 1C available from the Eumetsat archive system. This is important from a more technical standpoint, in that the current libraries in HYDRA for accessing HDF4 via Java are difficult to maintain, and will be replaced by the new Java-NetCDF library.

Recent progress in employing data and display software components to add HYDRA-type functionality to the McIDAS-V architecture is shown in Figure 4.1.9.2, a McIDAS-V display of IASI spectra and imagery demonstrating the interactive capability to investigate all IASI spectral bands. In addition to hyperspectral data support, work is progressing on the incorporation of CALIPSO and CloudSat data into McIDAS-V, as well as, several MODIS products. Work in the upcoming quarter will focus on incorporating analysis capabilities found in HYDRA into McIDAS-V, building on the work completed so far.

In October 2007 the first alpha release of McIDAS-V was made available to the McIDAS Users Group. The software is now freely available to all, and can be found at:
<http://www.ssec.wisc.edu/mcidas/software/v/>

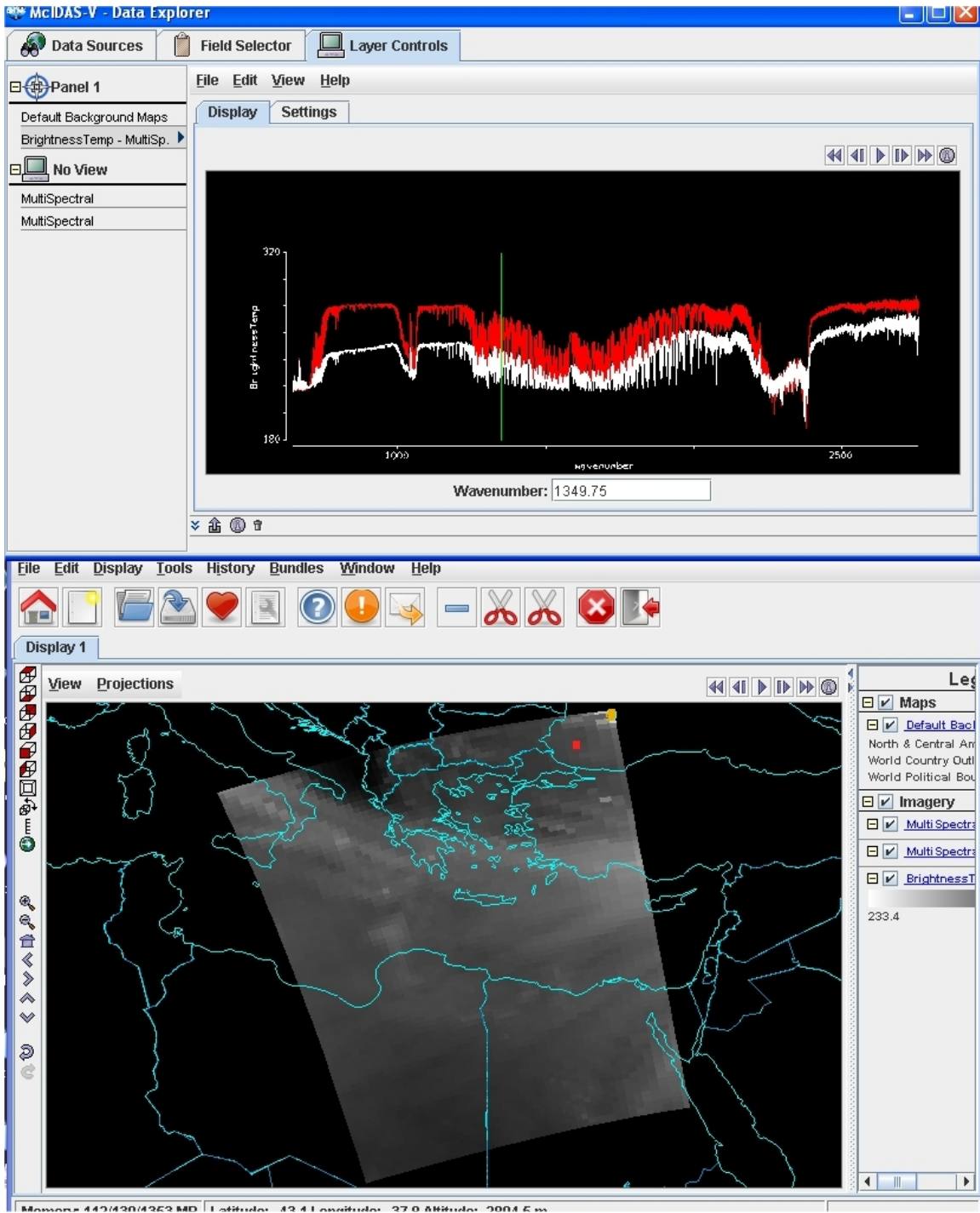


Figure 4.1.9.2: McIDAS-V display of IASI spectra (top) with slider bar to display spectral bands (bottom). The user can select points in the image and display the spectra for that pixel, or select the spectral band and display the image.



4.2. Cal/Val Efforts in support of GOES – Dave Tobin

Proposed Work

Proposed tasks for this effort included participation in GSICS meetings, participation in GOES-R Cal/Val planning, analyses of benchmark aircraft validation data sets in support of GSICS, simulation studies to estimate uncertainties in satellite sensor intercalibrations, and characterization and analysis of ARM site data for atmospheric sounding validation.

Summary of Accomplishments and Findings

Key accomplishments and findings include:

We performed simulation studies using MODIS data to assess the ability of a proposed infrared climate benchmark sensor (CLARREO) to intercalibrate operational sounders. This provides a robust and accurate way to assess the radiometric uncertainties in the sensor intercomparisons due to differences in the spatial and temporal sampling of CLARREO and the operational sounders. We find that with modest CLARREO radiometric noise performance that the collocation errors for monthly ensembles of intercomparisons are on the order of 0.01K. Future work involves studying the impact of the CLARREO footprint size on the intercomparison uncertainties and also using the same simulation framework to estimate the uncertainties in Simultaneous Nadir Overpass intercomparisons between existing observations such as between METOP-A IASI and Aqua AIRS.

Global intercomparisons of Aqua AIRS and MODIS infrared radiance observations over five years were performed to assess the calibration accuracy and trends of the observations. Preliminary analyses of the intercomparisons suggest that there are no significant changes in the observed biases as a function of time.

We performed intercomparisons of METOP-A IASI and Aqua AIRS infrared spectral observations using Simultaneous Nadir Observations over the METOP-A mission time period. The results to date confirm the hypotheses that the high spectral resolution sounder observations can be used as benchmark observations, to within a determined uncertainty, for assessment of other Geo and Leo observations with the GSICS framework. No significant trends are detected and mean differences are generally on the order of 0.1K or less. The remaining differences are under investigation. See accompanying Figure 4.2.1.

Quality control on ARM dedicated radiosonde launch data collected in the fall of 2007 were performed for METOP-A and Aqua overpasses of the ARM sites.

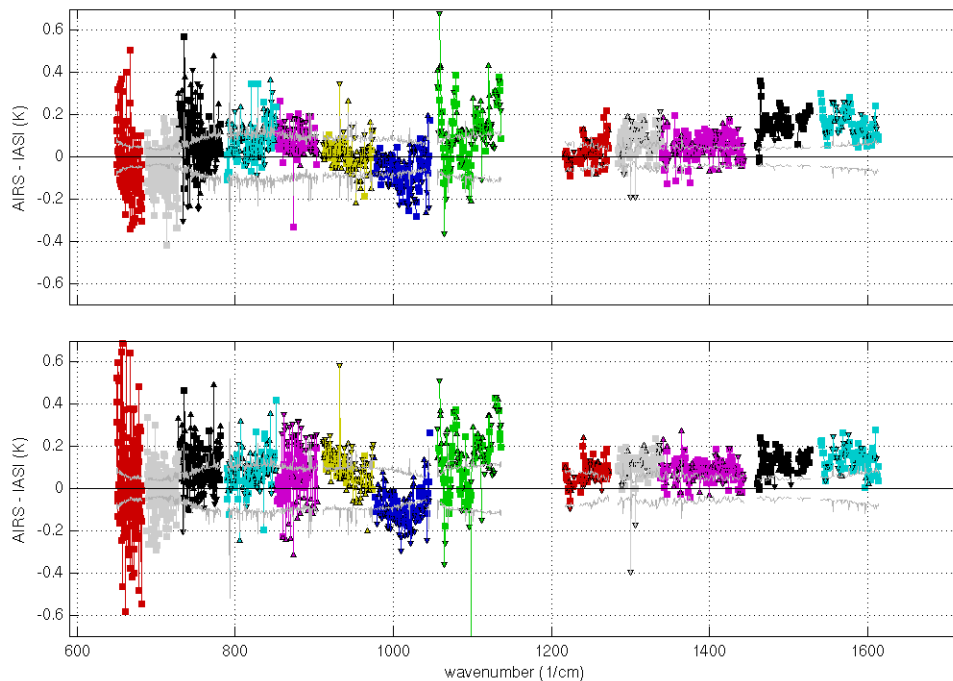


Figure 4.2.1: Differences between AIRS and IASI spectral radiances collected for Simultaneous Nadir Overpasses in the northern (top panel) and southern (bottom panel) hemispheres. The curves are color-coded according to the AIRS detector arrays and the uncertainty of the differences are shown as the grey curve.

Publications and Conference reports

Holz, R.E., F. Nagle, D.C. Tobin, R.O. Knuteson, S. Dutcher, H.E. Revercomb. An investigation of the capability of CLARREO to calibrate operation sounders with a focus on both spatial and temporal sampling uncertainties, (2007), *Eos Trans. AGU*, 88 (52), Fall Meet. Suppl., Abstract A31B-0313.

4.3. Nowcasting Activities – Ralph Petersen, Robert Aune

Proposed work

The overall goal of this project is to provide forecasters with new tools to help identify areas of convective destabilization 3-6 hours in advance of storm development based on the moisture data from current and future GOES satellites. This year's efforts were a logical continuation and progression of work performed during the past several years, including: 1) continued development and testing of the new Lagrangian-based dynamical nowcasting model, 2) improved utilization of satellite sounders by projecting GOES sounder products ahead in time and space to provide new nowcasting products, 3) development of visualization tools to view predicted Derived Product Images (DPIs) in formats identical to the current observational products and 4) initial interactions with NWSFOs, NSL and NCEP/SPC to evaluate new objective nowcasting products.

Summary of accomplishments and findings

Specific efforts this year have been directed toward three major tasks, including: Running the Lagrangian Nearcasting system running in real time, determining the optimal predictor for DPI Nowcasts, and determining the utility of Nowcasting products in WFOs.



Note: because the term “Nowcasts is being heavily used to describe 0-1 hr projections made by extrapolation of radar observations, these slightly longer range products based primarily on satellite data are now being described as “Nearcasts”, as will be the case throughout the remainder of this report.

Running the Lagrangian Nearcasting System running in real time

Transfer of the Nearcasting system from the developmental environment to fully automated Linux computers involved not only porting the codes from the current research-based computers, but also assuring that the highest-resolution DPI products and RUC-based initial wind data are available in a timely manner. Connections to the existing real-time page also needed to be completed for the products to be made available to users in real time.

Although these activities are almost completed, a number of modifications were added based on NWS preferences. Most importantly, output from the Nearcasting system is being made available primarily in the newly implemented WMO grid-point data communications standard (GRIB-II), with web-page output taking on a more secondary role. The decision to make this change was based on positive reception to the Nearcast products from a variety of NWS/WFO, especially at the Great Lakes Operational Meteorology (GLOM) Workshop. Providing the data in GRIB-II format allows the Nearcast products to be displayed directly on the NWS AWIPS operational workstations, and will provide a much more effective means of incorporating the new products into real-time use. Use on AWIPS workstations also provides an effective means of obtaining the user feedback necessary for future larger-scale implementation.

In September, a CCNY-CREST graduate student was trained on the use of the model at CIMSS with the goal of integrating the moisture prediction capabilities of the Nearcasting Model with the hydrological prediction efforts developing at CCNY. Discussions are underway to determine whether we should transfer the Linux-based version of the system to CCNY or whether we should initially expand our prediction domain to cover the New York area. The latter option reduces the complications of developing additional data ingest capabilities at CCNY before products become available there.

Determining the optimal predictor for DPI Nearcasts

Tests of the Nearcasting system were proposed using both multi-layer Total Precipitable Water (TPW) and Equivalent Potential Temperature (θ_e) as conservative tracers.

Efforts in this area have been concentrated in three areas, resolving imbalances in the RUC wind data used to initialize the DPI trajectories, adding information about cloudiness and product uncertainty, and verifying the accuracy and timing of the rapid moisture changes predicted by the Nearcasts after clouds have formed.

θ_e profilers have been obtained for the 13 April 2006 hailstorm case and are scheduled for testing as a truer definition of convective instability. Before the θ_e tests could be run, however, we needed to remove undesirable, small-scale ‘noise’ from the initial wind fields obtained from the RUC-II. Tests showed that significant smoothing was necessary to eliminate small-scale imbalances from the initial wind fields. The initial wind fields contain excessive divergence and deformation that can be amplified in the later 2-3 hours of the Nearcasts. Alternatives based on partial geostrophic and/or semi-geostrophic balance have shown little additional success. In the end, smoothed RUC 3-hour wind forecasts were chosen. This choice was made both because these forecasts appear to be more dynamically consistent than the initial analyses and because they are available immediately upon access to the GOES DPI data. Immediate access allows the Nearcasts to be run sooner.



It should be noted that after conversion to the Linux-based computers and the use of GRIB-II as the output medium, the gridded Nearcasts are now available within 2-3 minutes after the DPI products become available – meeting the goal of becoming a ‘real-time’ forecasting tool.

Based on feedback from forecasters and attendees at the 2007 AMS Annual Meeting, a change has been made to the Nearcast displays before training can begin at WFOs. The first of these involves a new procedure that adds ‘cloud obstruction’ information to the output fields. At every grid point, a display flag is added to indicate whether or not any DPI observations had been projected into the 10 by 10 km display boxes during the past several during the past six hourly Nearcast cycles. If no data have been present at that site, a shade of gray is displayed rather than extrapolating data from surrounding points. This feature assures users that the products are reflecting GOES *observations* and not simply a projection of a ‘first guess’ field.

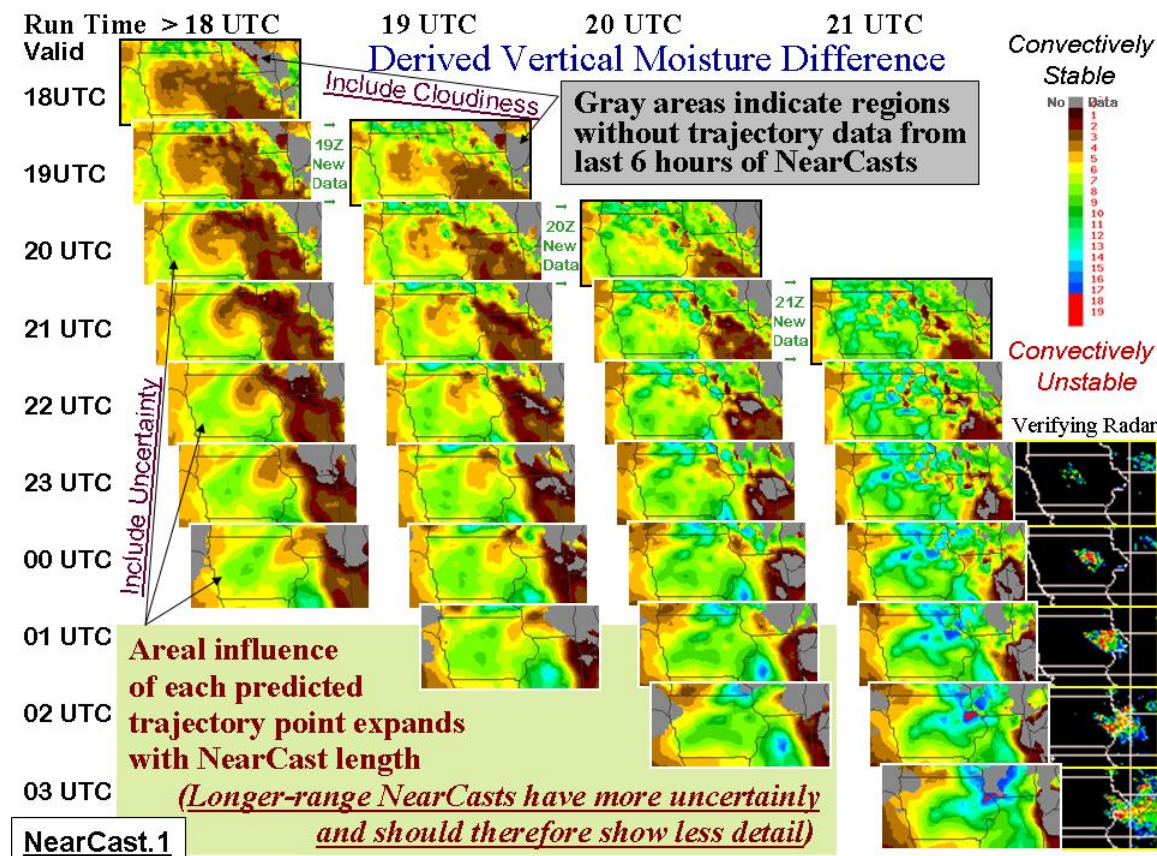


Figure 4.3.1: Illustration of Nearcast image output after adding 1) indications of areas where no DPI projections were available (“Cloudiness”), and 2) increasing uncertainty with Nearcast range. The second change involved the addition of ‘confidence’ into the output products, since users felt that very-small-scale details present in the 2-3 hour projections could be trusted more than those at longer ranges. To account for the increasing in uncertainty in the longer range Nearcast, the ‘radius of influence’ used to interpolate the Nearcast trajectory parcels during the process of creating regularly spaced output display grids was increased with each projection times. The change produces fields that retain full observation details at the initial times, but show less detail at longer prediction time.

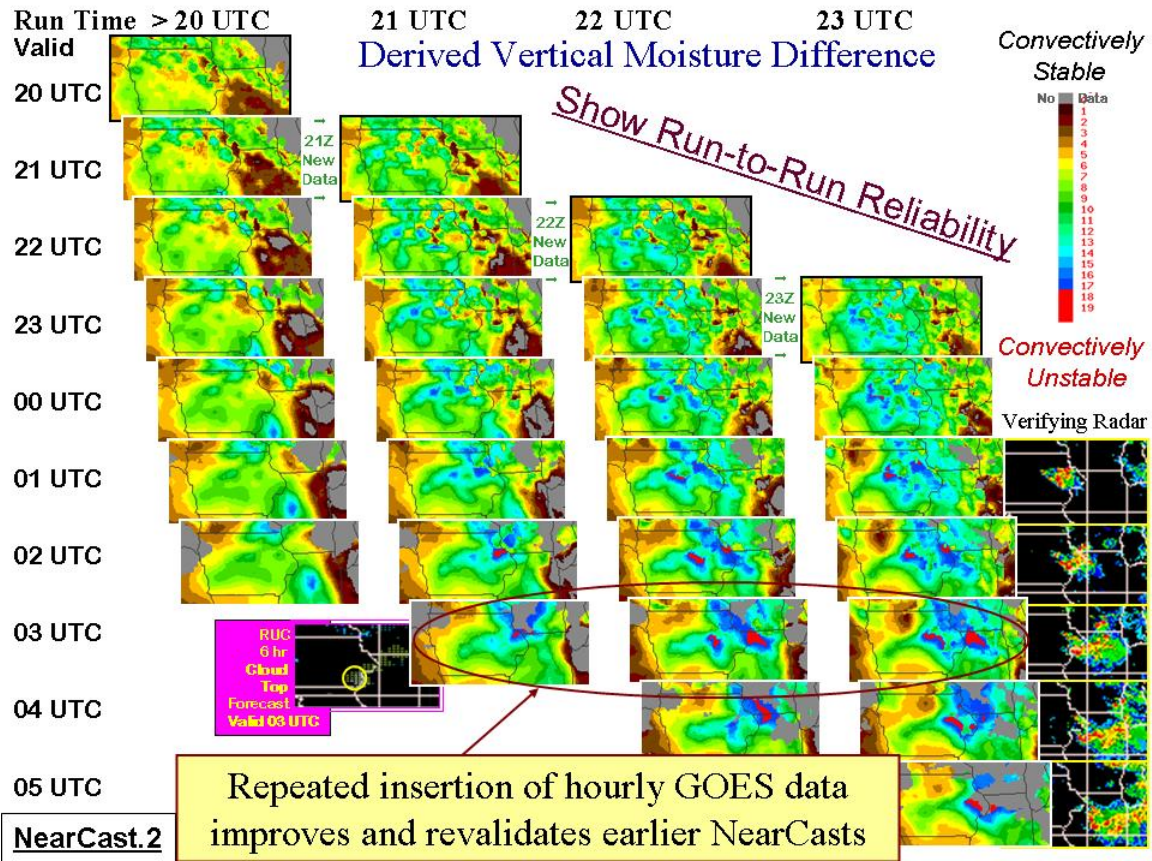


Figure 4.3.2: Illustration of temporal consistency and improvement of Nearcast projections from successive hourly runs with additional GOES DPI data insertions.

Because the Nearcasting products are updated every hour, forecasters can also improve their confidence in specific predictions by comparing sequences of output products for run-to-run consistency, as shown in Figure 4.3.2. This example not only shows very good agreement between successive runs regarding the location of the area of weaker stability across east-central IA and SW WI/NW IL, but also indicates that later runs indicated further weakening of the stability in SE WIS/NW IL where severe storms developed. If desired, additional time-lagged consensus products could be developed in the future.

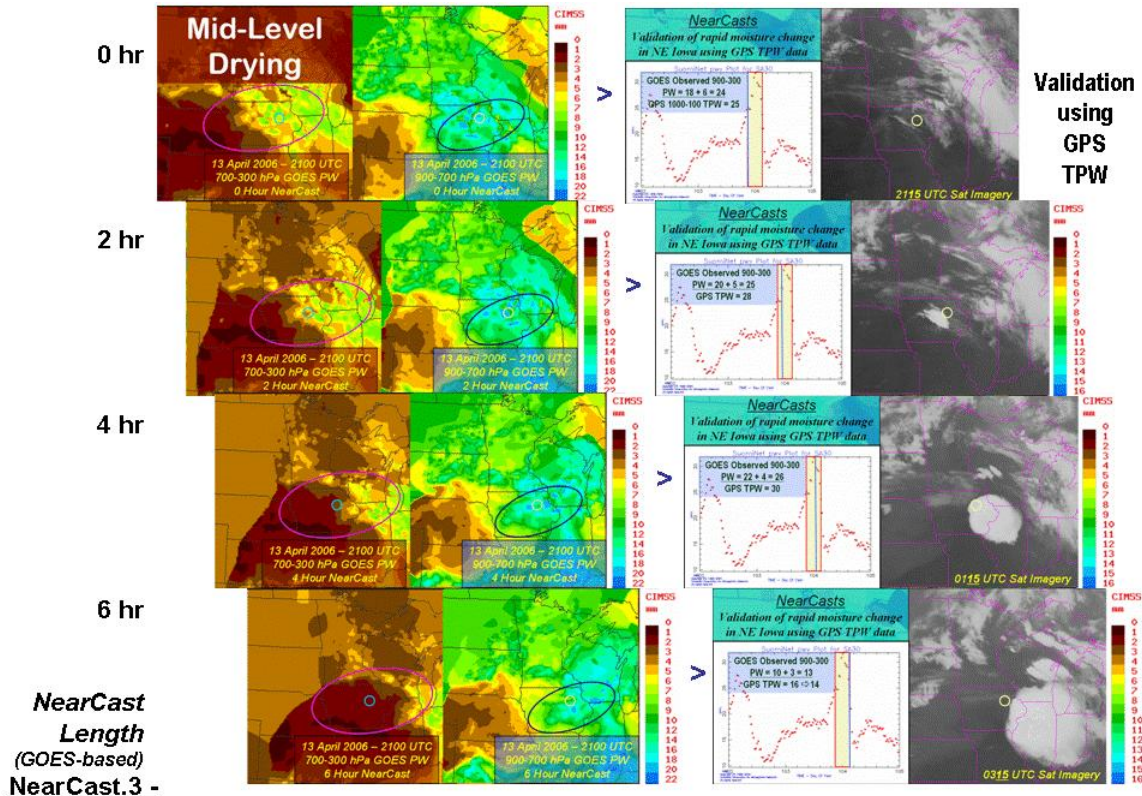


Figure 4.3.3: Point comparisons over NE Iowa of multi-layer Nearcasts of GOES DPIs between ~900-300 hPa with independent surface-based GPS Total-column Precipitable Water measurements.

Verifications were also made using surface-based GPS TPW as a standard (see Figure 4.3.3). These tests validate rapid successions of water vapor increases and decreases observed by GOES Nearcast products, but that were present as vividly in NWP guidance. For example, during the 13 April case, comparisons at a surface GPS site in NE Iowa show excellent agreement. The absolute values of the precipitable water agree very closely (indicating small biases). More importantly, both the rapid increase in lower-level moisture anticipated by the Nearcasts prior to the nearby thunderstorm development and the rapid decrease of moisture at both levels after the thunderstorm passage were well synchronized with the rapid increase and decrease in TPW noted by the independent GPI observations. The ability to capture both rapid local increase and decreases in moisture bodes well for the ability of forecasters to increase Probability-of-Detection and decrease False-Alarm-Ratios for convective events using the Nearcasting tools. These types of verifications with independent data sources are especially important for this project because verifications using other satellite systems are often difficult due to the development of clouds in the areas of interest.

Determine utility of Nearcasting products in WFOs

Possibly the most important work for the ultimate success of this effort is the education and training of forecasters in local WFOs on the concept and interpretation of the Lagrangian GOES Nearcasting systems for their everyday use, evaluation and feedback. In addition to overall system improvements, the objective of this evaluation is to improve forecasts of the timing and location of hard-to-predict isolated thunderstorms, and will help assess the utility of the DPI predictions of both 'event' and 'non-event' forecasts.



The NWS/WFO at Green Bay, WI (GRB) has already requested to be included in the Nearcast evaluation program. Other area offices (especially MKX) offered to participate at the NWS GLOM workshop in September. We plan to expand discussion to include the NWS Central region Headquarters and NCEP/Aviation Weather Center in 2008.

GRB has also offered to host a small regional workshop, which, among other things, is intended to expand the scope of the Nearcast model evaluation in January. This workshop would include all of their forecast staff plus Science and Operations Officers (SOOs) and forecasters from NWS Marquette. The final mix of display mediums (web-based or AWIPS) used for evaluation in these locations would be based upon initial experience in GRB. Although the initial feedback will be subjective, we will work with the WFOs to develop more objective feedback procedures, based in part of experience gained from the similar efforts at the NASA/SPoRT program.

Based on the WFO reaction to the DPI Nearcast products, preliminary interactions have begun with EUMETSAT regarding initiating pre-ABI tests using Meteosat products as a surrogate ABI database. One option would involve performing these risk-reduction tests over South Africa because that region has pre-convective severe weather signatures that are very similar to those found in the U.S. The South African Weather Service has already established an active applications program with Meteosat and staff members have expressed interest in collaboration.

Publications and Conference Reports

Petersen, R., R. Aune, 2007: An objective nowcasting tool that optimizes the impact of GOES Derived Product Imagery in very-short-range forecasts and Nowcasts. AMS Symposium on the Integrated Atmospheric Observing System, San Antonio, TX.

Petersen, R., R. Aune, 2007: An objective nowcasting tool that optimizes the impact of GOES Derived Product Imagery in very-short-range forecasts and Nowcasts. AMS Sattelite Meteorology Conference, San Antonio, TX.

Petersen, R., R. Aune, July. 2007: An objective Nearcasting tool that optimizes the impact of GOES Derived Product Imagery in very-short-range forecasts and Nowcasts. IUGG quadrennial meeting, Perugia, Italy.

Petersen, R., R. Aune, Sept. 2007: An objective Nearcasting tool that optimizes the impact of GOES Derived Product Imagery in fore casting isolated convection. NWS Great Lakes Forecasting Workshop, Milwaukee, WI.

Petersen, R., R. Aune, Sept. 2007: An objective Nearcasting tool that optimizes the impact of GOES Derived Product Imagery in fore casting isolated convection. Joint Eumetsat/AMS Satellite Conference, Amsterdam, The Netherlands.

4.4. Data Assimilation/Simulations – Jason Otkin and Allen Huang

To support GOES-R Risk Reduction and Algorithm Working Group research activities, two large-scale, high-resolution Weather Research and Forecasting (WRF) model simulations were performed on a high-performance supercomputer at the National Center for Supercomputing Applications (NCSA). The first simulation contained three nested domains configured to represent the anticipated GOES-R scanning regions (i.e. full disk, CONUS, and mesoscale). The outermost domain covered most of the GOES-R viewing area with 6-km horizontal resolution, while the inner two domains covered the CONUS and



mesoscale regions with 2-km and 667-m resolution, respectively. The simulation required 1 TB of memory and ~74,000 CPU hours to complete. A representative example of the simulated 300 hPa height and winds from the full disk domain is shown in Figure 4.4.1. Model-simulated temperature, moisture, and cloud data were subsequently passed through the Successive Order of Interaction (SOI) forward radiative transfer model in order to generate proxy Advanced Baseline Imager (ABI) radiance and reflectance data sets.

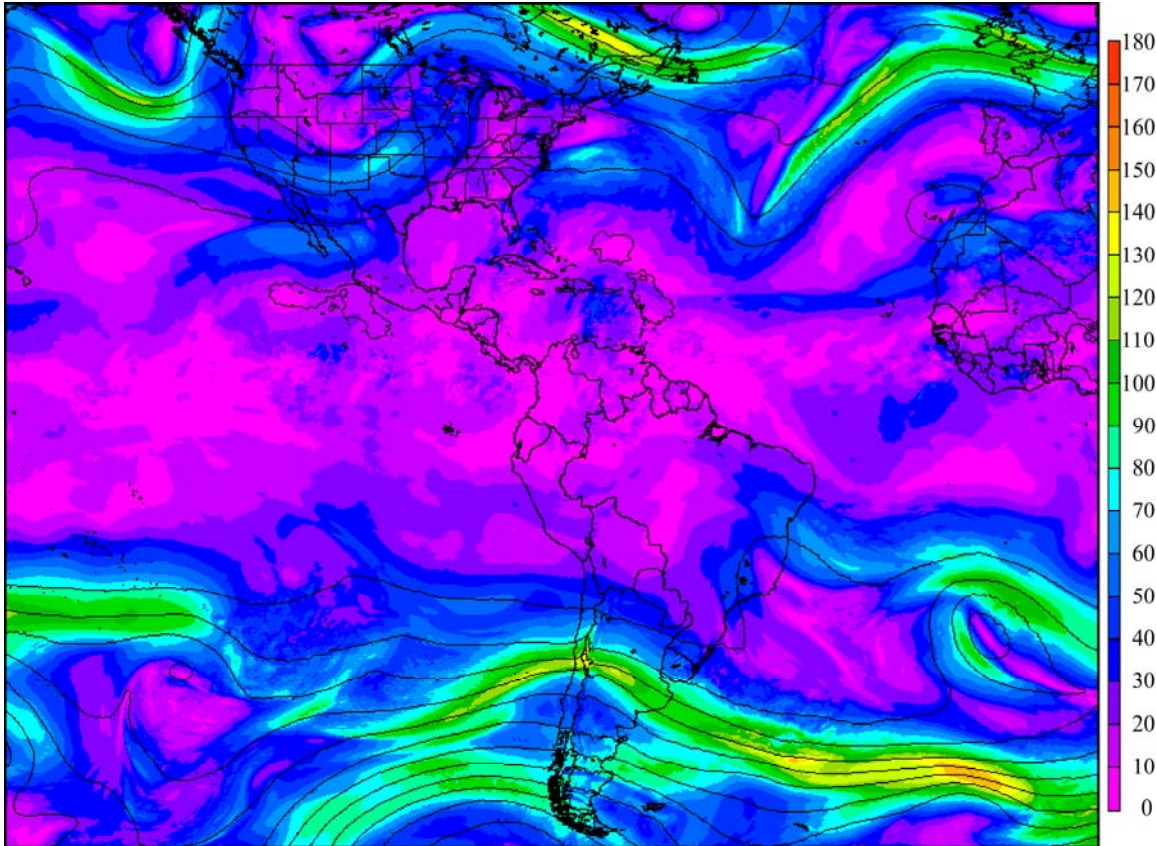


Figure 4.4.1: WRF-simulated 300 hPa height (black lines) and winds (kts; shaded) valid at 1800 UTC on 04 June 2005.

In an effort to more thoroughly characterize the realism of proxy ABI radiance data sets derived from numerical model output, an additional high-resolution model simulation was performed over the Meteosat viewing domain. The simulation contained a single domain covering the entire Meteosat viewing area between 58° S and 58° N with 3-km horizontal resolution. This domain was chosen in order to leverage the availability of many ABI-like channels on SEVIRI, as well as to utilize its high spatial and temporal resolution. Due to its large size, the simulation required 1.5 TB of memory and ~95,000 CPU hours to complete. Simulated SEVIRI visible reflectance and infrared brightness temperature data sets currently being generated for this case will be heavily utilized in an upcoming validation study. A representative example of simulated SEVIRI 10.8 μm brightness temperatures is shown in Figure 4.4.2.

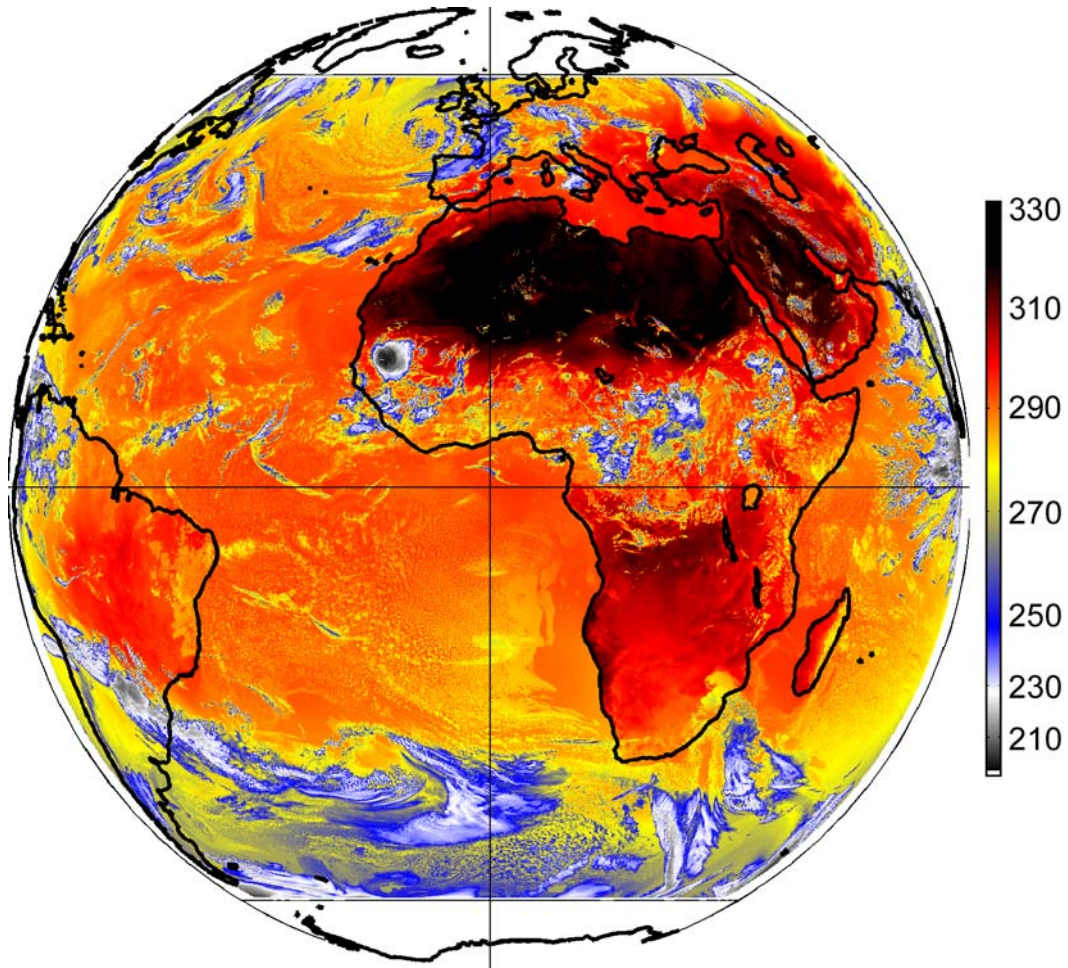


Figure 4.4.2: Simulated SEVIRI 10.8 mm brightness temperatures (K) valid at 1200 UTC on 16 August 2006.

Since the accuracy of simulated cloudy-sky radiances is strongly dependent upon the ability of the WRF model to realistically simulate cloud morphology, a detailed comparison of model-simulated and MODIS-derived cloud data was completed for a case study containing a wide assortment of cloud types. An ensemble of eight high-resolution model simulations was constructed using four cloud microphysical and two planetary boundary layer (PBL) parameterization schemes characterized by different levels of complexity. Inspection of the simulated data sets revealed that the PBL and microphysics schemes both exerted a strong influence on the spatial distribution and physical properties of the simulated cloud fields. Overall, the simulated cloud properties were broadly similar to the MODIS observations, although several large discrepancies were also identified. A journal article describing the results of this study was recently accepted for publication in *Monthly Weather Review*.

Publications and Conference Reports

Otkin, J.A., and T.J. Greenwald, 2007: Comparison of WRF model-simulated and MODIS-derived cloud data. *Mon. Wea. Rev.*, accepted for publication.

Otkin, J. A., and T.J. Greenwald, 2007: An intercomparison of MODIS-derived and WRF-simulated cloud data for an intense extratropical cyclone. 18th Conf. on Numerical Weather Prediction, Park City, UT.



Otkin, J.A., H.-L. Huang, T.J. Greenwald, E.R. Olson, and J. Sieglaff, 2007: Large-scale WRF-simulated proxy atmospheric profile data sets used to support GOES-R research activities. 15th Satellite Meteorology and Oceanography Conference, Amsterdam, Netherlands.

Otkin, J.A., and H.-L. Huang, 2007: Large-scale high-resolution WRF model simulations used for GOES-R research activities. 8th Annual WRF User's Workshop, Boulder, CO.

Otkin, J.A., and T. Greenwald, 2007: An intercomparison of MODIS-derived and WRF-simulated cloud data for an intense extratropical cyclone. 18th Conf. on Numerical Weather Prediction, Park City, UT.

Otkin, J.A., H.-L. Huang, T. Greenwald, E.R. Olson, and J. Sieglaff, 2007: Large-scale WRF-simulated proxy atmospheric profile data sets used to support GOES-R research activities. 15th Satellite Meteorology and Oceanography Conference, Amsterdam, Netherlands.

4.5. Ground Systems Processing – Maciej Smuga-Otto and Robert Knuteson

Proposed Work

In 2006, SSEC/CIMSS demonstrated a lightweight web-oriented system for distributed processing, management and visualization of hyperspectral data—nicknamed Origami. Extensions to Origami proposed for 2007 involved integration of new algorithms to the Origami framework, the packaging of Origami for distribution across multiple projects, and development of the infrastructure itself to make the Origami framework more robust.

Summary of Accomplishments and Findings

In 2007, several candidate algorithms slated for integration into Origami were moved to an XML (eXtensible Markup Language)-based interface description standard, and tools were developed to generate Origami-compatible source language interface files from this XML description. It is much easier to automatically generate a new source language (C/C++, Fortran, Java, etc.) interface file from an XML description than it is to translate an interface file written in one source language into another. The algorithms in question, used for calibration Level 1 of raw data from potential hyperspectral imaging sounder, already had well-established interfaces to very specific coding frameworks within which they were developed, and needed to be adapted to Origami. The XML interface files provided the cleanest way to do this, as they assured the least coupling between the algorithm code and the surrounding environment. The flexibility of this approach was further demonstrated when this approach was adapted, with few changes, to a similar challenge in deploying Level 2 candidate algorithms for Advanced Baseline Imager (ABI) work under separate funding. The GEOCAT development framework is being used as the application testbed for this GOES-R risk reduction demonstration of interactive computing.

The Origami task dispatcher, in order to fulfill its task, needs to know the interface to each algorithm, and can most easily obtain this information by parsing the XML algorithm interface file. Since this is the same file that was used to ultimately generate the executables, this guarantees that Origami has access to the most current version of the interface, and is thus aware of all currently implemented interface conventions for the algorithm in question.

Since the goal of Origami was to allow lightweight deployment of various algorithms in a distributed system as independent executables (outside of any previously constructed framework), the conversion of their interfaces to a format compatible with Origami, and the development of a matching XML-driven code generator is a major milestone in integration activity. Figure 4.5.1 shows the role of the XML interface in the Origami concept.

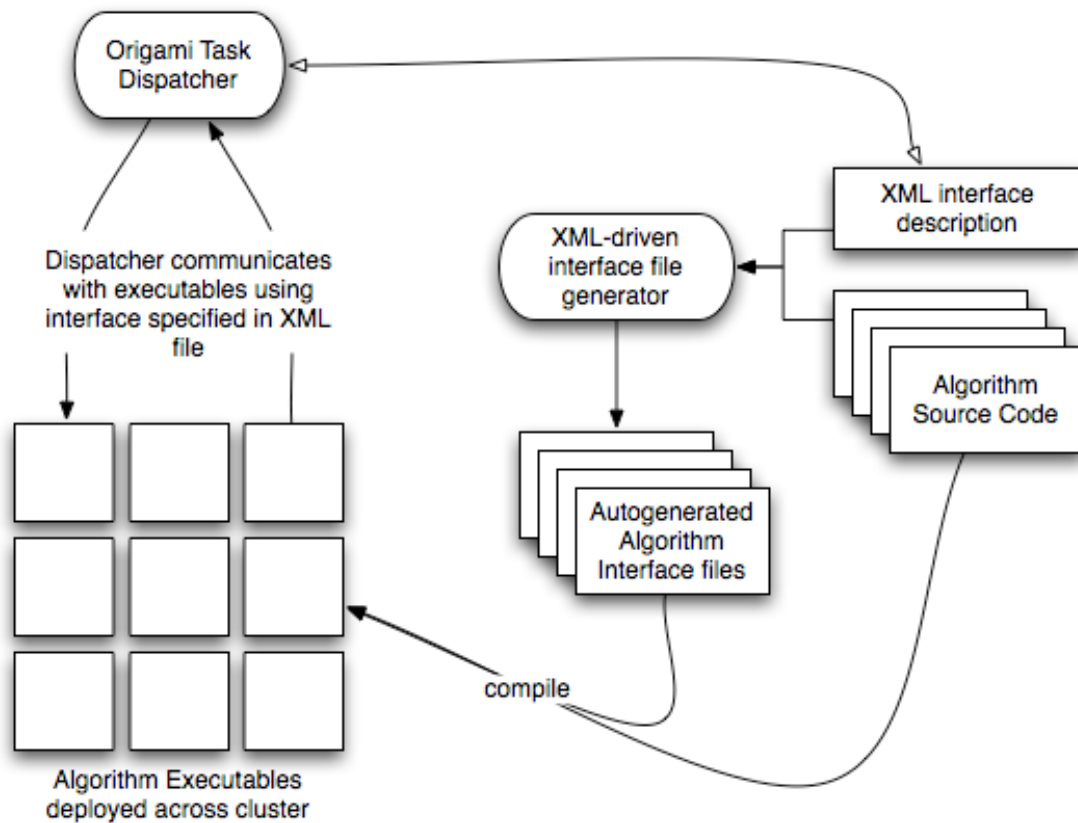


Figure 1: Role of XML interface and code generator in algorithms slated for Origami

Figure 4.5.1: Role of XML interface and code generator in algorithms slated for Origami.

In addition, preparatory steps were taken to integrate the distributed science workflow parts of Origami into the McIDAS-V visualization environment under development at SSEC. In the integrated workflow envisioned as a result of merging efforts from these two projects, the scientist will search for data sets and order-distributed computations of intermediate products (such as reprocessing calibrated data) directly from the visualization software interface, without having to cut and paste between the visualization software and the original Origami web interface. This adaptation can be performed while keeping most of the core Origami codebase, and only changing its lightweight user interface component.

The re-scoping of Origami as a component for integration into other applications prompted a rethinking of high-level design for science applications dealing with large volume data sets. The new design restructures the application space so that it allows for a component-by-component examination of whether to build a new solution or to adopt an existing one. A diagram of the new design as it relates to Origami was presented at this year's joint EUMETSAT/AMS meeting in Amsterdam, Holland and is shown here as Figure 4.5.2. A more detailed description of the Origami concept as it is being applied to McIDAS-V is contained in Garcia et al. (2008).

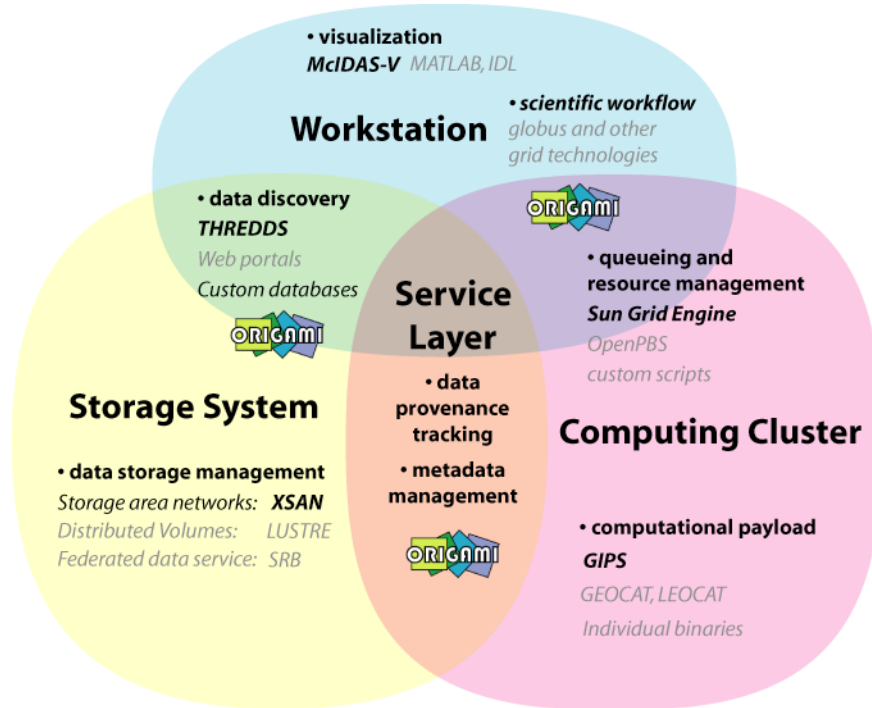


Figure 4.5.2: High level design of a distributed science workflow application for dealing with high volume data sets.

Publications and Conference Reports

Smuga-Otto, Maciej, R. Garcia, G. Martin, B. Flynn and R. Knuteson. Origami and GIPS: Running a hyperspectral sounder processing system on a lightweight on-demand distributed computing framework. Joint 2007 EUMETSAT Meteorological Satellite Conference and Satellite Meteorology and Oceanography Conference, 15th, of the American Meteorological Society, Amsterdam, the Netherlands, 24-28 September 2007. Proceedings. European Organization for the Exploitation of Meteorological Satellites (EUMETSAT), Darmstadt, Germany, 2007, Unpaged. Call Number: Reprint # 5582.

Garcia, Raymond K., B.M. Flynn, R.O. Knuteson, T. Whittaker, T. Rink, T. Achtor, S. Mindock, S.T. Dutcher, M.J. Smuga-Otto, G.D. Martin. Tools For Integrating Distributed Computing With Interactive Visualization In McIDAS-V, 88th American Meteorological Society Annual Meeting, 24th Conference on IIPS, New Orleans, LA, January 2008.

5. GOES R Algorithm Working Group

5.1. GOES-R Proxy Data Sets - Allen Huang and Tom Greenwald

Proposed Work

In 2007, the Proxy Data effort for the GOES-R AWG was concentrated on the refinement of the first version of data sets, models and documents that have been delivered to proxy team leaders. In addition, due to computing resources awarded by the National Center for Supercomputing Applications (NCSA), a new and enhanced comprehensive data set at spatial resolutions not achievable in the previous year was generated. The critical part of this large-scale simulation work is to adapt the supercomputing environment to perform WRF model simulations that can closely mimic similar data sets generated in the



previous year's work. For example, the generation of simulated full disk ABI data sets at a few km resolution requires more than a Terabyte of RAM and takes tens of thousands of CPU hours to complete. Successful execution of full disk NWP model simulations requires optimal use of the limited awarded computing resources.

Computation of Top of Atmosphere (TOA) ABI radiances also requires consideration of ABI sensor specifications, cloud and aerosol microphysical property modeling, and ocean and land surface property modeling. The CIMSS proxy work included meeting the common data set requirements requested by AWG application team members.

Summary of Accomplishments and Findings

A wide range of tasks was completed during this year's project.

Forward model development

Significant effort was spent enhancing and expanding the forward radiative transfer model (RTM) system that converts 3D WRF model fields into simulated ABI images. In terms of simulating the ABI IR bands (8-16), earlier work had used a simple 2-cloud-layer RTM for fixed 101-level profiles that were interpolated from variables at the WRF model's native levels. Radiance calculations had also been performed for the GIFTS spectrum and then convolved using the spectral response functions for a given ABI band. Unfortunately, it was found that the combination of interpolated profiles and the 2-cloud-layer RTM often produced large errors in the computed radiances in cloudy atmospheres. We decided instead to use the WRF model's native levels and the SOI RTM, which can accept any number of cloud layers.

The convolution approach was also abandoned in favor of using a single radiance calculation for each ABI band. Abandoning this approach not only saved computational time but also significantly reduced data volume because the radiances would not need to be saved for each of the GIFTS 3,074 bands. The Community Radiative Transfer Model (CRTM) was also integrated into our system and the Compact-OPTRAN model within it was used to compute gas optical depth profiles for input into the SOI RTM. Additional improvements included using the IR Sea Surface Emissivity Model (IRSSEM) that is also part of the CRTM.

Simulation of ABI solar bands (1-7) was a new task for this year. This task consisted of developing new code and acquiring various models and databases. Initial work involved the single-cloud-layer solar RTM developed by Dr. Ping Yang at Texas A&M. However, we found that the model suffered from inaccuracies that were traced to problems with the interpolation method used for the lookup tables. Furthermore, the lookup tables themselves were very large (about 410 MB for all 7 bands) and were limited to local zenith angles of 66° . Subsequently, a solar version of the SOI RTM (see section 4.1.4) and lookup tables for ice and liquid absorption/scattering properties replaced the single-cloud layer RTM. The new forward RTM system is applicable to a full range of solar angles and local zenith angles. Surface properties in the solar were specified by global MODIS-derived surface albedo data sets (0.01° resolution and two-week mean) and a sea surface reflectance model that accounts for sun glint, whitecaps and underlighting. Molecular scattering was also incorporated into the new solar forward RTM for bands 1-3, which had not been part of the single-cloud-layer RTM.

A deliverable was provided on 31 January 2008 that included documentation on a description of the 2-cloud-layer IR forward model and how to use it.

Production of simulated proxy data sets

A large-scale WRF simulation over North and South America (centered at 0° N and 75° W) for 4-5 June 2005 was the source of model-simulated atmospheric profiles used for the forward model systems. The



large domain consisted of 6 km grid spacing. Additional nested grids included a 2-km grid for CONUS and a small mesoscale-sized domain at 667 m grid spacing located in the central U.S. All of the forward model systems were written in Fortran 90, and have been found to be efficient and very stable. Much of this success is due to the use of a common data format (NETCDF) for most I/O and the application of simple text files to specify model input parameters. However, the sheer volume of data forced us to put considerable effort into developing an efficient means of processing and visualizing the simulated ABI data sets. This effort involved the creation of a series of BASH scripts that automatically move code and data to various nodes on our 80-core Opteron cluster. Because the WRF model data for each domain is actually broken up into many parts, another step involved piecing together these parts into a complete domain. We did so separately for each of the three domains. New software was also written that allows the simulated radiance/reflectance data in the WRF model projection to be remapped into the projection expected for the ABI in the IR (2 km at nadir). Finally, a series of MATLAB scripts was used to create low and high-resolution images and animations.

Table 5.1.1, Simulated ABI proxy data set archive. IR refers to ABI bands 8-16 and Solar refers to ABI bands 1-7.

Domain	Bands	Time Range (UTC)	Time Sampling	Data Volume*
Fulldisk	IR	0600 (4 June) – 0600 (5 June)	30 min	3.8 TB of raw model data, 4.0 GB per time for remapped IR ABI data, 2.7 GB per time for remapped solar ABI data, additional GOES-12 data also produced but not included here
Fulldisk	Solar	1745 (4 June)	-	
CONUS	IR	0600 (4 June) – 0600 (5 June)	30 min	3.4 TB of raw model data, 446 MB per time for remapped IR ABI data, 297 MB per time for remapped solar ABI data, additional goes-12 data also produced but not included here
CONUS	All	2200 (4 June) – 0000 (5 June)	5 min	
Mesoscale	IR	2200 (4 June) – 0000 (5 June)	1 min	2.8 TB of raw model data, 15 MB per time for remapped IR ABI data
Mesoscale	Solar	2200 – 2245 (4 June)	5 min	

* These totals do not include the 101-level interpolated atmospheric profile data sets or the unmapped radiance/reflectance data sets

Table 5.1.1 provides a summary of the simulated ABI proxy data sets produced thus far for 4-5 June 2005. Sample images of only a small portion of these data sets are depicted in Figures 5.1.1-3. Figure 5.1.1 shows a simulated ABI window IR band for one time step. Figure 5.1.2 shows the simulated ABI at all 16 bands for CONUS coverage at a single time step. Multiple time steps of the simulated ABI CONUS data and images have also been created for the AWG winds, clouds, and sounding teams, as well as the GRAFIIR team's algorithm development and products performance testing and evaluation. Animated files of much of the data summarized in Table 5.1.1 were delivered to the AWG program manager for his briefing at the AMS annual meeting for the GOES-R Users' Conference held in New Orleans, Louisiana in January 2008. Finally, Figure 5.1.3 demonstrates the high level of realism obtained



in the ABI visible (band 2) simulations for the CONUS domain. The significant progress made in solar forward model development has led to the availability of these much-needed ABI proxy data sets.

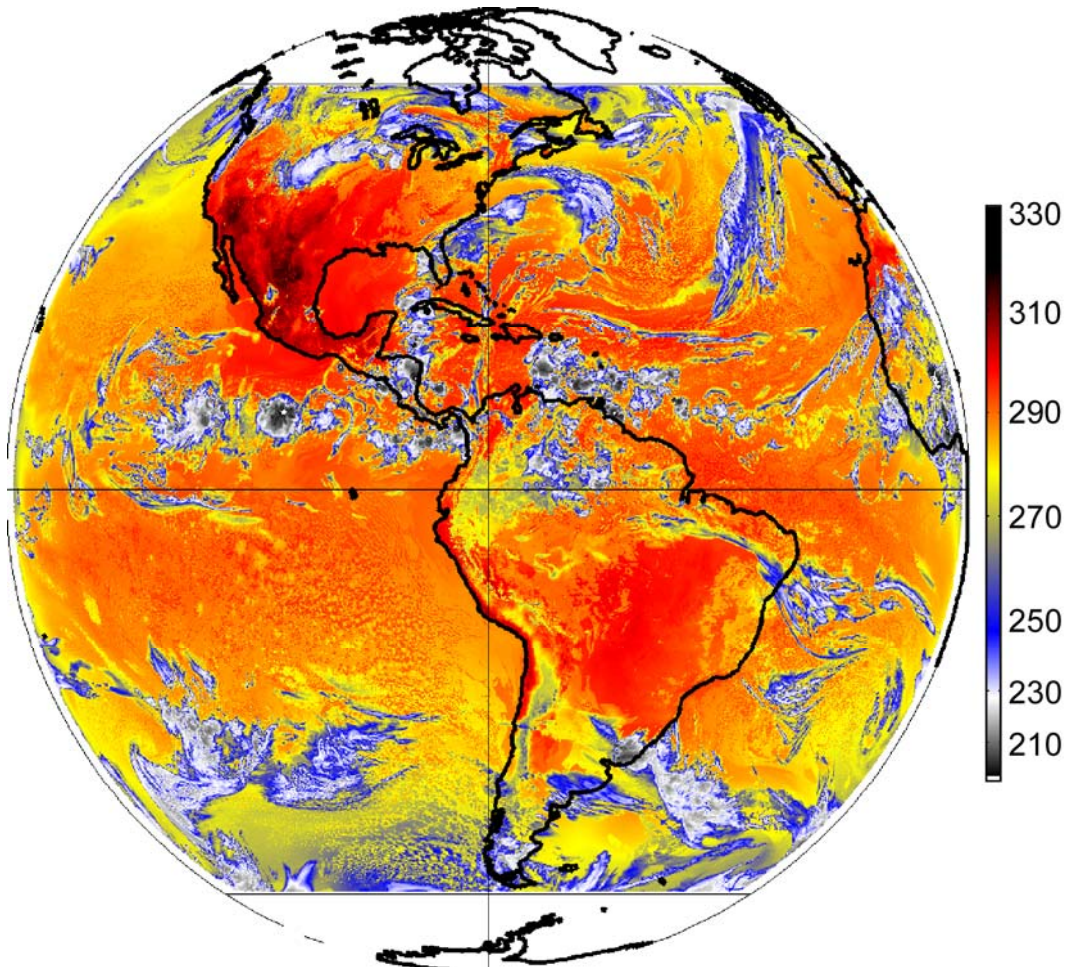


Figure 5.1.1: Simulated ABI band 14 (11.2 μm) brightness temperatures (K) for 1800 UTC on 04 June 2005.

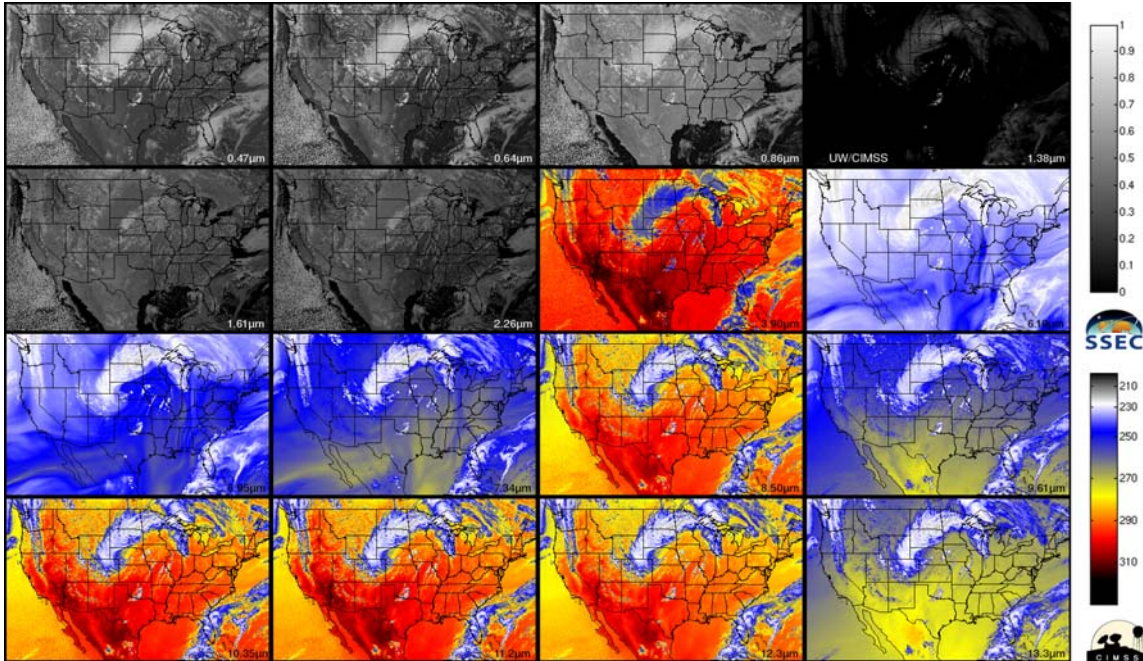


Figure 5.1.2: Simulation of all ABI bands for the CONUS domain at 2200 UTC on 04 June 2005. Band numbering starts at upper left corner and increases left to right.

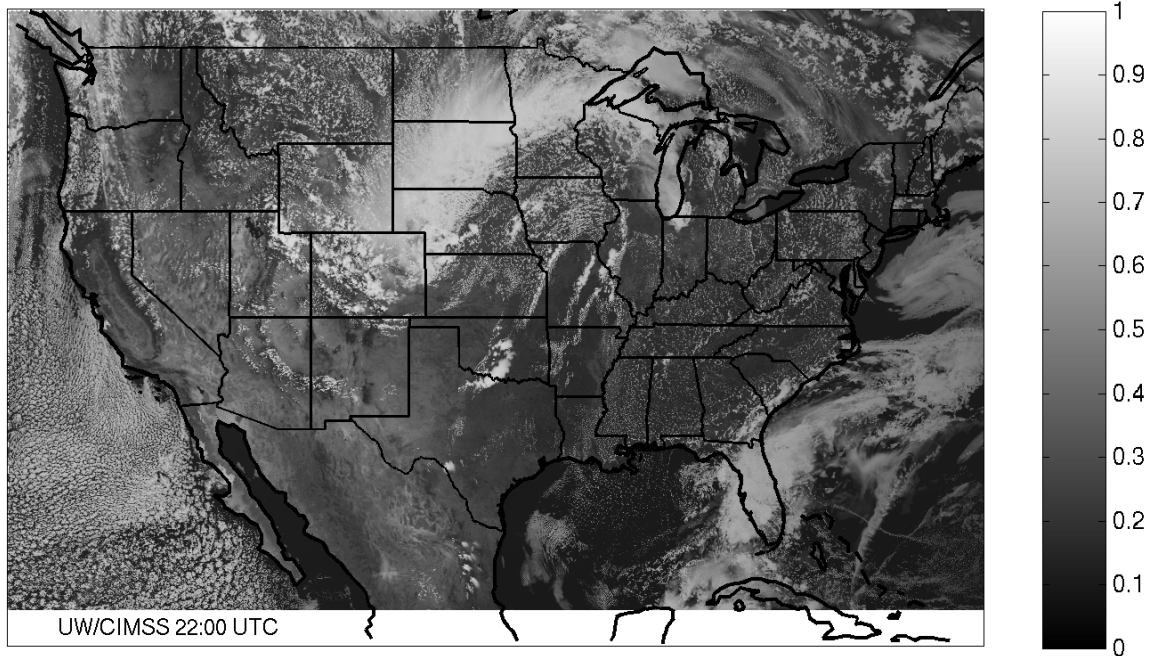


Figure 5.1.3: Expanded view of ABI band 2 (0.64 µm) shown in Figure 5.1.2.

Proxy data sets derived from MODIS data

Production of proxy data sets from MODIS data involves a number of steps. First, MODIS bands are selected that have central wavelengths similar to ABI bands. The IR MODIS data are then de-striped and averaged to the ABI spatial resolution. There is also a correction to the data based on the expected rebroadcast bit depth for the ABI. The cases selected cut across a wide range of weather and



environmental conditions, such as fire and smoke, mountain waves, dust storms, convective clouds, and daytime clouds. Recent work consisted of remapping the MODIS data into the ABI projection within McIDAS.

Data distribution

While only a small fraction of the ABI proxy data sets have been distributed, certain research teams have received subsets of these data sets to satisfy their work tasks. Simulated ABI IR-band proxy data for the CONUS between 2200 UTC on 04 June and 0000 UTC on 05 June were delivered to the AWG Sounding and Winds teams to test their algorithms. High-temporal resolution simulated ABI proxy data for the mesoscale domain during the same time period were also provided to Tim Schmit to demonstrate ABI's scanning capabilities.

MODIS-derived ABI proxy data sets for different weather/environmental phenomena were delivered to NOAA on 09 February 2008.

Validation

Assessing the validity of the simulated ABI proxy data sets is an ongoing task, but several limited evaluations were done. Since GOES-12 is located at the same position as where GOES-R is expected to be, data from the GOES-12 imager is the best choice for validation. However, to provide for a true comparison, additional simulations were done specifically for the GOES-12 imager bands. This process was straightforward, at least for the IR bands, since our forward RTM systems allow for many different types of instruments to be simulated. Once the pseudo-GOES-12 imager data were generated from the WRF model profiles, the data were remapped to the GOES-12 imager projection (4 km resolution at nadir). To facilitate comparisons between the simulated and real data sets, generalized code was written specifically for producing 1D and 2D frequency distributions.

Comparisons of the spatial averages of the thermal IR band brightness temperatures over the full disk domain (limited to local zenith angles of about 65°) revealed mixed results. The mean values were relatively close for band 4 (10.8 μm). However, the water vapor band (6.7 μm) comparison produced biases on the order of ~3-4 K. While the cause of these differences is not entirely clear, they may be due in part to water vapor biases in the global data sets used to initialize the WRF model run.

Another set of comparisons was performed involving the GOES-12 imager solar bands (1 and 2) as well as band 4, but only for cloudy regions at 1745 UTC on 04 June for most of the full disk domain. To examine how well the simulations reproduced different cloud types according to height and optical thickness, 2D frequency distributions of band 1 albedo versus band 4 brightness temperatures were compared. Results showed that while the model simulations broadly captured the behavior seen in the GOES-12 imager observations, the simulated band 1 albedos tended to be larger on average. This tendency indicates that the WRF model may have produced clouds that were too optically thick, particularly for lower level clouds. Another comparison involved 2D frequency distributions of band 2 (3.9 μm) albedo versus band 4 brightness temperatures. Band 2 albedos were derived using band 4 radiances to remove the thermal emission component from the band 2 radiances. Albedos at this band provide a measure of cloud particle size – larger albedos imply smaller particle sizes while smaller albedos imply larger particles. Results suggested the WRF model produced boundary layer clouds with smaller particle sizes than observed.

Publications and Conference Reports

Greenwald, T. J., J. Sieglaff, Y.-K. Lee, H.-L. Huang, J. Otkin, E. Olson, M. Gunshor, 2007: Verifying large-scale, high-resolution simulations of clouds for GOES-R activities, Submitted to 5th GOES Users' Conference, American Meteorological Society Meeting, New Orleans, Louisiana.



Greenwald, T. J., H.-L. Huang, E. Olson, J. Otkin, M. Gunshor, P. Yang, and J. Niu, 2007: CIMSS Forward Modeling for Production of ABI Proxy Data Sets. GOES-R AWG Annual Meeting, Leesburg, VA.

Greenwald, T. J., H.-L. Huang, D. Tobin, J. Otkin, E. Olson, M. Gunshor, and P. Yang, 2007: Evaluation of Simulated GOES-R ABI and Hyperspectral Radiance Measurements. 3rd Symposium on Future National Operational Environmental Satellites, American Meteorological Society Meeting, San Antonio, Texas.

Otkin, J. A., H.-L. Huang, E. R. Olson, and T. Greenwald, 2007: WRF-simulated atmospheric profile data sets used to support GOES-R research activities. GOES-R AWG Annual Meeting, Leesburg, VA.

Otkin, J. A., and H.-L. Huang, 2007: Large-scale high-resolution WRF model simulations used for GOES-R research activities. 8th Annual WRF User's Workshop, Boulder, CO.

5.2. GOES-R Analysis Facility Instrument for Impacts on Requirements (GRAFIIR) – Allen Huang

Proposed Work

In 2007, the GRAFIIR effort concentrated on developing an efficient facility to model specific ABI sensor effects. We also focused on developing the framework, which we planned to be similar to GEOCAT or a web-oriented system nicknamed Origami. Origami is a system for processing, managing and visualizing multispectral and hyperspectral data. In addition, the GRAFIIR team sought to provide a flexible platform to analyze multiple inputs and outputs to demonstrate the sensor impacts on many products. GRAFIIR planned to use Unidata's Integrated Data Viewer (IDV), Java WebStart technology and other existing graphic and data management software to enhance our system's analysis capability and to identify sensor components that might prohibit the ABI products meeting measurement requirements.

Summary of Accomplishments and Findings

Modeling of ABI Instrument Effects (conducted by M. Gunshor)

To date, four instrument effects have been applied to simulated ABI data that have been remapped to an ABI-like grid and quantized for ABI bit depth:

1. Noise (NEdT or NEdR)
 - Vis/NIR (bands 1-6): SNR is 300:1 at 100% albedo
 - IR (bands 7-15): NEdT at 300K is 0.1K, (band 16): 0.3K

Random noise is generated such that for m lines by n elements in an image a random number generator is used on all m x n points where the standard deviation of what will be added to those m x n points is the noise (such as the NEdR equivalent of 0.1K at 300K for IR bands or 300:1 in reflectance units).

2. Calibration Offset IR Bands: ABI Spec is for absolute accuracy of 1K
 - Vis/NIR Bands: ABI Spec is for absolute accuracy of 3%
3. Navigation Error:

Spec Navigation Error is 21 microradians. This spec is the largest of any of the navigation/co-registration type errors. To simulate this error, a random compass direction (0-359.99 degrees) is selected for each pixel and a normalized random distribution for distance based on 21 micro



radians (0.75km) is added. Then the radiance for that pixel is “smudged” in that direction using linear interpolation. The result is a new image with the original Lat/Lon grid but slightly altered radiances. A few pixels may have large differences from the original because they were on the edge of a feature such as a cloud.

4. Striping:

The striping specification is “not to exceed the noise.” Assuming the ABI will have a detector array that will result in 100 lines of remapped data, striping is added to one of the first 100 lines and every 100th line after that.

Combination of the above ABI instrument effects

Data sets were created that applied all four instrument effects at 1X spec and 3X spec to determine their effects on certain algorithms.

Other effects that will be simulated are:

- Co-registration Error
- Swath to Swath Offset

Modeling High Spatial Resolution Atmospheric Fields for ABI Simulation

Leveraging the Proxy Data effort, GRAFIIR simulated atmospheric fields were generated using version 2.2 of the WRF model (ARW core). The simulation was initialized at 00 UTC on 04 June 2005 with 1° GFS data and then run for 30 hours using a triple-nested domain configuration. The outermost domain covers the entire GOES-R viewing area (every 15 minutes) with 6-km horizontal resolution while the inner domains cover the CONUS (every 5 minutes) and mesoscale regions (every minute) with 2-km and 0.667-km horizontal resolution, respectively. The sounding, wind and cloud teams will then use these data sets to demonstrate the impact of ABI instrument effect on their product requirements.

ABI instrument effects on ABI Sounding, Wind and Cloud Products

The figures and tables below represent some of the GRAFIIR analysis results. Figure 5.2.1 demonstrates the noise impacts on the ABI legacy sounding retrieval of 300-500 layer relative humidity. The RH retrieval error increases from pure ABI measurements (no instrument noise), to nominal spec noise (1X) and three times of spec noise (3X). Error increases from less than 10% for pure to ~12% of spec noise and to ~20% of noise increases three fold.

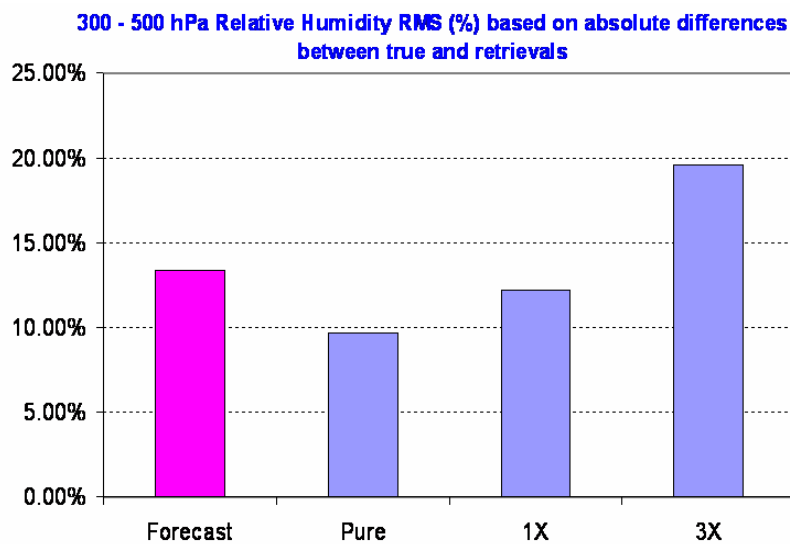


Figure 5.2.1: ABI instrument noise impacts on legacy sounding retrieval of relative humidity (300-500 mb). NWP forecast model error is also shown for comparison.



Figure 5.2.2 shows the noise impacts on ABI cloud mask classification. When noise increased from spec. noise to three times spec. noise, the classes of probable cloudy and clear increase. This preliminary analysis indicates that when noise increases the probability of confident discrimination of ABI pixel been clear or cloudy decreases.

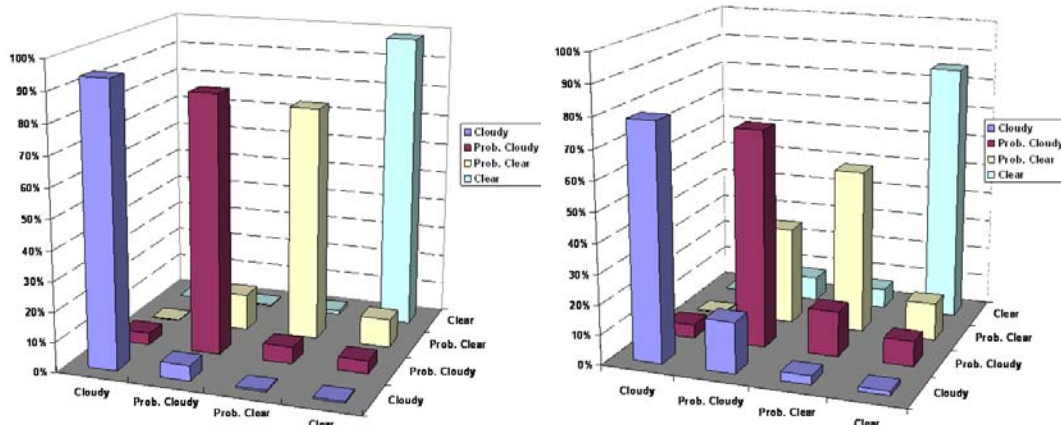


Figure 5.2.2: ABI cloud mask is impacted by the increase of noise from spec. noise (left) to three times spec. noise (right).

The noise impact on the ABI detection of cloud phase is also studied. Figure 5.2.3 indicates the relative change from liquid to ice and ice to liquid cloud. When noise is much higher, the cloud phase is biased toward selecting water clouds.

	Liquid Phase	Ice Phase
Noise Free Count	N=652573	N=636807
Noise 1x Spec Count	+1.3% N=661252	-2.9% N=618476
Noise 3x Spec Count	+29.4% N=844719	-14.3% N=545560

Cloud Phase Pixel Counts

	Noise 1x Spec	Noise 3x Spec
Ice to Liquid	N=29697	N=74108
Liquid to Ice	N=5186	N=2790

Cloud Phase Pixel Changes

Figure 5.2.3: Same as Figure 5.2.2 except for cloud phase determination.



The two tables below show the results of the noise impact on the water vapor and infrared winds derived from the tracking of water vapor and infrared images simulated for ABI. The noise impacts on the bias and root mean square errors are shown.

Table 5.2.1. Water vapor wind derived from ABI images simulated from different level of noise. Pure is without any noise, 3X means three times of ABI spec. noise.

Water Vapor (WV) Atmospheric Motion Vectors						
Image Interval (Minutes)	# Matches		Speed Bias (AMV-WRF)		Vrms (AMV Vs WRF)	
	Pure	3X AIE	Pure	3X AIE	Pure	3X AIE
5	3041	534	-0.064	1.6648	5.1523	6.1122
15	2693	1189	0.0554	1.6774	4.7039	5.2942
30	2124	1217	0.0698	1.4038	5.0002	4.8443

Table 5.2.2: Same as Table 5.2.1 but for Infrared motion wind.

Infrared (IR) Atmospheric Motion Vectors						
Image Interval (Minutes)	# Matches		Speed Bias (AMV-WRF)		Vrms (AMV Vs WRF)	
	Pure	3X AIE	Pure	3X AIE	Pure	3X AIE
5	4157	1615	-0.355	0.1657	4.449	4.7329
15	3754	2825	-0.564	0.7658	4.0065	3.8399
30	2484	1890	0.5022	0.7612	4.0185	3.4238

In summary, GRAFIIR’s first task was to build an infrastructure to conduct systematic and detail analysis of ABI instrument impacts on key products. With 2007 achievements, CIMSS is one step closer to reaching this goal.

5.3. Development of the Multilayer Cloudy Radiative Transfer Model for GOES-R Advanced Baseline Imager (ABI) - Bormin Huang

Proposed Work

Surface and aircraft observations show that many cloud types can appear simultaneously at the same location but at different altitudes. Furthermore, clouds may be continuous or broken at a given cloud level within a sensor’s field of view (FOV). The proposed work was to develop the GOES-R ABI multilayer cloudy radiative transfer model. The model must not be so complicated that it makes the cloudy retrieval problems unmanageable, but it must be generalized enough to handle multilayer clouds with defined effective cloud emissivity to include the multiple scattering effects. The clear-sky forward model is a special case where the cloud parameters are reduced to zero.



Summary of Accomplishments and Findings

The multilayer cloudy forward model for ABI was developed and implemented successfully. We are making products available for the science community. The accomplishments and findings are illustrated in the following four figures.

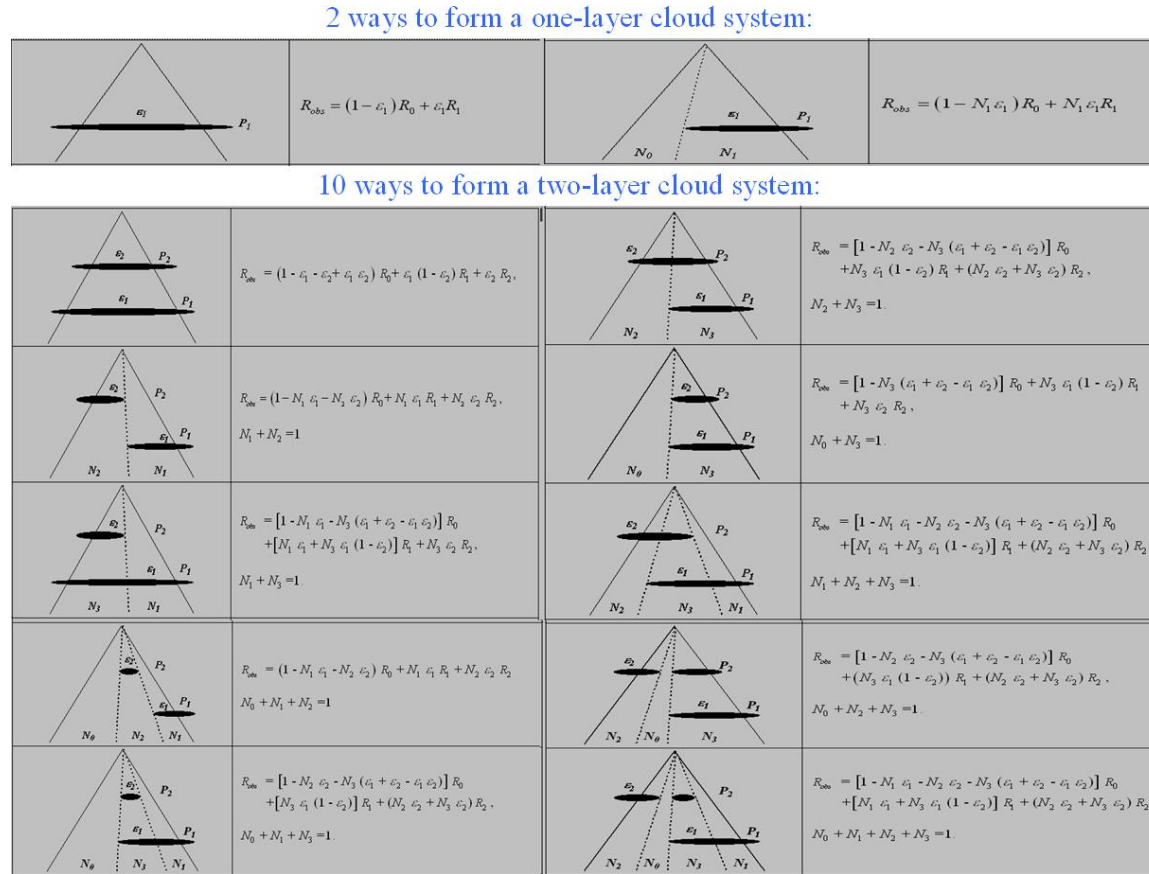


Figure 5.3.1: There are two ways to form a one-layer cloud system and ten ways to form a two-layer cloud system. The ABI multilayer cloudy forward model is capable to simulate all the cases.

ABI Multilayer Cloudy Forward Model

One-layer cloud system studies

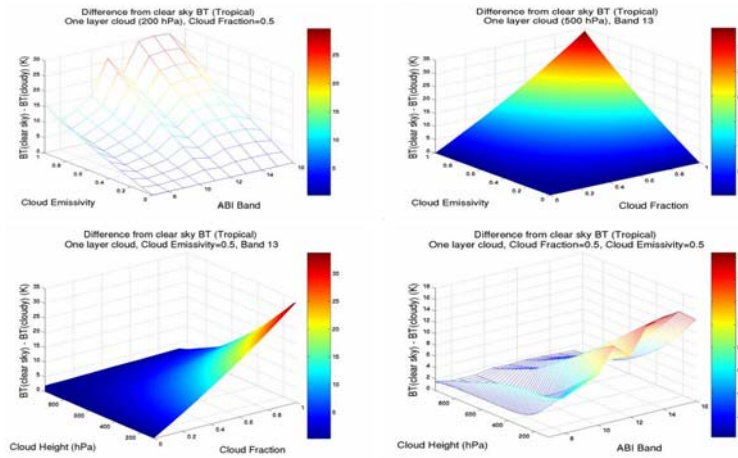


Figure 5.3.2: The simulated ABI brightness temperature spectra for various one-layer cloud systems in terms of various cloud heights, cloud emissivities, and cloud fractions.

ABI Multilayer Cloudy Forward Model

Two-layer cloud system studies

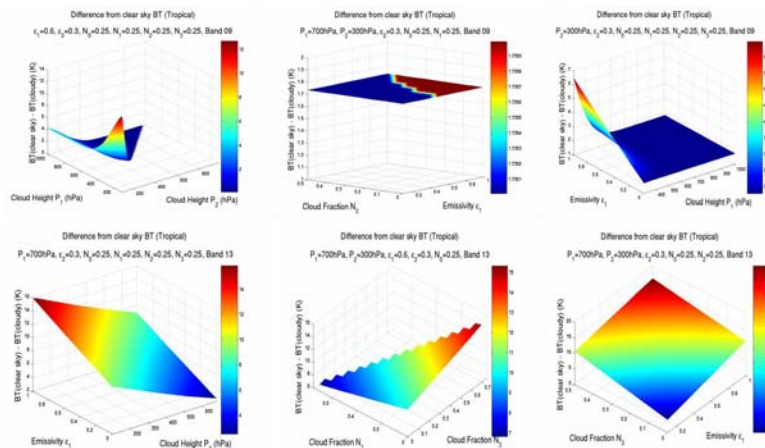


Figure 5.3.3: The simulated ABI brightness temperature spectra for various two-layer cloud systems in terms of various cloud heights, cloud emissivities, and cloud fractions. The developed multilayer cloudy forward model is capable of handling complicated cloud situations.

Multiple Solutions Exist for Multilayer Cloudy Retrieval

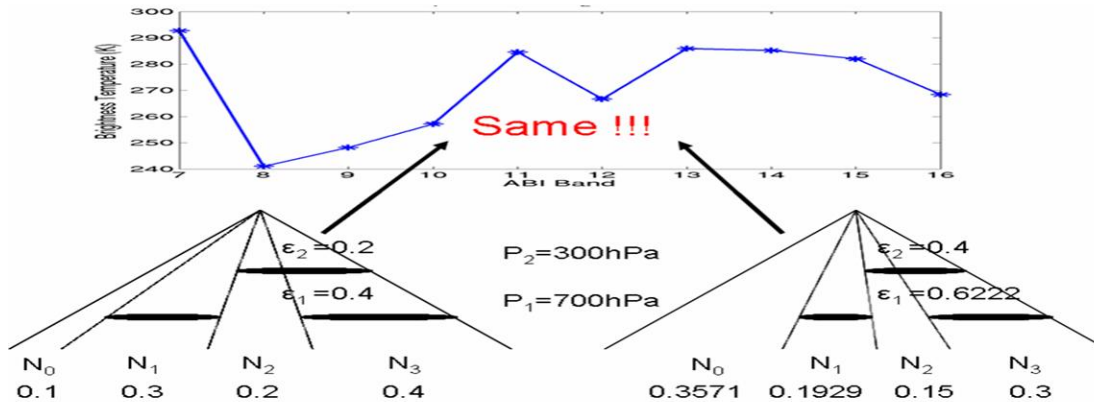


Figure 5.3.4: An example illustrates that two different two-layer cloud systems can correspond to the same observed spectrum. This new finding implies the existence of multiple solutions for multilayer cloudy retrieval.

Publications and Conference Reports

Part of the work was presented at the 2007 AWG meeting and the 2007 EUMETSAT/AMS conference. A paper was finished last year for journal submission.

5.4. Algorithm Integration Team (AIT) Technical Support – Ray Garcia and Maciej Smuga-Otto

Proposed Work

Our overall goal is to provide technical expertise to both the algorithm teams located at CIMSS and to the AIT in order to ease the integration of algorithm code from the science prototyping environment into the AIT framework, and eventually the production environment. This work includes standardizing algorithm interfaces; advising the AIT on framework design and implementation; tracking and managing inter-algorithm dependencies and data dependencies; supporting AIT development of software processes; attending AIT teleconferences and workshops; and assisting in software tools selection.

Summary of Accomplishments and Findings

- Advised the AIT on framework design.
- Provided technical expertise and direct assistance to science algorithm teams at CIMSS with preparation of code deliverables and flowchart packages.
- Worked toward defining and formalizing an internal software development process including versioning, provenance, documentation, and testing.
- Attended the May 2007 GOES-R AWG Developers' Retreat, which focused on coding standards, documentation requirements, programming languages, software tools, QA standards and software development model.
- Conducted a workshop with the AIT programming team at CIMSS in November 2007, focusing on technical issues related to framework implementation.
- Agreed on a common algorithm interface and other design features to allow interoperability of algorithms developed at CIMSS in the science prototyping environment (GEOCAT) and the AIT framework.



- Worked closely with the AIT to resolve issues and incompatibilities encountered while implementing and testing their framework, including data structure incompatibilities, problems arising from different programming languages and architecture-related differences.

5.5. Total Ozone from ABI – Chris Schmidt, Jun Li

Proposed Work

The Advanced Baseline Imager (ABI) on GOES-R has sufficient spectral coverage to retrieve total column ozone over its coverage area. The 9.6- μm ozone absorption band is particularly important. The legacy GOES I-M Sounder experimental total column ozone (TCO) algorithm from CIMSS can be applied to ABI. ABI ozone will provide high spatial and temporal resolution sampling of ozone features that primarily reflect ozone distribution in the stratosphere and upper troposphere; ABI ozone alone cannot meet requirements for measuring the tropospheric column ozone. ABI ozone will provide continuity with the current ozone capabilities and function as a part of an ABI Sounding package. Development of an ABI ozone algorithm begins with adapting the algorithm to EUMETSAT's Spinning Enhanced Visible and Infra-Red Imager (SEVIRI), which has similar spectral coverage to that proposed for ABI. Alongside using straight SEVIRI data as a proxy, the effort will also include using ABI proxy data derived from SEVIRI and MODIS data.

In 2007, CIMSS proposed to run the prototype algorithm on SEVIRI data in real time at full resolution, utilize proxy data sets for testing as they become available, iterate algorithm modifications and validation to minimize errors, and install and port algorithm software and test data sets to run on STAR demonstration platform.

Summary of Accomplishments and Findings

The primary focus of the 2007 effort was to transfer the SEVIRI ozone algorithm to GEOCAT and subsequent delivery to the Algorithm Implementation Team (AIT) along with the necessary flowcharts and diagrams. Additionally, the Algorithm Test Plan was developed and partially implemented. At the end of 2007, the ozone algorithm was running on the AIT's framework and implementation of the test plan was underway. As part of the implementation, computer hardware was purchased to provide the necessary power to run SEVIRI ozone under GEOCAT in real time, though that has yet to be implemented. The GEOCAT version utilizes the AWG Cloud Teams SEVIRI Cloud Mask, as it will when ABI is implemented.

The Proxy Teams at this time do not have the ability to model ozone beyond utilizing climatology, so SEVIRI data will be the only available proxy data set for the near term. MODIS data is a possibility though the radiances must be transformed to match those of ABI.

Figure 5.5.1 shows SEVIRI total column ozone on 01 August 2006 at 23 UTC. The patterns in the image are very promising and the data validates well against OMI, though the simplistic cloud screen used in this particular case (not the cloud team algorithm) is introducing error, most notably seen as cloud-like features in the ozone field.

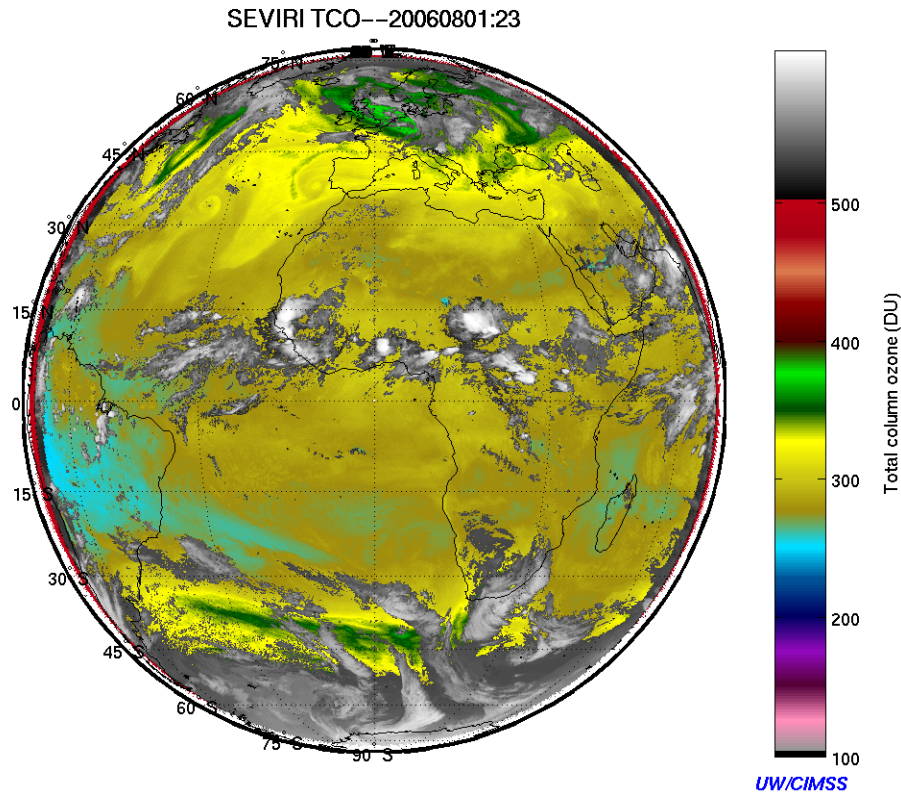


Figure 5.5.1: SEVIRI total column ozone on 01 August 2006 at 23 UTC.

Publications and Conference Reports

Schmidt, Christopher C., X. Jin, J. Li, and J. Li, 2007: GOES-R ABI Ozone Estimation, Algorithm Working Group Annual Meeting, National Conference Center, Landsowne, VA, 14-18 May 2007.

5.6. GOES-R Cloud Properties –Corey Calvert, Andrew Heidinger, Michael Pavolonis, Andi Walther and Pat Heck

Proposed Work

This project includes all of the CIMSS efforts relating to the GOES-R Algorithm Working Group (AWG) Cloud Application Team. The task of the team is to develop a set of consensus cloud algorithms and all documentation for delivery to the NESDIS/STAR integration teams. Our effort also includes development of validation tools to demonstrate that we meet performance requirements.

Summary of Accomplishments and Findings

The major accomplishment of this year was the development of the first version of algorithms to generate the 12 products for which this team is responsible. These 12 products are generated from five main algorithms: Cloud Detection, Cloud Typing, Cloud Height, Daytime Cloud Properties, and Nighttime Cloud Properties. The initial versions of these algorithms were delivered to the NOAA/NESDIS/STAR Algorithm Integration Team (AIT) in October 2007. We conduct all development, testing and validation with the Geostationary Cloud Algorithm Test-bed (GEOCAT). GEOCAT progress is reported in Section 5.8. Figure 5.6.1 provides a snapshot of the various products now being generated by Cloud Application Team.



It is important to point out that ABI cloud algorithms represent a significant advancement over the heritage algorithms. Development of algorithms was needed to properly use the advances in spectral, spatial and temporal information provided by the ABI. Our algorithm development in this year can be summarized as follows:

- Implementation of temporal signatures for cloud detection.
- Use of results from opaque cloudy regions to constrain properties of semitransparent cloudy regions.
- Development of infrared-only cloud typing.
- Optimization of cloud property lookup tables.
- Use of water vapor absorption bands in cloud height detection.

In addition, we are developing tools to use CALIPSO data to guide algorithm development and to validate our results. For example, we are using CALIPSO/CALIOP to provide distributions of cloud mask thresholds for known clear pixels and to provide statistics of cloud properties needed for the one-dimensional variational techniques employed in the algorithms. In terms of direct validation, CALIOP is being used to validate the cloud type/phase, cloud height and cloud emissivity.

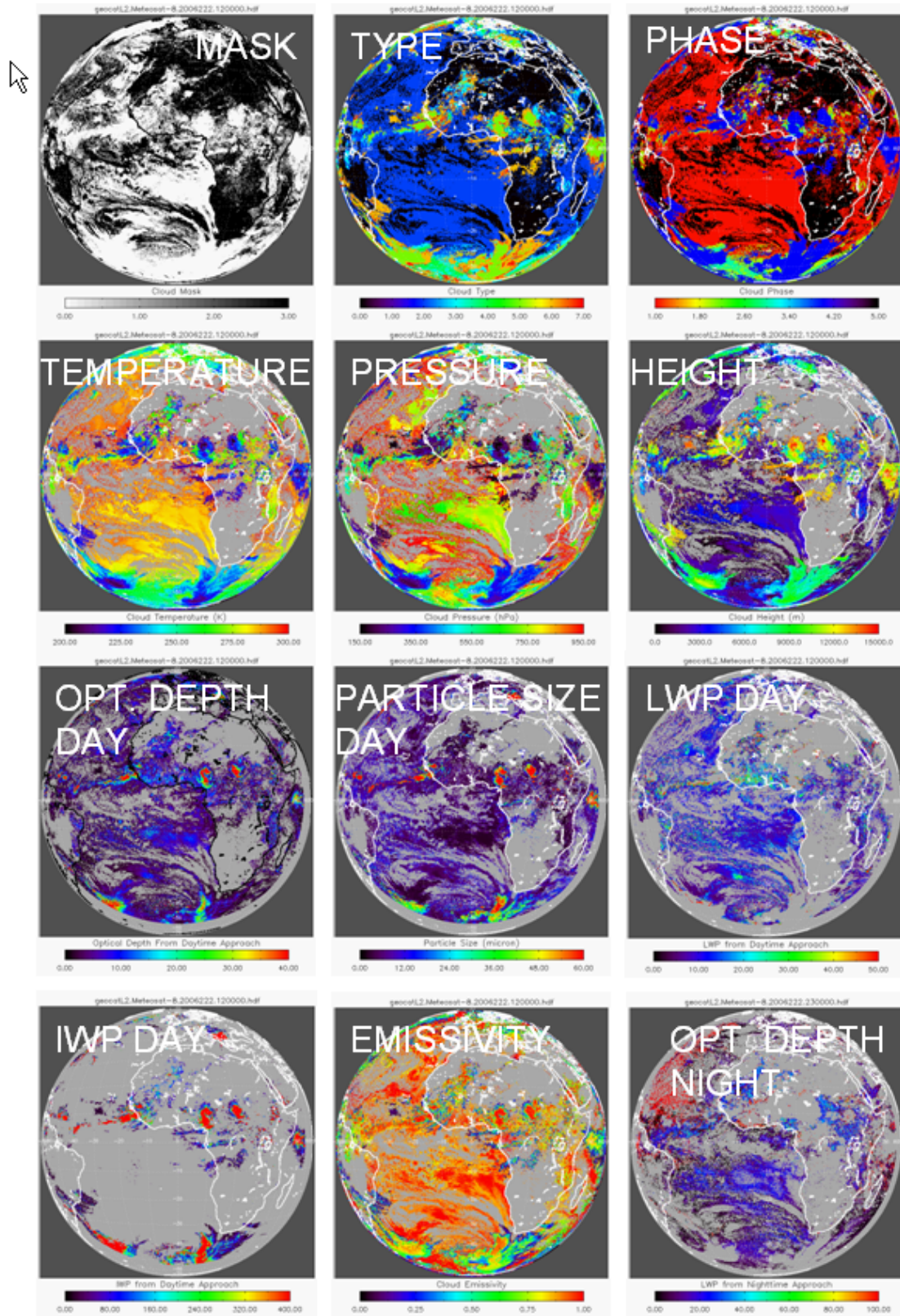


Figure 5.6.1: Examples of products generated by CIMSS Cloud Application Team.



Publications and Conference Reports

Heck, Patrick W., P. Minnis, R. Palikonda, C.R. Yost, F.L. Chang, and A.K. Heidinger, 2008: Nighttime Retrieval of Cloud Microphysical Properties for GOES-R. Fifth GOES User Conference, New Orleans, LA.

Heidinger, Andrew and Michael Pavolonis: Candidate Approaches for the Real-time Processing of Cloud Properties from GOES-R ABI. Fifth GOES Users Conference, New Orleans, LA.

5.7. Static Libraries for Retrieval of Cloud Optical and Microphysical Properties - Bryan Baum

Proposed Work

This project involves several steps that lead to the development of static libraries of ice/water cloud properties, which are critical for accurate retrieval of cloud optical thickness and effective particle size. To build these static libraries, one must first develop the bulk scattering and absorption models for ice and water clouds. These bulk scattering models provide information such as single-scattering albedo, asymmetry factor, scattering and absorption cross-sections, and scattering phase functions. All the parameters are a function of particle size. The inference of the bulk scattering properties for water clouds is straightforward as water clouds are assumed to be composed of spherical droplets. Ice clouds are more problematic as the particles are not spherical. In our development of ice cloud bulk scattering/absorption parameters, we used a mixture of hollow columns, solid columns, droxtals, hexagonal plates, aggregates, and 3D bullet rosettes.

Given the bulk scattering and absorption models for ice/water clouds, the next step in the process of building the static libraries is to employ a radiative transfer model to simulate a cloud layer over a range of cloud optical thicknesses, cloud heights, and cloud effective particle sizes. The final step is to organize all the radiative transfer simulations into a static library that may be used efficiently for operational retrievals using GOES data.

Summary of Accomplishments and Findings

Working with the GOES AWG cloud retrieval team, we have developed the bulk scattering and absorption models and have documented them in an Algorithm Theoretical Basis Document that is in progress. We have also developed static libraries for use with our proxy data set (SEVIRI), which has many spectral channels in common with GOES-R.

Publications and Conference Reports

The contribution of this effort is being documented in the GOES Cloud AWG ATBD that will be finished by the end of February 2008.

5.8. GEOCAT Enhancements and Documentation – Graeme Martin and Michael Pavolonis

Proposed Work

The Geostationary Cloud Algorithm Testbed (GEOCAT) was developed by the GOES-R Algorithm Working Group (AWG) Cloud Application Team to test and compare various cloud product algorithms and aid in the delivery of algorithm software to the GOES-R AWG Algorithm Implementation Team (AIT). GEOCAT provides navigated and calibrated geostationary imager radiances, ancillary data, and fast model generated clear sky radiance data structures to product producing subroutines (e.g. algorithms),



and provides a common algorithm output structure, whose definition is transparent to the algorithm developer. GEOCAT's design allows for multiple algorithms for the same and/or different products to be processed with a single invocation of the GEOCAT executable, making it a very useful algorithm testbed.

For this project, we proposed to expand upon the work of the AWG Cloud Application Team by making their algorithm processing software, GEOCAT, available to other GOES-R Algorithm Working Groups at the University of Wisconsin-Madison and to provide support for implementing non-cloud team algorithms into GEOCAT. This effort required that certain enhancements be implemented into GEOCAT and that the GEOCAT data structures, user instructions, and algorithm implementation processes be documented. While GEOCAT is already a flexible system, this project involved some additional updates to the main GEOCAT framework. The actual code enhancements were guided by specific non-cloud algorithm needs and Algorithm Integration Team (AIT) requirements (e.g. coding standards, output formats, etc.). Overall, this work allowed for a robust algorithm test tool to be available to AWG members, which will also aid in the delivery of algorithms to the AIT. GEOCAT-produced data sets such as navigated/calibrated SEVIRI radiances and certain cloud team products (e.g. cloud mask) were also made available to AWG members in a standard easy-to-read format (HDF4).

Summary of Accomplishments and Findings

- Completed a draft of the GEOCAT User's guide.
- Incorporated CIMSS ozone retrieval algorithm into GEOCAT.
- Transitioned CIMSS fire algorithm (detection and characterization) from McIDAS F77 routines to a GEOCAT F90 module.
- The ABI calibration, navigation, and fast model modules have been added to GEOCAT so that simulated ABI proxy can now be processed.
- A robust python script that converts simulated ABI data produced by the CIMSS Proxy Team into a GEOCAT compatible format has been written. Simulated ABI proxy data can now be readily processed in GEOCAT (see figures below).
- Generated one month of navigated/calibrated 15-minute SEVIRI full disk data and made it available to other AWG members.
- Added a variety of generic data manipulation routines into GEOCAT that are useful to algorithm developers.

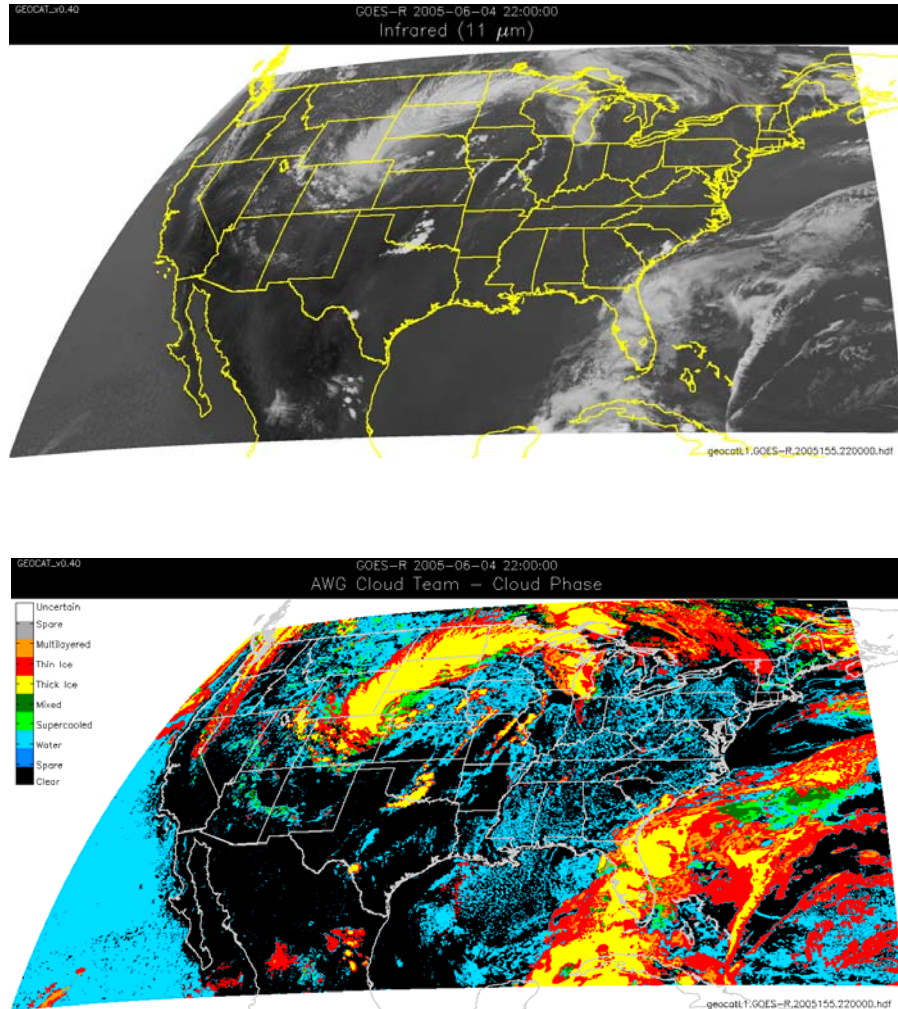


Figure 5.8.5: Example of GEOCAT output using model simulated ABI proxy data. The top image is an 11-micrometer image and the bottom is the official Cloud Team cloud type/phase product applied to the same scene. GEOCAT provides the capability to apply algorithms to simulated ABI, SEVIRI, MTSAT, and GOES 8-13 data.

5.9. ABI Fire Detection and Characterization Algorithm Development and Evaluation—Chris Schmidt and Elaine Prins

Proposed Work

The primary focus of this effort is to evaluate the current GOES Wildfire Automated Biomass Burning Algorithm (WF_ABBA) and adapt the algorithm for application with the GOES-R ABI. This activity builds on historical and current expertise at CIMSS in fire algorithm development for the GOES Imager and the global geostationary fire monitoring network (Met SEVIRI, MTSAT-1R, etc.).

CIMSS proposed to revise the WF_ABBA to address GOES-R ABI observational requirements utilizing the improved fire monitoring capabilities on GOES-R. This plan included: updating modules that identify and characterize sub-pixel fire activity, demonstrating and validating the prototype GOES-R ABI WF_ABBA using various GOES-R ABI proxy data sets, and providing a version of the algorithm for further evaluation by the AWG science team. This effort involves collaborating with MODIS and NPOESS VIIRS fire product development experts to ensure consistency between the GOES ABI and



NPOESS VIIRS fire algorithms to the extent possible and maximize future use of multiple data sources (geo and leo) that take advantage of the strengths of each system to create improved fused fire products. This activity also ensures enhanced future geostationary fire detection, diurnal monitoring, and characterization in the GOES-R era.

Summary of Accomplishments and Findings

During the past year the CIMSS fire monitoring team focused on adapting the current McIDAS GOES WF_ABBA to GOES-R ABI and evaluating the ABI fire algorithm for fire detection and sub-pixel characterization using model simulated ABI data provided by CIRA and MODIS simulated ABI data provided by CIMSS. CIMSS also began various documentation tasks. The fire team worked in collaboration with SSEC programming staff to construct fire algorithm flowcharts using the VISIO software. Drafts of the top-level flowcharts, detailed flowcharts and I/O tables for each of the two main components of the WF_ABBA were delivered to the AIT in April 2007. CIMSS has also made some progress on the Algorithm Theoretical Basis Document and the Algorithm Implementation and Test Plan Document.

Algorithm development activities involved adapting the current McIDAS GOES WF_ABBA (version 6.0) for application to GOES-R ABI with modifications to improve fire detection and characterization and to decrease the run time. These improvements were based on techniques developed and evaluated with GOES-R Risk Reduction funding. To date, the GOES WF_ABBA code has relied on a static look-up table approach to assign surface emissivity. The ABI WF_ABBA utilizes the dynamic multi-spectral UW Baseline emissivity database to more accurately reflect seasonal changes in surface emissivity. Application of the UW Baseline Fit emissivity data set allows for the identification of more fire pixels associated with a given fire. CIMSS also generated a new lookup table for atmospheric offsets as a function of total precipitable water and satellite view angle. Other modifications include rearrangement of tests to decrease the run time and threshold adjustments to accommodate a higher saturation threshold in the ABI 3.9 micrometer band.

Over the past several years, there has been increased interest in using fire radiative power to characterize sub-pixel fire activity. The ABI WF_ABBA now provides estimates of fire radiative power (FRP) based on GOES-R risk reduction efforts. The updated code also provides a fire mask, simple opaque cloud mask, and other metadata identifying block-out zones and pixels that could not be processed. The final user output file was revised to include latitude, longitude, satellite view angle, pixel size, observed 4- and 11-micrometer brightness temperatures, instantaneous estimates of fire size and temperature, fire radiative power, biome type, and fire confidence flag. Similar modifications were made to the experimental version of the next generation global geostationary WF_ABBA (version 6.5) that will be implemented in NESDIS operations in 2008 for GOES, Met-9, and MTSAT-1R. All of these changes were made in direct response to recommendations made by the international user community at the GOFC/GOLD Geostationary Fire Monitoring and Applications workshop held in December 2006.

The proposed CIMSS activities did not include eliminating dependencies on McIDAS from the ABI fire code. Regardless, the CIMSS fire team worked with other SSEC/CIMSS scientists and programming staff to integrate version 6.5 of the GOES WF_ABBA into GEOCAT and remove the McIDAS dependencies. Although there are a few issues that need to be resolved regarding the handling of image processing/navigation, pixel size determination, and ecosystem assignment in GEOCAT, the GEOCAT code is on track with most of the McIDAS routines adequately replaced with GEOCAT routines. In October 2007, CIMSS delivered a GEOCAT version of the updated GOES WF_ABBA to the AIT. The delivery included the GEOCAT fire code, a build document, and updated I/O tables. The ABI version will be integrated into GEOCAT and transferred as part of the second delivery (version 0.5).



The McIDAS ABI fire code was further developed and evaluated using a limited set of model simulated ABI data provided by CIRA and MODIS simulated ABI data provided by CIMSS. Version 6.5 of the current WF_ABBA was also applied to Met-8/-9 and MTSAT-1R data to provide an assessment of the effect of regridding/resampling on fire detection with the WF_ABBA (Met-8) and data from a large detector array (MTSAT-1R). The initial CIRA model simulated data set included three case studies where an array of fictitious fires was embedded in imagery in the Great Plains on 08 May 2003. These case studies provide examples for each of the following: constant fire with no cloud, variable fire with no cloud, and constant fire with cloud. The case studies span 6 hours with imagery every 5 minutes allowing CIMSS to test the robustness of the ABI WF_ABBA for fire detection and characterization under both clear and cloudy skies with prescribed fires. CIRA delivered a second data set for Central America (23 April 2004) that contains realistic fires and clouds. CIMSS has provided MODIS to ABI simulated data sets for 8 case studies in North, Central, and South America. Although truth is not known for the MODIS to ABI case studies, these data sets provide realistic examples of fire activity in the Western Hemisphere and can be produced in less than a day.

Results from the application of the ABI fire code to both the model simulated and MODIS to ABI simulated data are encouraging. Figure 5.9.1 shows the application of the ABI fire code to CIRA simulated ABI data for the variable fire with no cloud case study on 08 May 2003 at 19:15 UTC. Figure 5.9.2 shows the ABI fire mask for the MODIS simulated ABI data on 23 October 2007 at the height of the wildfire activity in Southern California. In both cases the CIMSS ABI fire code identifies over 95% of the fire clusters with no false alarms. Code was written to automatically compare the ABI fire code output with the CIRA and MODIS simulated ABI proxy data sets. For the CIRA constant fire no cloud truth data sets, the ABI fire code is able to detect fires in all fire clusters, although fringe fire pixels go undetected at times because the fire within a specific pixel is too small/cold or the majority of the hotspots lie outside of the core of the ABI pixel. When applying the ABI viewing geometry and Point Spread Function (PSF), some of the edge pixels around a fire are influenced by a small portion of the fire. It appears that the ABI fire code is able to detect more than 85% of the fire pixels in clear sky conditions based on the sensor's capability, with minimal false alarms (less than 5%). For fire detection, it appears that the algorithm is performing quite well and close to the X80 level.

We evaluated the ABI sub-pixel fire characterization performance for both the CIRA model simulated data and the MODIS simulated ABI data, though no truth is available for the MODIS simulated data. Unfortunately the majority of the CIRA model simulated fires resulted in saturated pixels. For those pixels that are not saturated or cloud covered, the average WF_ABBA fire size is about 60% of the corresponding CIRA fire size and the average WF_ABBA FRP for non-saturated fire pixels is about 76% of the corresponding CIRA FRP. This percentage is better than what is expected in clear sky conditions at this satellite view angle and we feel more "truth" data sets are needed to verify this result. There is no truth available for the MODIS simulated ABI data sets, but it is worthwhile to compare regional calculations of the operational MODIS FRP product with the ABI simulated product. For the 2003 wildfires in Southern California and the Central American case study, the MODIS and ABI derived FRP are on average within 10% of each other. Larger differences are observed in South America.

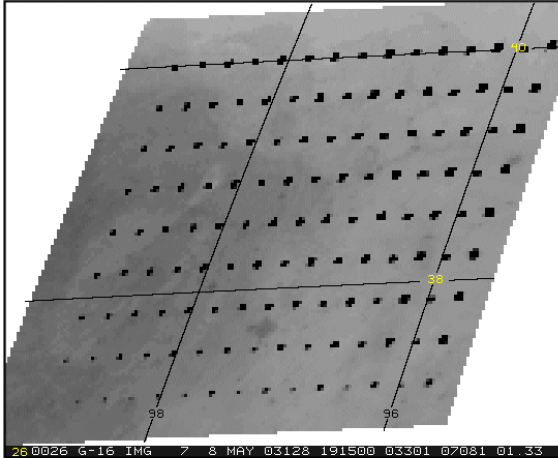


Application of Prototype ABI Fire Algorithm to Model Simulated Data over the Great Plains

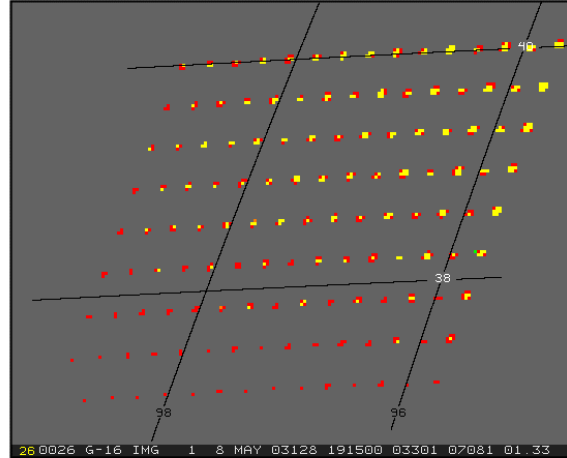
Date: 8 May 2003

Time: 19:15 UTC

Variable Fire - No Cloud Case Study



CIRA Model Simulated ABI
3.9 micron band



CIMSS ABI Fire Mask Product
Biome Block-Out Zone ■

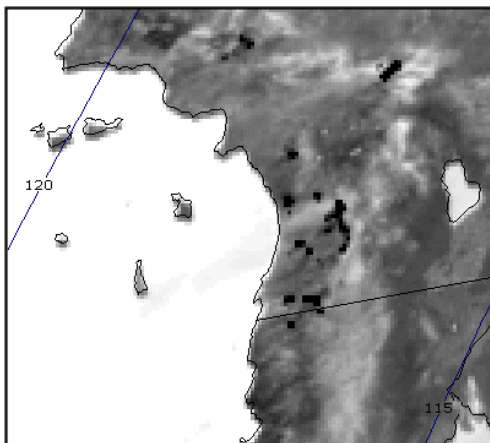


Figure 5.9.1: Application of the prototype ABI fire algorithm to model simulated data over the Great Plains.

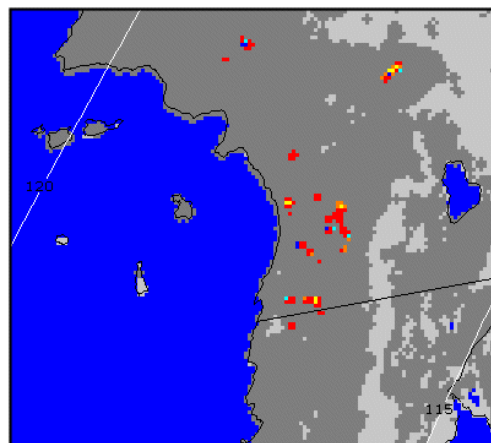
Application of Prototype ABI Fire Algorithm to MODIS Simulated ABI Data over Southern California

Date: 23 October 2007

Time: 18:25 UTC



MODIS Simulated ABI 3.9 micron band



GOES-R ABI Fire Product Mask



Figure 5.9.2: Application of the prototype ABI fire algorithm to MODIS simulated ABI data over Southern California.



Publications and Conference Reports

Schmidt, Christopher C., E.M. Prins, J.P. Hoffman, J.C. Brunner, S. Lindstrom, M. Gunshor, D. Santek, and G. Martin, 2007: GOES-R Fire Detection and Characterization, Algorithm Working Group Annual Meeting, National Conference Center, Landsowne, VA, 14-18 May 2007.

Schmidt, Christopher C., E.M. Prins, J.P. Hoffman, S. Lindstrom, J.C. Brunner, and J. Feltz, 2007: GOES-R ABI fire detection and monitoring with the WildFire ABBA, The joint 2007 EUMETSAT Meteorological Satellite Conference and the 15th America Meteorological Society (AMS) Satellite Meteorology & Oceanography Conference, RAI Center, Amsterdam, Netherlands, 24-28 September 2007.

5.10. GOES-R Legacy Profile Algorithm Evaluation and Selection - Jun Li and Tim Schmit

Proposed Work

1. Work on GOES-R sounding algorithm design review;
2. Develop Version 1.0 of ABI legacy profile retrieval algorithm;
3. Collaborate with GOES-R AWG cloud team (Dr. Heidinger) on applying cloud mask algorithm;
4. Demonstrate Version 1.0 algorithm by using WRF-simulated full disk ABI proxy data, which are provided by proxy team;
5. Evaluate and develop Version 1 of ABI retrieval algorithms;
6. Make available the version 1.0 code and documentation to STAR for implementation in the STAR collaborative environment;
7. Assist in the demonstration and interpretation of performance of the CIMSS algorithm on proxy data sets.

Summary of Accomplishments and Findings

AWG sounding algorithm design review (ADR) was held

GOES-R AWG sounding algorithm team (SAT) algorithm design review (ADR) was held on 21 June 2007. Co-chair Tim Schmit presented the ADR. Mitch Goldberg, Jaime Daniels, Monica Coakley, Chris Barnet, et al. attended the meeting. CIMSS sounding team helped prepare the ADR. The ADR went well, suggestions from AWG management will be included in legacy algorithm; the day one product will be based on the single time step radiances. Using single time step in algorithm avoids the collocation error and the complexity of clear/cloudy mixture between two times. The users can easily produce composite product from multiple times. In addition, better handling surface infrared emissivities and temporal information in sounding retrieval will be studied under GOES-R risk reduction project according to Mitch Goldberg's advice.

Version 1.0 algorithm has been delivered

The GOES-R AWG sounding algorithm version 1.0 (statistical approach) was delivered in August 2007 for Algorithm Integration Team (AIT) to test. The delivered package is available at: http://cimss.ssec.wisc.edu/goes_r/awg/sounding/. The version 1.0 algorithm uses a regression approach; it combines forecast and ABI infrared radiances for legacy soundings. The algorithm has been evaluated using one month's SEVIRI data and radiosonde observations. The legacy algorithm and software are implemented to process the simulated ABI infrared radiances. ABI simulated radiances are provided by proxy team, a pre-determined clear sky mask is used, the clear sky mask is assumed to be available from



AWG cloud team, ECMWF 6-hour forecast are used for algorithm demonstration and implementation purpose. The forecast can be replaced by other forecast model output.

Version 2.0 algorithm for SEVIRI (V2.0S) has been released to AIT

GOES-R AWG legacy profile version 2.0 algorithm/software (science codes) for SEVIRI processing was delivered to algorithm integration team (AIT) and GEOCAT team for implementation. The version 2.0 software is based on the physical iterative retrieval algorithm. The package contains science codes, technical document and a single footprint SEVIRI test data set. The GEOCAT team is working on the implementation of the algorithm/software. GEOCAT already has model forecast input temporally and vertically interpolated. Spatially interpolation is also expected to be performed for SEVIRI process. Version 2.0 is currently for SEVIRI data processing only, Figure 5.10.1 shows the Total Precipitable Water (TPW) image from SEVIRI. A version 2.0 package is also being developed for processing the simulated ABI (V2.0A) radiances developed by proxy team. Version 2.0A is expected to be released to AIT in February 2008.

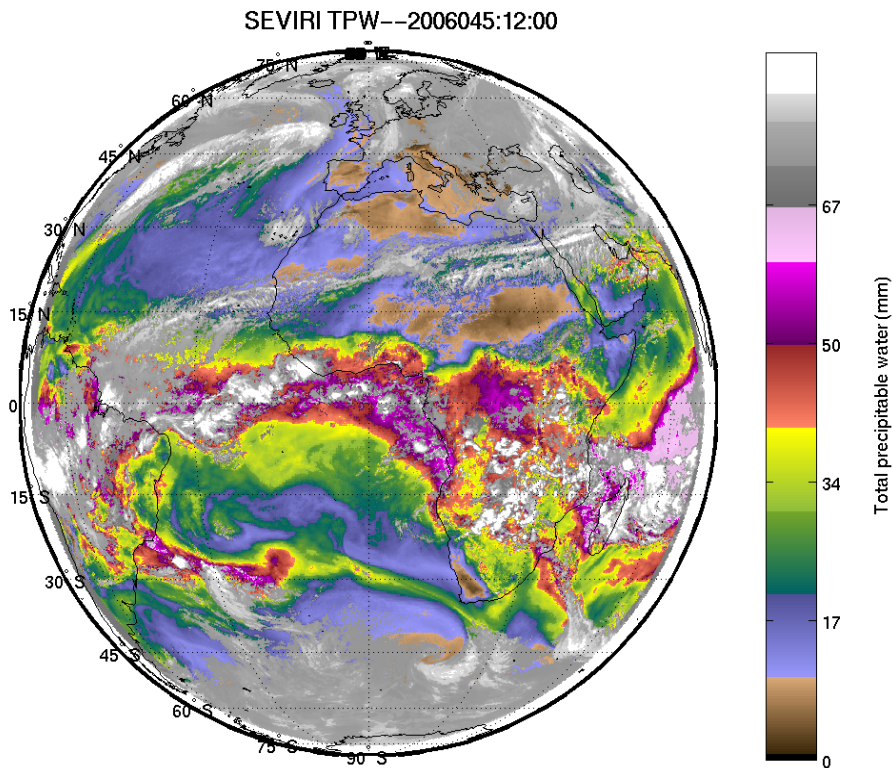


Figure 5.10.1: Very preliminary TPW overlay on the 11 μm brightness temperature (BT) image (black and white) from SEVIRI.

CIMSS legacy profile algorithm is recommended for EUMETSAT SEVIRI nowcasting product generation

The current EUMETSAT nowcasting SAF uses neural network (NN) for nowcasting product (LI, TPW, CAPE) generation from SEVIRI. Recently they proposed to use a physical retrieval algorithm to replace the NN approach. The CIMSS legacy profile algorithm is recommended. Based on the GOES-R Risk Reduction and AWG TAC advice on enhancing the international collaboration, the version 2.0 algorithm/documents for SEVIRI has been provided to EUMETSAT nowcasting SAF in Madrid, Spain for their operational implementation.



Legacy profile algorithm evaluated

The ABI legacy profile algorithm was initially evaluated with SEVIRI and Advanced Microwave Scanning Radiometer for Earth Observing System (AMSR-E). The SEVIRI TPW retrievals from ABI legacy profile physical algorithm (version 2.0) were compared with operational AMSR-E TPW product over ocean for August 2006. The temporal distance between SEVIRI and AMSR-E is less than 15 minutes, and the spatial distance between the two types of observations is less than 10 km. Figure 5.10.2 shows the TPW scatterplot between AMSR-E and SEVIRI. The two observations agree very well with correlation of 0.96. When SEVIRI TPW is less than 25 mm, SEVIRI has slight wet bias. When SEVIRI TPW is greater than 25 mm, SEVIRI has slight dry bias, which is consistent with the MODIS results (Seemann et al. 2003 - *JAM*). Initial evaluation over land was also carried out using radiosonde observations. Results show that substantial improvement from SEVIRI over the forecast can be seen between 300 and 700 hPa for moisture.

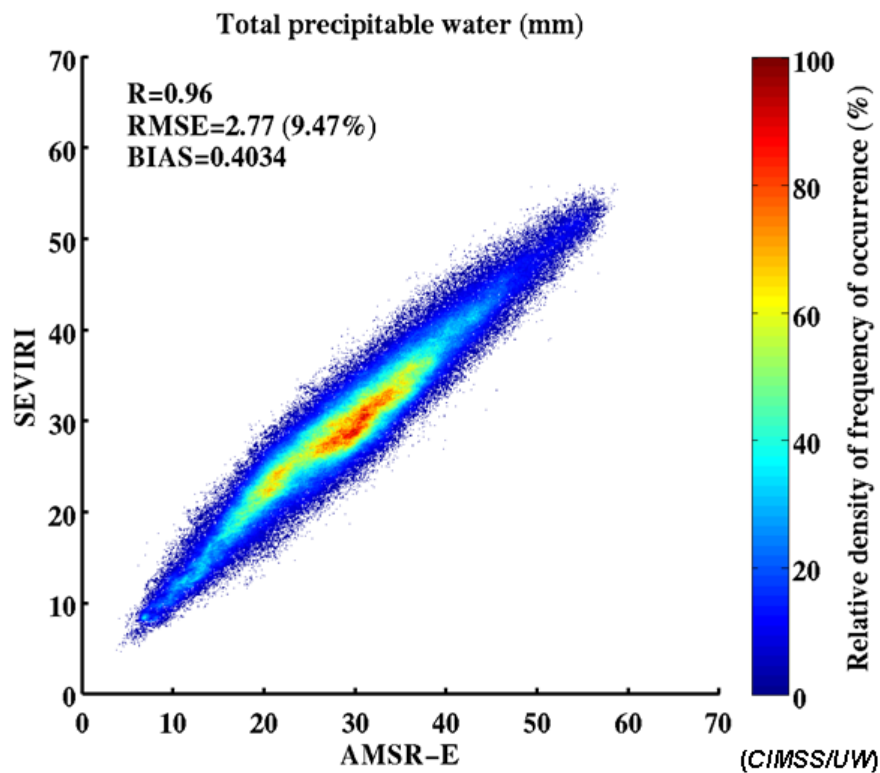


Figure 5.10.2: The TPW scatterplot between AMSR-E and SEVIRI for August 2006.

Publications

Jin, Xin, J. Li, J.P. Nelson III, C.C. Schmidt, Z. Li, T.J. Schmit, and M.D. Goldberg, 2007: An improved atmospheric profile retrieval system for GOES Sounder and SEVIRI data, *Proceedings of SPIE 6684*.

Schmit, Timothy J., J. Li, J.J. Gurka, M.D. Goldberg, K. Schrab, Jinlong Li, and W. Feltz, 2007: The GOES-R ABI (Advanced Baseline Imager) and the continuation of GOES-N class sounder products, *J. of Appl. Meteorol. Cli.* (conditionally accepted).



5.11. Sounding Product Evaluation and Validation – Dave Tobin and Tom Achtor

Proposed Work

Our plan was to produce and provide ARM site and aircraft-based data sets for AWG sounding algorithm validation, and to use the data sets to assess the algorithms. We have prior experience with both sets of data and with retrieval validation. After coordinating some details of the data sets (e.g. what timeframe to focus on, what sites) with other members of the Sounding AWG, we planned to begin to assemble the data sets. For the ARM sites, assembling the data sets will include best estimates of the surface, atmospheric temperature and water vapor profiles as well as cloud observations from an array of ARM site observations, along with coincident satellite observations including those from AIRS, MODIS, and GOES. The aircraft data sets will include the S-HIS and/or NAST-I radiance observations and coincident validation data, where the source of the validation data varies from campaign to campaign. We planned to assemble these data sets in a data analysis and visualization environment that will support the evaluation of the algorithm with optimal statistical methods and high quality visualization output products. This environment supports data fusion and facilitates the development of new techniques for analysis that may be needed.

Summary of Accomplishments and Findings

We assessed data set needs for validation and Sounding AWG members recently made available routine ABI legacy profile retrievals. Much of the resources allocated for this task have been saved until routine availability of these soundings have been put into place. DOE ARM and aircraft data sets are available for focused sounding validation.

The plan for remainder of FY2008 resources includes implementing a way to access DOE ARM data streams and ABI legacy sounding profile database into McIDAS-V. Doing so will allow robust validation of GEOCAT generated ABI profiles.

Milestone Plan for remainder of resources:

- Continue to coordinate data set needs with Sounding AWG Co-chairs and members.
Coordinate a two-pronged validation approach: validate August 2006 ABI legacy profiles simulated from SEVIRI proxy data using convectional and research grade validation resources; and integrate Jun Li's SEVIRI sounding package into GEOCAT to allow routine processing and to produce larger validation data sets.
- Continue to assemble ARM and aircraft data sets in suitable validation environment.
Continue to coordinate data from several European instrumented testbeds in England and Germany.
Use DOE ARM mobile facility data from Niger, Africa to validate August 2006 ABI legacy profiles.
- Perform ABI legacy profile algorithm validation analyses (Spring 2008).
Incorporate a GOES-R AWG sounding package that uses SEVIRI data as proxy data input into GEOCAT to allow routine "on-the-fly" profile quality control.
Implement match-up file creation in GEOCAT to make validation easier.

5.12. GOES-R AWG Winds – Chris Velden, Steve Wanzong and Iliana Genkova

Proposed Work

The development and automated processing of wind vectors from satellites has its heritage at CIMSS. The work plan research objectives seek to continue this heritage by adapting current methods and algorithms to NOAA's next generation of geostationary satellites, starting with GOES-R. The ABI will



provide both traditional and new spectral channels that the CIMSS winds team will test, process and validate using simulated and proxy data sets provided by other members of the GOES-R AWG project.

In 2007, we planned to use locally available hardware resources initially for software testing, with a phased transition to a collaborative testbed environment as it comes online. The proxy data took advantage of existing imagery from GOES and MSG/SEVERI. We also employed ABI simulated imagery for select case studies. The algorithm development, testing and validation will focus on heritage algorithms currently being used in NESDIS operations today to generate winds from satellite imagery. We leveraged and adapted current algorithms/software to expected ABI characteristics, focusing first on ABI heritage channels (VIS, IR-W, WV) for winds testing. We then focused on the new spectral capabilities afforded by the ABI for wind derivation. All software development followed accepted AWG standards, and has documentation.

This work ensures the readiness of the CIMSS/NESDIS automated winds algorithm for eventual operational implementation upon the deployment of GOES-R ABI.

Summary of Accomplishments and Findings

During this reporting year, the development of the winds retrieval algorithm for GOES-R ABI targeted the following goals:

- 1) Redesign the current operational winds code to meet the AWG standards in terms of documentation, programming language, and embedding it into a GOER-R ABI AWG framework;
- 2) Test the algorithm performance using simulated and proxy data sets;
- 3) Address the need for new approaches to vector height assignment and quality control.

The team prepared an Atmospheric Motion Vector (AMV) flowchart package for the AWG Integration Team to meet requirements. It includes top level and detailed flowcharts, a table of programs and subroutines, subroutines/function calling trees, tables of input and output files and directory listings for all AMV software modules – targeting and height assignment, tracking, and nine quality control modules. The targeting, feature tracking, and quality indicator routines have been rewritten and added to the current choice of ABI algorithm development framework, i.e. GEOCAT. Navigation and calibration steps are now in the part of the processing flow handling ABI radiances and are no longer a direct part of the winds algorithm.

Another major implementation involved using the AWG Cloud team's cloud heights product to assign AMV target heights. Pixel-level cloud-top heights are converted to target heights using the 25% coldest in terms of IR brightness temperature (BT) pixels and calculating the median value as an effective target height. We have also started using CALIPSO data to validate these assigned heights. However, this technique only applies to cloud-tracked vectors. The clear sky WV winds height assignment currently remains the same process.

To address calibration and navigation issues when extracting AMVs from spectral channels not currently available on NOAA satellites, we developed an ABI specific calibration module. IR and WV channels are included. It allows us to test the winds retrieval on simulated ABI and SEVIRI proxy data, including non-heritage IR and WV channels. We also worked on adding capabilities to GEOCAT to handle ABI simulated data and pass it to all AWG algorithms including the AMV retrieval.

Once the tools were developed to work with ABI synthetic data, we conducted two major GRAFIIR studies. The GRAFIIR idea was first introduced and implemented in May 2007, and presented at the GOER-R AWG meeting. In brief, it is a GOES-R effort to assess instrument impact on GOES-R retrieval



algorithm performance. Our studies are using synthetic data over CONUS (data set produced at CIMSS by the Proxy Team) having 2 km spatial and 5 min, 15 min, 30 min temporal resolution (the data for the first study was originally at 6 km pixel but remapped to 3 km). All IR and WV channels were available. We applied 1x, 2x and 3x times the specs' impacts (calibration, navigation errors, etc.) and prepared ABI simulated imagery to demonstrate the instrument impact on the AMV algorithm.

The following alterations are added to the pure ABI TOA radiances:

- CalOffset1K, CalOffset2K,
- NavError1x, NavError2x,
- NoiseFactor1x, NoiseFactor2x,
- Striping1x, Striping2x,
- CalOffset1K, NoiseFactor1x,
- CalOffset1K_NoiseFactor1x_NavError1x_Striping1x,
- CalOffset2K_NoiseFactor2x_NavError2x_Striping2x,
- NoiseFactor3x_NavError3x_Striping3x.

We found that the quality of the AMVs is generally preserved despite the added impacts – see Table 5.12.1.

Table 5.12.1: GRAFIIR Stats over CONUS – 04 June 2005

Water Vapor (WV) Atmospheric Motion Vectors						
Image Interval (Minutes)	Number of Matches		Speed Bias (AMV-WRF)		V (AMV vs. WRF)	
	Pure	3x AIE	Pure	3x AIE	Pure	3x AIE
5	3041	534	-0.064	1.6648	5.1523	6.1122
15	2693	1198	0.0554	1.6774	4.7039	5.2942
30	2124	1217	0.0698	1.4038	5.0002	4.8443
Infrared (IR) Atmospheric Motion Vectors						
Image Interval (Minutes)	Number of Matches		Speed Bias (AMV-WRF)		V (AMV vs. WRF)	
	Pure	3x AIE	Pure	3x AIE	Pure	3x AIE
5	4157	1615	-0.355	0.1657	4.4490	4.7329
15	3754	2825	-0.564	0.7658	4.0065	3.8399
30	2484	1890	0.5022	0.7612	4.0185	3.4238
All (IR & WV) Atmospheric Motion Vectors						
Image Interval (Minutes)	Number of Matches		Speed Bias (AMV-WRF)		V (AMV vs. WRF)	
	Pure	3x AIE	Pure	3x AIE	Pure	3x AIE
5	7189	2149	-0.232	0.5382	4.7588	5.1105
15	6447	4014	0.0971	1.0358	4.3116	4.3220
30	4608	3128	0.3029	1.0129	4.4977	4.0402

All AMVs were quality controlled and compared to RAOBs. Statistics for the Pure and the 3x tests, 3 temporal steps, and for low, mid and high winds were calculated for IR and WV heritage bands separately and together. These results were presented at the 5th GOES Users' Conference, 88th AMS Annual Meeting, New Orleans, LA, 21-24 January 2008 (Huang et al.).

We are currently performing a further analysis of the derived AMV data sets (ongoing work, which will continue in 2008). The 5, 15 and 30 min AMV data will be collocated, and statistics for the matched



RAOB winds will be calculated in a similar manner to the preliminary results described above. The final analysis will be presented at the 9th Winds Working Group workshop in April 2008.

Another important task is an exploration of the best quality assessment parameter for the AMV in addition to the widely approved and used quality indicator (QI). We examined the skill of a new index, the expected error (EE), and compared that to the QI's skill. Table 5.12.2 shows statistics of a set of AMVs compared to RAOBs as thresholded by a maximum EE. The number of matches, speed bias, rms-vector difference and average RAOB speed are included in the tables. GOES-12 IR AMVs from 03 August – 01 October 2007 were included in this data set. To better compare these results to the operational results, only QI values (forecast independent) greater than 0.5 are included, and matches with AMV – RAOB vector differences greater than 30 ms⁻¹ are omitted. As this table shows, and has been discussed in previous reports, the RMS vector differences decrease as the EE maximum decreases. The upper-level biases are fairly constant and the average RAOB speed decreases with decreasing expected error.

A similar table is shown for the QI in Table 5.12.3. This table shows the same statistics as in Table 5.12.2 except it uses QI minimums to threshold the data rather than EE maximums. The QI impacts the AMV – RAOB statistics quite differently than the EE does. The RMS vector differences at all levels drop only slightly with increasing QI minimum. In the mid-levels, RMS differences increase slightly as the QI minimum increases to about 0.8. The mid and upper-level speed biases generally decrease (in magnitude) as the QI minimum threshold is increased. The most striking difference, however, is that the average RAOB (and AMV) speed increases as the QI threshold minimum increases. Although the RMS vector difference of the QI stays fairly constant, the normalized RMS (by average RAOB speed) decreases linearly with increasing QI thresholds.

Table 5.12.2: AMV-RAOB statistics for the unmatched AMV data as binned by a maximum Expected error (EE). Lowering the allowable EE threshold reduces the RMS vector differences. To get AMV performance statistics close to those of the current Recursive Filter (auto-editor), the maximum allowable EE must be lowered to a threshold just lower than 6 m/s.

Expected Error Max		3	4	5	6	7	8	9	10	11	12
Number of matches	100 - 400	1845	7640	18328	30763	40417	46210	48962	50126	50576	50712
	400 - 700	750	2495	5000	7538	9576	10811	11387	11676	11763	11810
	700-1000	1920	3120	4065	4725	5070	5186	5209	5209	5209	5209
Spd Bias (AMV \bar{S} RAOB)	100 - 400	-1.63	-1.73	-2.02	-2.12	-2.17	-2.16	-2.14	-2.11	-2.06	-2.04
	400 - 700	-1.27	-1.33	-1.43	-1.47	-1.54	-1.54	-1.50	-1.43	-1.38	-1.34
	700-1000	-0.44	-0.42	-0.33	-0.27	-0.25	-0.24	-0.23	-0.23	-0.23	-0.23
RMS Vector Diff. (vs RAOB)	100 - 400	5.09	5.92	6.78	7.48	8.06	8.45	8.67	8.79	8.46	8.87
	400 - 700	4.20	4.79	5.39	6.01	6.58	6.97	7.20	7.31	7.37	7.42
	700-1000	3.78	4.10	4.48	4.74	4.84	4.88	4.89	4.89	4.89	4.89
Avg RAOB Speed	100 - 400	10.66	12.79	14.61	16.04	17.24	18.15	18.68	18.98	19.11	19.16
	400 - 700	9.63	11.15	12.36	13.11	13.82	14.34	14.60	14.75	14.82	14.84
	700-1000	7.55	8.12	8.43	8.60	8.65	8.68	8.68	8.68	8.68	8.68



Table 5.12.3: AMV-RAOB statistics for the unmatched AMV data as binned by a minimum QI. Raising the minimum QI reduces the RMS vector differences slightly. Unlike the EE, however, the average RAOB speed within the thresholds increases as the QI goes up.

QI Min	1.0	0.95	0.90	0.85	0.8	0.75	0.7	0.65	0.6	0.55	0.5	
Number of Matches	100 - 400	1960	11447	16869	20290	24572	27706	30550	33415	35760	39463	41705
	400 - 700	169	1290	2093	2664	3525	4171	4815	5497	6101	7353	8025
	700-1000	65	514	886	1135	1488	1760	2033	2300	2574	3107	3418
Spd Bias (AMV \bar{S} RAOB)	100 - 400	-0.48	-0.76	-1.02	-1.17	-1.36	-1.5	-1.6	-1.7	-1.8	-1.94	-2.02
	400 - 700	0.93	-0.02	-0.5	-0.61	-0.79	-0.88	-0.99	-1.1	-1.17	-1.25	-1.3
	700-1000	0.56	0.26	0.17	0.08	0.05	-0.04	-0.1	-0.18	-0.24	-0.22	-0.23
RMS Vector Diff. (vs RAOB)	100 - 400	8.43	8.3	8.39	8.43	8.49	8.55	8.6	8.66	8.72	8.82	8.89
	400 \bar{S} 700	8.1	7.55	7.49	7.38	7.33	7.25	7.29	7.32	7.33	7.45	7.46
	700-1000	4.81	4.28	4.42	4.48	4.51	4.55	4.59	4.68	4.7	4.86	4.89
Avg RAOB Speed	100 - 400	25.52	22.82	22.04	21.61	21.12	20.78	20.42	20.06	19.75	19.42	19.18
	400 \bar{S} 700	18.69	17.78	17.44	16.99	16.54	16.21	15.97	15.66	15.39	15.09	14.88
	700-1000	10.34	9.03	9.01	9.04	8.87	8.86	8.83	8.82	8.76	8.72	8.68

Publications and Conference reports

Wanzong, Steve, W. Bresky, I. Genkova, J. Daniels, C.S. Velden, and D.A. Santek: Status of atmospheric motion vector research for GOES-R ABI. Annual GOES-R AWG Conference, National Conference Center, Ashburn, Virginia, May 2007.

Genkova, Iliana, S. Wanzong, C.S. Velden, L. Grasso and M. DeMaria: Wind retrieval performance on synthetic GOES-R ABI imagery. Joint 2007 EUMETSAT Meteorological Satellite Conference and the 15th Satellite Meteorology and Oceanography Conference of the American Meteorological Society, Amsterdam, The Netherlands, September 2007.

Wanzong, Steve, C.S. Velden, I. Genkova, D.A. Santek, N. Bormann, J. Thepaut, D. Salmond, M. Hortal, J. Li, E.R. Olson, and J.A. Otkin: The use of simulated data sets in atmospheric motion vector research. Joint 2007 EUMETSAT Meteorological Satellite Conference and the 15th Satellite Meteorology and Oceanography Conference of the American Meteorological Society, Amsterdam, The Netherlands, September 2007.

Berger, Howard, C.S. Velden, S. Wanzong, and J. Daniels: Evaluation of a new quality indicator to estimate satellite-derived Atmospheric Motion Vector observation error. Joint 2007 EUMETSAT Meteorological Satellite Conference and Satellite Meteorology and Oceanography Conference, 15th, of the American Meteorological Society, Amsterdam, the Netherlands, September 2007.

5.13. GPSDI Hurricane Intensity from ABI – Chris Velden and Tim Olander

Proposed Work

Researchers at CIMSS obtained simulated GOES-Advanced Baseline Imager (ABI) data collected at CIRA. The simulated data set consists of all available high-resolution MODIS infrared imagery for selected North Atlantic tropical cyclones (TC). From these images, TC intensity estimates were derived



using the CIMSS Advanced Dvorak Technique (ADT). The ADT intensity estimates from the simulated GOES-ABI data were compared to ADT intensity estimates using coincident GOES infrared imagery as well as intensity estimates obtained from several operational TC forecast centers (OpCen). Statistical analysis of the ADT (for each GOES data set) and OpCen performance were compared to in situ aircraft reconnaissance measurements of mean sea level pressure (MSLP) to assess the impact of simulated GOES-ABI imagery over current GOES imagery.

Summary of Accomplishments and Findings

Homogeneous ADT estimates from the current and simulated GOES data sets (within +/- 15 minutes) were compared. 42 ADT estimates were obtained within one hour of a reconnaissance MSLP measurement and 30 minutes of one or more OpCen intensity estimates over 11 Atlantic basin storms between 2002 and 2006.

Table 5.13.1: ADT Bias and RMSE values for estimated TC MSLP (in hPa), as compared to aircraft reconnaissance measurements, for ADT intensity estimates using simulated GOES-ABI and coincident real GOES imagery, and operational TC forecast center estimates. The sample comprises 42 estimates.

Intensity	GOES-ABI		GOES-current	
	Bias	RMSE	Bias	RMSE
Raw T#8.72	19.18		12.58	19.65
Final T#	9.16	17.77	11.92	16.76
CI#	5.55	13.01	6.68	11.41
OpCen	3.15	11.87	3.15	11.87

Due to the small sample size, it is difficult to conclusively ascertain the impact of the ABI data over the current data on the ADT. In general, Table 5.13.1 shows the bias of the simulated GOES ABI data tends to be lower than the bias observed with real GOES data. However, the RMSE of the final CI number for the GOES-ABI is slightly inferior to the real GOES data. For example, the GOES RMSE is slightly better than that achieved by the OpCen consensus but the simulated GOES-ABI RMSE is slightly worse.

Some tuning of the ADT scene type and intensity determination schemes will be necessary to account for the improved ABI spatial resolution and resulting scene type samples (i.e. more eye scenes), which we suspect is causing much of the differences in the results. Figure 5.13.1 shows the scene type differences and resulting Raw T# values for the current GOES and GOES-ABI intensity estimates versus aircraft reconnaissance for Hurricane Wilma in 2005.

In addition, the likely increased temporal image frequency between the current GOES (15 or 30 min.) and GOES-ABI (5 or 15 min.) will require modifications to the time-averaging scheme and various time-base rules.



Hurricane Wilma – October 2005

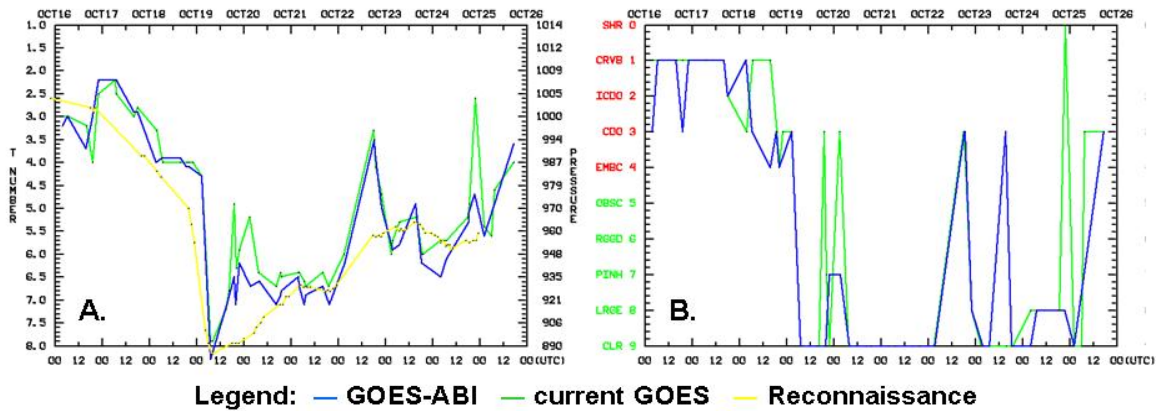


Figure 5.13.1: Hurricane Wilma (2005): A) ADT Raw T# Intensity Estimates: GOES-ABI (blue), current GOES (green), and aircraft reconnaissance (yellow). B) Scene type selection: green are eye scenes, red are non-eye scenes. Note scene type difference between CDO (GOES) to Pinhole Eye (PINH) (GOES-ABI) in B) around October 20/00UTC, and the coincident difference in Raw T# values in A).

5.14. Aviation – Wayne Feltz

Co-Chair Wayne Feltz and Chair Ken Pryor have been communicating monthly to produce a consistent schedule for all aviation related algorithm implementation. The Aviation AWG algorithm design review occurred on 16 November 2007. Aviation AWG team members Wayne Feltz and Michael Pavlonis attended the GOES-R AWG review in May 2007. Tony Wimmers also attended. He is conducting most of the turbulence research and algorithm implementation.

5.14.1. Volcanic Ash and SO₂ – Wayne Feltz and Michael Pavlonis

Proposed Work

We proposed to adapt advanced techniques for the detection of volcanic ash, the retrieval of ash cloud height, the retrieval of ash loading, and the detection of SO₂ for application to the GOES-R ABI. These techniques are based on relatively recent advances in infrared retrieval science, where measured radiances are converted into cloud emissivity. The information content of the measurements, with regard to volcanic aerosols, is maximized in cloud emissivity space. Simple brightness temperature differences offer far less sensitivity. This project involves algorithm and software development, testing on proxy data



sets, and validation. This work will ensure the readiness of the volcanic ash and SO₂ algorithms for operational implementation upon the deployment of GOES-R.

Summary of Accomplishments and Findings

We successfully developed and implemented a probabilistic ash detection scheme along with a volcanic ash cloud height and mass loading retrieval (see figures below). Both of these products are derived using infrared measurements (8.5, 11, 12, and 13.3 micrometers), so that they are spectrally day/night independent. A 7.3, 8.5-micrometer based SO₂ detection algorithm was also developed. All algorithms were implemented in the Geostationary Cloud Algorithm Testbed (GEOCAT) so that they can readily be delivered to the GOES-R Algorithm Implementation Team (AIT). The algorithms were applied to SEVIRI data, which has many spectral channels in common with ABI. The early results are very promising. The volcanic ash detection algorithm has a false alarm rate on the order of 0.001% and the ash cloud height and mass loading results are consistent with those derived from different techniques. The SO₂ detection algorithm has also showed great promise for extracting SO₂ signals from the measured 7.3 and 8.5-micrometer radiances. Finally, a detailed algorithm flowchart package was delivered to GOES-R AIT.

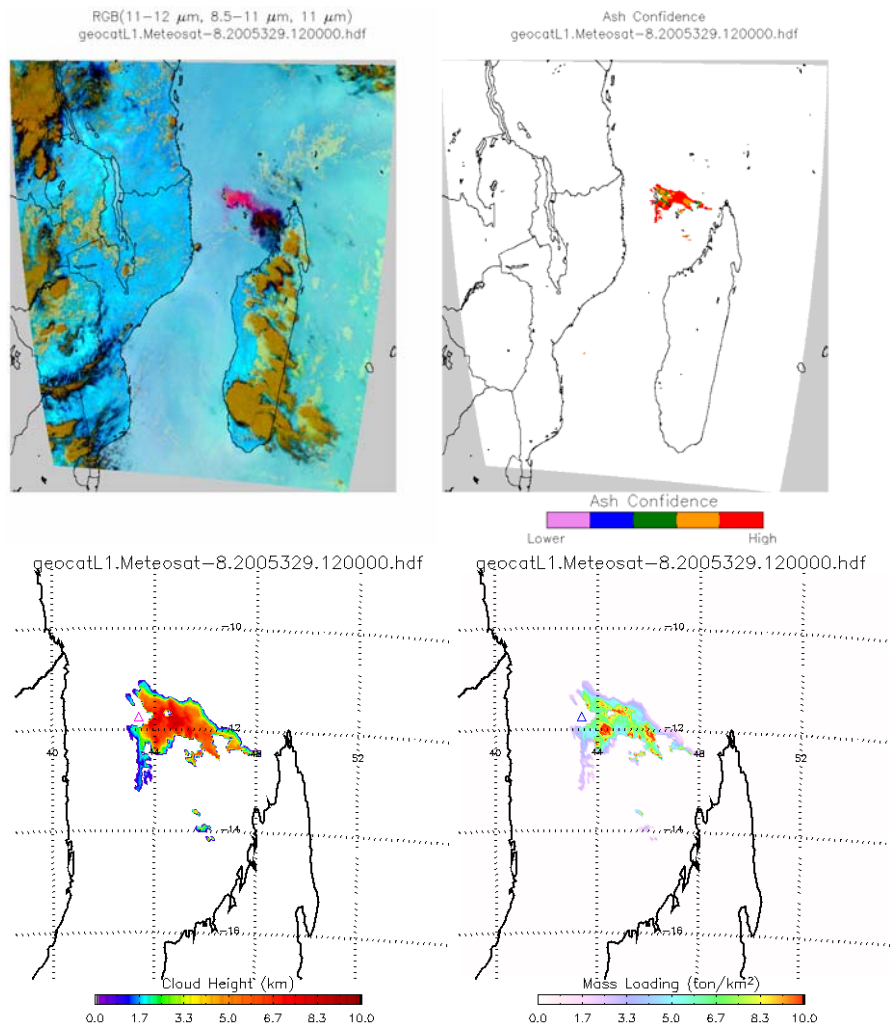


Figure 5.14.1.5: Top, left: An RGB image showing a volcanic ash cloud associated with the eruption of Karthala on November 25, 2005. Top, right: the results of the probabilistic ash mask. Bottom, left: The retrieved cloud top height (km). Bottom, right: The results of the mass loading retrieval (ton/km²).



5.14.2. Fog/Low Cloud – Wayne Feltz and Michael Pavlonis

Proposed Work

We proposed to adapt heritage techniques for the detection of fog/low cloud and the retrieval of fog depth for application to the GOES-R ABI. We also proposed to explore ways to enhance the performance of the heritage algorithms primarily through the use of additional channels that are available on ABI such as the 8.5-micrometer channel. This project involves algorithm and software development, testing on proxy data sets, and validation. This work will ensure the readiness of the fog/low cloud algorithms for operational implementation upon the deployment of GOES-R.

Summary of Accomplishments and Findings

We have successfully implemented the heritage NOAA/NESDIS fog detection and fog depth retrieval algorithms into the Geostationary Cloud Algorithm Testbed (GEOCAT) (see figure below). The heritage 3.9-micrometer based fog products were designed for nighttime only usage, so one of our goals is to mitigate this weakness so that reliable products can be retrieved for all solar zenith angles. With this goal in mind, we have explored ways to improve the algorithms using the 8.5-micrometer channel. The availability of the 8.5-micrometer channel on the ABI is significant. As an infrared channel, it offers day/night independent measurements. In contrast, use of the traditional 3.9-micrometer channel during the day is complicated by reflected sunlight. Our initial results indicate that, while the 8.5-micrometer channel is not quite as sensitive to fog/low cloud relative to other types of liquid water clouds, it does offer important information on the presence of fog. During the day, retrievals of cloud optical depth and particle size can be used to estimate fog depth. We have begun exploring the use of these products, derived by the cloud team, for gaining reliable fog depth estimates during the day. Finally, a detailed algorithm flowchart package was delivered to GOES-R AIT.

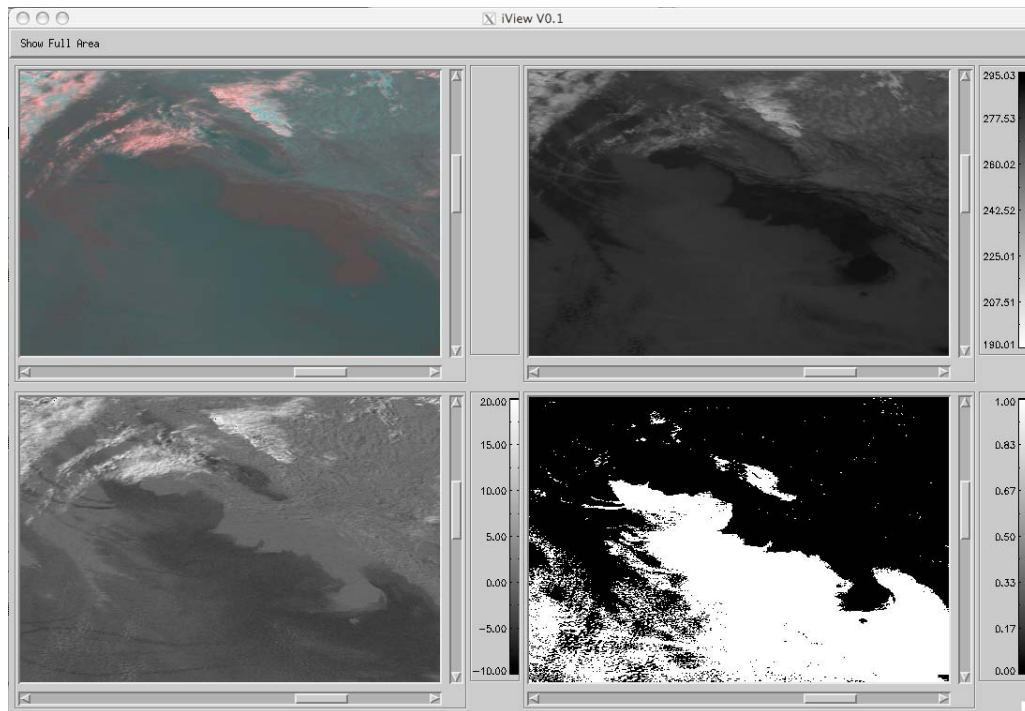


Figure 5.14.3.2: GOES-10 data and fog product output from GEOCAT for December 11, 2004 at 11:00 UTC over southern California and its coastal waters including (a) (upper left) RGB image using the 3.9 micrometer pseudo-



emissivity for the red gun and the 11 micrometer brightness temperature for the green and blue guns, (b) (upper right) 3.9 micrometer brightness temperature, (c) (lower left) 3.9 minus 11 micrometer brightness temperature difference, and (d) (lower right) heritage fog detection product which is based on the differences shown in image (c), white indicates fog/low cloud

5.14.3. Turbulence – Wayne Feltz and Tony Wimmers

Proposed Work

We proposed to adapt the technique used by Wimmers and Moody for the detection of upper tropospheric zones of turbulence to an application optimized for GOES-R (2004a, b). This project will involve software development, testing on proxy data sets, validation and documentation. This work will ensure the readiness of the turbulence detection algorithm for operational implementation upon the deployment of GOES-R.

Summary of Accomplishments and Findings

The accuracy of the tropopause-folding algorithm was improved by refining the criteria for satellite signatures corresponding to upper-tropospheric turbulence. We now consider gradient feature size, aircraft angle of approach, and distance from the tropopause fold. Also, the algorithm was tested on a 12-month data set of over two million automated, in-situ observations. Further turbulence prediction requirements were refined using model wind data. The algorithm was adjusted to fit more closely with the theory of clear air turbulence due to tropopause folding.

Validation of the tropospheric fold algorithm with NCAR United Airlines Eddy Diffusion Rate (EDR) objective turbulence reports over eastern United States from 01 May 2004 – 30 April 2006 was accomplished. The most robust prediction of turbulence occurred in the months of December – February. The high volume of data in the EDR reports enabled a determination of aircrafts' directional sensitivity to turbulence around the jet stream.

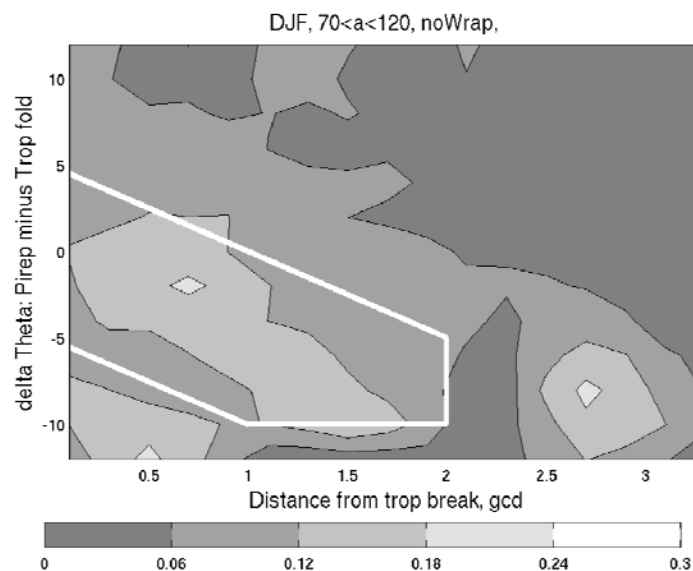


Figure 5.14.3.1: Vertical cross-section of turbulence probability at a tropopause fold. Horizontal axis is great circle degrees (gcd = 111 km); vertical axis is the potential temperature normalized for the tropopause height; solid white line is the expected area of turbulence.



A presentation about the turbulence algorithm was given at the EUMETSAT/AMS satellite conference in Amsterdam in September 2007. The presentation was titled “A prediction scheme for aircraft turbulence at tropopause folds using satellite imagery and EDR data.”

Finally, a detailed algorithm flowchart package was delivered to GOES-R AIT. Charts are available at: <http://www.orbit.nesdis.noaa.gov/star/goesr/FlowChartPackage/status.php>.

The Turbulence ADR was finished on 16 November 2007 and a presentation can be obtained at: http://www.orbit.nesdis.noaa.gov/star/goesr/ADR/adr_avn.zip.

Publications and Conference Reports

Wimmers, A., and W. Feltz, 2007: A prediction scheme for aircraft turbulence at tropopause folds using satellite imagery and EDR data. Joint 2007 EUMETSAT Meteorological Satellite Conference and Satellite Meteorology and Oceanography Conference, 15th, of the AMS, Amsterdam, the Netherlands, 24-28 September 2007. Proceedings. European Organization for the Exploitation of Meteorological Satellites (EUMETSAT), Darmstadt, Germany, 2007, Unpagged. Call Number: Reprint # 5572

5.15 Estimation of Sea and Lake Ice Characteristics with GOES-R ABI - Xuanji Wang, Yinghui Liu and Jeff Key

Proposed Work

To accomplish the goals outlined in the GOES-R AWG Project Plan, it is important to evaluate, improve, and develop sea and lake ice retrieval algorithms for application with GOES-R ABI. In this project, we are surveying and evaluating existing retrieval algorithms for sea and lake ice products (which includes ice concentration/extent, ice thickness/age, and ice motion) by comparing the products from other sources such as model simulations, submarine cruise measurements, and surface-based observations. The effort focuses on improving the current algorithms and developing new algorithms when necessary. The work will serve as a test-bed of the current algorithms for ice products, and will allow for algorithm testing and optimization to be done in consistent manner. AVHRR, MODIS, and SEVIRI data are being used as proxy data for the purpose of testing and validating candidate algorithms. This activity will ensure enhanced future geostationary cryosphere applications in the GOES-R era.

Summary of Accomplishments and Findings

The project started in May 2007, so this report covers approximately seven months of effort. Nevertheless, significant progress has been made; preliminary results are very promising and exciting for all ice products created from our algorithms. The survey and evaluation of potential algorithms has been completed, and improved and new algorithms have been proposed, coded, tested, and validated primarily with proxy data and validation data.

1. Ice concentration and extent

The sea ice concentration and extent algorithm is designed to combine the advantages of three existing ice concentration/extent retrieval algorithms: (1) a group threshold technique from the Earth Observation System (EOS) Moderate Resolution Imaging Spectroradiometer (MODIS) snow and sea ice mapping algorithms based on the normalized difference snow index and visible reflectance observations; (2) tie point analysis from the National Polar-Orbiting Operational Environment Satellite System (NPOESS) Visible/Infrared Imager/Radiometer Suite (VIIRS) fresh water ice algorithm; (3) tie point analysis from the Algorithm developed by Lindsay and Rothrock (1995). This algorithm is applied to proxy data, including AVHRR, MODIS and SEVIRI data, and the retrieved



products compare in good agreement with Advanced Microwave Scanning Radiometer - Earth Observing System (AMSR-E) Level-3 gridded daily mean products. An additional product, ice surface temperature retrieval, which is the first step to retrieve ice concentration particularly at night, is accomplished with the split-window technique developed by Key and Haefliger (1992).

2. Ice thickness and age

A variety of ice thickness estimation algorithms has been surveyed and evaluated, including the NPOESS/VIIRS sea ice thickness algorithm, a tracking algorithm for sea ice age (Fowler et al., 2004), a cluster algorithm for sea ice age (Massom and Comiso, 1994), and a sea ice slab model for sea ice thickness (Maykut and Untersteiner, 1971). We found it is necessary to develop a new algorithm specifically for GOES-R ABI applications based on comparisons between current algorithms and in-situ measurements. This One-dimensional Thermodynamic Ice Model (OTIM) is based on the surface energy balance at thermo-equilibrium that contains all components of the surface energy balance to estimate sea/lake ice thickness. Based on the knowledge of ice thickness, ice is then classified into open water, new/fresh ice, grey ice, grey-white ice, thin first year ice, medium first year ice, thick first year ice, multi-year ice. The OTIM has been implemented locally and applied to proxy data of AVHRR, MODIS, and SEVIRI, and also extensively compared and validated with numerical model simulations, submarine upward looking sonar ice draft data, and Canadian station measurements. The performance of the OTIM is the best in comparison with complicated numerical model simulations and other algorithms in terms of ground ‘truth.’

3. Ice motion

The heritage ice motion algorithm developed by Fowler et al (2004) has been adopted and implemented at the direct broadcast site in Tromsø, Norway using MODIS data as well as using archived SEVIRI data. This approach has been used to track ice over a given set of days and currently is used by the National Snow and Ice Data Center with AVHRR passes. A variety of time steps can be used to track the ice, though the best results are given when using images that are 24 hours apart. One downside to using this technique is that motion is detected in only a small fraction of the area due to the movement of clouds. Comparisons of Fowler code with the Medium Range Forecast Model (MRF) surface winds have yielded positive results, showing that the detected motion is similar that of the surface wind. Another algorithm developed by CIMSS for tropospheric winds, windco, has been also adopted and modified for ice motion estimation, using successive passes over the polar regions. A comparison between both ice motion algorithms has shown agreement in the direction of movement. Other options for validation, including the use of ocean buoys are being explored.

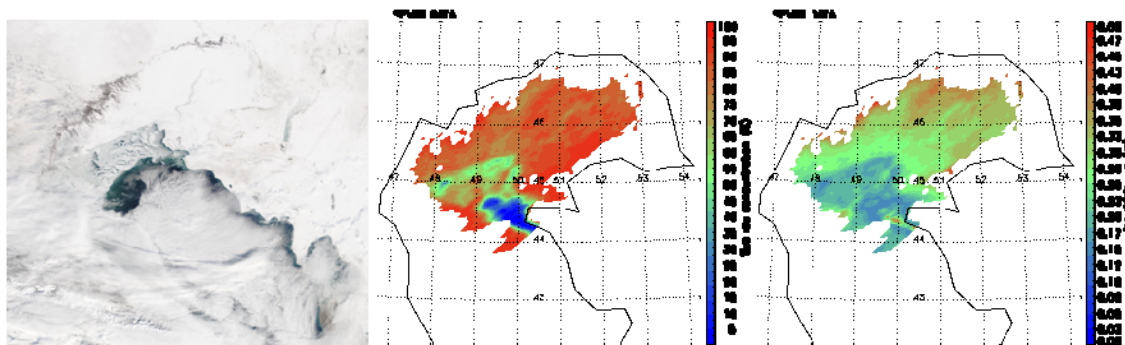


Figure 5.15.1: MODIS true color image (left) over the Caspian Sea on January 27, 2006 and the corresponding sea ice concentration (middle) and sea ice thickness (right) from SEVIRI at the same time.

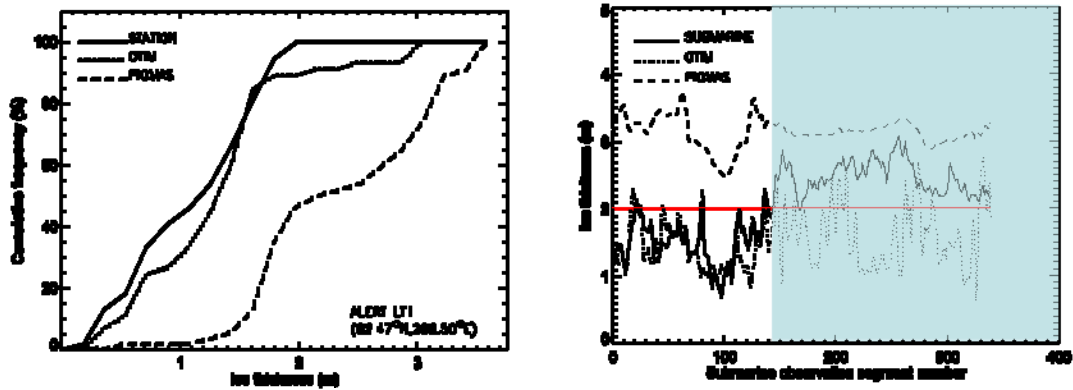


Figure 5.15.2: Comparison of ice thickness cumulative frequency distribution (left) from OTIM, Canadian station at Alert (82.47oN, 61.50oW), and Pan-Arctic Ice-Ocean Modeling and Assimilation System (PIOMAS) over 2002 ~ 2004, and a point-to-point comparison (right) of the ice thickness from OTIM, submarine, and PIOMAS during the SCICEX experiment in 1999 along the submarine track. OTIM ice thickness products were produced with AVHRR data.

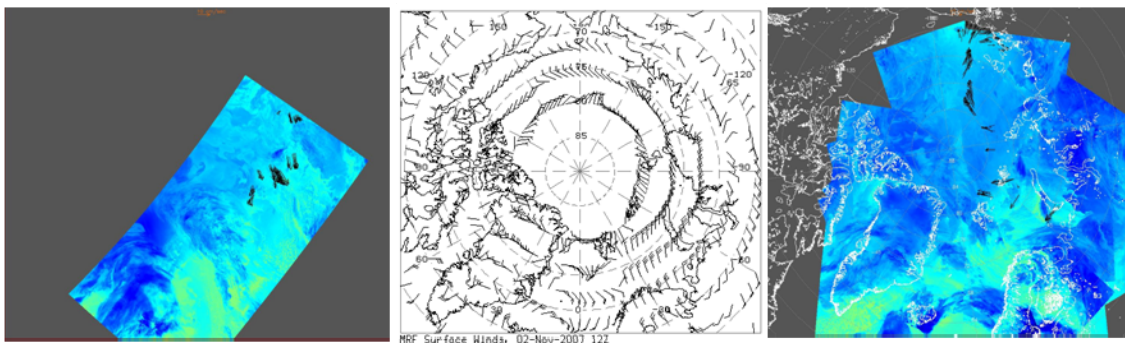


Figure 5.15.3: Comparison of ice motion from MODIS, utilizing the Tromsø direct broadcast site for 1252 UTC on 3 Nov, 2007, and the MRF model surface winds (middle) at 12 UTC. Orientation is the same on both images (left and middle). A composite for 19 December 19 2007 is shown on the right.

Publications and Conference Reports

Key, Jeff, P. Romanov, D. Cline, X. Wang, Y. Liu, and A. Rost, 2007: Evaluation of Snow and Ice Algorithms for GOES-R ABI, Annual GOES-R AWG Conference, 14-18 May 2007, National Conference Center, Ashburn, VA.

6. GOES-R (and beyond) instrument and requirement studies – Jun Li and Tim Schmit

Proposed Work

1. Continue to support necessary GOES-R reviews.
2. Continue to do necessary trade-off studies for next generation GOES sounding capability. (Note that this task is also partially supported by GOES-R Risk Reduction and AWG.)
3. Help to understand the ABI instrument and its relationship to various products.
4. Study the impact of GOES-R system characteristics and scan strategy on the science products and a wide variety of applications.
5. Demonstrate the values, merits, and benefits of GOES-R (and beyond).



6. Study the ABI continuation of current GOES Sounder class legacy products before hyperspectral IR on geostationary orbit.

Summary of Accomplishments and Findings

CIMSS-supported GOES-R reviews

CIMSS scientist Hank Revercomb was supported at Hyperspectral Environmental Suite (HES, end of formulation) and GOES-R reviews.

ABI continuation of current GOES Sounder legacy products studied

The feasibility of using the Advanced Baseline Imager (ABI) to continue the current operational GOES Sounder products is being studied. Simulations show that including the forecast information in ABI processing can provide similar results compared to current GOES Sounder class legacy products such as total precipitable water (TPW), Lifted Index (LI), etc. LI retrievals from GOES-12 also show that ABI can be used together with the forecast to continue the current GOES Sounder class legacy products before hyperspectral IR sounder is put on geostationary orbit. Figure 6.1 shows the scatterplot between true TPW and retrieved TPW with ABI + forecast, GOES-12 Sounder + forecast, and HES + forecast. The retrieval simulation is performed with radiosonde observations (RAOBs) over the Continental United States (CONUS) with lifted index less than zero, ABI noise is reduced to 10 km field-of-regard (FOR). The TPW retrieval simulation from approximately 300 unstable atmospheric profiles shows that ABI + forecast is similar to GOES Sounder + forecast, and both are better than forecast only. HES + forecast is much better than either ABI + forecast or GOES Sounder + forecast. On the other hand, ABI alone is slightly worse than the forecast, while the current GOES Sounder alone is better than the forecast. HES (final formulation) alone is much better than both forecast and the current GOES Sounder alone (not shown).

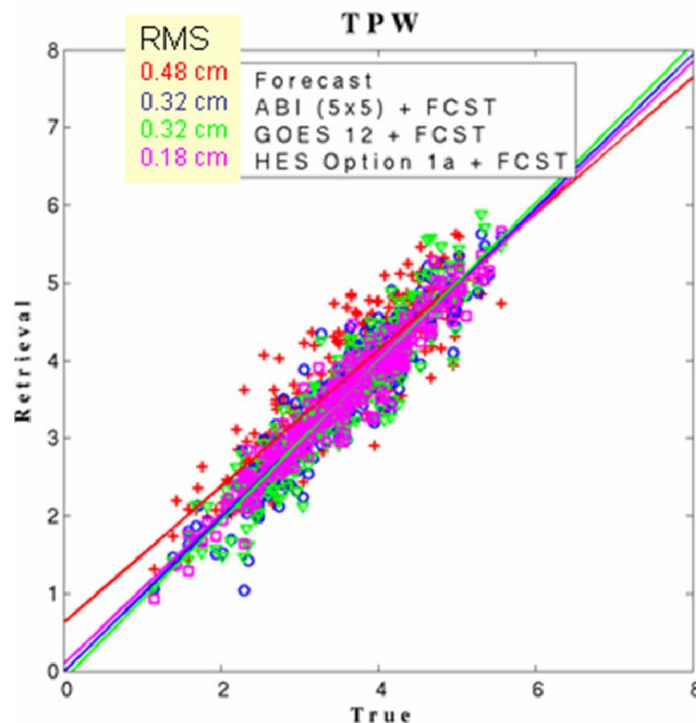


Figure 6.1: Scatterplot between true TPW and retrieved TWP with ABI + forecast, GOES-12 Sounder + forecast and HES + forecast.



Information content on ABI, GOES Sounder and GEO hyperspectral IR sounder studied

To clearly compare the sounding information content among future geostationary hyperspectral sounders, current GOES Sounder and the ABI, an eigenvector based information content analysis was performed. This information content analysis can be used with retrieval simulation to demonstrate the sounding performance of Geostationary Hyperspectral Sounder (GHS), current GOES Sounder and ABI. An eigenvector-based information content based on the CONUS 300 RAOB profiles is performed to ABI, the current GOES Sounder and GHS (HES is an example). Figure 6.2 shows the water vapor relative humidity (RH) information for RAOB, HES, GOES Sounder + forecast, ABI + forecast, GOES Sounder alone, and ABI alone. It can be seen that: (a) HES alone has the closest information to RAOB for both temperature (not shown) and water vapor; (b) HES alone has better information than any other options for both temperature (not shown) and water vapor; (c) ABI + forecast and GOES Sounder + forecast have the similar information for both temperature (not shown) and water vapor; and (d) both ABI + forecast and GOES Sounder + forecast have better water vapor information than the forecast.

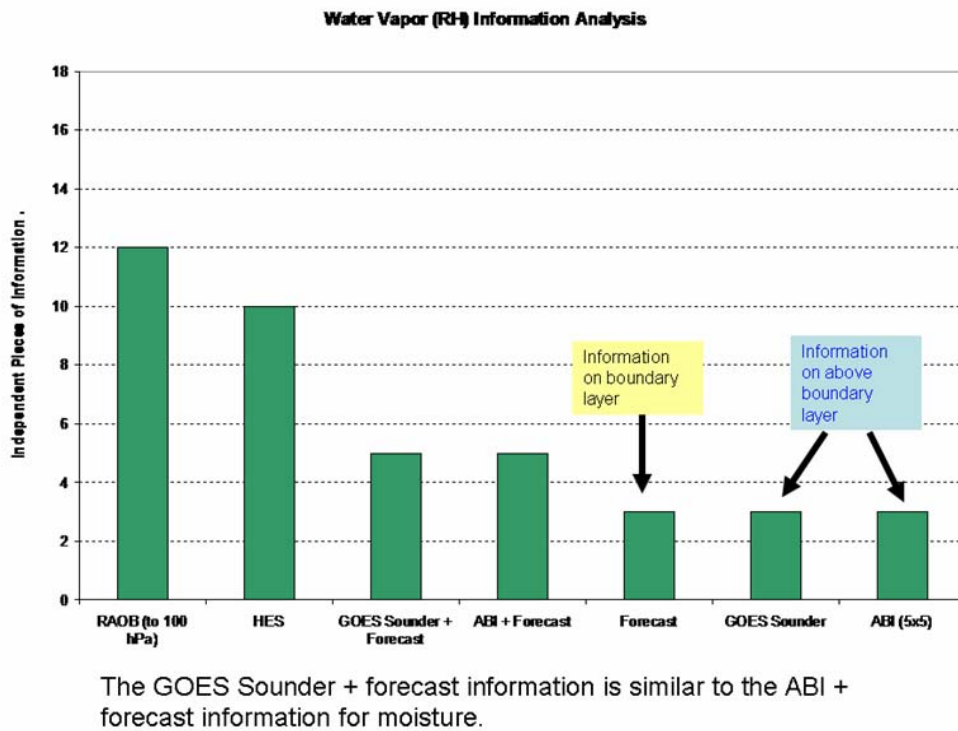


Figure 6.2: Water vapor relative humidity information content estimates from 300 RAOB profiles.

Advantages of GEO hyperspectral IR sounding system on severe storm nowcasting studied

A simulation was carried out to show the value of atmospheric nowcasting products (TPW, LI, etc.) from a geostationary advanced IR sounder for severe weather nowcasting. These nowcasting products indicate the cloud formation and atmospheric instability before the storm development. A convective storm case during the International H₂O Project (IHOP) was used in this study. The atmospheric field data was from MM5 with 2 km spatial and 5-minute temporal resolutions. Figure 6.3 shows the TPW (upper left panel) and Lifted Index (upper right panel) from IHOP (12 June 2002) MM5 model output. The lower left panel shows the TPW from simulated hyperspectral IR (blue) and current GOES Sounder (green), along with the “truth” (model) at the indicated location. The lower right panel is the same as the lower left panel but for lifted index. Grey colors in the upper panels are for cloud-top temperature. Results are preliminary. The advanced sounder provides nowcasting products with much better accuracy before the cloud formation and storm development than the current GOES Sounder.

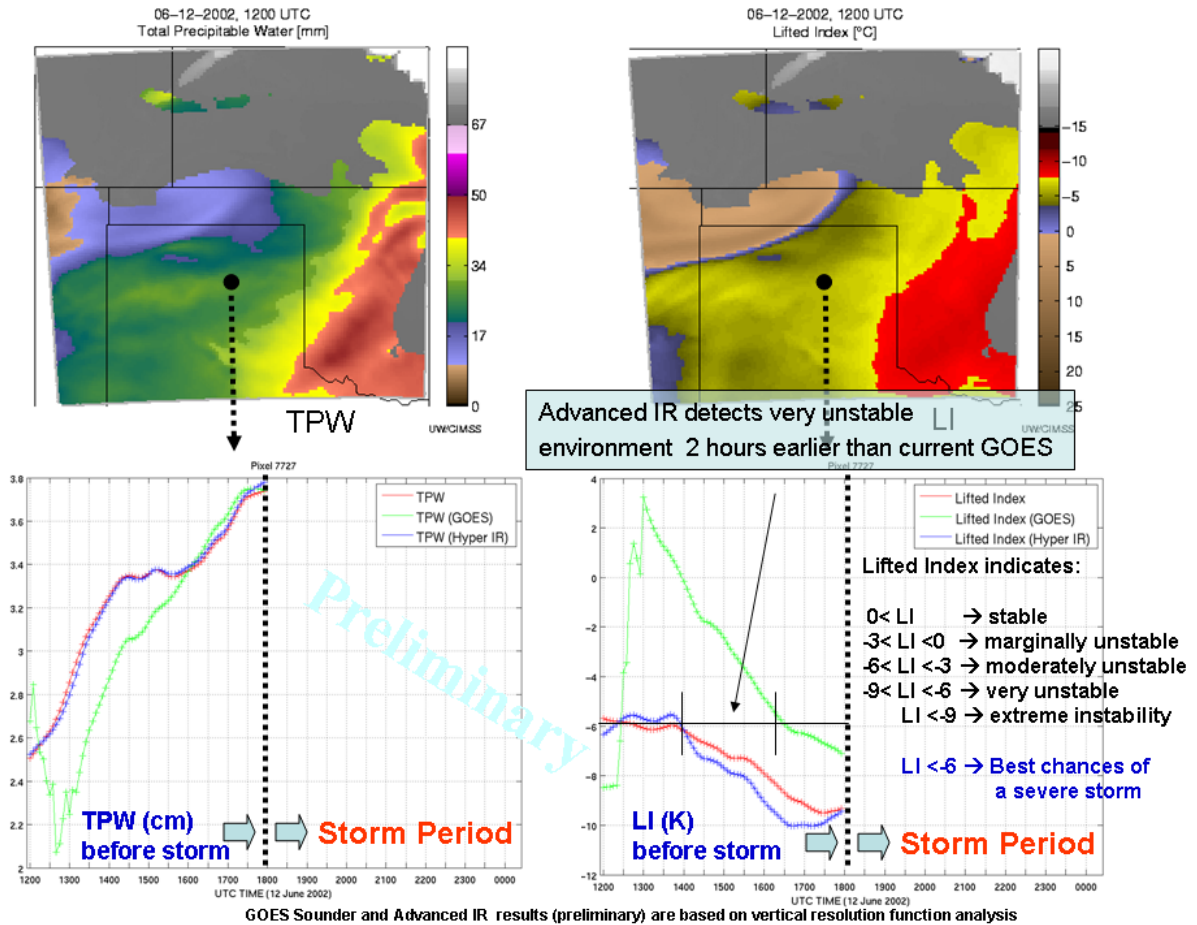


Figure 6.3: TPW (upper left panel) and Lifted Index (upper right panel) from IHOP (12 June 2002) model output (MM5, 2 km, 5 minutes). The lower left panel shows the TPW from simulated hyperspectral IR (blue) and current GOES Sounder (green), along with the “truth” at the indicated location. The lower right panel is the same as the lower left panel but for lifted index. Grey colors in the upper panels denote cloud-top temperature.

Advantages of ABI high spatial resolution on severe storm nowcasting studied

The advantage of ABI spatial resolution was also analyzed using data from the Moderate Resolution Imaging Spectroradiometer (MODIS) and the Advanced Very High Resolution Radiometer (AVHRR). Turbulence, tropical cyclone and super cell storm cases were used for the analysis. Figure 6.4 shows the 11- μ m brightness temperature (BT) images for 2 km resolution (ABI, left panel) and 4 km resolution (current GOES Imager, right panel). MODIS 1 km data were used in the simulation. Results showed that ABI depicts detailed structures of the hurricane eye better than the current GOES Imager. This study demonstrates that ABI’s high spatial resolution (2 km) will facilitate improved detection of the detailed structures of severe weather events such as convective storms and tropical cyclones

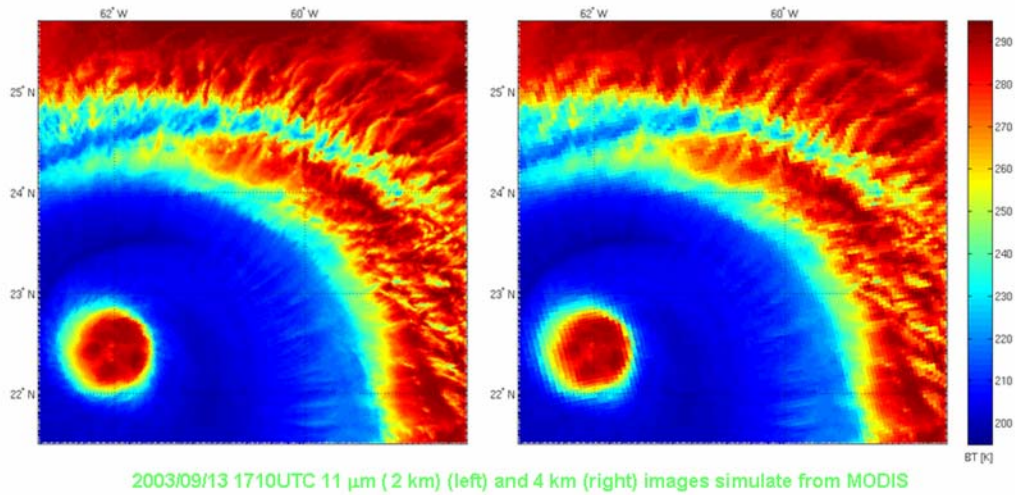


Figure 6.4: The 11 μm BT images at 2 km resolution (ABI, left panel) and 4 km resolution (current GOES Imager, right panel). MODIS data from 13 September 2003 were used for the simulation.

ABI footprint size in high latitude region studied

To determine how large the ABI footprint size will be in the high latitudes, which is related to ice motion estimates, snow/ice cover and other products, the ABI footprint size is estimated as a function of the local zenith angle.

Figure 6.5a shows the central GOES-R local zenith angles and Figure 6.5b shows the ABI IR bands footprint size distribution. The approximate footprint size of the current GOES Imager (assuming 4 km resolution) is shown in Figure 6.5c for comparison. The footprint size does not change significantly if the local zenith angle is less than 40° . However, the size doubles when the local zenith angle goes to 60° , and it increases significantly after 60° . Of course, with the GOES-R ABI, the field-of-view size is much finer at the sub-point.

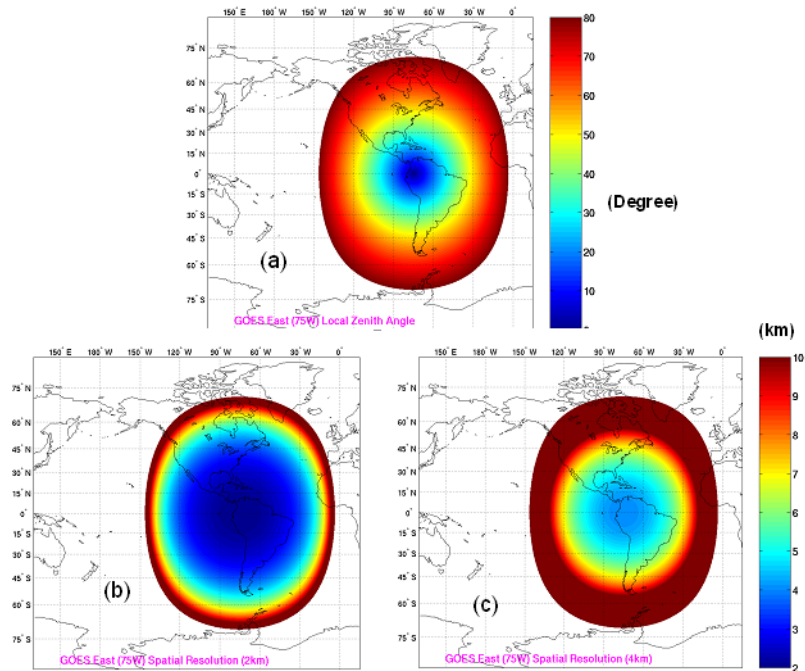


Figure 6.5: Local zenith angle (a), ABI IR bands footprint size, (b) GOES Imager IR bands footprint size, (c) for “central GOES” scenario.

The need for high temporal geostationary infrared soundings for hurricane measurements

High temporal geostationary infrared soundings for severe storm applications have been demonstrated. Atmospheric InfraRed Sounder (AIRS) data during the development of Hurricane Dean in August 2007 were collected for single field of view (SFOV) soundings. It is very difficult to obtain polar-orbiting hyperspectral IR data for a hurricane structure study because of the low temporal resolution and the orbital gaps. Figure 6.6 shows the AIRS coverage (color) and the GOES coverage (black/white) from 18:15 UTC to 20 UTC on 20 August 2007. Hyperspectral IR data from a geostationary satellite can provide detailed three-dimensional atmospheric temperature and moisture structures for hurricanes during their development and evolution. An animated GIF is available on request to show the needs of hyperspectral IR system on GOES.

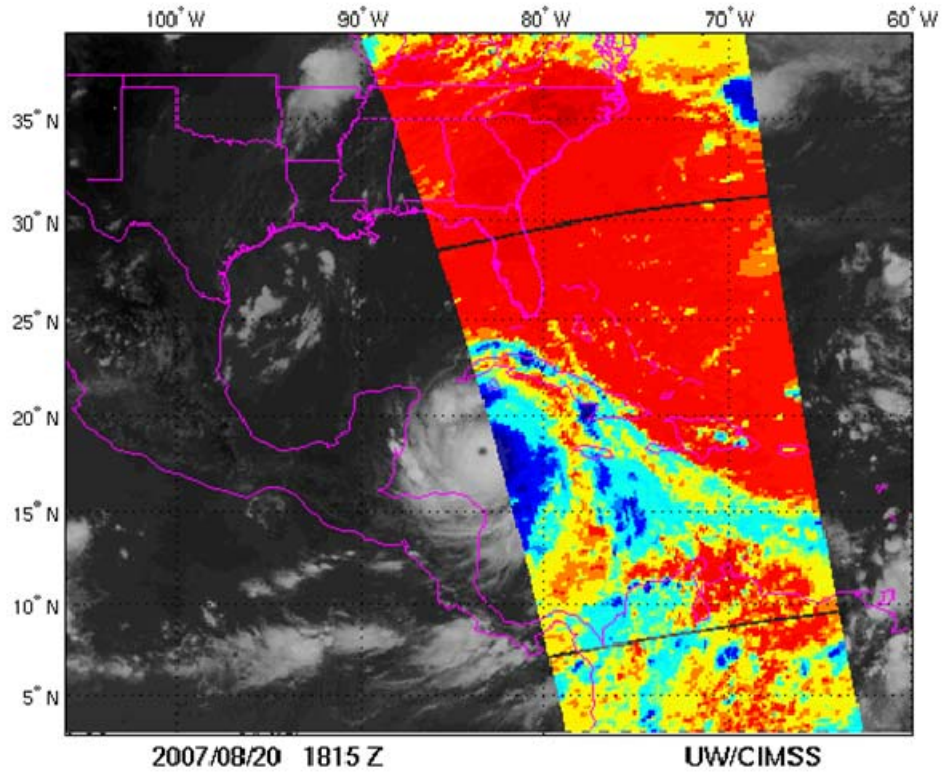


Figure 6.6: The AIRS coverage (color) and the GOES coverage (black/white) from 18:15 UTC to 20 UTC on 20 August 2007.

ABI scan scenario studied

ABI scan scenarios were studied. ABI has the capability to take a full disk scan in 15 minutes, a CONUS scan every 5 minutes, and a mesoscale scan every 30 seconds. The CIMSS AWG Proxy Team generated ABI simulated radiances in both clear and cloudy skies using Weather and Research Forecasting (WRF) model output. The outermost domain covers the entire GOES-R viewing area (every 30 minutes) with 6-km horizontal resolution while the inner domains cover the CONUS (every 5 minutes) and mesoscale regions (every 1 minute) with 2-km and 0.667-km horizontal resolution, respectively. The data were used to simulate ABI scan scenarios. Figure 6.7 shows the water vapor absorption band (7.34 μm) BT images at 23:04:38 UTC for each scan mode (Disk + CONUS + Meso). A loop of ABI scan scenario over 15 minutes is also available on request.

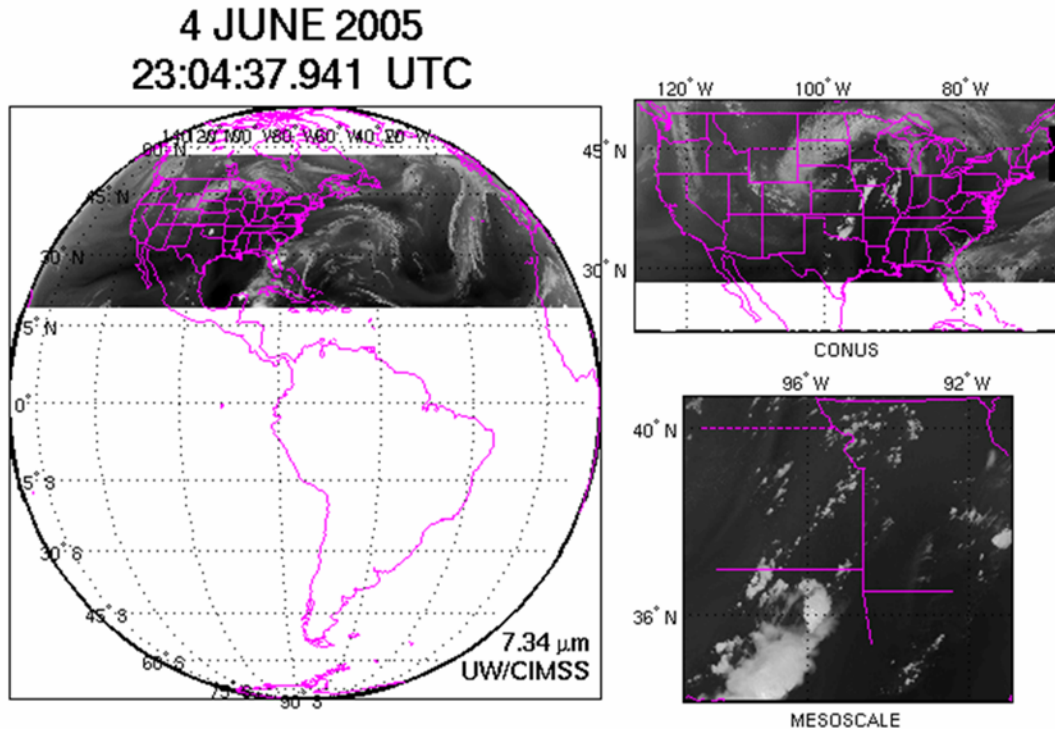


Figure 6.7: The water vapor absorption band (7.34 μm) BT images at 23:04:94 UTC for a scan mode (Disk + CONUS + Meso).

IASI/GOES Sounder real time comparison over CONUS

We have started to do the IASI/GOES Sounder real time comparison over CONUS. The purpose is to demonstrate the advantage of the hyperspectral IR sounder, and to help improve the GOES sounding processes over CONUS. The IASI single FOV soundings are from the CIMSS research algorithm. IASI data are accessed in near real time from NESDIS. Results will be reported in early 2008.

Publications and Conference Reports

Peer reviewed journal publications in 2007 (01 January – 31 December)

Jin, Xin, J. Li, C.C. Schmidt, T.J. Schmit, and Jinlong Li, 2008: Retrieval of Total Column Ozone from Imagers Onboard Geostationary Satellites, *IEEE Transactions on Geosciences and Remote Sensing*, 46, 479 - 488.

Li, Jun, P. Zhang, T.J. Schmit, J. Schmetz, and W.P. Menzel, 2007: Quantitative monitoring of a Saharan dust event with SEVIRI on Meteosat-8, *International Journal of Remote Sensing*, 28, 2181 – 2186.

Li, Z., J. Li, T.J. Schmit, W.P. Menzel, 2007: Comparison between current and future environmental satellite imagers on cloud classification using MODIS, *Remote Sensing of Environment*, 108, 311 – 326.

Li, Zhenglong, J. Li, W.P. Menzel, T.J. Schmit, J.P. Nelson, J. Daniels, and S.A. Ackerman, 2008: GOES sounding improvement and applications to severe storm nowcasting, *Geophysical Research Letters* (in press). doi:10.1029/2007GL032797.



Schmit, T.J., J. Li, J. J. Gurka, M.D. Goldberg, K. Schrab, Jinlong Li, and W. Feltz, 2008: The GOES-R ABI (Advanced Baseline Imager) and the continuation of GOES-N class sounder products, *J. of Appl. Meteorol. and Climatology*. (conditionally accepted).

Wang, F., J. Li, T.J. Schmit, and S.A. Ackerman, 2007: Trade studies of hyperspectral infrared sounder on geostationary satellite, *Applied Optics*, 46, 200 - 209.

Weisz, E., J. Li, W.P. Menzel, A.K. Heidinger, B.H. Kahn, and C.-Y. Liu, 2007: Comparison of AIRS, MODIS, CloudSat and CALIPSO cloud top height retrievals, *Geophysical Research Letters*, 34, L17811, doi:10.1029/2007GL030676, 2007.

Weisz, E., J. Li, Jinlong Li, D.K. Zhou, H.-L. Huang, M.D. Goldberg, and P. Yang, 2007: Cloudy sounding and cloud-top height retrieval from AIRS alone single field-of-view radiance measurements, *Geophysical Research Letters*, 34, L12802, doi:10.1029/2007GL030219.

Related Presentations in 2007 (01 January – 31 December)

Jun Li gave an oral presentation at the International TOVS Science Conference held from 4 to 10 Oct. 2006 in Maratea, Italy, the title is “GOES IR Sounder – future perspective from current applications”.

Tim Schmit gave a talk at the annual National Weather Association (NWA) meeting in Cleveland, OH, which was held in October 2006. The title is “Operational Applications of GOES-R.”

W. Paul Menzel gave a talk at the 87th AMS Annual Meeting, 14 January – 18 February 2007, San Antonio, Texas. The title is “The next GOES Sounder.”

Tim Schmit gave an oral talk at the 87th AMS Annual Meeting, 14 January – 18 February 2007, San Antonio, Texas. The title “Baseline instruments for the GOES-R series.”

Tim Schmit gave a poster presentation at the 87th AMS Annual Meeting, 14 January – 18 February 2007, San Antonio, Texas. The title is “The GOES-R ABI (Advanced Baseline Imager) and continuation of GOES-N class sounder products.”

Tim Schmit gave a poster presentation at the combined EUMETSAT/AMS Satellite Conference held from 23 to 28 September 2007 in Amsterdam. The title is “GOES-R baseline instruments.”

Jun Li gave an oral presentation at the joint EUMETSAT/AMS satellite conference held from 23 to 28 September 2007 in Amsterdam, The Netherlands. The title is “Single Field-of-View Soundings from Geostationary Infrared Sounder Radiances.”

7. A CIMSS Research Study of the Next Generation Geostationary Operational Environmental Satellite (GOES) Data Compression - Bormin Huang

Proposed Work

CIMSS is developing data compression techniques for the Geostationary Imaging Fourier Transform Spectrometer (GIFTS) program, which is a joint project between the National Oceanic and Atmospheric Administration (NOAA) and the NASA Langley Research Center. The National Academy of Sciences’ Committee on Earth Science and Applications from Space recommended that NASA and NOAA



complete the fabrication, testing, and space qualification of the GIFTS instrument. The use of robust data compression techniques for efficient and effective data rebroadcast and archiving will be essential for future NOAA geostationary environmental satellites.

Summary of Accomplishments and Findings

- Finished the GIFTS lossless data compression software for delivery to NOAA and NASA. The average lossless compression ratio is about 4.5 to 1, and the average execution time is about 6 seconds. These codecs meet the requirement of the GIFTS data production rate of ~200 MB per 12 seconds during a scanning mode.
- Contributed 20 data compression papers and one book chapter to the CCSDS Compression Working Group as per the group's request sent via NOAA; these documents will be placed on the CCSDS web site for reference.
- 13 data compression papers were accepted for publication in the IEEE and SPIE journals and conferences.
- Organized the 2007 SPIE International Conference on Satellite Data Compression, Communications, and Archiving, which was held in San Diego, CA, 26-30 August 2007.
- Invited to review 12 journal and conference papers for IEEE, SPIE, and other academic societies, and served as session chairs for several IEEE and SPIE conferences.

Publications and Conference Reports

Huang, Bormin, A. Ahuja, and H.-L. Huang: "Optimal compression of high spectral resolution satellite data via adaptive vector quantization with linear prediction," *Journal of Atmospheric and Oceanic Technology* (accepted).

Huang, Bormin, and Y. Sriraja: "Lossless Compression of Ultraspectral Sounder Data Using Integer Multiwavelet Transform," *IEEE Geoscience and Remote Sensing Letters* (accepted).

Huang, Bormin, and Y. Sriraja: "Predictor-guided lookup tables for lossless compression of hyperspectral imagery," *IEEE Signal Processing Letters* (accepted).

Huang, Bormin, and J. Ma: "On Asymptotic Solutions of the Lloyd-Max Scalar Quantization," *IEEE ICICS 2007*.

Wei, S.-C., and B. Huang: "Application of Independent Component Analysis to Lossless Compression of 3D Ultraspectral Sounder Data," *IEEE APPC 2007*.

Huang, Bormin, and S.-C. Wei: "Vector Quantization with Reversible Variable-Length Coding for Ultraspectral Sounder Data Compression: An Application to Future NOAA Weather Satellite Data Rebroadcast," *SPIE MIPPR 2007*.

Huang, Bormin: "Fast Minimum-redundancy Prefix Coding for Real-Time Space Data Compression," *Proc. SPIE*, 6683, 66830H, 2007.

Huang, Bormin, S.-C. Wei, H.-L. Huang, M. Smuga-Otto, R. Knuteson, H.E. Revercomb, and W.L. Smith: "Lossless data compression studies for the Geostationary Imaging Fourier Transform Spectrometer (GIFTS) with the bias-adjusted reordering preprocessing," *Proc. SPIE*, 6683, 668306, 2007.

Huang, Bormin, S.-C. Wei, H.-L. Huang, M. Smuga-Otto, R. Knuteson, H.E. Revercomb, and W.L. Smith: "Lossless compression studies for the Geostationary Imaging Fourier Transform Spectrometer



(GIFTS) Data via predictive partitioned vector quantization,” *Proc. SPIE*, 6683, 66830E, 2007. Wei, S.-C., B. Huang, and L. Gu: “Ultraspectral sounder data compression using the Tungstall coding,” *Proc. SPIE*, 6683, 66830G, 2007.

Wei, S.-C., and B. Huang: “Use of Independent Component Analysis for Lossless Compression of Ultraspectral Sounder Data,” *Proc. SPIE*, 6683, 668309, 2007.

Huang, Bormin, and H.-L. Huang: “Current Status of Lossless Compression of Ultraspectral Sounder and Hyperspectral Image Data,” Joint 2007 EUMETSAT Meteorological Satellite Conference and the 15th Satellite Meteorology & Oceanography Conference of the American Meteorological Society.

Huang, Bormin, A. Ahuja, Y. Sriraja, and H.-L. Huang: “Lossless Compression Studies for NOAA’s Future GOES Advanced Sounders,” in 23rd Conf. Interactive Information Processing Systems (IIPS) for Meteorology, Oceanography, and Hydrology, AMS Annual Meeting, 2007.

8. Joint Center for Satellite Data Assimilation (JCSDA)

8.1. The Development of IASI radiance and AIRS cloudy radiance assimilation techniques within the NCEP’s Global Forecast System – James Jung, Tom Zapotocny and Todd Schaack

Proposed Work

We proposed to conduct impact studies in greater detail with the new (version 5) Atmospheric Infrared Sounder (AIRS) data set generated by the National Environmental Satellite Data and Information Service (NESDIS) and the AIRS Science Team. We planned to start by investigating the new quality control and cloud height parameters, specific to this version of the data, with respect to fits to the model background to determine which parameters have value. We then proposed to investigate assimilating the cloud-cleared radiances with respect to cloud amount and number of cloud levels. The AIRS Science Team also suggested using a slightly different set of channels to improve forecast results. We proposed to conduct impact studies of this new channel set.

We proposed to continue to work with National Center for Environmental Prediction (NCEP) and NESDIS personnel to modify NCEP’s Gridpoint Statistical Interpolation (GSI) software to assimilate Infrared Atmospheric Sounding Interferometer (IASI) radiances. We have been working with NESDIS to resolve various issues with the Binary Universal Format for the Representation of meteorological data (BUFR) as well as other problems prohibiting operational use of the data. We have collected several months of IASI data and are archiving it on tape enabling us to conduct a two-season impact experiment. We planned to work with NCEP on quality control, channel selection and assimilation weights of the IASI data. We planned to conduct impact tests over two seasons to ensure the IASI data has a positive effect on NCEP’s weather forecasts.

Summary of Accomplishments and Findings

AIRS Cloud Cleared Radiance Tests

We have collected an older version of the AIRS cloud cleared radiance data and have run a seasonal impact study during January-February 2007. The initial control experiment used the current NCEP operational configuration – 152 AIRS channels from all AIRS footprints with operational thinning. The cloud cleared AIRS experimental run used the operational configuration minus the operational AIRS data, and added AIRS cloud cleared radiance file.



For these experiments, the May version of the GDAS/GFS was used at the operational resolution of T382L64. The AIRS radiances were processed as potentially cloud-affected, consistent with all other infrared radiances including the original AIRS data set. Use of the AIRS cloud cleared radiances in this manner resulted in a 10% increase in the number of observations used in the analysis from each radiance profile in this experiment. Forecast verifications of anomaly correlations for geopotential heights from Northern and Southern Hemisphere forecasts are seen in Figure 8.1.1 (a) and (b), and Figure 8.1.2 (a) and (b) for 1000 hPa and 500 hPa forecasts respectively. These figures provide an indication of potential gains that may be had by the use of cloudy radiances, which provide far greater spatial and spectral coverage than cloud free radiances alone.

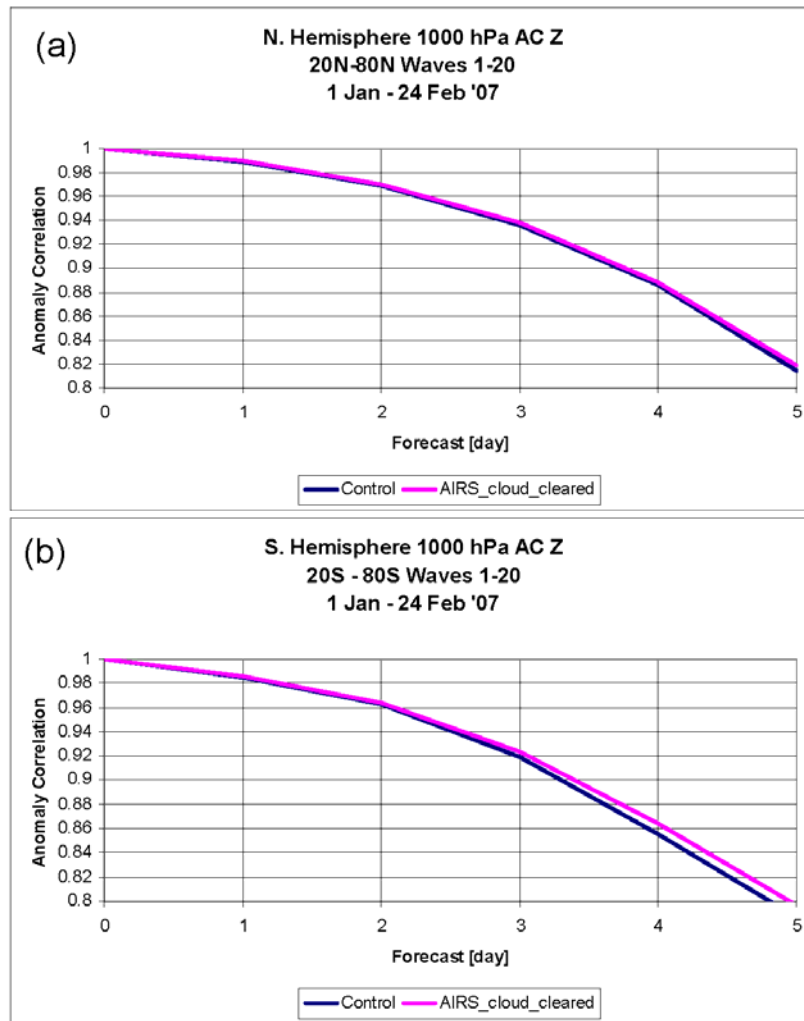


Figure 8.1.1: Anomaly correlation scores at 1000 hPa in the (a) Northern and (b) Southern Hemisphere for January-February 2007.

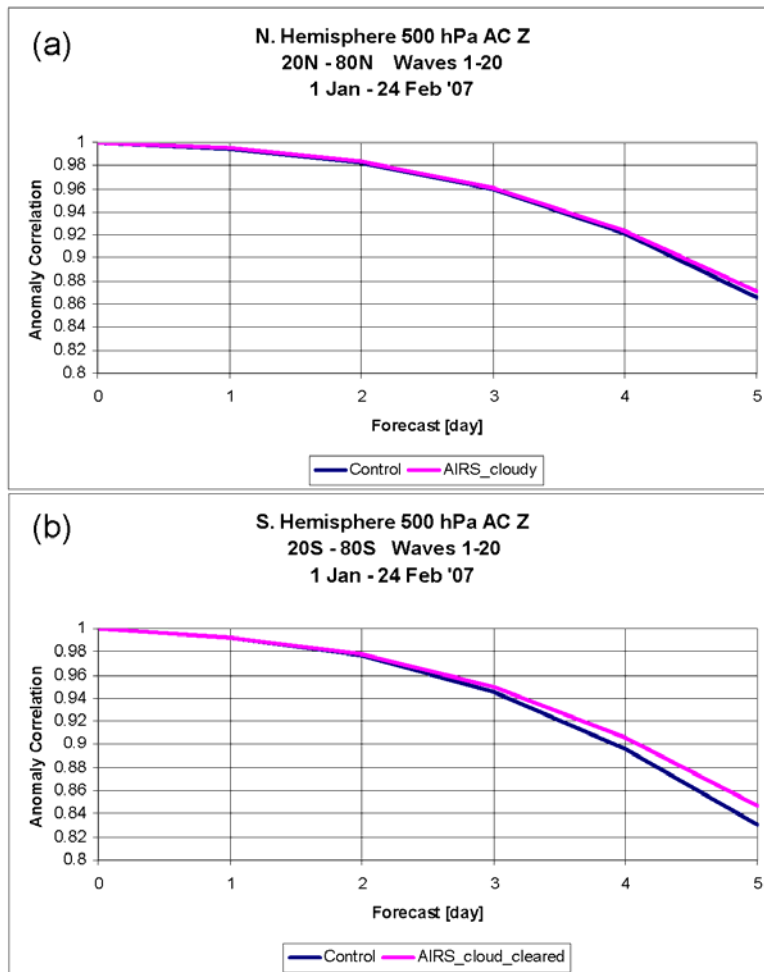


Figure 8.1.2: Anomaly correlation scores at 500 hPa in the (a) Northern and (b) Southern Hemisphere for January-February 2007.

We have been given a sample data set of the new formats for the new (version 5) AIRS cloud cleared radiances. We have modified the latest version of NCEP's GSI assimilation software to read and assimilate the new AIRS data. We are presently waiting for NESDIS to start delivery of the new data set.

Geostationary Winds Expected Error Assimilation Tests

The Expected Error (Le Marshall et al. 2004) was developed to predict the error that Atmospheric Motion Vectors have independent from the assimilation system in which they will be used. Preliminary studies shown in Figure 8.1.3 indicate that the Expected Error is able to reasonably predict the root mean square errors of the GOES Atmospheric Motion Vectors with respect to the GDAS model first guess (background). In Figure 8.1.3, the blue line is the speed bias and the magenta line is the RMS fit of the wind observations to the background to the Expected Error.

The Expected Error was then tested as a quality control flag (accept/reject) in the GDAS. The model background error for wind speed between 100 and 500 hPa was approximated to be 5.0 m/s. All Atmospheric Motion Vectors between 100 and 500 hPa, having an Expected Error of more than 5.0 m/s, were rejected. Figure 8.1.4 shows the improvement in the fit to the model first guess when these winds were removed.



The wind speed error in the background of the GDAS was estimated to be 5.0 m/s, 4.0 m/s and 4.0 m/s for 100-399 hPa, 400-699 hPa and 700 hPa -1000 hPa layers respectively. Using the background error values as Expected Error quality control cutoff flags, impact studies were conducted with NCEP's GDAS during 01 – 31 January 2007. Improvements in forecast skill (anomaly correlations) were found at mid-latitudes in both hemispheres when comparing using NCEP's standard winds assimilation technique to using the Expected Error quality control flag as shown in Figure 8.1.5.

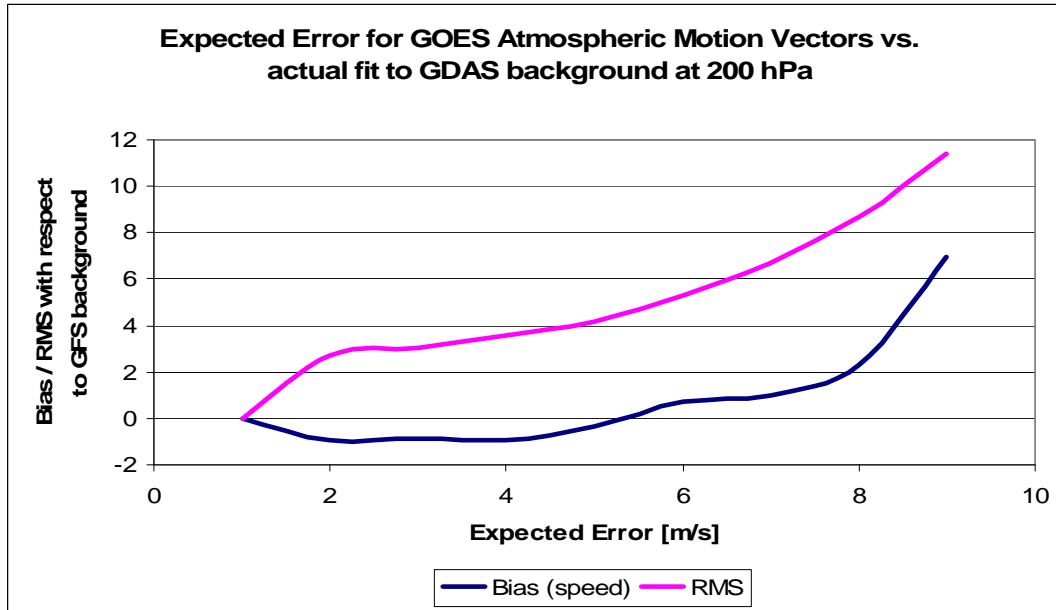


Figure 8.1.3: Comparison of the Expected Error for GOES Atmospheric Motion Vectors to the GDAS background. The blue curve is the Bias and the magenta line is the RMS.

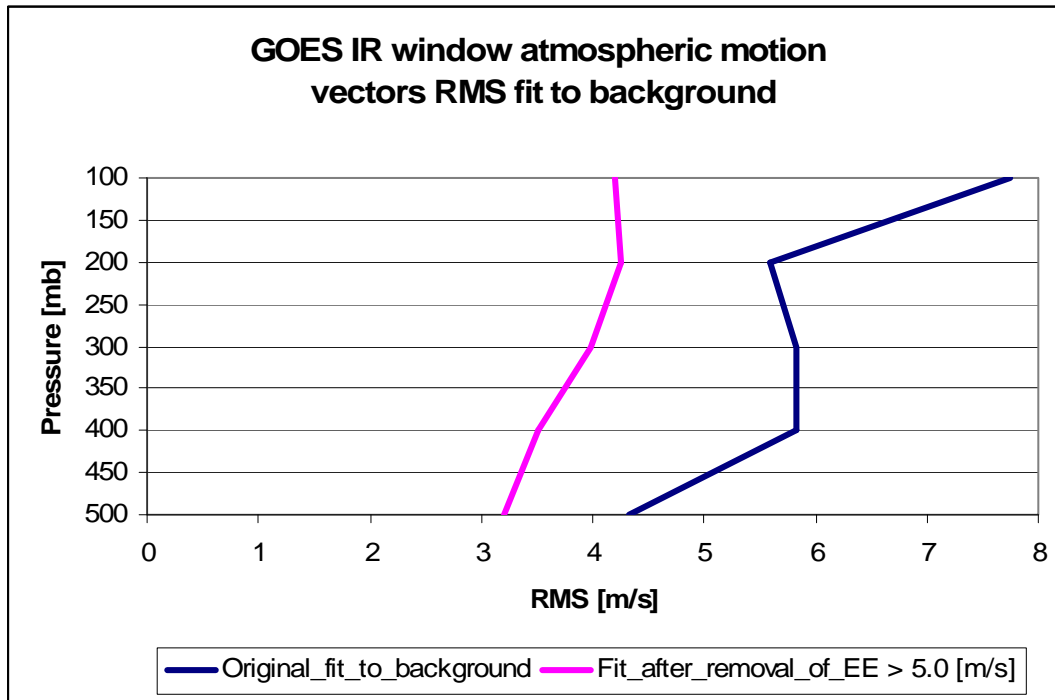


Figure 8.1.4: RMS fit of the GOES Atmospheric Motion Vectors above 500 hPa to the GDAS. The original fit is in blue. The fit after rejecting winds with an Expected Error above 5.0 m/s is in magenta.

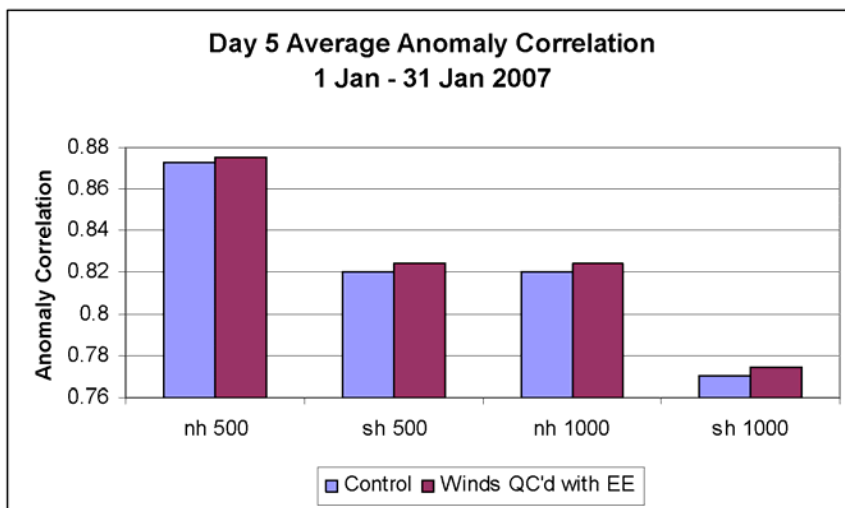


Figure 8.1.5: Summary of day 5 anomaly correlations during January 2007

Reference:

Le Marshall, J.F., Rea, A., Leslie, L., Seecamp, R. and Dunn, M., 2004: Error Characterization of Atmospheric Motion Vectors, *Aust. Meteor. Mag.*, **53**, 123 – 131.



IASI Radiance Assimilation Tests

We have been working with NESDIS and NCEP to resolve the logistics problems associated with assimilating IASI data. Software modifications were made and timing issues have been resolved and IASI data are now being processed in real time by NCEP. Some of the software modifications are scheduled to go into NCEP operations with the next (Spring 2008) upgrade.

A new version of the CRTM was required to incorporate new satellites and specifically IASI data into the GSI. We worked with NCEP personnel to incorporate and test this new version of the CRTM in the GSI on the present suite of operational satellites. This new version of the CRTM was implemented with the GSI into NCEP operations in December 2007.

The latest version of the GSI and its associated scripts has been modified to read, spatially thin, and assimilate the IASI data. We are presently waiting for updated coefficient files for the CRTM to conduct assimilation tests.

Publications and Conference Reports

Presented results at the annual Joint Center for Satellite Data Assimilation (JCSDA) Workshop, May 2007.

Jung, J.A., T. H. Zapotocny, J.F. Le Marshall and R.E. Treadon, 2007: A Two Season Impact Study of NOAA Polar Orbiting Satellites in the NCEP Global Data Assimilation System. Submitted to *Wea. Forecasting*.

Le Marshall, J., J. Jung, T. Zapotocny, C. Redder, M. Dunn, J. Daniels, and L.P. Riishogjaard, 2008: Impact of MODIS Atmospheric Motion Vectors on Global NWP. Submitted to *Aust. Meteor. Mag.*

Le Marshall, J., J. Jung, M. Goldberg, C. Barnett, W. Wolf, J. Derber, R. Treadon and S. Lord 2008: Using Cloudy AIRS Fields of View in Numerical Weather Prediction. Submitted to *Aust. Meteor. Mag.*

Le Marshall, J., L. Bi, J. Jung, T. Zapotocny, and M. Morgan, 2007: WindSat Polarimetric Microwave Observations Improve Southern Hemisphere Numerical Weather Prediction. *Aust. Meteor. Mag.* **56**, 35-40.

Zapotocny, T.H., J.A. Jung, J.F. Le Marshall, and R.E. Treadon, 2007: A Two Season Impact Study of Satellite and In-Situ Data in the NCEP Global Data Assimilation System. *Wea. Forecasting*, **22**, 887-909.

Zapotocny, T.H., J.A. Jung, J.F. Le Marshall, and R.E. Treadon, 2008: A Two Season Impact Study of four Satellite Data Types and Rawinsonde Data in the NCEP Global Data Assimilation System. Accepted in *Wea. Forecasting*.

8.2. Enhanced Cloud Height Assignment using CALIPSO – Steve Ackerman

Proposed Work

Accurate height assignment of atmospheric motion vectors is a key to good data assimilation of satellite derived cloud drift winds. Inappropriate altitude error bars assigned to good (in terms of speed and direction) cloud motion vectors (CMVs) may keep them from ultimately being assimilated into a forecast model and diminish the positive impact on NWP. To improve the number of cloud drift winds assimilated, it is necessary to better characterize the errors in the height assignment. This research effort will develop a method for utilizing cloud layer altitudes measured by Cloud-Aerosol Lidar and Infrared



Pathfinder Satellite Observation (CALIPSO) to improve the process of CMV height assignments derived from geostationary and polar orbiting satellites.

Summary of Accomplishments and Findings

The project is a three-step process:

1. *Compare MODIS and CALIOP for collocated scenes.* This comparison gives us an idea of the best possible comparison.
2. *Compare CALIOP heights with MODIS wind algorithm height assignment.* These two instruments are flown in tandem and will provide a comparison on cloud height winds from the lidar with the winds algorithm method. In addition, comparison against the results of step one will provide insight on if the method can be improved.
3. *Compare with GOES data.* The comparison with CALIOP and the MODIS wind algorithm will give us a better understanding of what to expect when a comparison is done with two different instruments in a similar orbit. Then the project will move on to the comparison with GOES. This will be the most trying comparison as the instruments are not only different, but the orbits are as well.

In this period we finalized the collocation of MODIS and CALIPSO to conduct initial comparison of winds. This activity was accomplished under a different project but was required prior to beginning this project. We have begun step two with the development of a data set of collocated CALIPSO and CMV heights derived from the MODIS polar winds processing scheme, which is similar to the GOES scheme.

8.3. Assimilating and Determining the Forecast Impact of Sea Surface Winds Measured by WindSat/Coriolis in the NCEP GDAS/GFS – Li Bi, James Jung and Steve Ackerman

Proposed Work

In collaboration with the Joint Center for Satellite Data Assimilation (JCSDA), we proposed to evaluate assimilation techniques and the forecast impacts obtained with both the National Environmental Satellite, Data, and Information Service (NESDIS) WindSat data and Navy's WindSat data in the National Centers for Environmental Prediction (NCEP) Global Data Assimilation/Forecast System (GDAS/GFS). We planned to start by investigating Quality Control (QC) in the assimilation process for both NESDIS and Navy's WindSat data, and the thinning and superobing for WindSat data. We then proposed to undertake three WindSat runs, fully testing and comparing the attributes of using the NESDIS WindSat data and the Navy's WindSat data. After completing the three WindSat runs, we proposed to compute the geographic distribution of Forecast Impact (FI) and compared the attributes of using the NESDIS and Navy WindSat data to a control experiment. We also proposed to conduct the area weighted Root Mean Square Error (RMS) calculation, and make a comparison between Navy WindSat experiment and control experiment. Ultimately these efforts should lead to the operational implementation of WindSat data in the NCEP weather forecast models.

Summary of Accomplishments and Findings

Progress to date includes completing three GFS simulations produced daily from 15 February to 30 March, 2007: 1) a control run, 2) a control run with NESDIS WindSat sea surface wind observations added, and 3) a control run with Navy's WindSat observations added. The operational version of the forecast model at the operational resolution of T382L64 was used along with a pre-implementation of the Gridpoint Statistical Interpolation (GSI).



Figure 8.3.1 displays a preliminary comparison of the RMS and bias by wind speed from the Navy WindSat and NESDIS WindSat experiments. Panel (a) shows the results from Navy WindSat and panel (b) shows the results from NESDIS WindSat. There is large RMS and bias for NESDIS WindSat retrieved wind for wind speed that is less than 4ms^{-1} .

The Anomaly Correlation (AC) comparisons are presented in Figure 8.3.2. The results presented show the 500 hPa day five geopotential height anomaly correlation from a control run and two WindSat experiments. The best (highest) anomaly correlations are achieved using the Navy's retrieved WindSat winds at 1000 hPa for both hemispheres and at 500 hPa in the Northern Hemisphere. Although not shown, other fields such as 1000 hPa wind also benefit from the addition of Navy's WindSat data. The geographic distribution of FI explained in Zapotocny et al. (2005) and Zapotocny et al. (2007) was used to show the improvement/degradation the WindSat data had on the daily forecasts. For this season assimilation and impact study, a time series of two-dimensional FI results were generated at different levels. Figure 8.3.3 displays geographic distributions of forecast impacts averaged over March 2007 for u component of the Navy WindSat retrieved winds at 10m level at forecast hours (a) 6, (b) 24. The range of FI is from -50 to 100. The 10m level is the level that is closest to where the WindSat wind observations are added to the assimilation system. Of the two fields shown, the largest impacts are in Africa, South America and Australia in the 6-hour forecast. There is a marked decrease in FI by 24 hours. Figure 8.3.4 shows the same FI diagnosis for the u component of the Navy WindSat retrieved winds at 500 hPa. Of the two fields shown, large impacts are found in tropics in the 6-hour forecast and there is also a marked decrease in FI by 24 hours.

Another diagnostic used here is the area weighted RMS calculation discussed by Zapotocny et al. (2007). The area weighted RMS calculation accounts for the reduction in area as for grid boxes approach the poles. The area weighted RMS comparison between the Navy WindSat experiment and control experiment are presented in Figure 8.3.5. The top panel (a) is the comparison for the u component of the winds and the bottom panel (b) is for the v component of the winds at 10m. The analysis from the experiment is used in this calculation. At 6 hour forecast, the area weighted RMS for Navy WindSat experiment has smaller RMS value than the Control run. By 24 hours, the difference decreased and a further decrease occurred at 48 hours.

Based on these assimilation experiments, and similar experiments conducted by NCEP, the Navy version of the WindSat retrievals are scheduled to be implemented in the next NCEP forecast system upgrade scheduled for spring 2008.

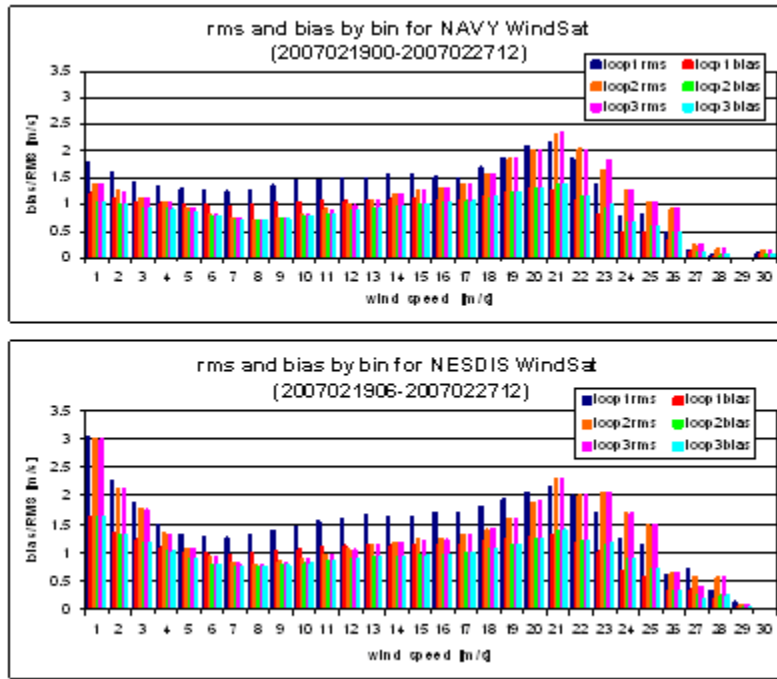


Figure 8.3.1: A preliminary comparison of the rms and bias by bin for Navy WindSAT and NESDIS WindSAT from WindSAT runs using either NESDIS or Navy WindSAT data. Panel (a) shows the results from Navy WindSAT and panel (b) shows the results from NESDIS WindSat.

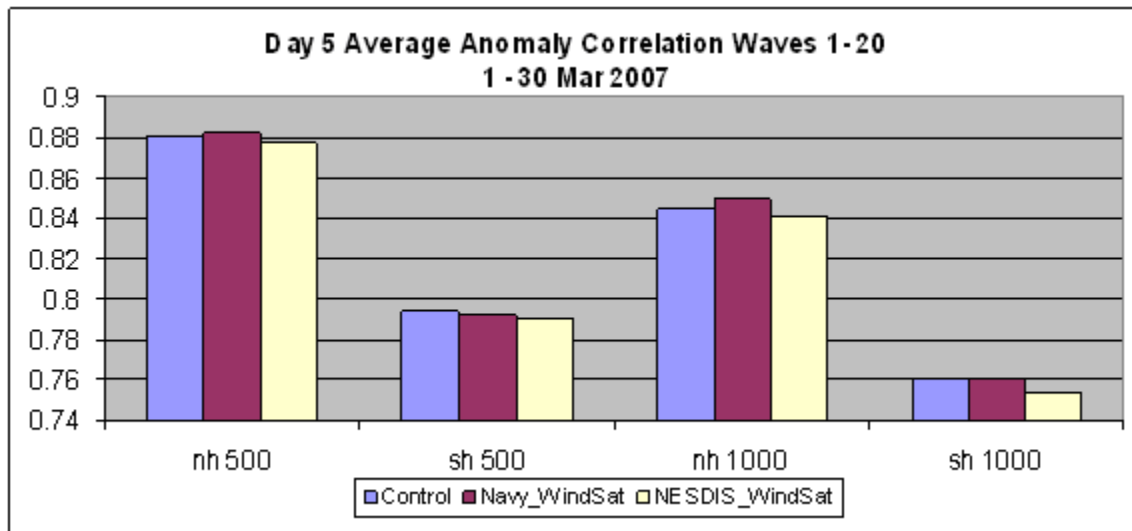
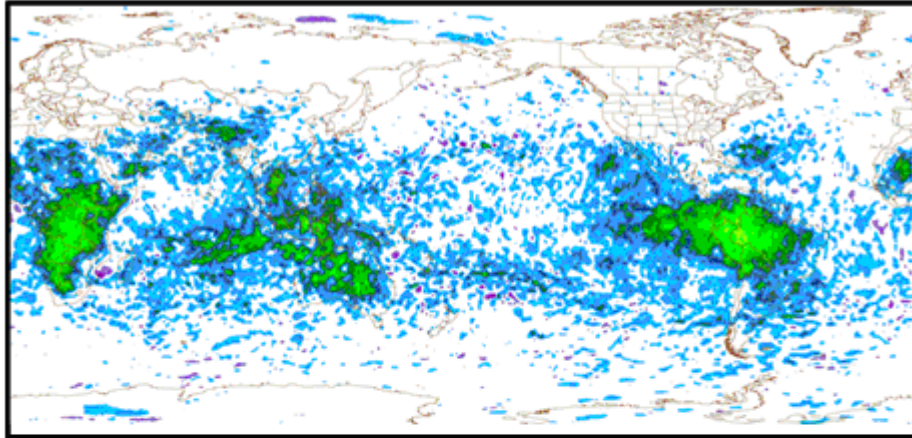


Figure 8.3.2: Three-way comparison of the Day Five geopotential height anomaly correlation for the period 01 – 30 March 2007.



(a) 10M UGRD FCST IMPACT 6HR NAVY WINDSAT
MARCH 1 – MARCH 30 2007



(b) 10M UGRD FCST IMPACT 24HR NAVY WINDSAT
MARCH 1 – MARCH 30 2007

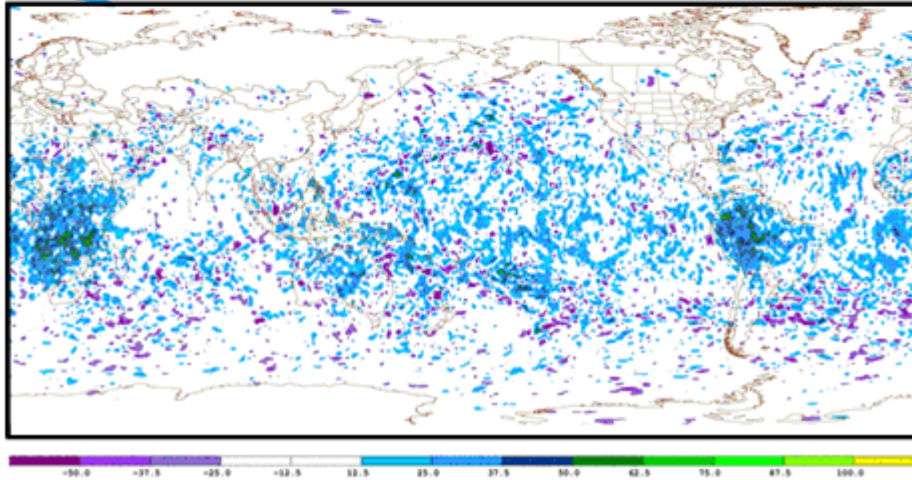
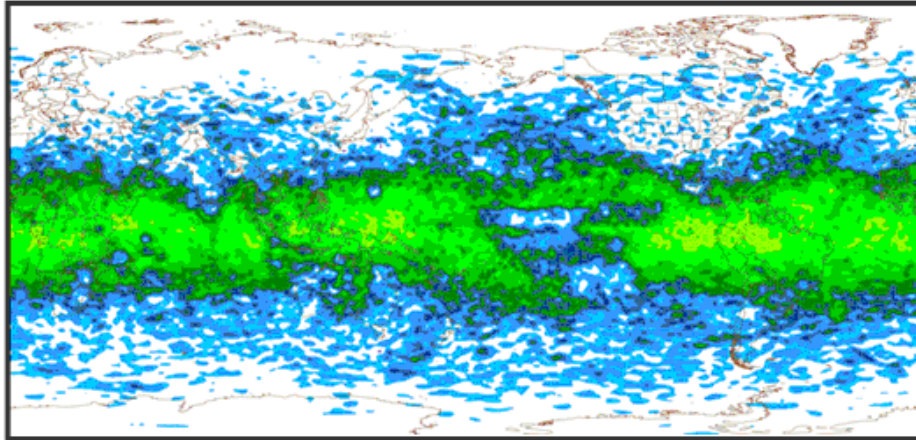


Figure 8.3.3: Geographic distribution of forecast impact from March 1 to March 30 for u component of the wind at 10m for Navy WindSat retrieved winds at forecast hours (a) 6 and (b) 24. The range of forecast impact is from -50 to +100.



(a) 500 hPa UGRD FCST IMPACT 6HR NAVY WINDSAT
MARCH 1 – MARCH 30 2007



(b) 500 hPa UGRD FCST IMPACT 24HR NAVY WINDSAT
MARCH 1 – MARCH 30 2007

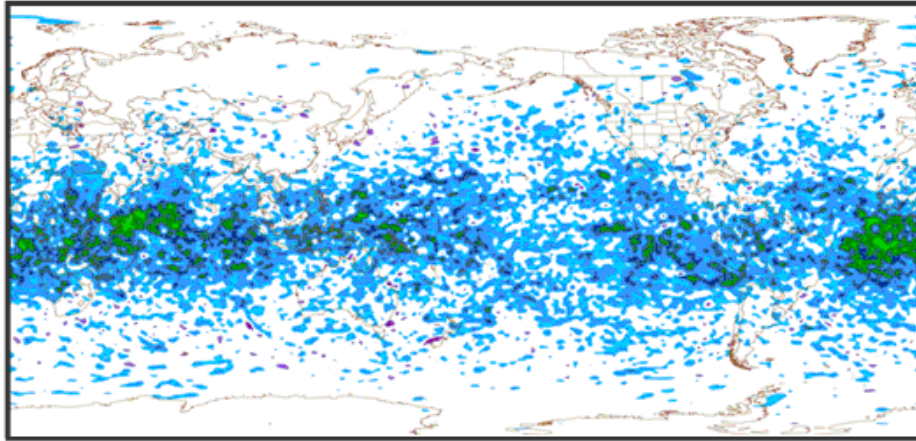
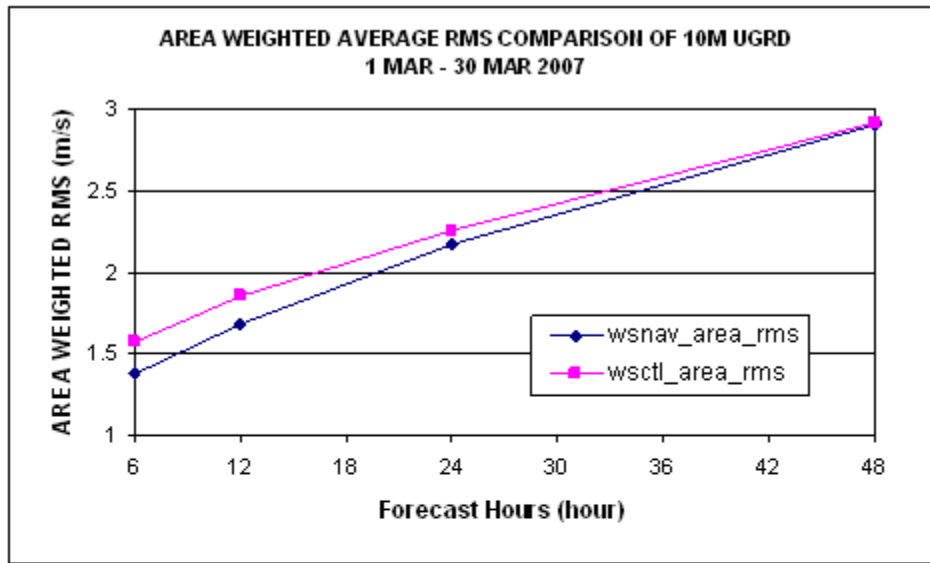


Figure 8.3.4: Geographic distribution of forecast impact from March 1 to March 30 for u component of the wind at 500 hPa for Navy WindSat retrieved winds at forecast hours (a) 6 and (b) 24. The range of forecast impact is from -50 to +100.



(a)



(b)

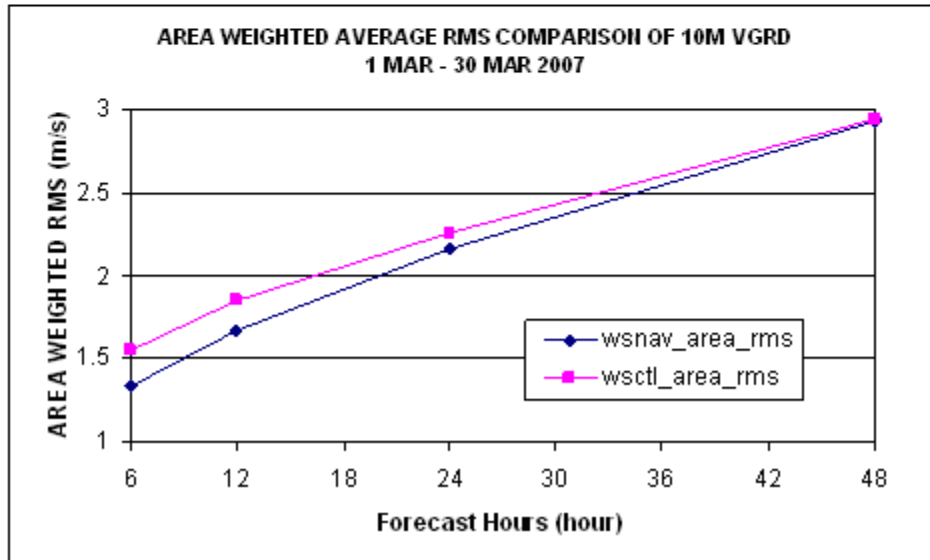


Figure 8.3.5: Area weighted average RMS comparison of 10m (a) u component and (b) v component for the Navy's WindSat experiment and control run from 01 March to 30 March 2007.

References:

Zapotocny, T., W.P. Menzel, J.A. Jung, and J.P. Nelson III, 2005: A Four Season Impact Study of Rawinsonde, GOES and POES Data in the Eta Data Assimilation System. Part I: The Total Contribution. *Wea. Forecasting*, **20**, 161-177.

Zapotocny, T., J.A. Jung, J.F. Le Marshall and R. Treadon, 2007: A Two-Season Impact Study of Satellite and In Situ data I the NCEP Global Data Assimilation System. *Wea. Forecasting*, **22**, 887-909.



Publications and Conference Reports

Attended the annual JCSDA workshop, May 2007.

Le Marshall, J., L. Bi, J. Jung, T. Zapotocny, and M. Morgan, 2006: WindSat Polarimetric Microwave Observations Improve Southern Hemisphere Numerical Weather Prediction. *Aust. Meteor. Mag.* **56**, 35-40.

Bi, L., J. Le Marshall, T. Zapotocny, M. Morgan, and J. Jung, 2007: Assessing the Forecast Impact of WindSat/Coriolis Data in the NCEP GDAS/GFS. Presented at the 87th AMS Annual Meeting.

Bi, L., J. Jung, M. Morgan and J. Le Marshall, 2008: A One-Season Assimilation and Impact Study of NESDIS and Navy's WindSat Retrieved Data in the NCEP Global Data Assimilation System. Presented at The 88th AMS Annual Meeting.

8.4. Observation error characterization for radiance assimilation of clouds and precipitation – Ralf Bennartz, Tom Greenwald and Andrew Heidinger

Proposed Work

The goals of this project are to:

1. Further develop, integrate, and test the Successive Order of Interaction (SOI) forward, tangent linear and adjoint infrared and microwave radiative transfer models within the Community Radiative Transfer Model (CRTM) framework.
2. Determine observation error covariances under cloudy and rainy conditions both in the infrared and microwave separating effects of: (1) radiative transfer solvers, (2) approximations in optical properties of clouds and precipitation, (3) cloud overlap assumptions, (4) neglecting three-dimensional radiative transfer and beam filling.
3. Quantify regional and global biases between GFS/GDAS and observations for different model setups as well as for different cloud microphysical parameterizations.

Summary of Accomplishments/Findings

Within the first year of this project we have continuously worked on the refinement of SOI and have started initial collaborations with NOAA and NCEP staff to evaluate the SOI model in the bigger CRTM framework. With respect to above the objectives 2 and 3, we have successfully installed the WRF model locally at UW and are currently running WRF to establish a model database. This database will then be used in conjunction with CRTM as well as Monte-Carlo models to study observation error covariances in an Observation System Simulator context.

Publications and Conference Reports

Kim, M.-J., M. Kulie, C. O'Dell and R. Bennartz, 2007: Scattering of ice particles at microwave frequencies: A physically based parameterization. *Journal of Applied Meteorology and Climatology*, Volume 46, Issue 5, 2007, pp.615-633

O'Dell C.W., P. Bauer and R. Bennartz, 2007: A fast cloud overlap parameterization for microwave radiance assimilation. *J. Atmos Sci.* 64 (11): 3896-3909.

Kulie, M.S., and R. Bennartz, 2007: Remote sensing of precipitation at higher latitudes using combined active and passive microwave observations. Joint 2007 EUMETSAT Meteorological Satellite Conference



and Satellite Meteorology and Oceanography Conference, 15th, of the American Meteorological Society, Amsterdam, the Netherlands, 24-28 September 2007. Proceedings.

Kulie, M.S., and R. Bennartz, 2007: A multi-sensor strategy to investigate precipitation at higher latitudes. 12th American Meteorological Society Conference on IOAS-AOLS, New Orleans, January 2007.

9. Continued Development of the Community Radiative Transfer Model (CRTM) – Paul van Delst

Proposed Work

The CRTM development planned for 2007 involved a number of upgrades to the atmospheric absorption model, addition of various infrared surface emissivity models, the development of a regression test suite, and preparation for the IASI interferometer instrument.

Summary of Accomplishments

Apart from the development of software to generate IASI instrument transmittances for regression fitting to generate atmospheric absorption coefficients, the remainder of the CRTM development and maintenance was driven by requests from within the JCSDA, NCEP/EMC, and NESDIS/STAR. As proposed, the IASI instrument was added to the list of sensors for the CRTM. Software was developed to reduce line-by-line (LBL) generated transmittances to the IASI spectral resolution. Different methodologies to handle the LBL resolution and effective bandwidths were investigated to balance accuracy and speed.

CRTM coefficients for other instruments were also generated at the request of various groups connected with the JCSDA. The NCEP reanalysis project requested an accurate model for the SSU instruments on NOAA-06, -07, -08, -09, -11, and -14. Working with Dr. Q. Liu (NESDIS/STAR/Perot), who successfully regenerated the SSU spectral responses (SRFs) as a function of CO₂ cell pressure, transmittance coefficients were developed and supplied to the NCEP reanalysis project, as well as NASA/GMAO. In addition, working with Dr. Y. Chen (NESDIS/CIRA), coefficients for the MeteoSat-08 and -09 SEVIRI instruments, and for special cases of the NOAA-17 and -18 AVHRR/3 with slightly shifted SRFs, were generated and supplied to the NESDIS Geostationary SST group.

Actual development of the CRTM itself has been restricted to the addition of the capability to apply microwave instrument antenna corrections to the AMSU-A, AMSU-B, and MHS. This capability was a request from the NCEP/EMC GSI developers to determine if assimilation of antenna, rather than brightness, temperatures, would improve the analysis. In addition, it has since been discovered that the instrument BUFR data for AMSU-A varies between antenna (NOAA-18 and MetOp-A) and brightness (NOAA-15 and -16) temperature, so the capability is needed for CRTM users that utilize NCEP BUFR data streams (e.g. NCAR).

10. NCEP International Modeling Support - Ralph Petersen

Proposed Work

CIMSS continued to cooperate with NCEP to support the reporting and representation of NCEP activities and numerical models at international and national meetings and training programs. Specifically, CIMSS planned to provide support for the NCEP goals of preparation for and participation in the WMO SWFDP NWP Training Course held in Pretoria, South Africa.



Note: In the past, resources to allow CIMSS to participate in these cooperative efforts have been provided through proposals initiated with NCEP/EMC. Beginning with this proposal, funding was provided directly by NWS/IA.

Summary of Accomplishments and Findings

The WMO-organized seminar on Forecasting Hazardous Weather was given in conjunction with the UK Meteorological Office and the South African Weather Service (SAWS) in Pretoria, South Africa. CIMSS contributions include 1- to 2-hour training sessions on NWP formulation, NWP model characteristics and strengths, means of accessing NWP data, Ensemble forecasting, as well as a session of severe weather applications of NWP output. The use of satellite data in and in conjunction with NWP models is also emphasized, both in the present and future.

A total of approximately 20 forecasters from roughly 10 countries in southern Africa attended. The UK Met Office conducted evaluations of the workshop. CIMSS also participated in post-workshop support of students using web-based tools developed by the UK Met Office.

Both NCEP and CIMSS benefited from these interactions. We shared advances with the UK Met Office and the SAWS and increased our understanding of the forecasting needs of developing countries. This task was completed in the first quarter of 2007.

Publications and Conference Reports

No published presentation made during the past year. Copies of training materials were provided to the participants, WMO, UK Met Office and SAWS. Additional copies are available on request.

11. Support for the WVSS-II Field Program – Ralph Petersen and Wayne Feltz

Proposed Work

CIMSS conducted a second ground-truth assessment of the WVSS-II systems being flown on UPS aircraft at Louisville, KY during weekdays from 7-18 November 2006. Proposed objectives included: 1) assessing the accuracy of WVSS-II observations by comparing them to rawinsonde observations and 2) providing guidance to develop optimal observing strategies through the ongoing evaluation of temporal moisture variability intended to help define the temporal and spatial requirements for aircraft observations.

Summary of Accomplishments and Findings

The report is divided into two parts. The first provides a detailed summary of the November 2006 rawinsonde-WVSS-II intercomparison test, and the second provides preliminary information needed to determine the optimal spacing and timing of operational aircraft moisture observations.

Observing Systems Available for WVSS-II Validation

All non-aircraft observations were made at a site on the Kentucky Air National Guard (ANG) facility immediately adjacent to the Louisville airport. Observations were taken from the portable “AERIbago” vehicle 24 hours/day during weekdays throughout the full experiment period. Primary observational systems included: a portable surface station reporting temperature, dewpoint temperature and wind information; a NWS standard Ceilometer; a GPS receiver for use in calculating total precipitable water (GPS-TPW); an upward-looking AERI to measure boundary layer temperature and moisture at 10 minute temporal resolution; and a Vaisala GPS rawinsonde system. Model RS-92 sensors were used for all rawinsonde launches. To avoid the possible introduction of previously observed instrument “aging”



errors, the moisture sensors were all less than three months old. Data taken by the UW-CIMSS systems have been archived at UW-CIMSS for future use and are available at:

<ftp://ftp.ssec.wisc.edu/validation/exper/wvssii/>.

The full set of aircraft data has also been collected from the FSL MADIS data retrieval system for use in the UW-CIMSS assessment.

Status of Rawinsonde vs. Aircraft Co-location Data

The most critical surface-based observations for this report were the rawinsonde reports. Three rawinsonde launches were scheduled each night: one immediately before the majority of the UPS arrivals at about 0400 UTC; another between the rush of descents and ascents at about 0730 UTC; and a third after the majority of departures at about 1045 UTC. Exceptions were made on Mondays and Fridays when, due to scheduling of WVSS-II equipped aircraft by UPS, only two launches were possible on several occasions. All 28 launches were successful, with no equipment failure. On a typical day, about 5-10 aircraft co-locations were available, but not all fell within the narrow time and space windows used in this assessment.

Constraints on assessment due to instrument shortcomings

A number of engineering and software modifications were made to the WVSS-II systems and the on-board reporting system to correct deficiencies noted during the first assessment conducted by CIMSS in 2005. Although it had been hoped that all of the WVSS-II sensors and software modifications would have been included on the participating UPS aircraft before the second assessment period began, the complete conversions were not completed until the end of the November 2006 data collection period. As such, the comparisons of the WVSS-II data with the rawinsonde standard were again limited in the following ways:

1. The engineering changes to correct the erroneous reports in areas of high humidity and clouds during in descent did not entirely solve the problem. Because the objective of the experiment was to assess the quality of good reports made by both the aircraft and rawinsonde, the intercomparisons focus on rawinsonde co-locations with aircraft ascents.
2. Moisture problems persisted in some units. When small amounts of moisture enter the laser sensing unit, the moisture reports are too high. Because this bias was particularly apparent in areas of extremely low mixing, the assessments were again limited to regions where the observed mixing ratio was greater than 2 g/kg.
3. A number of the aircraft had biases in their temperature sensors. To correct this issue, assessments of moisture were again made in terms of the primary WVSS-II water vapor observation, which is mixing ratio (as reflected in specific humidity), and then transformed in to Relative Humidity using rawinsonde temperatures. A comparison using aircraft temperature reports was also made for reference.
4. Not all of the UPS aircraft had an updated version of the software developed by CIMSS to correct a deficiency to reduce the precision of the WVSS-II observations exceeding 10 g/k. The assessment was again limited to reports of less than 10 g/kg.

Conventions for identifying aircraft/rawinsonde co-locations

Based on experience gained in the four previous aircraft/rawinsonde co-location tests performed by UW-CIMSS, all co-location data used for the initial assessment were limited to time and space windows of +/- 60 minutes and 50 kilometers. These limitations minimized the impact of transient weather features in the area, such as frontal passages, and ensured that an adequate number of reports were available for statistical calculations.



A total of 50 ascending rawinsonde/WVSS-II matches were within the above limitations (from aircraft ascents only). The matches included data from 16 different rawinsonde releases (three of the release times had matches only with descending data and were not included in the assessment) and close to 50% of the approximately 25 available aircraft. Numerical differences between the aircraft and rawinsonde data were calculated at each aircraft reporting level and then 'binned' into 10 hPa deep layers for display and statistical calculations.

Displays of rawinsonde and aircraft profiles of temperature and specific humidity were made for each of the 13 rawinsonde-aircraft match-up times. Comparisons of individual soundings from the two observing systems showed a range of similarities and differences between the two observing systems, seemingly related to the specific mix of aircraft reporting and the uniformity of the weather regime present each day. Based on these findings, data from all aircraft that showed consistently large deviations from the co-located rawinsonde reports were eliminated from the statistical assessments.

Statistics for the full period

Weighted average rawinsonde reports were compiled for the full test period. The averages were weighted according to the number of aircraft matches for each rawinsonde launch. This weighting method reduces the influence of an individual sounding during an extreme weather event that has only one aircraft match-up, and increases the influence on the average of a report with many aircraft matches. Corrections for the influence of solar radiation of the rawinsondes were unnecessary because all of the rawinsonde launches were made after sunset and before dawn. The average temperature profile for the two-week assessment period showed a weak temperature inversion in the lowest 50 hPa, capped by a weak lapse rate that becomes nearly adiabatic by 500 hPa. A very weak secondary temperature inversion is also present between 850 and 820 hPa. The moisture profile showed a slight increase in moisture immediately above the surface, with steadily decreasing specific humidity from just above the surface to 500 hPa.

Statistical fits of the WVSS-II Specific Humidity (SH) data to the rawinsonde reports were obtained for the full observation period using all WVSS-II systems except those that showed consistent erratic behavior. Although a minimum of 20 match-ups was needed to calculate significant statistics at any level, between 30-40 observational matches were made at most levels.

The WVSS-II SH data (Figure 11.1 - top) show very small, though generally negative biases (-0.1 to -0.3 g/kg) from the surface to about 800 hPa. Above that level, the bias reduces to between 0.0 and -0.1 g/kg. Peaks in the bias appear at about 850 and 800 hPa. The Root Mean Square (RMS) fits of the full set of aircraft data to the rawinsonde reports showed variability of about 0.7 g/kg from the surface to 800 hPa. Above 800 hPa, RMS values decrease to between 0.5 and 0.3 g/kg. Again, peaks in the RMS appear near 850 and 800 hPa. The fact that the Standard Deviation (Stdev) also shows the unexplained peaks at 850 and 800 hPa indicates that the error is not due entirely to systematic differences between the observing systems (the bias is very small in this region), but instead must be due to a random factor, possibly related to atmospheric variability near this level.

Inter-comparison among the WVSS-II observations showed very good consistency between individual WVSS-II instruments, and provides evidence for the source of the peaks in the differences in the two data sets near 850 and 800 hPa. For observations taken within 15 minutes of each other, both the SH and Temperature (T) data show similar degrees of consistency from the surface to 500 hPa. The SH RMS ranged from ~0.7 to ~0.4 g/kg with increasing height while the T RMS increased from ~0.6° to ~0.8°. The agreement between independent WVSS-II observations made within 15 minutes was approximately the same as the agreement between WVSS-II and rawinsondes. This agreement not only corroborates the WVSS-II-to-rawinsonde statistics, but also provides evidence both of the consistency between individual



WVSS-II systems and the reproducibility of the WVSS-II data – a factor important for the future use of these data in NWP-based data assimilation systems.

At longer time intervals, however, the variability between observations at lower levels increased markedly. The source of this increased variability was traced to a combination of frontal passages and the progressive subsidence of a layer of dry air into the region of lower-level moisture during several periods of the test. Although gradual, the intrusion of the dry air from aloft into the lower levels was rapid enough to affect one or more of the 10 hPa deep layers used to generate statistics. In several cases, WVSS-II reports showed an area of extremely dry air capping a substantial moist layer extending from the surface to about 800-850 hPa. For example, if the WVSS-II reported about an hour before the rawinsonde, the statistic would indicate a disagreement – but this disagreement results from the time difference in a rapidly changing environment rather than an instrumentation error.

In an effort to reduce the impact of rapid changes in moisture observed between very thin layers on the co-location process, three additional constraints were placed on the statistical calculation. First, the 2 g/kg lower limit and 10 g/kg upper limits using in the 2005 tests were reintroduced. These limits eliminate the possible influences of WVSS-II biases caused by mechanical leaks in the sensor housings as well as errors caused by air-to-ground transmission deficiencies remaining on some aircraft. The second constraint was to eliminate individual cases in which successive rawinsonde reports showed that the variability in moisture in individual 10 hPa layers exceeded 7% per hour. Lastly, we eliminated cases where the rawinsonde reports showed vertical changes in relative humidity greater than 10% between successive 10 hPa levels.

Results using the additional restrictions (Figure 11.1 – middle) show that the additional processing constraints had very little impact on either the number of rawinsonde-aircraft matches or the statistical evaluation below 900 hPa. Below this level, the WVSS-II data show a slight dry systematic error (bias) of approximately -0.3 g/kg and random error component (Stdev) of about 0.6-0.7 g/kg, well within WMO requirements. Above 880 hPa, the number of rawinsonde-aircraft matches reduced at the uppermost levels (nearly all reports were eliminated above 700 hPa) and the magnitude of the bias increased slightly to about -0.2 g/kg. Both of these changes occurred because we eliminated reports of less than 2 g/kg, which tended to have a moist (+) bias. Additionally, the random error (Stdev) was reduced to between 0.2-0.4 g/kg in the entire region above 900 hPa. Although the peaks in bias and Stdev, which were present before the tests for large atmospheric temporal changes were added, have been eliminated, small peaks in the random error are still present near and above 900 hPa. This trend is likely due to the fact that the number of rawinsonde-aircraft matches is very low here because of the additional check for large vertical and temporal moisture changes. Not only has the sample size been reduced by over 30% in this region, but the probability that large environmental variations could still be affecting the remaining data and the sample could reduce the reliability of the statistics in this region.

When contrasted with results obtained during the spring 2005 assessment (Figure 11.1 – bottom), it appears that the engineering changes made after the 2005 test were at least partially successful in removing error in data taken during ascent. First, the positive biases that were present above 850 hPa in the 2005 data sets have been essentially eliminated. In addition, the unexplained bi-modal character of ‘systematic’ error (negative biases below 850 hPa and positive above) has been eliminated. Instead, the re-engineered systems now produce a small negative bias that appears to be consistent at all levels. The random error component has also improved. Although the Stdev (and RMS) below 900 hPa were similar in the two different tests (Stdev values averaging between 0.6-0.7 g/kg across the region), the performance above 900 hPa improved greatly with random errors in this region on the order of 0.4 g/kg— a 50-65% reduction from the 2005 tests.

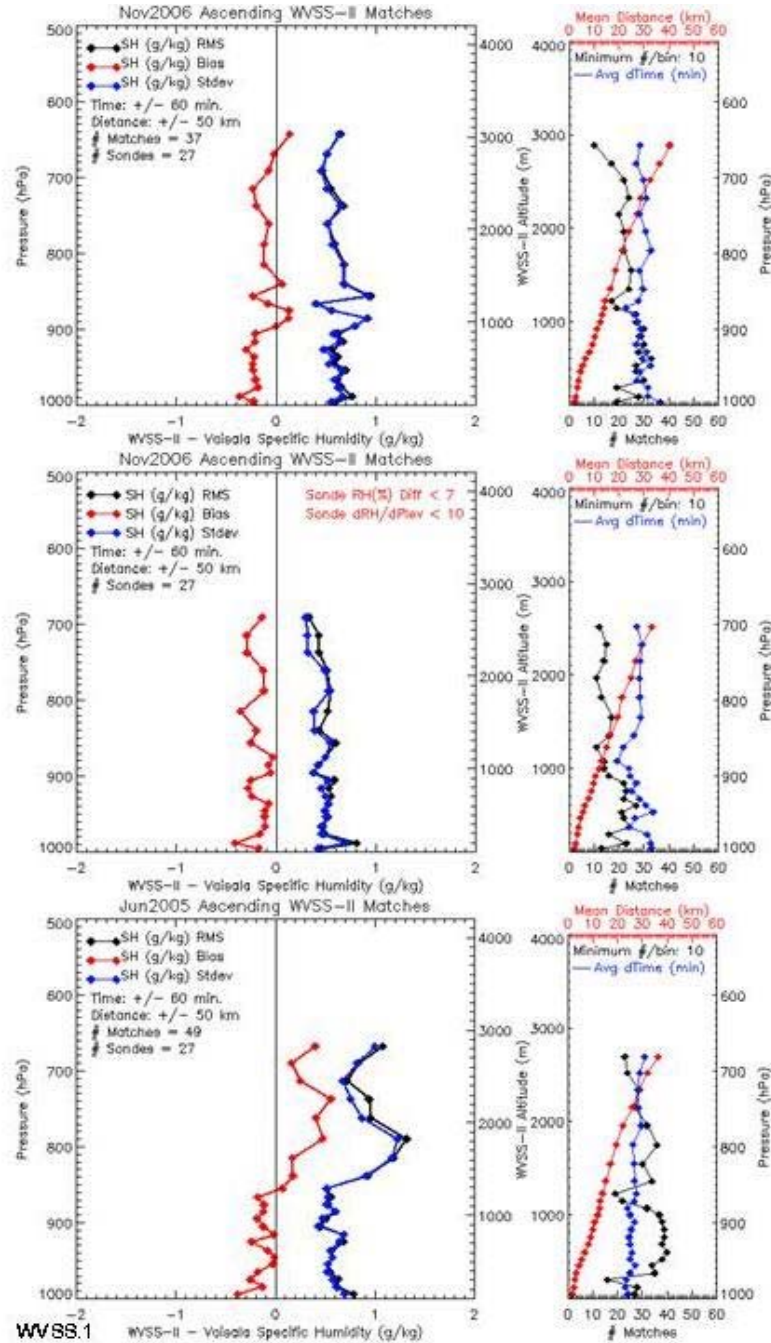


Figure 11.1: Top: Left - Statistical comparison of Rawinsonde and all WVSS-II moisture observation for the period 7-18 November 2006 at Louisville KY. Bias, Root Mean Square (RMS) and Standard Deviation (Stdev) between data sets (g/kg). **Top Right** - Number of observations used to calculate statistics (matched within +/- 60 minutes and 50km) and mean distance between observations shown in left panel. **Middle:** Same as top panel but with limitations imposed on WVSS-II observation range and vertical and temporal changes in rawinsonde data. See text for details. **Bottom:** Same as middle panel but for June 2005 tests and with limitations only on WVSS-II observation range.

Although not part of the WVSS-II system itself, statistics were also obtained for the aircraft temperature data. These data show a clear warm bias at all levels above the immediate boundary layer. Values range



from about 0.0 to 0.5°C. Random errors (Stdev) range from about 0.5°C in 500 hPa to ~1.0°C down to 950 hPa to 1.5°C near the surface. When the WVSS-II specific humidity and aircraft temperature are used to determine RH as an additional means of comparing the WVSS-II and rawinsonde observations, the warm bias shown in the temperature data makes the derived Relative Humidity data appear excessively dry. The relative humidity data derived by combining aircraft temperature and WVSS-II data has a dry bias of about 2-3% at almost all levels. Although this comparison does not provide a valid approximation of the error in the WVSS-II instrument, it does provide important information about the types of observational errors that should be used in data assimilation systems that might use the WVSS-II data.

A better representation of the RH error of the WVSS-II system was obtained by comparing calculations of RH obtained by combining the specific humidity measured by the WVSS-II and rawinsondes with the temperature measured by the rawinsonde. In this representation, the RH statistics represent *only* the effects of differences in the moisture observations between the two observing systems, independent of the temperature differences. The results (Figure 11.2 – left) reflect only the biases noted in the SH results (Figure 11.2 - right), with a very slight systematic dry bias averaging between -1 and -2% from the surface through 700 hPa. Similarly, the random errors of 0.6-0.7 g/kg below 900 hPa and 0.2-0.4 g/kg above 900 hPa translate into RH errors of approximately 9% throughout the column. The uniformity in the calculated RH error relative to the decreases in SH error from lower to upper levels is the result of the decrease temperature with height observed in this region of the atmosphere. *These levels of data quality meet or exceed all WMO observational requirements.*

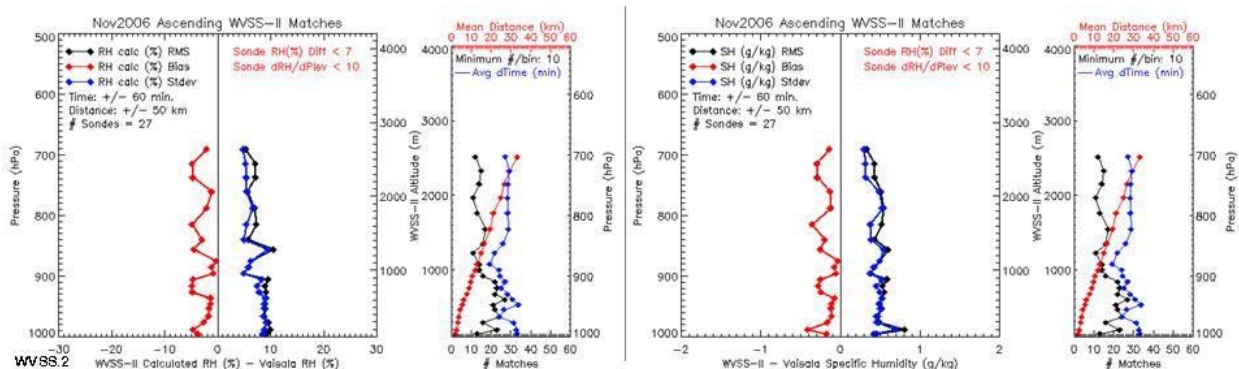


Figure 11.2: *Left Panels* - Statistical comparison of relative humidity (RH-%) calculated by combining specific humidity data from rawinsonde and WVSS-II with rawinsonde temperature observation for the period 7-18 November 2006 from Louisville KY - Number of observations used to calculate statistics (matched within +/- 60 minutes and 50 km) and mean time (min) distance (km) between observations. *Right Panels* - Statistical comparison of WVSS-II specific humidity (SH-g/kg) and rawinsonde observation for the period 7-18 November 2006 at Louisville KY, excluding WVSS-II observations <2 g/kg or > 10 g/kg and cases where relative humidity (RH) between successive rawinsonde reports in distinct 10 hPa layers varied by more than 7%/hr and where rawinsondes showed extreme vertical moisture gradients (RH changes greater than 10 % between adjacent 10 hPa).

Results of evaluations of alternative assessment methodologies

In an attempt to reduce the uncertainty due to the lack of precise time matching between the WVSS-II equipped aircraft and the validating rawinsondes, several additional assessment approaches were investigated conducted using alternative computational approaches. These included 1) time interpolation of the rawinsonde data (which were made immediately before and after the series of WVSS-II ascents and descents) to the time of the aircraft departures and 2) use of data derived from hourly numerical analyses of the Rapid Update Cycle (RUC – available via the web from NOAA’s Environmental Systems Research



Laboratory) as a means of further reducing the gap in time between the aircraft and validation data sets. Results of using both of these approaches are discussed here.

Tests of time-interpolated rawinsonde data as an evaluation standard

In the first of the alternative assessments technique tests, rawinsonde data acquired before and after each of the WVSS-II profiles were time-interpolated to the beginning time of each aircraft ascent. In doing so, it was anticipated that some of the effects of the rapid moisture changes observed on several days of the test period could be included more fully in the assessment.

When time-interpolation was used as a means of expanding the number of WVSS-II reports that could be used in the assessment by removing the +/-60 minute time matching constraint, the number of matches nearly doubled at most levels, going from near 30 to over 50 below 900 hPa. The Bias and RMS/Stdev statistics, however, became generally worse. Below 900 hPa, the Bias nearly doubled, while the RMS/Stdev increased at all but the upper-most levels. The increased differences between the full set of WVSS-II observations and the time-interpolated rawinsonde data were especially apparent near 900 hPa, where the RMS/Stdev increased by ~50%. Because many of the aircraft that were added in the longer-period tests were the same aircraft that had been shown to be providing high quality data in the +/-60 minute evaluations, the only explanation for the increased differences between the two data sets must be the inability of the linear time-interpolation of the 3-4 hourly rawinsonde data to account for the higher time-frequency variations observed in the WVSS-II moisture data at time separations greater than 1 hour. This conclusion is consistent with the WVSS-II temporal variability analysis discussed earlier. Even when using WVSS-II/Rawinsonde pairs that are time-matched to be within 1 hour, linear interpolation of 4 hourly rawinsonde data can not fully account for local variability seen in the much higher frequency WVSS-II reports (e.g., the miss-matches observed around the quickly changing moisture inversion). As such, the approach of eliminating areas of large temporal/vertical gradients was used instead of a time-interpolation approach.

Tests of utility of RUC analysis data as an evaluation standard

In the second alternative assessments technique tests, hourly RUC analyses made immediately before and after each of the WVSS-II ascents were tested as the evaluation standard. Again, it was anticipated that some of the effects of the rapid moisture changes observed on several days of the test period might be included more fully in the assessment using the higher time-resolution of the hourly RUC analyses instead of the 3-4 hourly rawinsonde data. Again, evaluations were made for both temperature and water vapor.

A total of 3 different comparisons were made for both the temperature and moisture data. These included using 1) all aircraft observations that passed Quality Control within +/-60 minutes of the rawinsonde launch compared with the rawinsonde report nearest in time without any time-interpolation, 2) all observations that passed Quality Control compared with the closest hourly RUC analysis data taken from the model grid point nearest the Louisville airport, and 3) comparison for rawinsonde data with hourly RUC analysis data taken from the model grid point nearest the Louisville airport. It should be noted both 1) that the rawinsonde data used in the earlier for comparison discussed in this report were not used in the RUC analyses and 2) that aircraft temperature data were available for use in the RUC temperature analyses.

Although temperature intercomparisons show generally similar results when inter-comparing the three systems, with the RUC analyses having many more matches than the rawinsonde data, as is to be expected, the picture for moisture observations is less promising. In this case, the fit of the RUC moisture analysis to the rawinsonde data taken at Louisville showed both large Biases and large RMS/Stdev values from the surface through 600 hPa. The Biases range from more than -1 g/kg below 800 hPa to more than



0.7 g/kg near and above 700 hPa. These Biases translate to RH differences of about -15% to nearly +20%. The random error is even larger throughout the lowest 400 hPa of the atmosphere, with Stdev values exceeding 1g/kg at almost every level. The maximum value > 1.5 g/kg at 700 hPa, corresponds to a RH difference of nearly 50%. By comparison, the Stdev fit of the WVSS-II data to rawinsondes was generally 0.5 g/kg or less at all levels. The fact that the two independent observational data sets were in close agreement validates the quality of the rawinsonde reports as a comparison standard and points to inaccuracies in the RUC analyses as being the source of the large differences (both systemic and random) between the two data sets. The effects of the large differences between the rawinsonde data and the RUC analyses were also apparent when comparing the RUC and WVSS-II data, with generally positive Biases and RMS/Stdev values between 1 and 1.5 g/kg.

From these data alone, it is unknown whether the large differences are due the inability of the RUC analyses to capture small-scale variation in observed moisture fields, or whether the RUC is adding small-scale features to its moisture analyses which are either unrealistic or out of phase with observations. Additional examination of temporal and spatial moisture variability being carried out under this proposal should help to address that question.

Although these results show that the RUC can be useful as a measure temperature observation accuracy, the fact that the errors in the RUC moisture analyses when compared to independent rawinsonde are much larger than the differences between the rawinsonde and WVSS-II data makes it inappropriate to use the RUC analyses (or short range forecasts) as a validation standard for any moisture observation.

Summary of November 2006 WVSS-II Co-location Assessment

This report presents a summary of the accuracy of mixing ratio observations made by WVSS-II equipped commercial aircraft during a two-week period in November 2006. Because errors due to engineering deficiencies were again noted in some of the descending data, the evaluation here again focused on data taken during aircraft ascent. The results (summarized in Fig 11.2) show small, negative Biases, on the order of -0.1 to -0.3 g/kg, and more vertically uniform than those observed in 2005. RMS fits average around 0.5 g/kg, notably less than that observed in 2005. This accuracy is well within NWS and WMO requirements

It should also be noted that care was needed to eliminate localized areas of excessive changes between successive rawinsondes and thereby minimize the impact of atmospheric variability in the instrument evaluation. Similar procedures may be needed for future use of these data with NWP data assimilation systems.

Temporal Moisture Variability Evaluation

Analyses of existing high time resolution boundary layer moisture profiles were also begun to help determine the optimal moisture observing frequency. Using-term time series of 7.2 minutes frequency AERI moisture profiles from surface-700 hPa made at the DOE ARM CART site at Lamont OK are being used to assess the observed temporal (and spatial in future) moisture variability. A two-sided quality control procedure similar to that used in the Wind Profiler evaluation discussed in the report form last year was applied to the AERI moisture profiles as an additional check for possible cloud contamination or other intermittent errors. It should be noted that these data were only available in clear sky conditions.

Initial results show that the time rate of change of moisture (measured in g/kg/hr) increases greatly as the time interval between observation decreases. Specifically, analysis of observations made throughout the entire day (Figure 11.3 - top) show that although the 95% of 12 hourly differences show normalized moisture variability less than 0.25 g/kg/hr, 50% of the observations made within 1 hr have variability *greater* than 0.25 g/kg/hr. In addition, 10% of the observations made within $1\frac{3}{4}$ hrs throughout the entire



day have variation > 1.0 g/kg/hr. These results validate the assertion that rawinsonde observations made every 12 hours are incapable of capturing realistic pictures of small-scale moisture variability in the atmosphere.

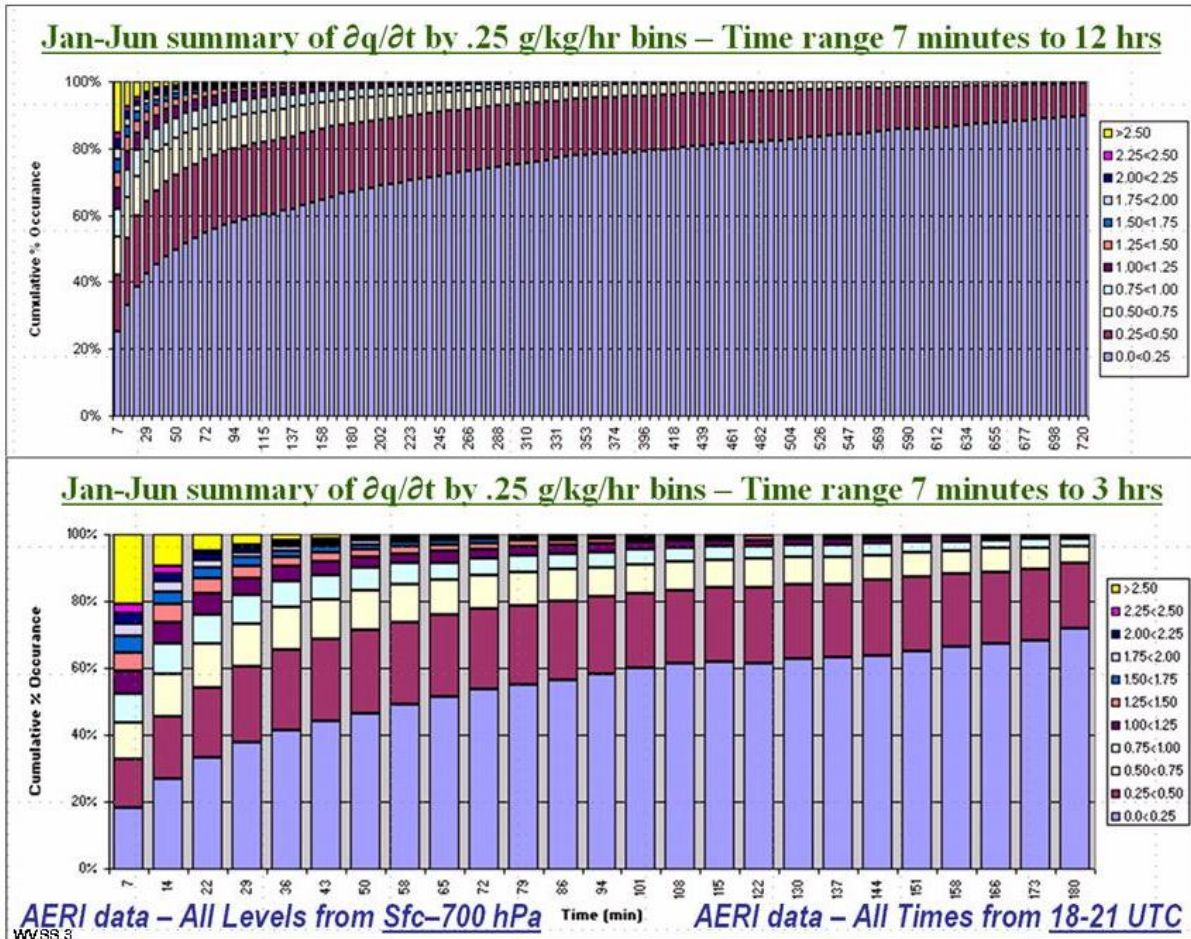


Figure 11.3: Results of 7.2-minute frequency time-series analyses of AERI moisture profiles from 2006 at Lamont, OK. Frequency of occurrence of temporal moisture tendencies (normalized to 1 hour changes) given in 0.25 g/kg/hr bins shown as full day averages (top panel) and 18-21 UTC averages (bottom panel).

Examinations conducted for shorter time intervals throughout the day showed substantial diurnal variability in moisture tendency. For example, tendencies calculated between 18-21 UTC (11.3 - bottom) showed greater variability than the full-day means, especially for the shortest time intervals. 85% of 3 hourly tendencies showed variability < 0.25 g/kg/hr, $\sim 10\%$ of observations made within 1 hr had variability > 1.0 g/kg/hr, $\sim 20\%$ of observations made within 30 min changed by > 1.0 g/kg/hr, and $\sim 5\%$ of observations made within 30 min changed by more than 2.0 g/kg/hr.

From these results, it can be inferred that observations of moisture changes taken no more frequently than 1 per hour may not be sufficient to detect many significant moisture changes which occur in the atmosphere. Additional evaluations are underway to better understand implications of these results as a function of year, time-of-day and/or time-of-year, relative to significant weather events and in terms of changes in the vertical moisture structure.



Although these results will provide information about observations frequency, these results will have to be combined with wind data to determine optimal special spacing. Before that can be done, the expected errors in Wind Profiler reports co-located with the AERI data at Lamont, OK must be determined.

In an extension of work reported last year, additional analyses of time- and space-series of Wind Profiler and co-located Rawinsonde data were used to determine the vertical structure of Wind Profiler errors and Local Wind Variability. Assuming wind errors in rawinsondes of 0.7m/s, Wind profile errors (Figure 11.4 - top) range from 0.5 m/s at 650 hPa to over 1/5 m/s above 250 hPa. At the same time, the Local Wind Variability (Fig 11.4 - bottom) decreases from about 1.5 m/s at 650 hPa to 1.25 m/s at 250 hPa.

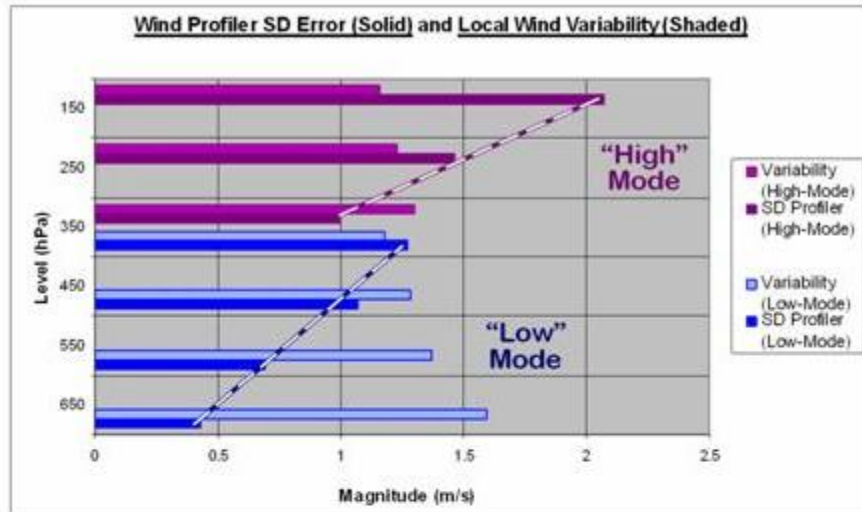
These results show that *six-minute* data from the National Wind Profiler Network:

- Are of excellent value, *if* subjected to 2-sided Quality Control procedures before use.
- Data in lower portions of both low- and high-lode are best.
- Use of six-minute date removes the time 'lag' present when using hourly NWP data and thereby reduces errors.
- Data show good time continuity, with greater variability in the boundary layer during day
- Wind Profiler data agree well with precisely co-located rawinsonde data
- "Representativeness Error" of both types of data can be calculated as function of level, distance and time offset between different observations.

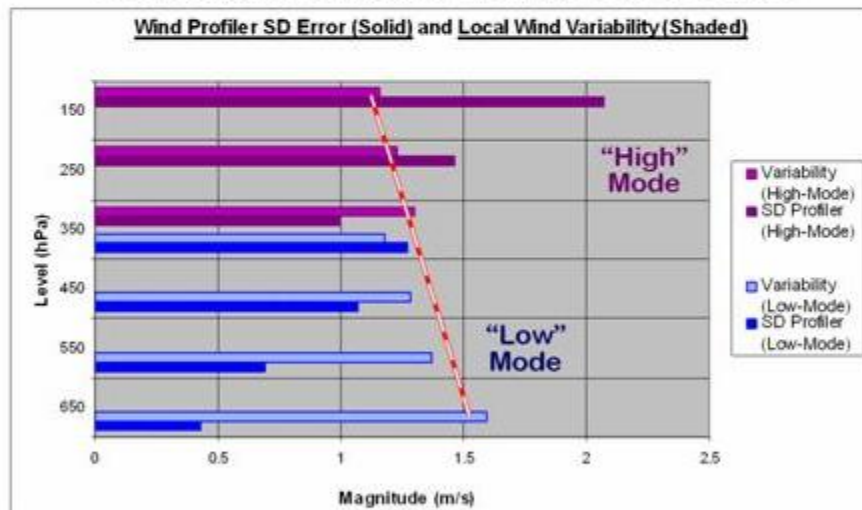
In addition to its use in determining optimal aircraft data spacing, information about the temporal and spatial variability (representativeness) of wind data will important for future meso-scale data assimilation systems, which will need different wind balances than current 'large scale' analyses, be nonlinear, need to include observed divergence (and wind tendencies) as input.



Wind Profiler Error from 700 to 100 hPa



Local Wind Variability from 700 to 100 hPa



- “Low” Mode Wind Profiler data error increase from $< 0.5 \text{ ms}^{-1}$ to $> 1.2 \text{ ms}^{-1}$ from 700 to 300 hPa
 - “High” Mode Wind Profiler data error increase from $\sim 1.0 \text{ ms}^{-1}$ to $> 2.0 \text{ ms}^{-1}$ from 400 to 100 hPa
 - Local Wind Variability decreases from $> 1.5 \text{ ms}^{-1}$ to $< 1.2 \text{ ms}^{-1}$ from 700 to 100 hPa
 - Similarity of calculations at 350 hPa using independent “Low” and “High” mode Profiler data give added credibility to the method
- WVSS.4

Figure 11.4: Results of analysis of time- and space-series of co-located Wind Profiler and Rawinsonde data from Lamont OK separating Wind Profiler instrument error from Local Wind Variability for low- and high mode Profiler reports.

Acknowledgements

The authors thank the large group of people who have been involved in the WVSS-II development and implementation efforts. Special thanks during the co-location tests need to be given to Dave Helms of NOAA/NWS, Randy Baker of UPS, Bill Moninger of NOAA/OAR, Rex Fleming of UCAR, Jeffery



Sarver KYANG of MSG, and the graduate students and staff of CIMSS who made this verification exercise possible. The work was supported by the NWS/Office of Climate, Water and Weather Services, Aviation Weather Branch through the NESDIS-UW CIMSS agreement.

Publications and Conference reports

Petersen, R. 2007: Sensor Development and Characteristics, Jan. 2007: Invited Paper, AMS Workshop on Applications of Aircraft Weather Data, San Antonio, TX.

Petersen, R., S. Bedka, W. Feltz and E. Olson, Jan. 2007: Evaluation of the WVSS-II Moisture Sensor using co-located, in-situ and remotely sensed observations, AMS Symposium on the Integrated Atmospheric Observing System, San Antonio, TX.

Petersen, R., S. Bedka, W. Feltz and E. Olson, Feb. 2007: Evaluation of the WVSS-II Moisture Sensor using co-located, in-situ and remotely sensed observations, Invited Poster, NCAR Workshop on Mesoscale Verification, Boulder, CO

Petersen, R., S. Bedka, W. Feltz and E. Olson, July 2007: Evaluation of the WVSS-II Moisture Sensor using co-located, in-situ and remotely sensed observations, IUGG quadrennial meeting, Perugia, Italy.

Petersen, R., S. Bedka, July 2007: Determining the Accuracy and Representativeness of Wind Profiler Data, IUGG quadrennial meeting, Perugia, Italy.

12. VISIT Activities – Steve Ackerman, Scott Bachmeier and Scott Lindstrom

Proposed Work

We proposed to continue exploring methods of improving and enhancing the content and techniques utilized for effective distance learning activities that are part of the Virtual Institute for Satellite Integration Training (VISIT) program.

Summary of Accomplishments and Findings

During the January-December 2007 period, there were four updates made to the VISITview software, and several support inquiries from the VISITview user community were addressed to improve the functionality of the software. Following a visit to EUMETSAT to present information on VISITview, a \$10K grant was received from EUMETSAT to make further updates to the software for internationalization.

The capability of utilizing operational real-time Advanced Weather Information Processing System (AWIPS) workstations at CIMSS was further refined and leveraged in 2007. This in-house AWIPS capability greatly enhances the process of VISIT lesson content creation by allowing immediate access to a diverse array of meteorological data sets from current weather events, in a format that is familiar to National Weather Service (NWS) forecasters. We facilitated the insertion of MODerate-resolution Imaging Spectroradiometer (MODIS) imagery, GOES sounder derived product imagery, and CIMSS Regional Assimilation System (CRAS) model forecast products into the AWIPS Operational Build 7, which is currently running at CIMSS.

Eight CIMSS-developed VISITview lessons (“MODIS Products in AWIPS”, “CRAS Forecast Imagery in AWIPS”, Mesoscale Convective Vorticies”, “Water Vapor Channel Satellite Imagery”, “The Enhanced-V: A Satellite Indicator of Severe Weather”, “TROWAL Identification”, “Basic Satellite Interpretation”, and “Water Vapor Imagery and Potential Vorticity Analysis”) were offered on the VISIT training calendar during 2007, with a total of 71 training sessions being conducted by CIMSS staff during the year



(the tally of National Weather Service forecast offices participating in these CIMSS VISIT lessons was 174). Two new VISITview instructional modules were developed and delivered during 2007. The first new VISIT lesson was “Water Vapor Imagery and Potential Vorticity Analysis” (an intermediate-level lesson intended as a more advanced follow-on to the introductory-level “Water Vapor Channel Satellite Imagery” lesson), which highlights water vapor satellite signatures associated with dynamical structures, using the framework of potential vorticity (PV) thinking, PV anomalies, and the dynamic tropopause. The use of water vapor imagery (in conjunction with GOES sounder Total Column Ozone products and synthetic water vapor image forecasts from the CRAS model) to assess Numerical Weather Prediction model output is demonstrated in this lesson. The second new VISIT lesson “Basic Satellite Principles” serves as an entry-level or a refresher course in satellite imagery interpretation, discussing topics such as pixel size/variability, parallax, and the variety of satellite channels and products that are currently available on AWIPS.

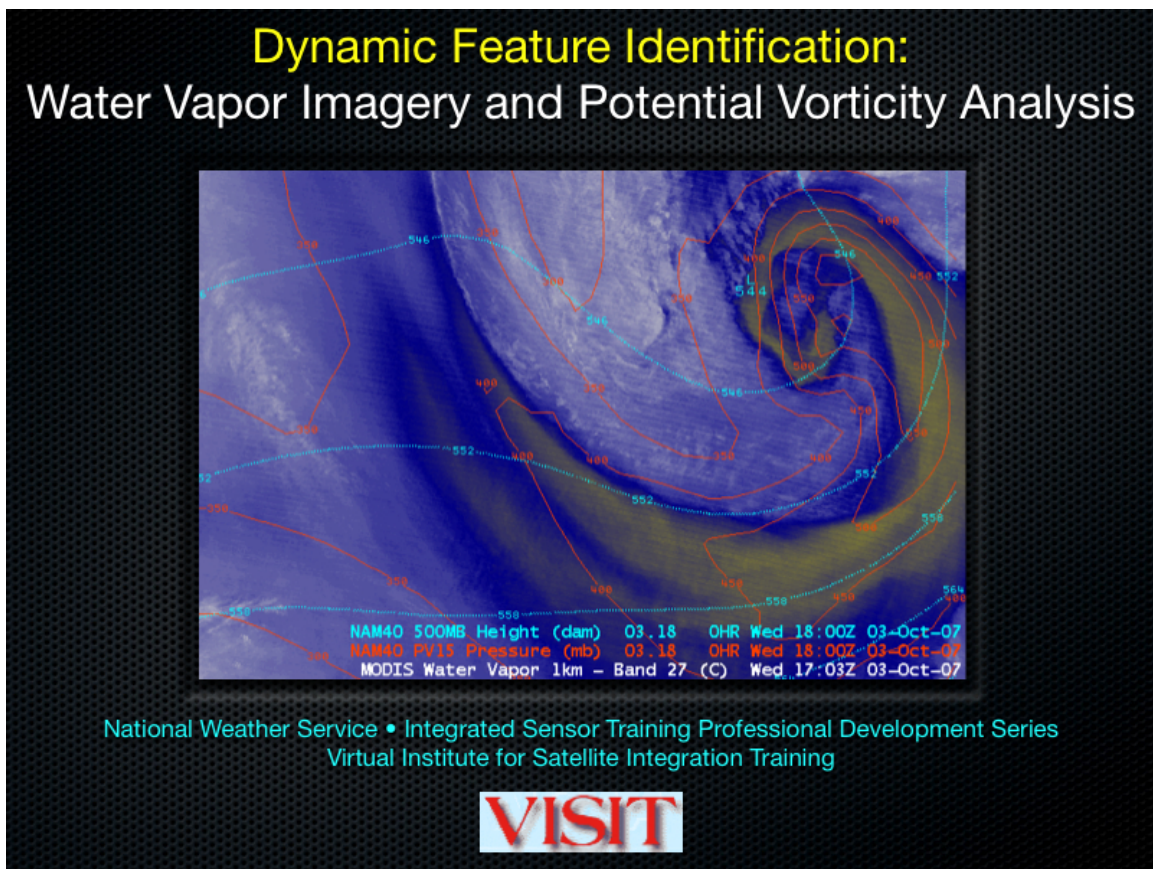


Figure 12.1: Title slide from the new “Water Vapor Imagery and Potential Vorticity Analysis” VISITview lesson, which was the most popular CIMSS VISIT lesson during 2007 (with 46 NWS offices participating).

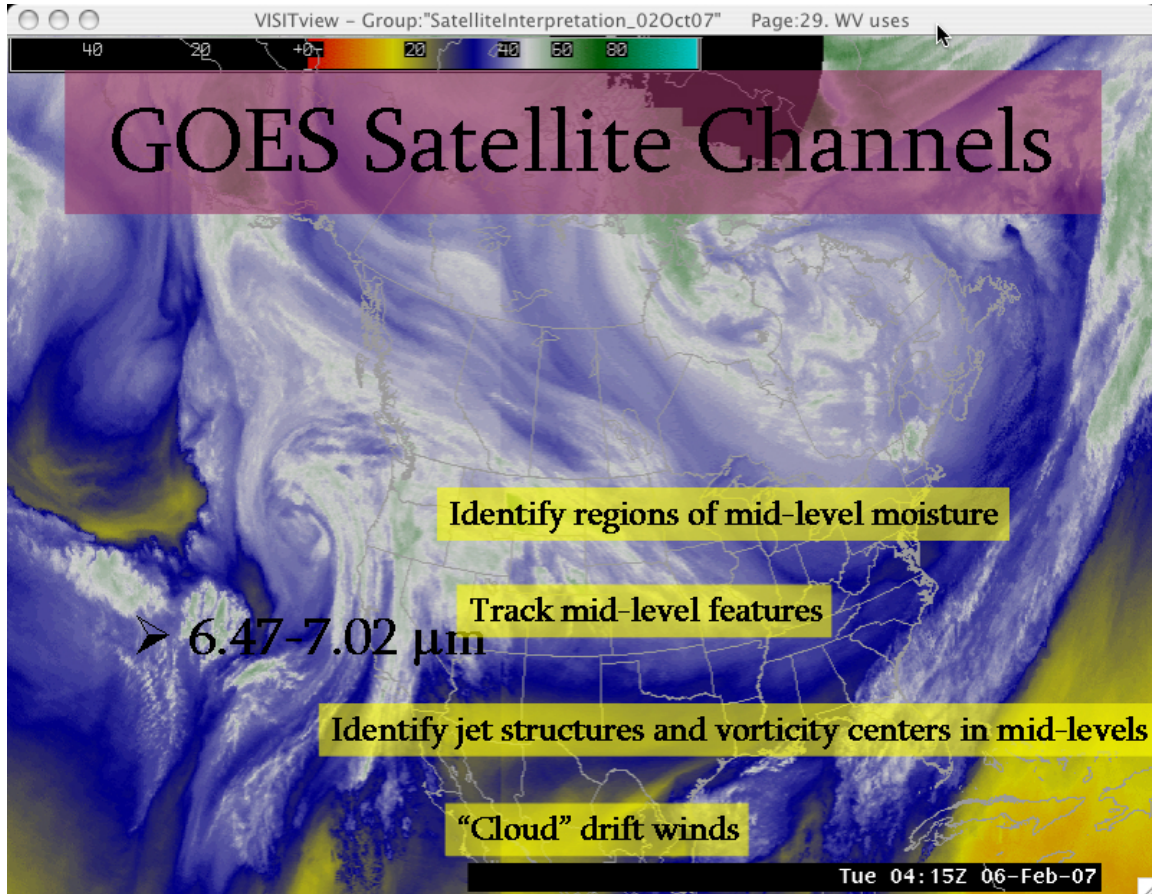


Figure 12.2: Screen capture from the new “Basic Satellite Principles” VISITview lesson, which provides an overview of the primary GOES satellite channels (such as the water vapor channel) and their uses in weather analysis and forecasting.

Work also continued to update existing versions of the “TROWAL Identification,” “Mesoscale Convective Vorticies,” “Water Vapor Channel Satellite Imagery,” “GOES High Density Winds,” “The Enhanced-V Signature: A Satellite Indicator of Severe Weather,” and “GOES Sounder Data and Products” VISITview lessons, adding new examples collected using the real-time AWIPS workstations at CIMSS. The ongoing process of periodically revising these existing instructional modules with new content helps to keep the material relevant and follow the pace of today’s changing learning objectives.

Publications and Conference Reports

A lecture and laboratory exercise “Satellite Applications: Dynamic Feature Identification” was given as part of the COMET Mesoscale Analysis and Prediction (COMAP) course in June 2007. A poster “Applications of Lightning Data at the Cooperative Institute for Meteorological Satellite Studies (CIMSS) at the University of Wisconsin–Madison” was given at the American Meteorological Society Annual Meeting. In addition, a presentation was given at an AMS Annual Meeting panel discussion on Societal Impacts, highlighting VISITview and the High Profile Training Event.



13. SHyMet Activities – Steve Ackerman and Scott Bachmeier

Proposed Work

CIMSS continued to further develop the Satellite Hydro-Meteorology (SHyMet) training course through close collaboration with experts at the Cooperative Institute for Research in the Atmosphere (CIRA) at Colorado State University, Colorado. The role of CIMSS in SHyMet is to 1) provide advice on the educational design of the program, 2) assist in the development of the curriculum, 3) support distance education activities, 4) develop and test appropriate satellite education materials, and 5) assist in the teaching of the courses as appropriate.

Summary of Accomplishments and Findings

CIMSS hosted the November 2007 SHyMet/VISIT workshop in Madison WI. (Attendees included: Tom Achtor, Bob Aune, Scott Bachmeier, Dan Bikos, Jeff Braun, Bernie Connell, Jeff Craven, Mark DeMaria, Jim Gurka, Brian Hahn, Scott Lindstrom, Tony Mostek, Brian Motta, Bill Sjoberg, Tom Whittaker). The goal of the meeting was to review the current status of and make plans for the VISIT and SHyMet plans for coming year.

SHyMet Statistics as of November 2007:

- 60 of 131 registered NOAA users have completed the program
- 8 of 16 Non-NOAA users have completed the program
- 29 SHyMet teletraining sessions for: GOES Sounder Data and Products, GOES High Density Winds, Cyclogenesis, and Intro to Satellite Severe Weather.

The teletraining portion of the course is being met by utilizing the already established Virtual Institute for Satellite Integration Training (VISIT) program. Previously, CIMSS developed and delivered lessons for the training topics “GOES Sounder Data and Products” and “GOES High Density Winds”. The “GOES Sounder Data and Products” lesson provides an introduction to the data and products available from the latest generation of GOES Sounder instruments, along with examples of sounder Derived Product Imagery (DPI) and their applications to weather analysis and forecasting. The “GOES High Density Winds” lesson reviews techniques for measuring satellite winds (atmospheric motion vectors), and provides details on the display of GOES high density winds on AWIPS. These distance learning courses were again delivered in 2007 using the VISITview software. CIMSS staff are charged with maintaining the lessons, evaluating feedback from the course and make appropriate modifications making any needed updates, where were not required.

14. Polar Winds from Satellite Imagers and Sounders – Chris Velden, Jeff Key and Dave Santek

Proposed Work

The primary objective of this project is to develop a satellite-based, tropospheric wind product covering both polar regions using a combination of instruments.

At CIMSS we are continued the development of the MODIS cloud-drift and water vapor winds product. We worked with our co-investigators at Rutgers University, NESDIS/STAR, and Colorado State University on 1) variational thermal wind estimation methods for use with ATOVS and AMSU; 2) combining the imager and sounder winds for a vertically and horizontally complete, satellite-based polar wind observation system; 3) extending the polar winds record back in time approximately 20 years using the AVHRR and TOVS instruments; and 4) working closely with the NASA Global Modeling and Assimilation Office, as well as the Joint Center for Satellite Data Assimilation (JCSDA) to improve the



use of the satellite-derived polar winds in numerical weather prediction (NWP) models. We also worked to 5) quantify the impact of including the polar winds in numerical weather forecast systems, and 6) to understand why the polar winds have the impact that they do. The combined polar winds product will be a very important tool for investigating the robustness of the assimilation system through an examination of differences in satellite-derived and modeled temperature and wind fields.

The project was funded by the NASA Earth Observing System (EOS) program through NESDIS (J. Key, PI). It ended December 31, 2007.

Summary of Accomplishments and Findings

During the third and final project year, the following was accomplished:

- A MODIS polar winds product was further developed and produced in near real-time with a 3-5 hour delay. The product is used operationally by ten (10) numerical weather prediction (NWP) centers in six countries. The NASA GMAO played a leading role in model experiments.
- Model output from several different experiments was investigated to determine possible mechanisms that propagate the polar wind information into mid- and low-latitudes. It was found that the addition of the polar winds modified the ageostrophic wind field near the polar jet stream, which has an effect on the speed and amplitude of baroclinic waves that extends from the jet stream into lower latitudes in later forecast times.
- A system to generate MODIS winds with direct broadcast (DB) data was developed and implemented at McMurdo, Antarctica; Tromsø, Norway; and Sodankylä, Finland. A similar system is under development at Fairbanks, Alaska. The U.S. Navy and the Met Office began operational use of the DB winds.
- Comparisons were performed between TOVS, AVHRR, and ERA-40 winds. Results are very encouraging and indicate that a combined TOVS/AVHRR product will provide an accurate, detailed wind product for the Arctic region.
- Historical AVHRR winds have been generated for a 21-year period (with additional funding from STAR).
- One PhD dissertation and one Master's thesis were completed.

Overall, the impact of the MODIS polar winds on numerical weather forecasts is positive. Most NWP centers have demonstrated a positive impact in the Arctic and Antarctic. Results for the Northern and Southern Hemisphere (poleward of 20 degrees latitude) vary, in most cases positive but in some cases negative or neutral. Most recently the MODIS winds were found to have a positive impact on hurricane track forecasts. Ten NWP centers now use the MODIS winds in their operational forecast systems: the NASA Global Modeling and Assimilation Office (GMAO), the European Centre for Medium-Range Weather Forecasts (ECMWF), the (UK) Met Office, the Canadian Meteorological Centre (CMC), the Japan Meteorological Agency (JMA), the U.S. Navy's Fleet Numerical Meteorology and Oceanography Center (FNMOC), Deutscher Wetterdienst (DWD), the National Centers for Environmental Prediction (NCEP) through JCSDA, MeteoFrance, and the National Center for Atmospheric Research (NCAR).

The direct broadcast (DB) winds are becoming increasingly important. Generally, the final MODIS polar wind product lags the observing time (the time MODIS views an area) by about 3-5 hours. The lag is largely due to the delay in the availability of the level 1B MODIS data from the NASA Goddard Space Flight Center via a NOAA computer system (the NOAA "bent pipe"). The 3-5 hour delay in the availability of wind information is too long for many regional or limited area data assimilation systems. (This includes a somewhat artificial delay of 100 minutes because a triplet of three consecutive orbits is used, and the final wind vector time is assigned that of the middle orbit.) In 2005, a system was developed to generate the MODIS winds with direct broadcast MODIS data in order to reduce the overall processing time. The system has been implemented at McMurdo, Antarctica, and Tromsø, Norway. All



processing is done on site. The Fleet Numerical Meteorology and Oceanography Center (FNMOOC, U.S. Navy) and UK Met Office began operational use of the MODIS winds that are generated on-site in McMurdo and Tromsø, Norway, in 2007. EUMETSAT now distributes the winds via EUMETCast. Other weather prediction centers are expected to use the DB winds operationally in the near future. A polar winds system is currently being developed at NESDIS' Fairbanks Command and Data Acquisition Station (FCDAS). Real-time results are available at <http://stratus.ssec.wisc.edu/db/>.

Publications and Conference Reports (Since project inception)

Santek, David, J. Jung, T. Zapotocny, J. Key, and C. Velden, 2006: Mechanisms that propagate polar satellite-derived atmospheric motion vector information into lower latitudes. *Proceedings of the 14th Conference on Satellite Meteorology and Oceanography*, American Meteorological Society, Atlanta, GA, 29 January-2 February 2006.

Velden, C., and many co-authors, 2005: Recent innovations in deriving tropospheric winds from satellites. *Bull. Amer. Meteor. Soc.*, **86**, 205-223.

Francis, J.A., E. Hunter, J. Key, and X. Wang, 2005: Clues to variability in Arctic minimum sea ice extent. *Geophys. Res. Lett.*, 32, L21501, doi:10.1029/2005GL024376.

Francis, J., E. Hunter, C. Zou, and J. Key, 2004: Arctic tropospheric winds from satellite sounders, 7th *International Winds Workshop*, Helsinki, Finland.

Key, J., D. Santek, C.S. Velden, J.M. Daniels, W. Bresky, and W.P. Menzel, 2005, Polar winds from satellite imagers for numerical weather prediction and climate applications, *Proceedings of the 8th Conference on Polar Meteorology and Oceanography*, American Meteorological Society, San Diego, California, 10-13 January 2005.

Zou, C.-Z., and W. Zheng, 2005, An improved algorithm for atmospheric wind retrievals from satellite soundings over the polar region, 8th Conference on Polar Meteorology and Oceanography, American Meteorological Society, San Diego, California.

Zou, C.-Z., 2005, An improved algorithm for atmospheric wind retrievals from satellite soundings over the polar region, 8th Conference on Polar Meteorology and Oceanography, American Meteorological Society, San Diego, California.

Theses

Dworak, R., 2007, Historical AVHRR Satellite-Derived Winds Archive (1982-2002), Validation and Comparison to the ERA-40, M.S. thesis, University of Wisconsin-Madison.

Santek, D.A., 2007: The global impact of satellite-derived polar winds on model forecasts. PhD dissertation University of Wisconsin-Madison, 141 pp.

15. Monitoring Global Variability with PATMOS-x – Amato Evan and Andrew Heidinger

Proposed Work

Firstly, we have proposed to incorporate real time satellite products from the operational cloud algorithm (CLAVR-x), part of the larger AVHRR Pathfinder Atmospheres Extended (PATMOS-x) reprocessing effort, into a format that is readable within Google Earth. We also have proposed to continue our efforts in understanding long term variability of the climate system (specifically clouds and aerosols), utilizing this unique data record.



Accomplishments

In mid December we launched our AVHRR Google Earth web site (<http://www.ssec.wisc.edu/google-earth/avhrr/>), which currently offers global AVHRR false color and sea surface temperature imagery at a 1km resolution. While it is difficult to measure the success of the project, we do note that between 4 and 5 GB of data are downloaded every week by users. With regards to understanding the climate with data from PATMOS-x (which currently spans the years 1981 through 2006); we have determined that 1) no substantial global long-term changes in cloudiness are evident in the AVHRR record -multidecadal variability in cloud cover is dominated by changes in the onset and duration of monsoon systems, 2) there are strong upward (Arabian Sea, Yellow Sea), and downward (Atlantic Ocean) trends in dust storm activity over the worlds oceans over the course of the record, and 3) there is a strong long-term inverse relationship between dust storms and hurricanes in the Atlantic via the aerosol direct effect. All of these findings have been published in the peer review literature referenced below.

Publications and Conference Reports

Evan, A.T., R. Bennartz, V. Bennington, H. Corrada-Bravo, A.K. Heidinger, N.M. Mahowald, C.S. Velden, G. Myhre and J.P. Kossin (2007): Ocean temperature forcing by aerosols across the Atlantic tropical cyclone development region. *Geochem. Geophys. Geosyst.*, accepted pending minor revision.

Evan, A.T., N. Mahowald and L. Remer (2007): Aerosols, State of the Climate in 2006, Horvitz, A., ed., *Bull. Am. Meteorol. Soc.*, 88 (6), pp. S23-S25.

Heidinger, A.K., A.T. Evan and B. Baum (2007): Cloudiness, State of the Climate in 2006, Horivtz, A., ed., *Bull. Am. Meteorol. Soc.*, 88 (6), pp. S17-S18.

Evan, A.T. (2007): Comment on "How Nature Foiled the 2006 Hurricane Forecasts." *EOS Trans.*, 88(26), pp. 271.

Evan, A.T., et al., (2007): Satellite-Observed West African Dust Outbreaks and the Relationship with North Atlantic Hurricane Activity, 15th AMS Conference on Satellite Meteorology, Amsterdam, Netherlands.

Evan, A.T., et al. (2007): Quantifying the impact of dust on tropical Atlantic Ocean temperatures, Joint AGU Meeting, Acapulco, Mexico.

Evan, A.T., et al. (2007): Saharan dust forcing of North Atlantic sea surface temperature. European Geosciences Union 2007 Annual Meeting, Vienna, Austria.

Heidinger, A.K., et al. (2007): Characterization of the 25 year PATMOS-x satellite cloud climatology using advanced sensors. European Geosciences Union 2007 Annual Meeting, Vienna, Austria.

Evan, A. T. & C. S. Velden (2007) Dust in the 2006 hurricane season. 61st Interdepartmental Hurricane Conference, New Orleans, Louisiana.



16. Developing Training Materials for McIDAS-X Users and Programmers – Dee Wade

Proposed Work

SSEC proposed to create a training course and materials for McIDAS users, as well as those wanting to do their own programming within McIDAS. The course design included both lectures and hands-on training. Lectures were supplemented by the use of Microsoft PowerPoint presentations, the McIDAS Learning Guide and the McIDAS Programmer's Manual.

SSEC and NOAA/NESDIS/IPD/SSD agreed to develop and evaluate training course material. SSEC would provide McIDAS instructors (two for user training and two for programmer training) to the NOAA Satellite Operations Facility (NSOF) building in Suitland, Maryland, to conduct a one-week McIDAS training session. The training sessions covered the details of McIDAS and how users and software programmers can efficiently use and write operational programs.

Summary of Accomplishments and Findings

The week of 10-14 September 2007 four SSEC instructors provided a week of McIDAS training to approximately 35 people at the NOAA Satellite Operations Facility (NSOF). The training consisted of a combination of lectures, including specially designed Power Point presentations for the McIDAS User and McIDAS Programmer training and interactive "hands-on" exercises on workstations. Specific user and programmer documentation was provided in the form of handouts.

Jay Heinzelman and Barry Roth provided McIDAS User Training on the first three days, 10-12 September. A short demo of McIDAS-V, the new McIDAS software, which is under development, was also provided on the Wednesday, 12 September.

Russ Dengel and Scott Lindstrom provided McIDAS Programmer Training on 13-14 September.

17. NPOESS Studies

17.1. Generating and Validating Snow and Ice Products in Polar Regions – William Straka III and Jeff Key

Background

The goal of this project is to generate NPOESS VIIRS snow and ice products in an operational environment at direct broadcast (DB) sites in the Arctic and Antarctic, and to provide automatic validation of these products. Snow/ice and cloud products are being generated with contractor code (Northrop Grumman Space Technology, NGST) and with our own algorithms, then validated with surface measurements and other data sets, when and where available, in real-time. MODIS data is being used as a proxy for VIIRS data.

Products of interest included: ice/snow surface temperature, ice/snow albedo, sea ice age, sea ice motion, and snow and ice cover. We also planned to look at cloud detection, cloud pressure, and cloud particle phase, and to work with the Cloud Team in this regard. Additionally, we wanted to investigate other high-latitude products that may eventually become VIIRS Environmental Data Records (EDRs) will be generated and validated, notably polar winds. The proposed system would build on DB product generation systems and product suites already in place and running at McMurdo, Antarctica and at Tromsø, Norway. The benefits of using real-time direct broadcast data are that: (1) it provides for an unlimited number of validation cases, as opposed to the more common situation where only a few ideal



test cases are used; (2) it provides a truly operational environment; and (3) it prepares us for future DB implementations of NPP and NPOESS products.

Summary of Accomplishments and Findings

The core parts of each EDR operational code set are used in our direct broadcast processing system, which operates on MODIS Level 1b data. The ice surface temperature (IST) operational code is currently running at Tromsø, Norway (since May 2006) and McMurdo, Antarctica (IST only; since June 2006). Additionally, the snow cover code is running at Tromsø. The two VIIRS IST algorithms are being compared to each other as well as comparing them to the IST algorithm that was being generated at the sites previously (Key et al., 1997). Less than 0.5% of the pixels in the 1-channel VIIRS IST algorithm have a larger than 2 degree difference when compared the two 2-channel algorithms (VIIRS 2 channel and Key et al., 1997). The areas and magnitudes of the differences between the 2-channel and 1-channel algorithms are similar.

Other VIIRS EDRs are being generated with our algorithms, in some cases at one or more DB sites and in other cases only with test data. The product suite now includes (“experimental” means code developed at CIMSS/NESDIS; “testing” means not running at DB sites; “DB” means routinely generated at DB sites):

Ice surface temperature (contractor and experimental; DB)

Snow cover (contractor and experimental; DB)

Ice motion (experimental; DB)

Ice concentration (experimental; testing)

Ice age/thickness (experimental; testing)

In addition to inter-comparing the various algorithms, we are also comparing the satellite-derived ice surface temperatures to surface observations. We are looking at established WMO surface sites as well as other observational systems, particularly the Automatic Weather Stations (AWS) across Antarctica. The SSEC Antarctic Meteorological Research Center and their international partners maintain the AWSs. There are six sites in the Arctic (all WMO sites) and nine sites in Antarctica that are currently being used in the validation study. More sites may be added in the future as data becomes available. Daily analyses, statistics and histograms are being produced in real-time for evaluation of the various algorithms. In addition, a 10-day time series of the differences is generated.

The latest product implemented Tromsø is ice motion. It is generated with code developed at the University of Colorado (C. Fowler) for AVHRR. A variety of time steps can be used to track the ice, though the best results are given when using images that are 24 hours apart. One downside to using this technique is that motion is detected in only a small fraction of the area due to cloud cover. An example is shown in Figure 17.1.1. Comparisons of satellite-derived ice motion with the Medium Range Forecast Model (MRF) surface winds have yielded positive results, showing that the detected motion is similar that of the surface wind. Another algorithm developed by CIMSS for tropospheric winds has been also adopted and modified for ice motion. A comparison between both ice motion algorithms has shown agreement in the direction of movement. Other options for validation, including the use of ocean buoys are being explored.

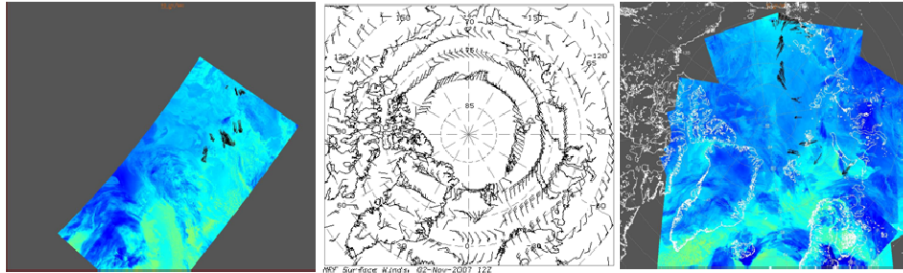


Figure 17.1.1: Ice motion (right and left) on 02 November 2007 based on MODIS data acquired at Tromsø, Norway, and the MRF model surface winds (center) at approximately mid-day.

Publications

Frey, R., S. Ackerman, Y. Liu, K. Strabala, H. Zhang, J. Key, and X. Wang, 2007: Cloud Detection with MODIS, Part I: Recent Improvements in the MODIS Cloud Mask, *J. Atmos. Ocean. Tech.*, accepted (January 2008).

Hall, D.K., J. Key, K.A. Casey, G.A. Riggs, and D.J. Cavalieri, 2004: Sea ice surface temperature product from the Moderate Resolution Imaging Spectroradiometer (MODIS), *IEEE Trans. Geosci. Remote Sensing*, 42(5), 1076-1087.

Key, J. et al., 2007: Integrated Global Observing Strategy Cryosphere Theme Report, WMO/TD-No. 1405, World Meteorological Organization, Geneva, 100 pp.

Liu, Y., J. Key, R. Frey, S. Ackerman, and W.P. Menzel, 2004, Nighttime polar cloud detection with MODIS, *J. Appl. Meteorol.*, 92, 181-194.

17.2. Cloud Studies for NPOESS – Richard Frey, Andrew Heidinger and Michael Pavolonis

Proposed Work

The main effort and outcome of this proposal was to work with the IPO, NGST, and NPP to improve the VIIRS Cloud Environmental Data Records (EDRs) using our experience with the heritage products from the current NOAA operational imagers. To date, we have been successful in collaborating with NGST on the VIIRS cloud mask and cloud type algorithms. In terms of the VIIRS cloud mask, we have helped NGST correct errors and implement new tests aimed at improving the SST performance. For the VIIRS cloud type, we have suggested algorithm improvements that mitigate errors noted by NGST in the baseline algorithm. In addition, we plan to expand this direct collaboration into other cloud EDR algorithms.

The secondary goal of this study is to start processing global MODIS data through VIIRS algorithms in partnership with NPP Atmospheric PEATE. By processing MODIS data through VIIRS algorithms globally, we can use our traditional validation approaches to expose weakness in VIIRS algorithms that might go unnoticed until after launch. In addition, we plan to run modified algorithms in parallel with the VIIRS baseline algorithms and demonstrate improvements for future algorithm updates.

Lastly, this study allows for the support of VOAT/IPO analyses that arise, as NGST or the IPO require assistance in defining new specifications or modifying EDR algorithms. The investigator of this project currently serves the VIIRS operational algorithm team (VOAT) Atmospheres Group lead.



Summary of Accomplishments and Findings

In the past year, we have handed on the Low Earth Orbiter Cloud Algorithm Test-bed (LEOCAT) to the NPP PEATE located at CIMSS. The PEATE intends to use LEOCAT as the core MODIS and VIIRS processing system. Through this partnership with the PEATE, we can process VIIRS algorithms globally on MODIS data. We have used this data to compute the distributions of VIIRS cloud mask test metrics using known clear pixels from CALIPSO/CALIOP. This has allowed us to validate the VCM thresholds and to suggest improvements. We have also used this data to being to explore true probabilistic cloud detection strategies. This work has been presented to NGST and at two conferences.

In addition, we have used MODIS and CALIPSO to explore the microphysical assumptions employed by the Nighttime VIIRS IR cirrus algorithm, which is used to estimate the height, opacity and particle size of cirrus clouds. CIMSS has much experience in validating these algorithms. We have coded this algorithm into IDL to allow for direct inspection of the intermediate steps in the retrieval process. In addition, we have developed an analysis that allows us to directly test the microphysical parameterizations in the NGST algorithm. The figure below demonstrates the current parameterizations differ significantly from both observations and theory. Discussions are ongoing with NGST to remedy this.

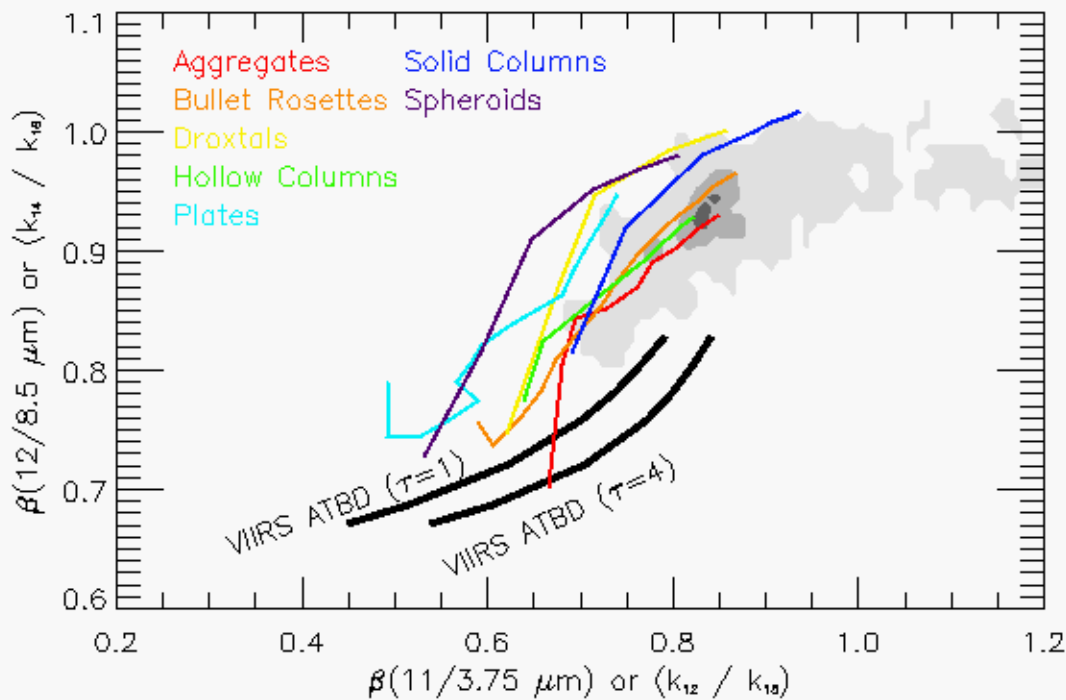


Figure 17.2.2: A comparison of the beta or k-ratio values used in the NGST VIIRS Infrared Nighttime Cirrus Retrieval algorithm against theory and CALIPSO observations. Our goal here is to use our analysis tools to point the way to improving the VIIRS algorithms.

Publications and Conference Reports

Heidinger, Andrew, B.A. Baum and P. Yang (2006): Consistency of cloud ice properties estimated from MODIS, AVHRR and SEVIRI. Conference on Atmospheric Radiation, 12th, and Conference on Cloud Physics, 12th, Madison, WI, 9-14 July 2006.



Heidinger, A.K., and M.J. Pavolonis (2008): Estimation of cloud height and emissivity from METOP/AVHRR and VIIRS The VIIRS cloud mask. Symposium on Future National Operational Environmental Satellites, 4th, New Orleans, LA, 20-25 January 2008

17.3. VIIRS Radiance Calibration / Validation, VIIRS / CrIS Cloud Property Investigations, and CrIS / ATMS / GPS Soundings – Paul Menzel, Eva Borbas, Youri Plokhenko, Chris Moeller and Dan LaPorte

Proposed Work

The proposed efforts are in five categories:

1. Continue participation in VIIRS instrument pre-launch testing and characterization;
2. Test VIIRS plus CrIS cloud property definition by exploring alleviation of VIIRS cloud problems using CrIS;
3. Study CrIS/ATMS/GPSOS Soundings and publish paper on combining geometric (radio occultation) CHAMP data with radiometric (infrared and microwave) AIRS/AMSU data;
4. Study sounding retrieval optimization with CrIS by quantifying sensitivity of temperature and moisture profile retrievals to CO₂ and O₃ profiles;
5. Develop HYDRA visualization tools for interrogation of multispectral data and demonstrate with MODIS and AIRS and IASI data

Summary of Accomplishments and Findings

Assessing VIIRS Pre-launch Performance (supported by IPO and NPP Cal/Val)

Chris Moeller and Dan LaPorte continued participation in VIIRS Technical Data Reviews and Algorithm Working Groups over the last quarter as well as reviewing FU-1 ambient phase II test data results.

- (a) FU-1 M9 RVS analysis and atmospheric correction has focused on analysis of FP-10 (RVS). SSEC/CIMSS has undertaken a study to improve the SBRS model-based atmospheric correction for M9 (1.38um) RVS retrieval. This work has shown considerable improvement in reducing the uncertainty of the M9 RVS retrieval (Figure 17.3.1) down to about 0.1%. The UW-Madison atmospheric correction has been tested on both HAM Side A and B M9 RVS with similar good results. Individual detector RVS has also been calculated, showing only small RVS variation from detector to detector. This work must be repeated when FU-1 RSR become available for M9.
- (b) In response to EDU RSR Characterization findings, several recommendations were given for FU-1 RSR testing regarding match spectral sampling and characterizing all detectors along a focal plane.

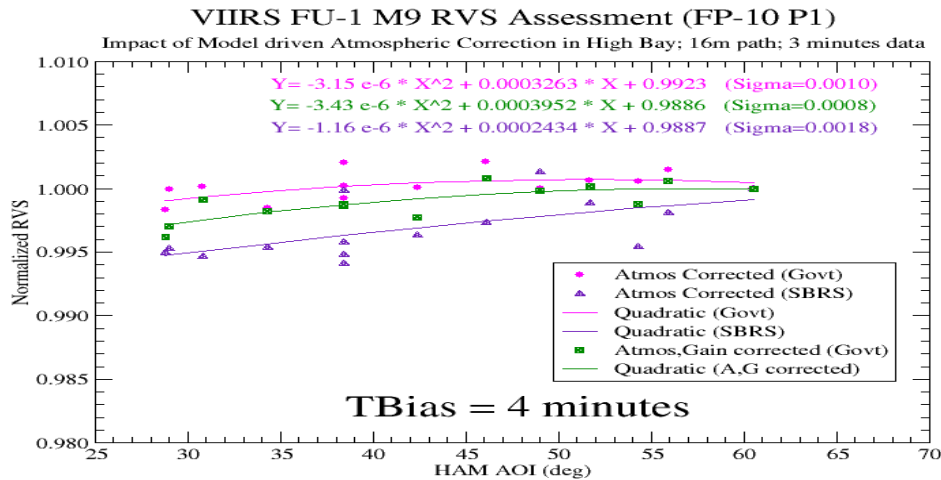


Figure 17.3.1: VIIRS M9 RVS retrieval for three analyses: SBRS atmosphere corrected (purple), UW atmosphere corrected (magenta), and UW atmosphere and gain corrected (green). The resulting fitting residuals are given in parentheses at the end of the quadratic fitting equation. All three analyses meet the 0.3% uncertainty threshold for M9 RVS; however the UW analyses reduce the fitting residuals considerably, creating margin in the M9 RVS uncertainty budget.

Estimating cloud profiles from AIRS measurements

An algorithm to estimate the cloud amount profile from AIRS high spectral resolution infrared measurements has been developed and tested. The cloud radiative transfer model adjusts cloud amount and cloud top pressure in each of 25 levels (spaced to provide uniform vertical resolution as much as possible) to match calculated with measured radiances for the AIRS spectral bands. An AIRS granule coincident with CALIPSO measurements has been processed (see Figure 17.3.1). The agreement in cloud vertical structure estimated from the AIRS radiances and measured by the CALIPSO backscatter is surprisingly good; both find the cloud extended between 5 and 15 km in height with denser segments near cloud bottom in similar locations. MODIS CO₂ slicing cloud top pressures indicate the radiative mean of these thinner high clouds.

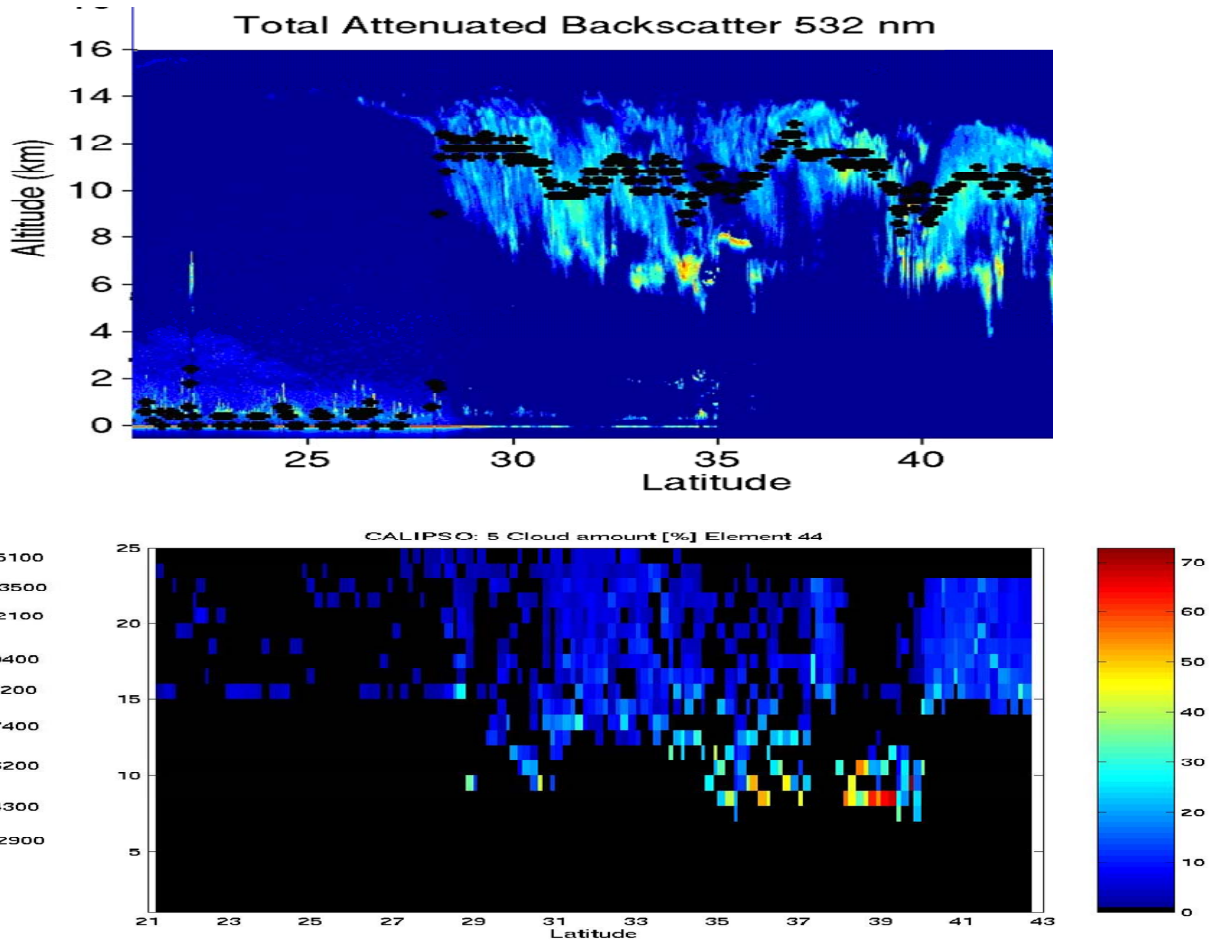


Figure 17.3.2: (top) CALIPSO attenuated backscatter (at 532 nm) and Aqua MODIS cloud top heights (black pluses) for a flight segment on 15 June 2006, zoom on high cirrus at 30° to 40° N latitude; (bottom) Vertical distribution of effective cloud amount derived from AIRS measurement along collocated scan element 44.

GPS and Sounders

The *Journal of Applied Meteorology and Climate* accepted a paper on combined CHAMP/AIRS/AMSU profile retrievals by E. Borbas, W. P. Menzel, E. Weisz, and D. Devenyi. The paper reports that AIRS/AMSU temperature retrievals show an improvement of about 0.5 C in the tropopause region after inclusion of GPS data.

Studying the sensitivity of AIRS retrievals to CO₂ / O₃ amounts

Studies continued on the effects of CO₂ concentration on residuals between AIRS measured radiances versus radiative calculations (via SARTA). The radiative transfer code was tested on an AIRS granule; the residuals between calculated radiances from profile retrievals and measured radiances are shown in Figure 17.3.2. It was found that residuals (indicated in brightness temperatures) ranged up to 1 K in the H₂O sensitive part of the spectrum while they remained less than 0.3 K in the O₃ and CO₂ sensitive parts of the spectrum. Varying CO₂ concentrations to minimize the residuals also lead to changes of 3 to 5 ppmv in CO₂ concentrations.

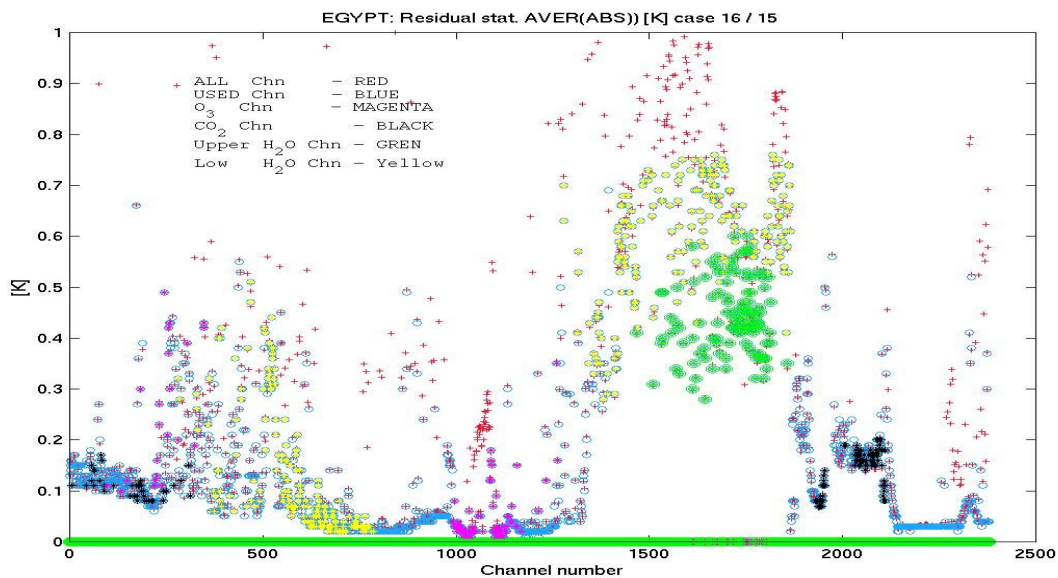


Figure 17.3.3: Residual statistics Aver(ABS(dT)) [K] where RED indicates all the AIRS channels (including those not used in profile retrieval). BLUE indicates the channels that were used, BLACK shows the CO₂ channels, MAGENTA the O₃ channels, GREEN the upper tropospheric H₂O channels, and YELLOW the lower tropospheric H₂O channels

Visualization Tools

HYDRA continues to add capabilities for interrogating and visualizing imager and sounder data. Currently it can accommodate data from MODIS, AIRS, IASI, SEVIRI, and GOES Imager and Sounder. In addition, HYDRA displays CALIPSO lidar images of clouds collocated with MODIS data of the same scenes. The transition of HYDRA capabilities into the next generation of McIDAS (the Man computer Interactive Data Access System – called MCIDAS-V) has begun (mostly funded through other resources). The goal is that hyperspectral analyses and visualizations can be combined/compared with model output and non-satellite (conventional) data. HYDRA is the main vehicle for training and research among the UW-Madison team preparing for NPP and NPOESS.

Publications and Conference Reports

T. Rink, W. P. Menzel, P. Antonelli, T. Whittaker, K. Baggett, L. Gumley, and A. Huang published a paper on “HYDRA – a Multispectral Data Analysis Toolkit” in the February 2007 issue of the *Bull. Amer. Meteor. Soc.* It introduces the multi-spectral data analysis toolkit, describes the various functions, and presents several examples with MODIS and AIRS data.

E. E. Borbas, W. P. Menzel, E. Weisz, and D. Devenyi co-authored a paper on “Deriving atmospheric temperature of the tropopause region/upper troposphere by combining information from GPS radio occultation refractivity and high spectral resolution infrared radiance measurements” accepted by *J. Appl. Meteor. Clim.* in January 2008.

Plokhenko, Y., W. P. Menzel, H. E. Revercomb, E. E. Borbas, P. Antonelli, and E. Weisz published a paper on “Analysis of multi spectral fields of satellite IR measurements: Using statistics of second spatial differential of spectral fields for measurement characterization” in the *Intl. J. Remote Sens.* in early 2008.



17.4. Cal/Val Verification and Validation Activities – Hank Revercomb and Fred Best

Proposed Work

The proposed work under the general task of “IPO Cal/Val Verification and Validation Activities” was composed of the tasks listed below. This section contains a summary of progress during the past year for each of these tasks.

- Perform Technical Evaluation of CrIS Performance
- Support CrIS SOAT Team
- Plan and Conduct Field Campaigns With S-HIS and NAST
- Evaluate JAIVEx Mission Data
- Support NAST Instrument and Calibration
- Refine NIST Traceability of Scanning-HIS Measurements
- Summary

Summary of Accomplishments and Findings

Perform Technical Evaluation of CrIS Performance

This task includes participation in the review of instrument test data obtained to characterize the sensor performance and to uncover performance anomalies and deficiencies, the development and utilization of proxy data sets for evaluating the impact of performance anomalies on CrIS Sensor Data Record (SDR) and Environmental Data Record (EDR) products, and strategies for mitigating performance issues.

In the past year, efforts under this task included:

- Participation in CrIS Flight Model 1 Test readiness reviews
- Participation in CrIS SDR Algorithm Reviews
- Participation in the testing and analysis of CrIS FM1 test data
- Development/refinement of a CrIS RDR data reader and test analysis software
- Examination of IASI data to characterize the effects of non-uniform scenes on the Instrument Line Shape and development and assessment of a novel correction technique

Regarding our input to the CrIS FM1 test plans and analyses, we have made significant contributions in the areas of ECT and ICT characterization, SDR algorithm refinements, and the addition of diagnostic mode data collection for the characterization of radiometric nonlinearity. The nonlinearity of FM1 is greater than anticipated (approximately three times spec). We are now working to adapt nonlinearity correction algorithms previously developed for Scanning-HIS and NAST-I to CrIS, and to analyze the CrIS test data to characterize its nonlinearity.

Regarding the effects of non-uniform scenes on the CrIS Instrument Line Shape, the launch of IASI was the first opportunity to use real satellite data to characterize and quantify these effects. For typical ensembles of Earth view scenes, we find that that the non-uniform scene effects can produce ILS effects as large as +/- 30 ppm (parts per million in spectral calibration knowledge) with highly non-Gaussian distributions. The effects are found to be highly correlated with scene non-uniformity derived from collocated imager data. Uncorrected, these effects manifest in brightness temperature errors as large as +/- 1 K in the LW band of IASI and +/- 3 K in the SW band of IASI. Using principle component analysis techniques, we have also developed a simple and accurate correction algorithm for these effects. The +/- 30 ppm effects are reduced to approximately +/- 3 to 4 ppm. Assessment and improvement of the correction algorithm is ongoing. See Figure 17.4.1. Also, as part of this effort, we have developed a simple yet very accurate method (at the tenths of ppm accuracy level) to determine and monitor the inter-FOV spectral calibration differences of IASI and CrIS.

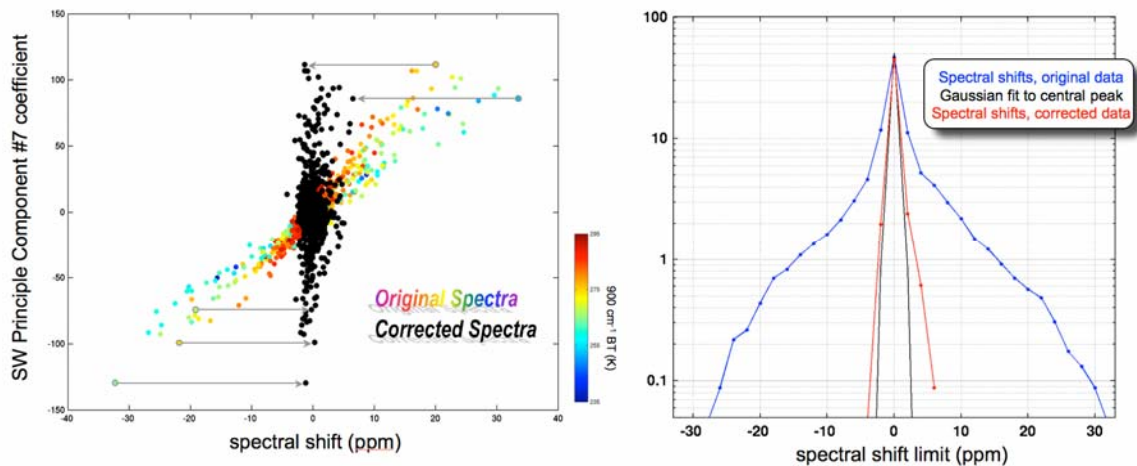


Figure 17.4.1: *Left panel:* Spectral shifts for an ensemble of original and corrected IASI spectra versus the magnitude of the non-uniform scene effects present in a principle component containing the non-uniform scene ILS signature. The correction reduces +/- 30 ppm spectral shifts to +/- 3 ppm shifts. *Right panel:* The percentage of spectra in the ensemble with spectral shifts greater than a certain limit for the original and corrected spectra. For example, 2% of the spectra have shifts greater than +10 ppm (and ~2% have shifts less than -2 ppm) before correction, while no spectra have shifts greater than 10 ppm (or less than -10 ppm) after correction.

Support CrIS SOAT Team

The SOAT team was inactive this year – we expect that it will be rejuvenated the next year.

Plan and Conduct Field Campaigns With S-HIS and NAST

Field experiment support was provided for both the Scanning High-resolution Interferometer Sounder (S-HIS) and the NPOESS Airborne Sounder Testbed – Interferometer (NAST-I) during the JAIVEx campaign conducted out of the NASA Johnson Space Center in Houston TX, April – May 2007. S-HIS and NAST-I are aircraft-based high spectral resolution infrared spectro-radiometers that have participated in numerous satellite validation campaigns in the past decade. Applications of the data have included sensor trade studies, radiative transfer model and atmospheric sounding algorithm development and validation, atmospheric sounding of temperature and water vapor and other trace gases, and surface and cloud remote sensing. The observations are also benefiting GSICS. Flying at high altitude and collecting observations which are coincident with the satellite overpasses, the S-HIS and NAST-I observations are providing NIST-traceable validation of the on-orbit satellite observations. Underflights to date have focused on validating the calibration accuracy of the high spectral resolution sounders AIRS on Aqua and IASI on METOP-A. The AIRS and IASI data were then used to intercalibrate other polar-orbiting and Geosynchronous infrared sensors via the Simultaneous Nadir Overpass techniques employed by various GSICS investigators. The periodic aircraft campaigns and NIST-traceable characterization tests thus provide a firm and quantitative basis to not only intercalibrate other sensors, but also provide an absolute benchmark for the GSICS analyses.

During JAIVEx, the NASA WB-57 completed ten science flights totaling roughly 50 science flight hours, with the S-HIS collecting science data for approximately 49 of these 50 science flight hours (~98%), with no loss of at-altitude data (only data losses were during ascent/descent). Figure 17.4.2 shows the WB-57 flight path for the April 19th CART site flight, overlaid on a IASI thermal image

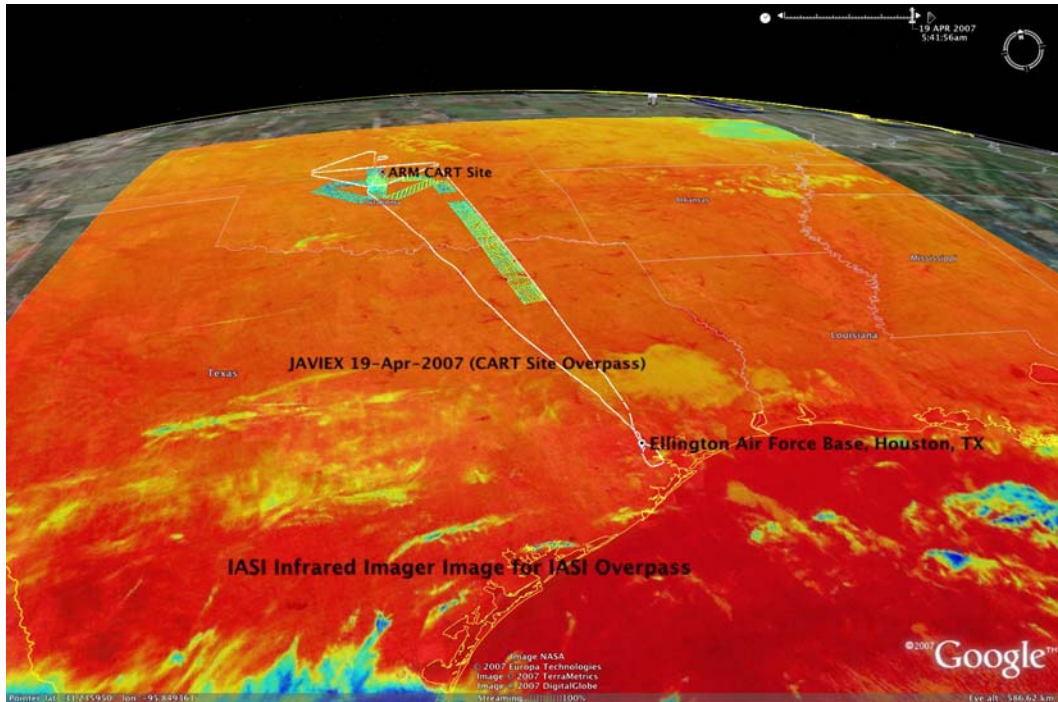


Figure 17.4.2: 19-Apr-2007 CART Site overpass. WB-57 flight path shown overlaid on the IASI infrared imager image for the overpass time.

NAST-I support during the JAIVEx field campaign included:

- Level 1 data processing (calibrated radiances) and quicklook generation
- NAST-I instrument support
- Local and remote NAST-I and S-HIS data transfer and distribution
- On-site technical computing and IT support
- Weather forecast support for flight planning activities

Evaluation of JAIVEx Mission Data

As part of JAIVEx, the first underflights of IASI were obtained. A sample result obtained for clear sky conditions over the Atmospheric Radiation Measurement (ARM) site in north central Oklahoma is shown in Figure 17.4.3 for portions of the IASI longwave, midwave, and shortwave band.

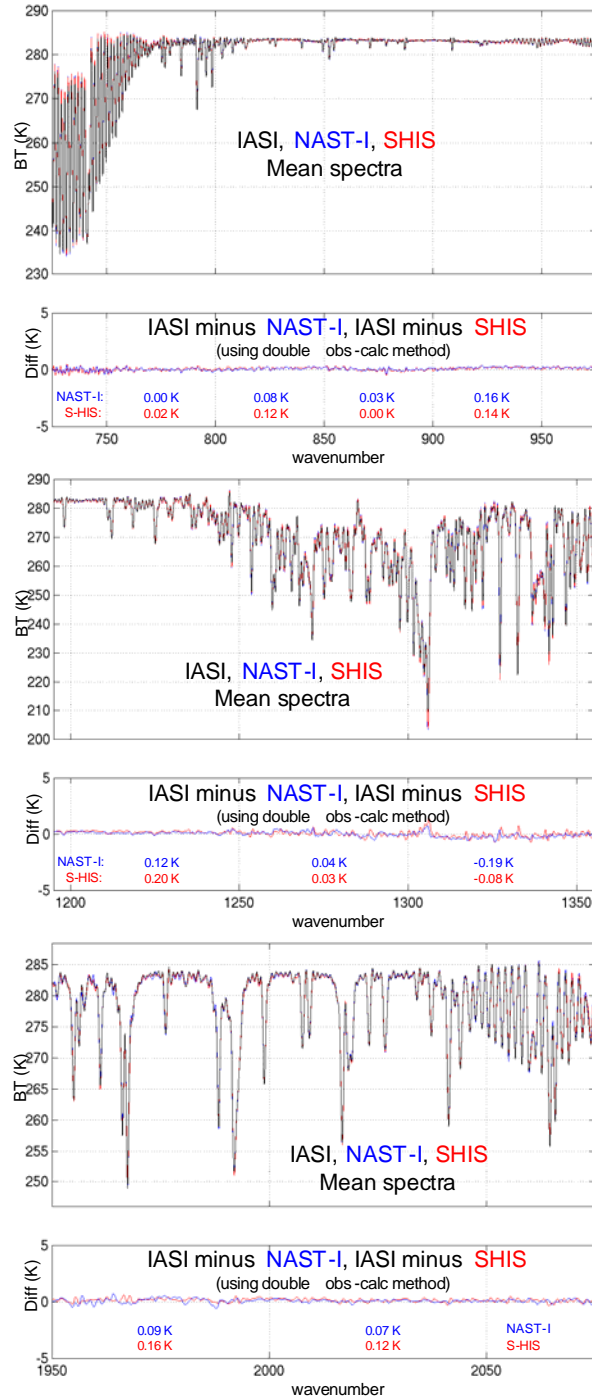


Figure 17.4.3: Validation of IASI spectral radiance observations using S-HIS and NAST-I data collected on 19 April 2007 over the Oklahoma ARM site. Longwave (top), Midwave (middle), and Shortwave (bottom) are shown respectively.

The analysis shows that the IASI absolute calibration is accurate to 0.1 to 0.2 K, within the calibration and intercomparison accuracy of the aircraft data. Similar results have been obtained for AIRS for past and recent flights; details of the analyses techniques and more results are available in the literature (e.g. Larar et al. 2003, Tobin et al. 2006).



One of the challenges for using advanced IR sounder data over land is the accuracy to which the surface emission can be accounted for in the retrieval inversion or 1-D variational data assimilation. Uncertainty in the characterization of surface emission in atmospheric sounding channels can lead to top of atmosphere radiance errors comparable to the small signals that contain the fine scale vertical structure information. This trend is particularly true of data collected in the important atmospheric boundary layer, the lowest one to three kilometers above the surface, where land/atmosphere coupled processes are most important. An evaluation of temperature, water vapor, and ozone retrieved profiles was made for the same coincident case study used for radiance validation of IASI with S-HIS. The retrievals from both IASI and SHIS use the same optimal estimation retrieval methodology (Rodgers 2000) in order to assess the quality of the IASI radiances on retrieved meteorological variables. A comparison of IASI, SHIS, and radiosonde measurements of temperature and water vapor are shown in Figure 17.4.4. The results include a unique method for the simultaneous retrieval of land surface emissivity within the optimal estimation scheme. The results were presented at the AMS/EUMETSAT joint satellite conference in September 2007 and at an IASI workshop in November 2007.

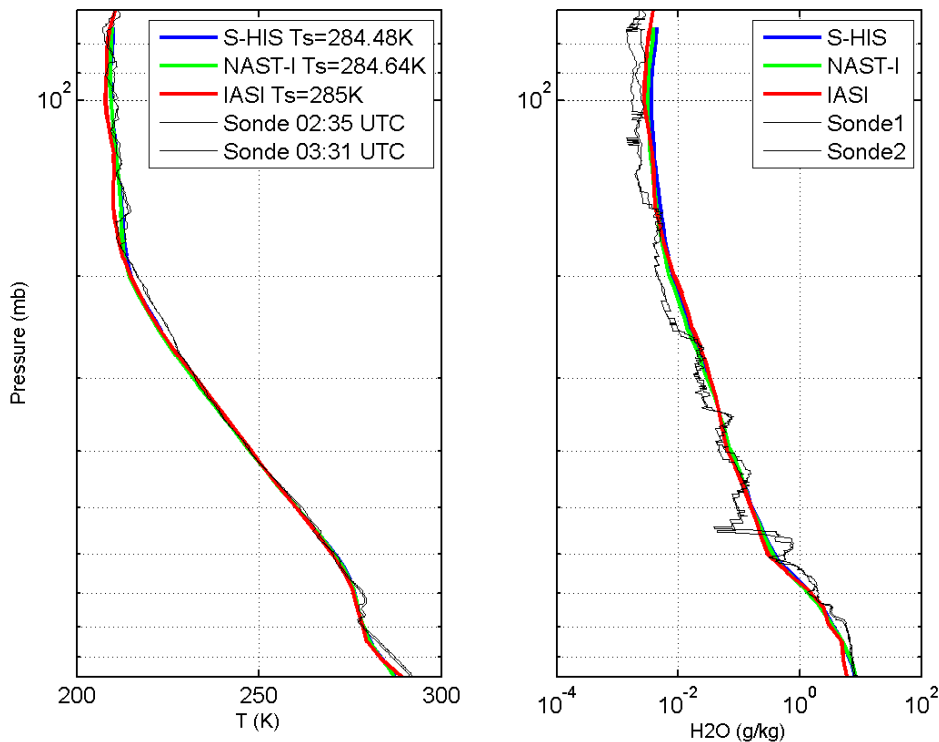


Figure 17.4.4: The temperature and water vapor profile derived from the same 19 April 2007 IASI and S-HIS spectra used in the radiance comparison are shown compared to two radiosondes launched from the ARM Southern Great Plains central facility before and after the satellite overpass. The IASI and S-HIS retrievals of T/WV are in good agreement with each other as expected from the excellent radiance comparison.

Support NAST Instrument and Calibration

Most of the effort related to NAST-I support was focused on getting the instrument operationally ready and properly calibrated for the JAIVEx field experiment.



Calibration Support

In order to improve the calibration accuracy of the NAST-I instrument, calibration pipeline modifications were designed and calibration coefficients were evaluated. Improvements that were implemented include:

- PC Filtering of Blackbody Radiances
- Adding a test of the blackbody controller cyclic redundancy check field when flagging reference radiances to be omitted from the calibration pipeline
- Verification and optimization of the nonlinearity and finite field of view calibration coefficients.

Because the NAST-I optical alignment had been adjusted since the prior end-to-end calibration assessment at SSEC, tests of the instrument near field response (NFR) and far field of view map were conducted prior to the JAIVEx field campaign. The far field of view map was completed for the NAST-I MW band. The results showed that the far field was well aligned with the theoretical field of view, and there was no evidence of field of view clipping in the far field. The NFR testing was completed for all three bands (SW/MW/LW) at the blackbody reference positions. Results indicated that all three bands were adequately centered and within the aperture diameter at blackbody positions.

End-to-end NAST-I calibration assessments were completed before and after the JAIVEx deployment. The tests were conducted at SSEC and included:

- Side-by-side clear atmosphere observation with AERI-08 and AERIBAGO instruments with simultaneous radiosonde launch and corresponding computed theoretical atmosphere comparison.
- Ice Bath Blackbody reference source (see Figure 17.4.5).
- Intermediate Blackbody reference source (318K, 333K).



Figure 17.4.5: NAST-I External Ice Bath Blackbody reference source test configuration, used both before and after the JAIVEx field campaign.

In another important calibration task this year, the SSEC participated in the planning phases for the NAST-I radiance validation test that will be conducted in a thermal vacuum chamber at NASA LaRC. In this test, the NAST-I will be maintained at flight temperature while viewing the SSEC AERI blackbody S/N 41 (recently validated by the NIST TXR). The blackbody will be controlled at several different temperatures from 230 to 295 K, representing most of the expected earth scene temperature range. Test



support included: designing and fabricating specialized blackbody cables, writing operating procedures for the unique blackbody configuration, and helping to develop the calibration validation procedure. The cal/val procedure was developed based on our experience with the Scanning-HIS radiance validation tests with the NIST TXR.

Instrument Support

SSEC provided diagnostic help with a blackbody controller problem reported during the WB-57 NAST-I test flights prior to the JAIVEx field campaign. NASA LaRC reported occasional missing and/or corrupted blackbody data packets. Subsequent testing of the UW Blackbody Controller subsystem at SSEC showed 100% data packet integrity and transmission to and from the controller for the duration of the tests, narrowing the problem to the instrument side. To further isolate the source of the problem, a detailed test plan was developed for the NAST-I hardware and software interfaces to the blackbody controller and forwarded to NASA LaRC. Further diagnosis of this problem will be conducted in the near future.

Refine NIST Traceability of Scanning-HIS Measurements

To verify the calibration accuracy and provide direct NIST traceability of the aircraft radiance observations, laboratory tests of the S-HIS and the NIST Transfer Radiometer (TXR) were conducted this year. The TXR was used to accomplish a more direct connection to the blackbody reference sources maintained by NIST than the normal traceability of blackbody temperature scales and paint emissivity measurements. The test involved the S-HIS and the TXR each observing a highly stable and accurate AERI blackbody for a wide range of scene temperatures (227 to 290 K) while operating the S-HIS under typical flight conditions, with the optical bench at about 260 K (see Figure 17.4.6). The test results, summarized in Figure 17.4.7 for the TXR longwave channel, show brightness temperature differences between the TXR and the S-HIS to be, on average, less than 40 mK. These results verify the S-HIS calibration accuracy, and provide NIST traceability of the S-HIS radiance observations and of the satellite validation results. Results for the TXR 5 μ channel are awaiting further analysis, but are expected to show good agreement—the mean difference between the S-HIS measured and AERI blackbody computed radiance is less than 40 mK.

It is anticipated that periodic satellite underflights and laboratory characterization tests will be continued into the future as a prelude to the on-orbit benchmark measurements, such as those recommended in the recent National Academy of Sciences Decadal Survey for the CLARREO mission.

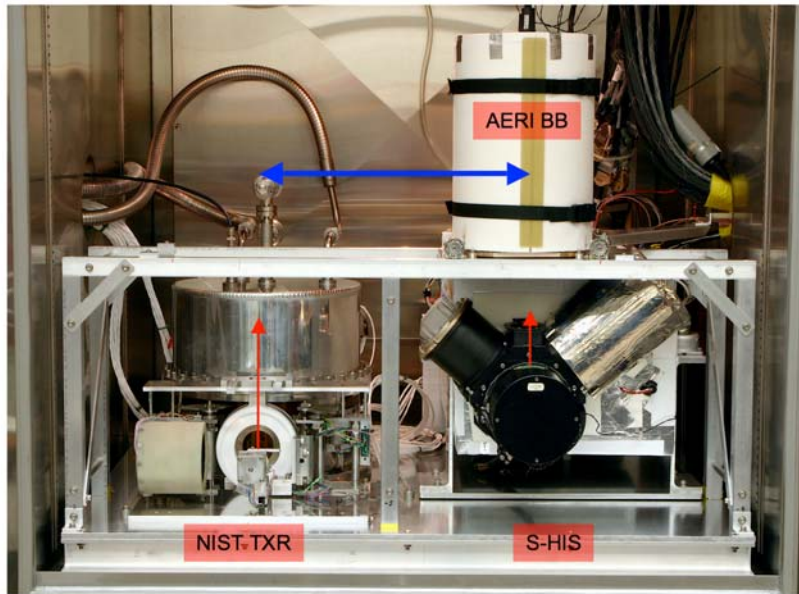


Figure 17.4.6: A photograph of the S-HIS / NIST TXR test setup. At each calibration temperature the AERI blackbody was sequentially moved into the view of either the NIST/TXR or S-HIS. Radiance measurements were then compared.

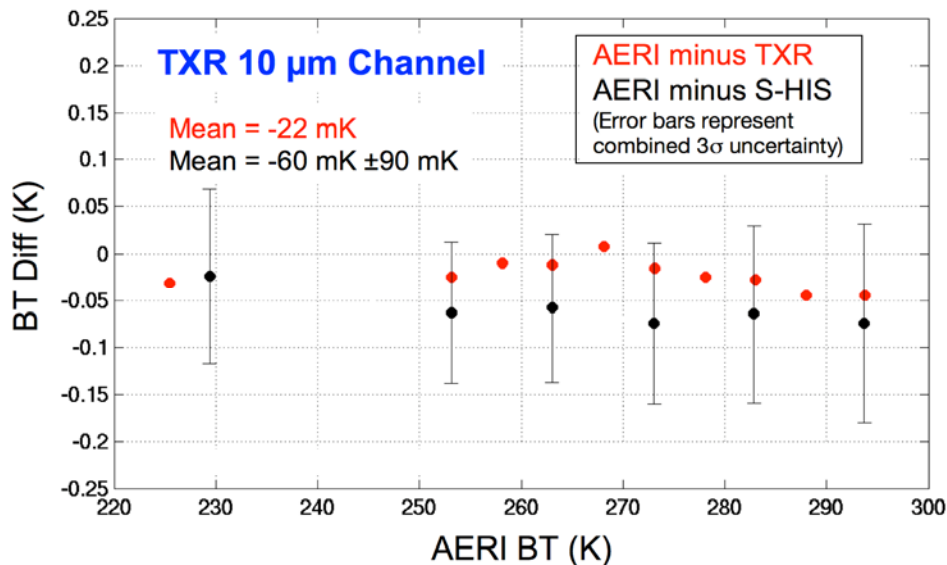


Figure 17.4.7: Difference between predicted AERI blackbody radiance and the measured S-HIS radiance and the predicted AERI blackbody radiance minus the measured TXR radiance for the 10 μm TXR channel.

Summary

This has been a productive year supporting our IPO Cal/Val Verification and Validation Activities. The significant accomplishments are highlighted below:

- Participated in the Joint Airborne IASI Validation Experiment (JAIVEx), supporting Scanning HIS & NAST-I.
- Analyzed radiance comparisons and cataloged data set releases.



- Quantified issue with CrIS spectral shifts from non-uniform fields and identified a new basis for a correction algorithm.
- Identified need and planned for development of CrIS non-linearity correction algorithm.
- Participated in CrIS Test Planning Reviews.
- Conducted retrieval algorithm development to handle complex surface emissivity conditions for EDR validation.
- Determined Direct NIST traceability for Scanning HIS and NAST-I calibration.
- Completed 18 Publications and Conference Presentations.

Publications and Conference Reports

A chronological listing of the publications and conference reports related to our IPO Cal/Val Verification and Validation Activities is included below:

Taylor, Joe K., Henry E. Revercomb, Erik E. Olson, Steve T. Dutcher, Fred A. Best, David C. Tobin, Nick C. Ciganovich, Scott Ellington, Ray K. Garcia, H. Ben Howell, Robert O. Vinson, Mark Werner, Results for Operational Correction of Tilt Induced Sample Position Error for the Scanning High-resolution Interferometer Sounder (S-HIS), in *Fourier Transform Spectroscopy and Hyperspectral Imaging and Sounding of the Environment on CD-ROM* (The Optical Society of America, Washington, DC, 2007), ISBN: 1-55752-828-4

Knuteson, Robert O., Szu Chia Moeller, David C. Tobin, and Henry E. Revercomb, A Proposed Methodology for the Determination of Surface Temperature and Effective Infrared Emissivity for Advanced Infrared Sounder Fields of View at High Latitudes, TGARS Special Issue on Remote Sensing and Modeling of Surface Properties – Impact on Satellite Products and Numerical Weather Prediction, submitted, Mar 2007.

Tobin, D. C., P. Antonelli, H. E. Revercomb, S. Dutcher, D. D. Turner, J. K. Taylor, R. O. Knuteson, and K. Vinson, Hyperspectral data noise characterization using principle component analysis: application to the atmospheric infrared sounder, *J. Appl. Remote Sens.* 1, 013515 (2007) doi: 10.1117/1.2757707

Taylor, Joe, Joseph O'Connell, Joseph Rice—National Institute of Standards and Technology; Henry Revercomb, Fred Best, David Tobin, Robert Knuteson, Douglas Adler, Nick Ciganovich, Steven Dutcher, Daniel LaPorte, Scott Ellington, Mark Werner, Ray Garcia, *NIST TXR Validation of Scanning HIS Radiances and a UW-SSEC Blackbody*, 2007 CALCON Technical Conference, 10-13 September 2007.

Tobin, David, Hank Revercomb, Fred Best, Joe Taylor, Steven Dutcher, Robert Holz, Daniel Deslover, William Smith, Allen Larar, *Radiometric and Spectral Validation of Infrared Atmospheric Sounding Interferometer (IASI) Observations*, 2007 CALCON Technical Conference, 10-13 September 2007.

Revercomb, Hank, Expected On-orbit Calibration Performance of CrIS, 2007 CALCON Technical Conference, 10-13 September 2007.

Taylor, J. et al., Improved radiance validation products: results for operational correction of Tilt induced interferometric errors for the Scanning High-resolution Interferometer Sounder (S-HIS), Joint 2007 EUMETSAT Meteorological Satellite & 15th AMS Satellite Meteorology and Oceanography Conference, Amsterdam, The Netherlands, 24 – 28 September 2007.

Smith, W. et al., *Joint Airborne IASI Validation Experiment (JAIVEx) - An Overview of the US component and capabilities*, Joint 2007 EUMETSAT Meteorological Satellite & 15th AMS Satellite Meteorology and Oceanography Conference, Amsterdam, The Netherlands, 24 – 28 September 2007.



Revercomb, H. et al., High accuracy infrared radiances for weather and climate, Part 2: Airborne validation of IASI and AIRS and the role for future benchmark satellites, Joint 2007 EUMETSAT Meteorological Satellite & 15th AMS Satellite Meteorology and Oceanography Conference, Amsterdam, The Netherlands, 24 – 28 September 2007.

Knuteson, R. et al., *Aircraft validation of infrared emissivity derived from advanced infraRed sounder satellite observations*, Joint 2007 EUMETSAT Meteorological Satellite & 15th AMS Satellite Meteorology and Oceanography Conference, Amsterdam, The Netherlands, 24 – 28 September 2007.

Best, F. et al., High accuracy infrared radiances for weather and climate, Part 1: NIST TXR Validation of scanning HIS radiances and a UW-SSEC blackbody, Joint 2007 EUMETSAT Meteorological Satellite & 15th AMS Satellite Meteorology and Oceanography Conference, Amsterdam, The Netherlands, 24 – 28 September 2007.

Taylor, J. K., L. O’Connell, J. P. Rice, H. E. Revercomb, F. A. Best, D. C. Tobin, R. O. Knuteson, D. P. Adler, N. C. Ciganovich, S. T. Dutcher, D. D. LaPorte, S. D. Ellington, M. W. Merner, R. K. Garcia, (2007), NIST TXR Validation of S-HIS radiances and a UW-SSEC Blackbody, *Eos Trans. AGU*, 88 (52), Fall Meet. Suppl., Abstract A31B-0311.

Smith, W. L., S. Kireev, A. Larar, X. Liu, D. Zhou, C. Lee, S. Newman, J. Taylor, S. Mango, H. Revercomb, D. Tobin, P. Schluessel, Comparison of IASI and NAST-I Physical Retrievals: Validation Using Radiosondes and Dropsondes during JAIVEx, 13-16 November 2007, Anglet, France.
Knuteson, R. O., M. E. Evansen, S. C. Moeller, H. E. Revercomb, D. C. Tobin, Comparison of Land Surface Infrared Spectral Emissivity Derived from MetOP IASI and Aqua AIRS, 13-16 November 2007, Anglet, France.

Tobin, D. C., H. E. Revercomb, P. Antonelli, Principle Component Analysis of IASI Spectra, IASI Conference, 13-16 November 2007, Anglet, France.

Best, F. A., H. E. Revercomb, D. C. Tobin, R. O. Knuteson, D. P. Adler, N. C. Ciganovich, S. Dutcher, J. K. Taylor, D. D. LaPorte, S. D. Ellington, M. W. Werner, R. K. Garcia, J. O’Connell, J. P. Rice, NIST TXR Validation of Scanning-HIS radiances and a UW-SSEC Blackbody, 13-16 November 2007, Anglet, France.

Revercomb, H. E., D. C. Tobin, R. O. Knuteson, F. A. Best, D. P. Adler, N. C. Ciganovich, S. Dutcher, R. K. Garcia, J. K. Taylor, D. D. LaPorte, S. D. Ellington, M. W. Werner, K. Vinson, W. L. Smith Sr., Spectral Radiances provide a new standard in absolute accuracy: Direct IASI radiance validation results from aircraft, 13-16 November 2007, Anglet, France.

Taylor, J. K., H. E. Revercomb, F. A. Best, N. C. Ciganovich, S. T. Dutcher, S. Ellington, R. K. Garcia, H. B. Howell, R. O. Knuteson, D. D. LaPorte, E. E. Olson, D. C. Tobin, K. Vinson, M. Werner, Performance of and FTIR sounder on several airborne platforms: the Scanning High-resolution Interferometer Sounder (S-HIS), 13-16 November 2007, Anglet, France.



17.5. The International Polar Orbiting Processing Package for Direct Broadcast Users - Allen Huang and Liam Gumley

Proposed Work:

CIMSS/SSEC proposed to coordinate with IPO and the NASA Direct Readout Lab (DRL) in executing the common work plan established in the March 2007 TIM. CIMSS/SSEC planned to:

1. Participate and engage in IDPS Algorithm Transformation Evaluation to evaluate the existing approaches for transforming IDPS algorithms into a form where they can be run on Linux. A study report on the advantages and disadvantages of each approach will be generated to recommend a strategy for adoption by IPOPP.
2. Evaluate selected IDPS algorithms for
 - a. Ancillary data requirements;
 - b. Algorithm interdependencies;
 - c. Suitability for real-time direct broadcast processing.
3. Provide assistance for NISGS installation on Draca for testing and evaluation.
4. Install NISGS on SSEC cluster for testing and evaluation.
5. Assemble initial test data sets.
6. Collect and provide important documents to the IPOPP team.
7. Establish IPOPP team website and/or mailing list.
8. Establish software development environment on Draca.
9. Create draft of IPOPP user web site (e.g., FAQ, relevant documents, schedules)
10. Support DRL, in time for Polar Max 2007, in the creation of a real-time processing system that runs a subset of VIIRS and equivalent MODIS algorithms in parallel driven by Aqua MODIS direct broadcast proxy data. Candidate algorithms include Cloud Mask, Fire Mask, cloud top property, and SST.

In addition, CIMSS/SSEC planned to work to accomplish the following tasks as part of the IPOPP “Build 2” effort in 2007:

1. Analyze VIIRS ancillary data requirements,
2. Analyze VIIRS gridded intermediate products, and
3. Build VIIRS cloud mask.

Summary of Accomplishments and Findings

During the year of 2007 following tasks were accomplished:

VIIRS OPS build 1.5 integration into LEOCAT

VIIRS OPS v1.4 cloud mask code, including the required ancillary and gridded IP stand-in data sets, are successfully implemented in LEOCAT framework. Work is also underway to upgrade to the use of v1.5 cloud mask code. An update of LEOCAT in Eclipse was also conducted. Eclipse has recently improved its support for C and Fortran projects. The projects associated with LEOCAT for IPOPP are being updated to take advantage of these improvements. Work is also underway to provide the development environment for implementing algorithms compatible with LEOCAT. The current algorithm development environment is being extended so that builds can be preformed both in and out of the Eclipse environment. For example, LEOCAT real-time DB operations at SSEC have demonstrated that LEOCAT is suitable for operation in the SSEC direct broadcast real-time processing environment.

MOD09 land surface reflectance for DB

Updated MOD09 code from Eric Vermote was received on November 15, and patched into the version we have running in real-time. It was also delivered, at Eric’s request, to the CSIR site in South Africa. The code has been running reliably at SSEC since the update was added, and reports from CSIR in early



January confirm that it is running reliably in their environment. SSEC has also delivered the MOD09 package to DRL. SSEC will need to review the package (once the SPA wrapper has been added) before it is released to the public.

MODIS real-time true color imagery over CONUS in support of DB real time data/products usage

SSEC released the new “MODIS Today” real-time true color image web site to the public on 12 December 2007: <http://www.ssec.wisc.edu/modis-today/>. It was picked up by several of the popular Google Earth blogs, and is currently featured on the home page of the NASA EOS website: <http://eos.nasa.gov/>

Conferences and meeting participation

Liam Gumley attended the “Earth from Space” conference in Moscow (4-6 December 2007) and co-chaired a session on real-time applications of DB data. He gave a presentation titled “EOS Direct Broadcast Real-Time Products for the US National Weather Service.”